

Nanoparticles for Oil Well Drilling Fluids and Cement

By

Muhammad Awais Ashfaq Alvi

Thesis submitted in fulfillment of
the requirements for the degree of

PHILOSOPHIAE DOCTOR
(PhD)



University of
Stavanger

Faculty of Science and Technology
Department of Energy and Petroleum Engineering

2024

University of Stavanger
N-4036 Stavanger
NORWAY
www.uis.no

©2024 Muhammad Awais Ashfaq Alvi

ISBN: 978-82-8439-210-3

ISSN: 1890-1387

PhD: Thesis UiS No. 738

*This dissertation is dedicated to my family who
instilled in me the virtues of perseverance and
commitment and relentlessly encouraged me to
strive for excellence.*

Acknowledgments

I would like to extend my appreciation to my supervisor Mesfin Belayneh for giving me an opportunity to work on this project. I would like to thank him for his continuous support, suggestions, and valuable feedback throughout the PhD work. His support with experimental work enabled me to generate a great amount of data. I would like to thank my co-supervisors Kjell Kåre Fjelde and Sulalit Bandyopadhyay for facilitating the progress of the thesis. Their mentorship and insightful feedback have been instrumental in shaping the direction and quality of this work.

I would like to express my gratitude to Arild Saasen and Mahmoud Khalifeh who generously shared their time, knowledge, and experience for this work. Their insights and suggestions have greatly contributed to the refinement and improvement of this thesis. My special thanks to lab technicians and engineers working at the department of Energy and Petroleum engineering, especially Caroline Ruud, Mona Minde (Head of the Department, Department of Mechanical and Structural Engineering and Materials Science), Kim Andre Nesse Vorland, Inger Johanne Munthe-Kaas Olsen and Jorunn Hamre Vrålstad.

I would like to thank my friends and PhD colleagues for their support, encouragement, and stimulating discussions. Their presence has provided a sense of camaraderie and made this academic endeavor a more enjoyable experience.

I would like to extend my heartfelt appreciation to my parents and wife for their encouragement, unconditional love, motivation, and understanding throughout this journey. Their unwavering support and belief in my abilities have been a constant source of motivation. Special thanks to my wife, Javeria Habib, for motivating me to finish this thesis and tolerating my demanding work schedule. Finally, to my son, Awliya Ahmed who accompanied me during the thesis writing sessions to make sure that I let him write a few lines in the thesis.

Summary

Drilling fluids and oil well cement are essential elements of the drilling process and well construction. Drilling fluids play a crucial role in the drilling process, ensuring the safety and efficiency of well construction. Continuous monitoring and adjustment of drilling fluids are required to optimize the drilling process and solve potential problems. The job of drilling fluids is to perform several important functions, such as carrying cutting from the bottom of the hole to the surface, providing cooling and lubrication to the drill bit, maintaining hydrostatic pressure to prevent the inflow of formation fluids, stabilizing the wellbore, and creating filter cake on the wellbore wall to control fluid loss. To perform these functions, the properties of drilling fluids, such as viscosity, density, yield stress, gel strength, and filtration, are important. The typical formulation of drilling fluids is based on water and oil. Typically, drilling fluids contain additives such as clay minerals, weighting agents, polymers, and various other additives. Factors such as well conditions, environmental considerations, and formation characteristics dictate the selection of appropriate drilling fluids. Conventional water-based and oil-based drilling fluids encounter certain challenges, such as fluid loss, formation damage, stuck pipe, differential sticking, or even wellbore collapse. Maintaining proper wellbore stability requires appropriate drilling fluid formulation.

Oil well cementing involves the placement of cement slurry into the annular space between the wellbore wall and casing to achieve zonal isolation, well integrity, and structural support. Conventional oil well cement can encounter various issues that can impact the well integrity, short-term and long-term performance. These include fluid loss, improper placement and setting, strength development, and formation of micro annuli, among others. Addressing these issues requires the use of specialized additives and advanced formulations tailored for specific well conditions. In addition to the above shortcoming, conventional oil well cement contributes to significant CO_2 emissions. Therefore, researchers are looking into possible alternative materials. Geopolymer is one of the alternatives to

conventional cement. It is a cementitious material typically produced by combining aluminosilicate sources with the hardener solution. While geopolymer can offer several advantages, it has shortcomings that need to be addressed, such as workability, low tensile strength, long-term durability & performance, and limited industry adoptions.

Nanoparticles (NPs) have gained immense attention for their potential application in drilling fluids, oil well cement, and geopolymer. The emergence of NPs is due to their ability to improve the performance of these materials. Notably, NPs are extensively researched as a multifunctional additive in these materials. However, to maximize the benefits and ensure safe and effective application in these materials, the optimal selection of NPs, dosage, and compatibility with other additives present in these materials still needs consideration. Therefore, the current work focuses on applying various NPs in these materials. This thesis is based on four publications and unpublished work.

The first section of this work deals with the application of different NPs (with respect to shape, size, surface charge, and surface functionality) on water-based drilling fluids (Papers I, IV, and unpublished work). The work investigated the performance of NPs based on iron oxide nanoparticles (IONPs), carbon nanotubes, and silica NPs on bentonite and potassium chloride (KCl) water-based drilling fluids. The results indicate that NPs can influence the properties of water-based drilling fluids. For instance, IONPs and nanotubes presence in the bentonite drilling fluids increases the gel strength and yield stress of the fluid. However, surface modification of IONPs with silica and polymer controls the gel-forming ability of the fluid and reduces gel strength. Moreover, silica NPs reduce bentonite drilling fluid's gel strength and yield stress. In addition, all types of NPs in the bentonite drilling fluids promote the shear thinning behavior by reducing the excessive gel formation at low shear rates. Adding NPs to the bentonite drilling fluids significantly reduces the friction values, and low concentration of IONPs and nanotubes in the drilling fluids show better performance than high concentration. Surface modified silica NPs however provide a higher

reduction in friction values. Fluid loss results suggest that NPs provide better reduction for bentonite-based fluids; NPs filled the pores in the filter cake and control the fluid flow. Microscale analysis of filter cake confirmed this behavior. In case of KCl drilling fluids, adding IONPs and nanotubes reduces the gel strength values of the fluid. While surface modification of IONPs with Si and silica NPs improves the gel strength of KCl fluids. Moreover, the yield stress of KCl fluids increased by adding silica NPs. Furthermore, NPs in KCl drilling fluids reduce friction values. While in case of KCl-based fluids, there was no significant reduction in fluid loss owing to the non-uniform distribution of NPs. Also, NPs adsorbed in the cake structure without filling the pores.

The second section includes the impact of hydrophobic IONPs on oil-based drilling fluids (Paper II). This work investigates the ability of IONPs to influence yield stress, HPHT fluid loss, mechanical friction, and barite sagging. The results suggested that NPs can increase the yield stress of oil-based drilling fluids at high temperature. Moreover, barite sagging, mechanical friction, and fluid loss were reduced by adding NPs to the drilling fluids. Also, drilling fluids with NPs produced a thin filter cake owing to the reduced permeability of the filter cake.

The third part of the thesis (paper III and unpublished work) focuses on applying aluminum oxide and carbon nanotubes to the fluid state and mechanical properties of cement and geopolymer materials. Additionally, the impact of NPs on the morphology and mineralogy of materials is tested. NPs in the cement and geopolymer slurry increase the viscosity of the slurries, as NPs control the segregation of materials by providing better cohesion. Fluid loss results for cement show that NPs delay the gelation of cement at high pressure and temperature and increase the fluid loss values. While for geopolymer, nanotubes show a significant reduction in fluid loss. NPs delays the pumpability of cement and geopolymer slurries at high temperature and pressure. Furthermore, NPs increase the compressive strength of cement and geopolymer, especially after 28 days. While only nanotubes provide improvement in the tensile strength of cement. In case of geopolymer,

NPs improve the tensile strength significantly until 7 days. However, after 28 days, only nanotubes show improvement in tensile strength. Microstructure and mineralogy analysis reveal that NPs are present throughout the structure of cement and geopolymer.

Abbreviations and Symbols

A	=	Pre-exponential factor
C_i	=	Concentration of solute at the interface of crystal-solution
C^*	=	Equilibrium solubility
C	=	Concentration of solute in supersaturated solution
f_{sm}	=	Volume fraction of solids in drilling fluids
f_{sc}	=	Volume fraction of solids in filter cake
h_{mc}	=	Filter cake height
k	=	Consistency factor
k_B	=	Boltzmann constant
k_{mc}	=	Permeability of filter cake
k_d	=	Coefficient of mass transfer based on diffusion
k_r	=	Rate constant in case of surface reaction
n	=	Flow factor
n_{ls}	=	Low shear curvature exponent
n_{hs}	=	High shear curvature exponent
S	=	Supersaturation
T	=	Temperature
V_f	=	Cumulative volume
ϕ	=	Factor represents the reduction in surface energy
γ	=	Interfacial tension
$\dot{\gamma}$	=	Shear rate
$\dot{\gamma}_s$	=	Surplus shear rate
μ_f	=	Viscosity of filtrate
μ_c	=	Casson plastic viscosity
λ	=	Wavelength
v	=	Molecular volume
ρ	=	Density
σ_c	=	Uniaxial stress
σ_t	=	Tensile stress
τ	=	Shear stress
τ_s	=	Surplus shear stress
τ_y	=	Yield stress
τ_c	=	Casson yield stress

ΔG_{crit}	=	Thermodynamic parameter
ΔP	=	Differential pressure
Al_2O_3	=	Aluminum oxide
AL-NPs	=	Short form for Al ₂ O ₃
API	=	The American petroleum institute
B_C	=	Bearden unit of consistency
BHCT	=	Bottom-hole circulating temperature
BWOC	=	By wight of cement
C-S-H	=	Calcium silicate hydrate
Ca (OH) ₂	=	Calcium hydroxide
CNTs	=	Carbon nanotubes
CVD	=	Chemical vapor deposition
ECD	=	Equivalent circulation density
EDS	=	Energy dispersive X-ray spectroscopy
Fe NPs	=	Short form for IONPs
Fe (CO) ₅	=	Iron pentacarbonyl
FeCl ₂ 4H ₂ O	=	Ferrous chloride tetrahydrate
FeCl ₃ 6H ₂ O	=	Iron (III) chloride hexahydrate
Fe-XG	=	Iron oxide NPs coated with xanthan gum
Fe-Si	=	Iron oxide NPs coated with silica
GGBFS	=	Ground granulated blast furnace slag
HPHT	=	High pressure high temperature
HSR	=	High sulphate resistance
IONPs	=	Iron oxide NPs
KCl	=	Potassium chloride
LPLT	=	Low pressure low temperature
LVE	=	Linear viscoelastic region
MPa	=	Megapascal
MWCNTs	=	Multi walled carbon nanotubes
WCNT-OH	=	Multi walled carbon nanotubes functionalized with hydroxyl groups
MWCNT-COOH	=	Multi walled carbon nanotubes functionalized with carboxyl groups
MW	=	Short form for MWCNTs
MW-OH	=	Short form for MWCNT-OH
MW-COOH	=	Short form for MWCNT-COOH

NCS	=	Norwegian continental shelf
NH_4OH	=	Ammonium hydroxide
NPs	=	Nanoparticles
OAm	=	Oleylamine
OBM	=	Oil-based mud
ODE	=	Octadecene
OPC	=	Ordinary Portland cement
P&A	=	Plug and abandonment
PSA	=	Petroleum safety authority
SiO_2	=	Silica
SEM	=	Scanning electron microscope
Si NPs	=	Silica NPs
Si-C NPs	=	Surface coated silica NPs
Si-N NPs	=	Silica NPs supplied by nycol
STEM	=	Scanning transmission electron microscopy
SWCNTs	=	Single walled carbon nanotubes
TS	=	Tensile strength
UCS	=	Uniaxial compressive strength
UCA	=	Ultrasonic cement analyzer
XG	=	Xanthan gum
XRD	=	X-ray diffraction
YM	=	Young's modulus

List of Publications

Paper I:

Alvi, M. A. A., Belayneh, M., Bandyopadhyay, S., & Minde, M. W. (2020). Effect of iron oxide NPs on the properties of water-based drilling fluids. *Energies*, 13(24), 6718. <https://doi.org/10.3390/en13246718>

Paper II:

Alvi, M. A. A., Belayneh, M., Fjelde, K. K., Saasen, A., & Bandyopadhyay, S. (2021). Effect of hydrophobic iron oxide NPs on the properties of oil-based drilling fluids. *Journal of Energy Resources Technology*, 143(4). <https://doi.org/10.1115/1.4048231>

Paper III:

Alvi, M. A. A., Khalifeh, M., & Agonafir, M. B. (2020). Effect of NPs on properties of geopolymers designed for well cementing applications. *Journal of Petroleum Science and Engineering*, 191, 107128. <https://doi.org/10.1016/j.petrol.2020.107128>

Paper IV:

Alvi, M. A. A., Belayneh, M., Saasen, A., & Bandyopadhyay, S. (2021, June). Impact of Various NPs on the Viscous Properties of Water Based Drilling fluids. In *International Conference on Offshore Mechanics and Arctic Engineering (Vol. 85208, p. V010T11A066)*. American Society of Mechanical Engineers. <https://doi.org/10.1115/OMAE2021-62612>

Candidate Contributions

The candidate is the main contributor to the publications, which include: Conceptualization, Methodology, Investigation, Planning and performing experiments, Data curation, Writing - original drafts, Writing-review & editing.

Additional Publications

Alvi, M. A., Belayneh, M., Saasen, A., & Aadnøy, B. S. (2018, April). The effect of micro-sized boron nitride BN and iron trioxide Fe₂O₃ NPs on the properties of laboratory bentonite drilling fluids. In SPE Norway one day seminar. OnePetro. <https://doi.org/10.2118/191307-MS>

Alvi, M. A. A., Belayneh, M., Saasen, A., Fjelde, K. K., & Aadnøy, B. S. (2018, June). Effect of MWCNT and MWCNT functionalized-OH and-COOH NPs in laboratory water based drilling fluids. In International Conference on Offshore Mechanics and Arctic Engineering (Vol. 51296, p. V008T11A069). American Society of Mechanical Engineers. <https://doi.org/10.1115/OMAE2018-78702>

Akram, A., Alvi, M. A. A., & Belayneh, M. (2018). The Impact of MWCNT on XG Polymer/Salt Treated Laboratory Water Based Drilling fluids. *Int. J. Nano Sci. Nanotechnol*, 9(1), 1-8.

Sharma, Anuvansh; Antony, Jibin; Raghunathan, Karthik; Alvi, Muhammad Awais Ashfaq; Glomm, Wilhelm; Bandyopadhyay, Sulalit. (2018) FunNano – Functional NPs for Diverse Applications. Det 21. Landsmøte i kjemi. Norsk Kjemisk Selskap; 2018-10-16 - 2018-10-18.

Contents

Acknowledgments	v
Summary	vii
Abbreviations and Symbols	xi
List of Publications	xv
Additional Publications	xvii
1 Introduction	1
1.1 Water-Based Drilling Fluids	1
1.2 Oil-Based Drilling Fluids	3
1.3 Oil Well Cement and Geopolymer	5
1.4 Scope and Objective	10
1.5 Contribution of the Dissertation	12
1.6 Thesis Outline	13
2 Literature Review	15
2.1 Application of NPs in Water-Based Drilling Fluids	15
2.2 Application of NPs in Oil-Based Drilling Fluids	21
2.3 Application of NPs in Oil Well Cement	22
2.4 Application of NPs in Geopolymer	28
3 Nanoparticles Synthesis	31
3.1 Co-Precipitation	35
3.2 Thermal Decomposition	36
3.3 Silica NPs	36
3.4 Aluminium Oxide NPs	37
3.5 Carbon Nanotubes	38
3.6 Surface Modification of NPs	39
4 Materials and Methodology	41
4.1 Synthesis of Iron Oxide NPs	41

4.2	Coating of Xanthan Gum on Iron Oxide NPs and Fe-Si NPs	42
4.3	Silica NPs and Surface Modification	42
4.4	MWCNTs	43
4.5	Aluminium Oxide NPs	44
4.6	Drilling fluids Formulation	44
4.7	Cement and Geopolymer Formulation	45
	4.7.1 Cement and Geopolymer Slurry Preparation	47
4.8	Characterization Techniques and Test Methods	49
	4.8.1 Scanning Transmission Electron Microscopy (STEM)	49
	4.8.2 Scanning Electron Microscopy (SEM)	49
	4.8.3 Dynamic Light Scattering (DLS) and Zeta Potential	50
	4.8.4 Viscosity	51
	4.8.5 Fluid loss	53
	4.8.6 Mechanical Friction	53
	4.8.7 Viscoelasticity	54
	4.8.8 Barite Sag Test for Oil-Based Drilling Fluids	54
	4.8.9 Temperature and Pressure Conditions for Cement and Geopolymer Tests	54
	4.8.10 Consistency	55
	4.8.11 Uniaxial Compressive Strength	55
	4.8.12 Indirect Tensile Strength Measurement	56
	4.8.13 Sonic Strength Development	56
	4.8.14 X-ray Diffraction (XRD)	57
4.9	Iron Oxide NPs	58
4.10	Commercial and Surface Modified NPs	59
5	Application of NPs in Water Based Drilling Fluids.	63
5.1	Rheological Parameters of Drilling Fluids with NPs	63
	5.1.1 Shear Stress Measurement	63
	5.1.2 Gel Strength	69
	5.1.3 Low and High Shear Curvature Exponents	73
	5.1.4 Yield and Surplus Stress	77
	5.1.5 Viscoelastic Properties	81
5.2	Mechanical Friction	84

5.3	Fluid Loss	88
5.4	Microscale Analysis of Filter Cake	91
5.5	Energy Dispersive X-ray Spectroscopy	101
6	Application of IONPs in Oil-Based Drilling Fluids.	111
6.1	Rheological Parameters of the Drilling Fluids	111
6.1.1	Gel Strength	112
6.1.2	Yield and Surplus Stress	113
6.1.3	Low and High Shear Curvature Exponents	113
6.1.4	Barite Sagging	114
6.2	Friction Measurement	115
6.3	Effect of NPs on the Fluid Loss and Filter Cake	116
7	Application of Nanotubes and AL NPs in Cement and Geopolymer	119
7.1	Rheological Properties	119
7.2	Fluid-Loss Test	122
7.3	Pumpability	123
7.4	Mechanical Properties	126
7.4.1	Uniaxial Compressive Strength (UCS)	126
7.4.2	Modulus of Elasticity	127
7.4.3	Compressive Strength to Young Modulus Ratios	129
7.4.4	Tensile Strength (TS)	130
7.4.5	Tensile Strength to Young's Modulus Ratios	131
7.5	Sonic Strength	132
7.6	X-ray Diffraction	134
7.7	Microstructure Analysis	136
8	Conclusions and future work	143
8.1	Conclusions	143
8.2	Future Work	149
	References	151
	Appendix	199

List of Figures

Figure 1.1 Well barrier envelopes (blue as primary and red as secondary) and NORSOK D-010 cement requirement.	5
Figure 1.2 Categories of well barrier element failures in the Norwegian sector of the North Sea.	7
Figure 3.1 Top-down and Bottom-up approaches to synthesize NPs.	31
Figure 3.2 Mechanism of NPs nucleation and growth, illustrated by Lamer diagram.	34
Figure 4.1 a) STEM image of IONPs produced by coprecipitation method b) Size distribution of NPs c) STEM image of IONPs produced by thermal decomposition method d) Size distribution of NPs (Paper I, Paper II).	58
Figure 4.2 SEM images of NPs a) MW b) MW-OH c) MW-COOH d) Si NPs e) Si-C NPs f) Si-N NPs g) Fe NPs h) Fe-XG NPs i) Fe-Si j) Al NPs (Paper IV).	60
Figure 5.1 Impact of Fe, Fe-XG, and Fe-Si NPs on shear stress of water-based drilling fluids a) Bentonite drilling fluids with 0.0095wt.% and 0.019wt.% Fe NPs b) Bentonite drilling fluids with 0.038wt.% Fe and Fe-XG NPs c) Bentonite drilling fluids with 0.0095wt.% and 0.019wt.% Fe-Si NPs d) KCl drilling fluids with 0.0095wt.% and 0.019wt.% Fe NPs e) KCl drilling fluids with 0.038wt.% Fe and Fe-XG NPs f) KCl drilling fluids with 0.0095wt.% and 0.019wt.% Fe-Si NPs (Paper I).	64

Figure 5.2	Impact of SiO_2 NPs on shear stress of water-based drilling fluids a) Bentonite drilling fluids with 0.0095wt.% and 0.019wt.% Si NPs b) Bentonite drilling fluids with 0.0095wt.% and 0.019wt.% Si-C NPs c) Bentonite drilling fluids with 0.0095wt.% and 0.019wt.% Si-N NPs d) KCl drilling fluids with 0.0095wt.% and 0.019wt.% Si NPs e) KCl drilling fluids with 0.0095wt.% and 0.019wt.% Si-C NP f) KCl drilling fluids with 0.0095wt.% and 0.019wt.% Si-N NPs.	66
Figure 5.3	Impact of MWCNTs on shear stress of water-based drilling fluids a) Bentonite drilling fluids with MW b) Bentonite drilling fluids with MW-OH c) Bentonite drilling fluids with MW-COOH d) KCl drilling fluids with MW e) KCl drilling fluids with MW-OH f) KCl drilling fluids with MW-COOH. . . .	68
Figure 5.4	Impact of Fe, Fe-XG and Fe-Si NPs on gel strength of water-based drilling fluids a) 10 sec gel strength of bentonite drilling fluids b) 10 min gel strength of bentonite drilling fluids c) 10 sec gel strength of KCl drilling fluids d) 10 min gel strength of KCl drilling fluids (Paper I).	69
Figure 5.5	Impact of SiO_2 NPs on gel strength of water-based drilling fluids a) 10 sec gel strength of bentonite drilling fluids b) 10 min gel strength of bentonite drilling fluids c) 10 sec gel strength of KCl drilling fluids d) 10 min gel strength of KCl drilling fluids. . .	71
Figure 5.6	Impact of MWCNTs on gel strength of water-based drilling fluids a) 10 sec gel strength of bentonite drilling fluids b) 10 min gel strength of bentonite drilling fluids c) 10 sec gel strength of KCl drilling fluids d) 10 min gel strength of KCl drilling fluids. . .	72
Figure 5.7	Impact of Fe, Fe-XG and Fe-Si NPs on n_{ls} and n_{hs} of water-based drilling fluids a) n_{ls} of bentonite drilling fluids b) n_{hs} of bentonite drilling fluids c) n_{ls} of KCl drilling fluids d) n_{hs} of KCl drilling fluids (Paper IV).	74

Figure 5.8 Impact of SiO_2 NPs on n_{ls} and n_{hs} of water-based drilling fluids a,b) n_{ls} and n_{hs} of bentonite drilling fluids c,d) n_{ls} and n_{hs} of KCl drilling fluids (Paper IV).	75
Figure 5.9 Impact of MWCNTs on n_{ls} and n_{hs} of water-based drilling fluids a,b) n_{ls} and n_{hs} of bentonite drilling fluids c,d) n_{ls} and n_{hs} of KCl drilling fluids (Paper IV).	76
Figure 5.10 Yield stress and surplus stress of water-based drilling fluids with Fe, Fe-XG and Fe-Si NPs a) Yield stress of bentonite drilling fluids b) Surplus stress of bentonite drilling fluids c) Yield stress of KCl drilling fluids d) Surplus stress of KCl drilling fluids (Paper IV).	78
Figure 5.11 Yield stress and surplus stress of water-based drilling fluids with Si, Si-C and Si-N NPs a,b) Yield and surplus stress of bentonite drilling fluids c,d) Yield stress and surplus stress of KCl drilling fluids (Paper IV).	79
Figure 5.12 Yield stress and surplus stress of water-based drilling fluids with MW, MW-OH, MW-COOH a,b) Yield and surplus stress of bentonite drilling fluids c,d) Yield stress and surplus stress of KCl drilling fluids (Paper IV).	80
Figure 5.13 Friction values of water-based drilling fluids a, b) Bentonite-based fluids with NPs c, d) KCl-based fluids with NPs (Paper I).	85
Figure 5.14 Friction values of water-based drilling fluids with SiO_2 NPs a,b) Bentonite drilling fluids with NPs c,d) KCl drilling fluids with NPs.	86
Figure 5.15 Friction values of water-based drilling fluids with MWCNTs a,b) Bentonite drilling fluids with nanotubes c,d) KCl drilling fluids with nanotubes.	87
Figure 5.16 Filtrate volume of water-based drilling fluids after fluid loss test a,b) Bentonite-based fluids with NPs c, d) KCl-based fluids with NPs (Paper I).	88

Figure 5.17 Fluid loss of water-based drilling fluids a,b) Bentonite drilling fluids with NPs c,d) KCl drilling fluids with NPs.	90
Figure 5.18 Fluid loss of water-based drilling fluids a,b) Bentonite drilling fluids with nanotubes c,d) KCl drilling fluids with nanotubes.	91
Figure 5.19 SEM images of filter cake of bentonite drilling fluids a,b) Structure of filter cake for base fluid c,d) Structure of filter cake for Fe NPs e,f) Structure of filter cake for Fe-XG (Paper I).	92
Figure 5.20 SEM images of filter cake of bentonite drilling fluids a,b) Structure of filter cake for base fluid c,d) Structure of filter cake for Fe-Si NPs.	93
Figure 5.21 SEM images of filter cake of KCl drilling fluids a,b) Structure of filter cake for base fluid c,d) Structure of filter cake for Fe NPs e,f) Structure of filter cake for Fe-XG (Paper I).	94
Figure 5.22 SEM images of filter cake of KCl drilling fluids a,b) Structure of filter cake for base fluid c,d) Structure of filter cake for Fe-Si NPs.	95
Figure 5.23 SEM images of filter cake of bentonite drilling fluids a,b) Base fluid c,d) Si NPs e,f) Si-C NPs g,h) Si-N NPs.	96
Figure 5.24 SEM images of filter cake of KCl drilling fluids a,b) Structure of filter cake for base fluid c,d) Structure of filter cake with Si NPs fluid e,f) Structure of filter cake with Si-C NPs g,h) Structure of filter cake with Si-N NPs.	97
Figure 5.25 SEM images of filter cake of bentonite drilling fluids a,b) Base fluid c,d) MW e,f) MW-OH g,h) MW- COOH.	99
Figure 5.26 SEM images of filter cake of KCl drilling fluids a,b) Base fluid c,d) MW e,f) MW-OH g,h) MW-COOH.	100
Figure 5.27 EDS analysis of filter cake formed by bentonite drilling fluids a,b) Base fluid c,d) Base fluid with Fe NPs e,f) Base fluid with Fe-XG NPs (Paper I).	101

Figure 5.28 EDS analysis of filter cake formed by bentonite drilling fluids a,b) Base fluid c,d) Base fluid with Fe-Si NPs.	102
Figure 5.29 EDS analysis of filter cake formed by KCl drilling fluids a,b) Base fluid c,d) Base fluid with Fe NPs e,f) Base fluid with Fe-XG NPs (Paper I).	103
Figure 5.30 EDS analysis of filter cake formed by KCl drilling fluids a,b) Base fluid c,d) Base fluid with Fe-Si NPs.	104
Figure 5.31 EDS analysis of filter cake formed by bentonite drilling fluids a,b) Base fluid c,d) Base fluid with Si NPs e,f) Base fluid with Si-C NPs g,h) Base fluid with Si-N NPs.	105
Figure 5.32 EDS analysis of filter cake formed by KCl drilling fluids a,b) Base fluid c,d) Base fluid with Si NPs e,f) Base fluid with Si-C NPs g,h) Base fluid with Si-N NPs.	106
Figure 5.33 EDS analysis of filter cake formed by bentonite drilling fluids a,b) Base fluid c,d) Base fluid with MW e,f) Base fluid with MW-OH g,h) Base fluid with MW-COOH.	108
Figure 5.34 EDS analysis of filter cake formed by KCl drilling fluids a,b) Base fluid c,d) Base fluid with MW e,f) Base fluid with MW-OH g,h) Base fluid with MW-COOH.	109
Figure 6.1 Effect of temperature and IONPs on shear stress at different shear rates for oil-based drilling fluids (Paper II).	111
Figure 6.2 Gel strength a) 10 sec and b) 10 min of drilling fluids and drilling fluids with 0.5 wt.% IONPs and 1.0 wt.% IONPs at different temperatures (Paper II).	112
Figure 6.3 Effect of temperature on a) Yield and b) Surplus stress of oil-based drilling fluids and drilling fluids with IONPs (Paper II).	113
Figure 6.4 a) n_{ls} and b) n_{hs} of oil-based drilling fluids and drilling fluids with IONPs (Paper II).	113

Figure 6.5	Static and dynamic barite sagging of oil based drilling fluids and drilling fluids with NPs (Paper II).	114
Figure 6.6	Impact of NPs on the coefficient of friction of oil-based drilling fluids (Paper II).	115
Figure 6.7	Filtrate volume after fluid loss test for oil-based drilling fluids with IONPs (Paper II).	116
Figure 7.1	Effect of temperature and NPs on the rheological behaviour of a) Cement b) Geopolymer (Paper III).	119
Figure 7.2	Apparent viscosity of a) neat cement with NPs and b) geopolymer modified with AL NPs, and MW-OH (Paper III).	120
Figure 7.3	Impact of AL NPs and nanotubes on static fluid loss of a) cement and b) geopolymeric slurries (Paper III).	123
Figure 7.4	a) Effect of AL NPs on setting time of the cement slurry b) Effect of MW-OH on setting time of the cement slurry c) Effect of MW on setting time of the cement slurry.	124
Figure 7.5	a) Effect of AL NPs on setting time of the geopolymer slurry b) Effect of MW-OH on setting time of the geopolymer slurry (Paper III).	125
Figure 7.6	Unconfined compressive strength for a) Neat cement with AL NPs and nanotubes b) Neat geopolymer with AL NPs and MW-OH (Paper III).	126
Figure 7.7	Estimated Young's modulus values a) Neat cement with NPs b) Neat geopolymer with NPs (Paper III).	128
Figure 7.8	Ratio of unconfined compressive strength to Young's modulus a) Cement samples b) Geopolymer samples (Paper III).	129
Figure 7.9	Indirect tensile strength a) Neat cement with NPs b) Neat geopolymer with NPs (Paper III).	130
Figure 7.10	Ratio of average tensile strength to Young's modulus of a) Cement samples b) Geopolymer (Paper III).	131

Figure 7.11 a) Sonic Strength development of cement b) Modified with AL NPs c) Modified with MW-OH c) Modified with MW.	133
Figure 7.12 Sonic Strength development of a) Geopolymer modified with AL NPs b) Modified with MW-OH (Paper III).	133
Figure 7.13 XRD pattern for the neat cement and cement with AL NPs and nanotubes.	134
Figure 7.14 XRD pattern for the neat geopolymer and geopolymer with AL NPs and MWCNT-OH indicating additional peaks and peak shifts for geopolymer with NPs (Paper III).	135
Figure 7.15 SEM images of the neat cement a) Overview of the structure b, c) Internal structure.	136
Figure 7.16 SEM images of cement with AL NPs a) Overview of the structure b) Internal structure showing AL NPs and cement c) AL NPs presence in the structure of cement.	137
Figure 7.17 SEM images of cement with MW-OH a) Overview of the structure b) Internal structure showing MW-OH and geopolymer c) MW-OH presence in the structure of geopolymer.	138
Figure 7.18 SEM images of cement with MW a) Overview of the structure b) Internal structure showing MW and cement c) MW presence in the structure of cement.	139
Figure 7.19 SEM images of the neat geopolymer a) Overview of the structure b, c) Internal structure (Paper III).	140
Figure 7.20 SEM images of geopolymer with AL NPs a) Overview of the structure b) Internal structure showing AL NPs and geopolymer c) AL NPs presence in the structure of geopolymer (Paper III).	141
Figure 7.21 SEM images of Geopolymer with MW-OH a) Overview of the structure b) Internal structure showing MW-OH and geopolymer c) MW-OH presence in the structure of geopolymer (Paper III).	142

List of Tables

Table 4.1	Composition of bentonite drilling fluids.(Paper I).	44
Table 4.2	Composition of KCl drilling fluids (Paper I).	44
Table 4.3	Composition of oil-based drilling fluids (Paper II).	46
Table 4.4	Chemical composition of cement.	46
Table 4.5	Chemical composition of geopolymer (Paper III).	47
Table 4.6	Composition of the AL NPs modified geopolymer (Paper III).	48
Table 4.7	Composition of the MW-OH modified geopolymer (Paper III).	48
Table 4.8	Size and zeta potential of NPs at 25 °C (Paper I, IV).	61
Table 4.9	Size and zeta potential of NPs at 50 °C (Paper I, IV).	61
Table 5.1	Yield stress and flow point (Oscillatory) for bentonite drilling fluids (Paper I).	81
Table 5.2	Yield stress and flow point (Oscillatory) for KCl drilling fluids (Paper I).	82
Table 5.3	Yield stress and flow point (Oscillatory) for bentonite drilling fluids.	83
Table 5.4	Yield stress and flow point (Oscillatory) for KCl drilling fluids.	83
Table 5.5	Yield stress and flow point (Oscillatory) for bentonite drilling fluids.	84
Table 5.6	Yield stress and flow point (Oscillatory) for KCl drilling fluids.	84
Table 6.1	Filter cake properties and filter volume (Paper II).	118
Table 7.1	Casson Yield stresses and Casson plastic viscosities of cement (Paper III).	121
Table 7.2	Casson Yield stresses and Casson plastic viscosities of geopolymer (Paper III).	121

1 Introduction

1.1 Water-Based Drilling Fluids

The primary stage to approach an oil and gas reservoir is to perform a drilling operation. Drilling is the process of connecting the surface with the reservoir to extract the hydrocarbons. Therefore, to enhance productivity, it is essential to put more emphasis on this operation. Drilling fluids are an integral part of the drilling operation of oil and gas reservoirs. The drilling fluids can be defined as a material that helps drilling tools to create a borehole. Water's use as drilling fluid dates back to the Zhou dynasty (1122-250 B.C.). During this period, wells were drilled to get access to water, gas, and brines, where water was employed as drilling fluid to lift the cutting and soften the rock surface [1]. Through the years, with the oil and gas industry's development, drilling fluids also developed as advanced materials composed of various additives to perform different functions. Drilling fluids are circulated from the surface using a drill pipe to perform functions like cleaning the bottom of the well & carrying cutting from the bottom of the well to the surface, cooling & lubricating of drill bit, maintaining wellbore stability, controlling the inflow of fluids from the wellbore (permeable rocks), and formation of thin filter cake with low permeability so the pores and holes which are present in the formation can be sealed [2–5]. In addition to these functions, the drilling fluids should not damage the formation as well as they should be environmentally friendly and non-hazardous to the drilling personnel [5].

Generally, drilling fluids are classified as water-based, oil-based, synthetic, and gas or pneumatic-based fluids [6]. Water and oil-based are the most common drilling fluids, where water is the continuous phase of water-based fluids with solid particles suspended in water to form a colloidal suspension. While oil is the continuous phase in oil-based fluids with suspended solid particles, and brine or water is added to form an emulsion [1]. Solids such as organic colloids and clays are added to provide the required filtration and viscous properties to

the water-based drilling fluids. Moreover, minerals such as barite are added when required to raise the density of the fluid. Also, lubricating agents and salts are added to the fluid for various purposes [1]. Since drilling fluids perform various tasks during drilling operations, proper design of drilling fluids is crucial to perform these functions effectively. However, conventional water-based drilling fluids are not able to perform these functions in an efficient way which leads to problems like formation damage owing to the interaction of water-based drilling fluids and rock. Moreover, high fluid loss from drilling fluids into the formation can increase the pressure, ultimately impacting the wellbore's strength. Also, water-based fluid can react with shale formations and cause shale swelling. Solid-induced drill string stuck can occur due to the drilling fluid's ineffective cutting holding capacity. In addition, the formation of a thick filter cake can cause differential sticking issues [7–10]. These problems can be more severe as the temperature and pressure increase during the drilling process for high-pressure/high-temperature (HPHT) wells due to polymer degradation and flocculation of bentonites [10, 11]. Significant financial losses are associated with these problems, and in the worst case, these can lead to the shutdown of the well. The drilling fluid's viscous, filtration, and frictional properties are critical to minimize these problems. These properties depend on the chemical additives type, concentration, shape, and size used to formulate the drilling fluids. Therefore, continuous laboratory-scale experiments must characterize and test suitable parameters. Moreover, oil-based drilling fluids can deal with these complex situations. However, the use of oil-based drilling fluids is sometimes limited due to environmental regulations [12]. Furthermore, since no blowout preventer (BOP) is present in the top-hole section of the well, water-based fluids are used for drilling these sections. Several strategies are employed to mitigate the issue with conventional water-based drilling fluids, such as using polymeric additives to minimize fluid loss and using KCl and silicate-based drilling fluids to control shale swelling [10, 13]. However, these microparticles and bigger-sized additives are not very promising in enhancing the drilling fluid's performance. Therefore, the petroleum industry is now searching for a small, multifunctional, stable under

extreme conditions, biologically degradable as well as environmentally sound option to formulate drilling fluids that are efficient and will perform satisfactorily during a drilling operation [14].

1.2 Oil-Based Drilling Fluids

As previously mentioned, water-based drilling fluids are ineffective in the case of reactive shale and at HPHT conditions. [15]. Moreover, owing to low friction values, better geomechanical and thermal stability oil-based drilling fluids are preferred in extended-reach wells and directional drilling [16–18]. However, the oil-based drilling fluids experience stability issues in HPHT wells, such as barite sagging problems. Similar to water-based drilling fluids, barite is also used as a weighting material in oil-based fluids due to its low environmental impact, cost, and high specific gravity [19]. However, the settling of barite particles at HPHT conditions can cause serious problems. For instance, the proper control of well pressure can be challenging due to variations in the drilling fluids density, especially the presence of light clear fluid in the vertical parts of the well [20]. Furthermore, these settled particles can lower the penetration rate by increasing the chances of drill string sticking. Barite sagging can occur both under dynamic and static conditions. *Zamora and Bell. (2004)* [21] suggested that close monitoring of the rheological parameters of drilling fluids can minimize this phenomenon. Moreover, rheological parameters are dependent on the stability of water in oil emulsion formed by oil-based drilling fluids. Therefore, the long-term stability of water in oil emulsion is crucial at high temperature. The harsh conditions of deep water and depleted reservoirs can further complicate the drilling process due to operating in a small pressure window [22]. It is critical to optimize operational parameters and drilling fluids properties to reach the target well depth under these circumstances. Choosing suitable drilling fluids with optimum densities for the different well sections is essential. To maintain pressure control and ensure operational success, the proper drilling fluid design for each section is vital. Since well hydraulics impact parameters such as pump pressure, wellbore cleaning, and equivalent

circulation density (ECD), it is critical to optimize the well hydraulics by fine-tuning the viscous properties of the drilling fluids. Moreover, to act as a primary barrier element, the drilling fluids should have stable density under extreme downhole conditions.

One of the techniques to enlarge the operational pressure margin is wellbore strengthening. The interaction of particles in the drilling fluids and surrounding rock defines the success of the wellbore strengthening technique. The type, concentration, and size distribution of particles in the drilling fluids are crucial to achieve wellbore strength [18, 23]. Operational examples employ wellbore strengthening to support or possibly increase the fracture gradient [24] as well as to show the importance of particle size, concentration, and type in lowering fluid losses [18]. Various wellbore strengthening techniques are available, combining two or more techniques typically shows the best performance. *Jacob et al. (2014)* provided the overview and benefits of different wellbore strengthening techniques [25]. One of the studies suggests the application of NPs to attain wellbore strengthening [26]. Lowering the fluid loss from oil-based drilling fluids to the formation is critical in achieving wellbore strength. It is vital to control fluid and mud losses to the permeable formation by formulating optimum drilling fluids. Filter cake formed by drilling fluids is also crucial as thick cake can cause differential sticking and excessive fluid loss to the formation, which can lead to formation damage [27]. To control this flow of fluids, the filter cake formed by the oil-based drilling fluids should be thin and impermeable [28–31]. Chemical additives and particles used in drilling fluids will define the filter cake formed by the fluid [28]. Therefore, it is vital to formulate a drilling fluid that can form an effective filter cake. The thickness, particle size distribution, permeability, and structure of filter cake are vital to optimize the drilling fluids formulation [22]. Different studies use various additives to mitigate the barite sagging problem [32–35]. However, these additives impact the rheological parameters of drilling fluids [36]. Moreover, various additives are suggested to resolve the fluid loss issue [1, 29, 37]. However, there is still a requirement to add suitable additives to drilling fluids that can solve the barite sagging and fluid loss issue. The additive should not significantly impact the

rheological parameters to avoid operational issues such as staying within pressure margins and excessive frictional pressure losses.

1.3 Oil Well Cement and Geopolymer

Oil well cement is one of the crucial well barrier elements used during well construction, completion, and plug & abandonment (P&A) phases. Oil well cementing involves the placement of cement around the casing, and the primary function of well cementing is to seal annular spacing between casing-casing or casing-formation, providing structural integrity and preventing formation fluid from leaking to the surface [38]. Improper zonal isolation can create leak paths, as shown in Figure 1.1 (modified from [39, 40]).

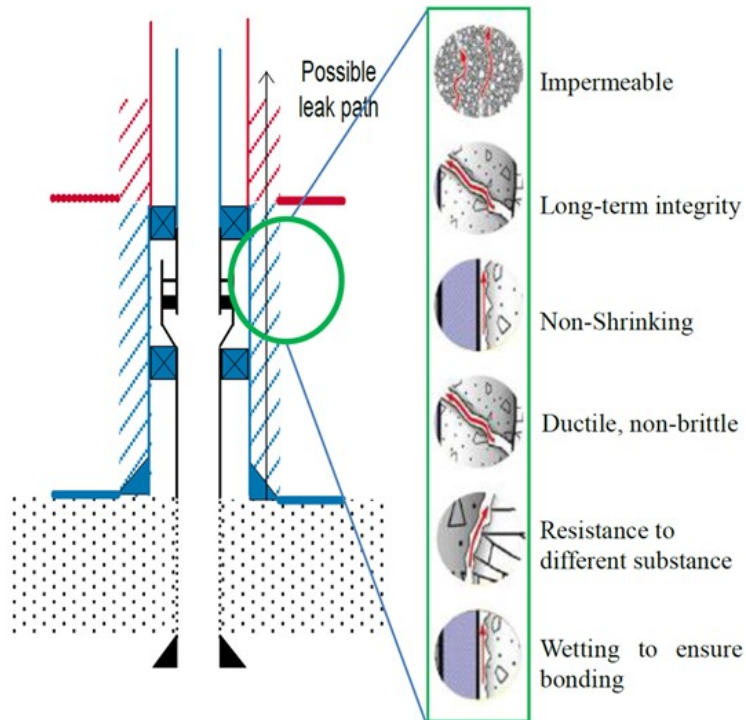


Figure 1.1: Well barrier envelopes (blue as primary and red as secondary) and NOR-SOK D-010 cement requirement.

Possible leak paths from the well could be through cement due to the permeability of cement. Low permeability and porosity of cement are crucial as the cement behind the casing sustains the pressure of formation fluids. Moreover, downhole stresses (e.g., thermal shocks, tectonic stresses, post-cement operations) can create cracks in the cement structure. Furthermore, leak paths can form in the micro annuli at the interface of casing-cement or cement-formation due to shrinkage of cement and/or improper wetting to ensure bonding between casing and cement. The brittleness of cement can also contribute to the formation of leak paths. A successful cementing operation can be achieved by adequately designing the cement slurry and following general guidelines and requirements relevant to well integrity. *NORSOK D-010 (2013)* [39] defines well integrity as “*the application of a technical, operational, and organizational solution to minimize the risk of an undesired leak during the lifetime of the well*”.

Studies have reported the well integrity issues in different parts of the world. *Vignes and Aadnøy (2010)* [41] based on data obtained from seven operators reported the integrity status of the Norwegian Continental Shelf (NCS) wells. As shown in Figure 1.2, their investigation indicated that out of the 75 wells (i.e., 48 production and 27 injection wells), casing and cement integrity issues recorded 11% of well integrity issues each [41]. The Petroleum Safety Authority PSA in Norway performed a survey on 1995 wells from 13 operators and reported that 30% of the wells have well integrity issues [42]. In addition, a recent report published by PSA shows that from 2011 to 2020, around 1292 wells were abandoned temporarily. The data from these wells show that the number of wells without any major well integrity issues reduced from 62% to 45% [43]. Various abandoned wells in Alberta, Canada, have been assessed by *Watson and Bachu (2009)* [44] with respect to leakage potential. This work shows that one of the reasons for leaks from the wells is improper zonal isolation.

As indicated in Figure 1.1, depending on the completion and well design, qualified cement can be considered either as a well barrier element in the primary or secondary barrier envelope. Also, *NORSOK*

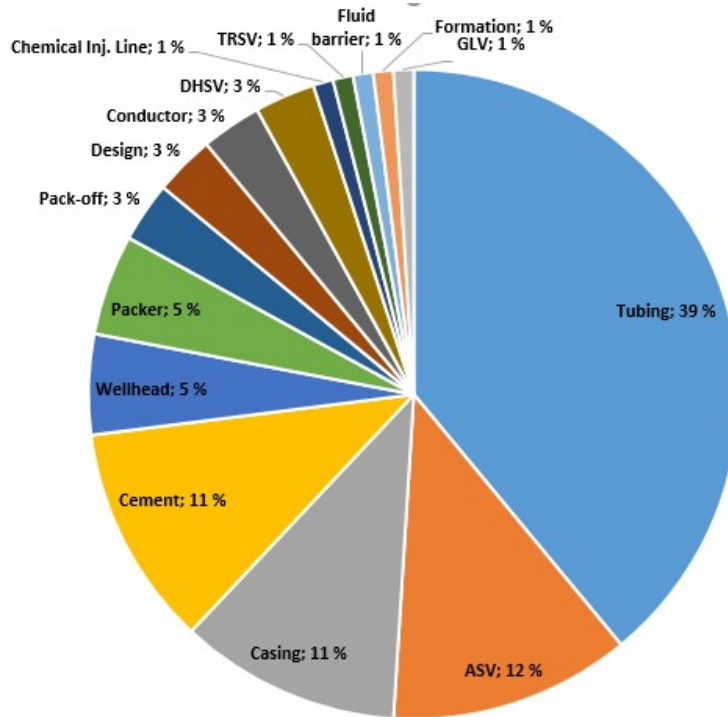


Figure 1.2: Categories of well barrier element failures in the Norwegian sector of the North Sea.

D-010 (2013) [39] defines the well integrity and sets criteria for barrier material used for zonal isolation or P&A. The standards state that the barrier material should be impermeable, able to withstand mechanical loads/impact, and non-shrinking. In addition, the candidate material shall resist downhole chemicals and ensure bonding with steel and formation. Since there are failure mechanisms associated with the Portland cement such as the formation of cracks due to changes in temperature and pressure regimes, volume changes causing possible micro annuli, and low ductility of cement, i.e., brittleness [45]. Also, poor cementing practices can result in channels through cement, for example, at high temperature, the cement sets too fast, causing channelling in the cement structure [46]. Furthermore, tectonic stresses [45, 47, 48] are circumstances that intensify the risk of material failure. Moreover, cement slurry in high-temperature wells

contributes to high fluid loss and strength loss phenomenon commonly called strength retrogression. Due to the above shortcomings with Portland cement, researchers are trying to look for supplementary materials as well as to improve the properties of cement. Several factors contribute towards to the strength of cement such as curing conditions and time [49, 50], additives used to form cement slurry [51, 52] and environmental conditions [53]. Additives are added to the cement slurry to influence its properties. For example, accelerators and retarders are added to reduce and increase the thickening time of cement slurry respectively. Moreover, additives are added to alter mechanical strength, such as compressive & tensile strength, fluid loss, density, and cement viscosity. In addition, additives are used to produce lightweight, expansive, corrosion-resistant, and stable against hydrogen sulphide cement [54]. Even though smart polymers, self-healing, and fiber materials are available owing to technological advancement, the challenge of attaining longer-term zonal isolation in severe oil well conditions still exists.

To mitigate the risk of well barrier failure, researchers and operators suggested to replace the Portland cement with alternative materials [45, 48, 55–57]. Moreover, a significant amount of CO_2 emissions is associated with cement production. As an example, the production of one ton of Portland cement can emit between 650-1100 kg of CO_2 [58, 59]. It has been documented that the manufacturing of Portland cement contributes to 5-8% of global CO_2 emissions [60, 61]. The scientific community suggests several strategies to solve CO_2 emissions from the production of Portland cement. One important strategy is partially replacing cement with fly ash or slag. However, this affects the short-term mechanical properties and does not deliver a radical CO_2 reduction. In addition, several alternative materials, such as bismuth-based materials [62], resins, creeping formation, and geopolymer, have been proposed or used as an alternative to Portland cement [45, 63, 64]. Geopolymers have been used in the construction industry and suggested as a supplementary material to cement for well construction [64–67]. Geopolymers belong to inorganic polymers that are made of a long chain of aluminosilicate materials formed by the process of geopolymerization. Geopolymerization

is the term introduced by *Joseph Davidovits* in 1978 [68, 69]. In this process, reactive alumina, and silica-based materials, known as precursors, act as source material. The source material is mixed with a hardener, an alkali silicate solution, to activate the geopolymerization process. Mechanisms such as dissolution, nucleation, orientation, and polycondensation are associated with the geopolymerization reaction [70, 71]. The tetrahedrons SiO_4 and AlO_4 are bonded alternately by sharing the oxygen ions as Si–O–Al–O to form the geopolymer structure with 3-D network gel [71, 72]. Various precursor materials such as kaolinite, metakaolin, feldspar, and solid wastes like rice husk, fly ash, blast furnace slag, and several others can produce geopolymer. The source material's properties define the geopolymer's strength and stability. Some of these properties may include but are not limited to fineness, particle size distribution, chemical composition, and reactive content of the geopolymeric precursors [73]. Moreover, the concentration of soluble silicate, water content, and pH level of the hardener are also important factors [70]. Researchers studied the advantages and existing limitations of geopolymers compared to conventional cement. Some of the advantages include lower permeability [74–76], durability in corrosive environments [76, 77], higher structural flexibility [78], lower chemical shrinkage [57, 65, 75, 79], and lower CO_2 emission during production [74]. However, current shortcomings limit the use of geopolymer for well construction. These include problems related to controlling the pumpability of geopolymer slurry at elevated temperature for an acceptable time [65], and lower tensile strength compared to Portland cement. Moreover, geopolymer technology has yet to be tested in the field and is not qualified for use in the field.

The application of nanotechnology in the oil and gas industry is under research and development phases. Research results indicated the potential application of nanotechnology in different fields of the oil and gas industry [80]. Intensive research at the laboratory scale is required before application in the field scale. The application of NPs in the oil and gas industry is focused on application in drilling fluids and oil well cement [81]. This indicates significant potential for using the NPs in these areas and should be explored further to

fill the gaps and find optimum solutions for the existing problems. Nanotechnology is the science that addresses the process that occurs at molecular and atomic levels. It concerns the design, synthesis, and characterization of nanostructures by regulating the size and shape at the nanoscale. NPs can be defined in terms of diameter as the particles that have at least one dimension in the range from 1 to 100 nanometres [82]. NPs have gained immense attention from researchers in recent years due to their size-dependent properties and high surface area to volume ratio which finds applications in different fields like catalysis, oil & gas industry, drug delivery, imaging and so on. Magnetic, thermal, and electrical properties of these NPs also vary from the bulk properties due to the transition to the nano regime [83–85].

1.4 Scope and Objective

Although extensive research is done on applying NPs in drilling fluids and oil well cement, more studies are needed that test different NPs (concerning sizes, shapes, surface charges, and functionalities) in similar drilling fluids formulations. In addition, most of the research in the literature is focused on the addition of NPs in bentonite-based drilling fluids. This work also studied the impact of NPs on the KCl-based drilling fluids. Further studies on the application of NPs in oil-based drilling fluid do not elaborate on the nature of tested NPs. Moreover, testing barrier materials with NPs using relevant testing conditions and characterization techniques also needs further work. In addition, testing of NPs in alternative materials such as geopolymer needs further investigation. Also, most of the existing research work reported the addition of higher concentrations of NPs in the oil well drilling fluids and cement, while in this work, a very low amount of NPs was added. Adding a low concentration of NPs is beneficial because of the cost and handling of NPs on a larger scale.

The scope and objective of this thesis work is an experimental investigation of the impact of the commercial and in-house synthesized NPs in oil well fluid materials. The objectives of this work are summarized as follows,

- To investigate the effect of in-house prepared and commercial NPs on the properties such as viscous, filtration, and mechanical friction of conventional bentonite and KCl-based drilling fluids formulated in the laboratory. In addition, the microstructure analysis of filter cake is studied (**Paper I, Paper IV**).
- To investigate the impact of hydrophobic iron oxide nanoparticles (IONPs) on the viscous, fluid loss, barite sagging, thermal stability, and mechanical friction properties of conventional oil-based drilling fluids (**Paper II**).
- To investigate the impact of commercial NPs on the fluid state properties such as viscous, fluid loss, and pumpability of G-class cement and geopolymer. Moreover, the potential of NPs to improve the mechanical and elastic properties of barrier materials is investigated. Finally, the influence of NPs on the mineralogy and microstructure of cement and geopolymer is investigated (**Paper III**).
- This work comprehensively investigates different NPs with respect to size, shape, surface charge, and functionality. This work provides the platform for using a small concentration of NPs in drilling fluids, oil well cement, and emerging barrier material such as geopolymer.

The research questions addressed are,

- Can the NPs (with different sizes, shapes, surface charges, and functionalities) alter the rheological parameters of drilling fluids?
- Can NPs reduce the mechanical friction of conventional water-based drilling fluid?
- Can NPs reduce the fluid loss of conventional water-based drilling fluid?
- Can NPs alter the filter cake microstructure produced after the fluid loss test?
- To assess how changing the nature of NPs will impact the

performance of oil-based drilling fluids?

- Can hydrophobic NPs provide more stability to oil-based drilling fluid at high temperature?
- Can NPs significantly reduce mechanical friction and fluid loss of oil-based drilling fluids?
- How can NPs impact the rheological parameters of cement and geopolymer?
- How can NPs impact the pumpability of cement and geopolymer slurries?
- Are NPs improving the strength of cement and geopolymer?
- How can NPs impact the microstructure and mineralogy of cement and geopolymer?

1.5 Contribution of the Dissertation

The PhD thesis contributed to the improvement of oil well drilling fluids and cement materials. The results from this work can be used to improve the formulation of drilling fluids and cement slurries for practical field applications. Moreover, the performance of alternative barrier materials, such as geopolymer, can be improved with the NPs. The results from this work improve the existing knowledge in applying NPs in drilling fluids and oil well cement.

1.6 Thesis Outline

The thesis is divided into eight chapters,

Chapter 2 presents an extensive literature review on the application of NPs in drilling fluids, cement, and geopolymer.

Chapter 3 looks into the theory of NPs synthesis and methods for iron oxide NPs (IONPs) synthesis. Also, it provides a brief overview of silica (SiO_2) NPs, Aluminium oxide (Al_2O_3) carbon nanotubes (CNTs), and surface modification of NPs.

Chapter 4 covers the description of the synthesis procedure of NPs and surface modification of NPs. It presents the in-house made and commercial NPs used in the thesis. Also, the chapter provides details of drilling fluids, cement, and geopolymer formulation. In addition, it discusses the characterization techniques used in this study. In the end, results for in-house produced and commercial NPs are discussed.

Chapter 5 discussed the main results of the application of NPs in water-based drilling fluids.

Chapter 6 covers the application of IONPs in oil-based drilling fluids.

Chapter 7 presents the findings from the study done on the application of multi-walled carbon nanotubes (MWCNTs) and Aluminium oxide (Al_2O_3) NPs in cement and geopolymer. The last chapter lists the main conclusions from this work.

Published articles (**Paper I**, **Paper II**, **Paper III**, and **Paper IV**) are the basis of this thesis's main body and are attached at the end.

2 Literature Review

This chapter presents the literature review on the application of NPs in drilling fluids, cement, and geopolymer.

2.1 Application of NPs in Water-Based Drilling Fluids

Extensive research has been done on applying NPs in water-based drilling fluids. Few studies report reviews on the application of NPs in drilling fluids [86–88]. Researchers reported the ability of NPs to influence the rheological parameters at low pressure/low temperature (LPLT) and HPHT of drilling fluids [89–94], minimize friction [93, 95–97], lower the fluid loss & thickness of cake formed after fluid loss [89, 96, 98, 99], improvement in heat transfer & thermal conductivities [99–101], prevent shale swelling and strengthen the wellbore [102–105]. Various NPs have been tested in water-based drilling fluids; however, this work will focus on the application of IONPs, SiO_2 NPs, and MWCNTs in water-based drilling fluids.

IONPs find extensive application in various fields due to their biocompatibility, low toxicity, and ease of synthesis [106, 107]. In the oil and gas industry IONPs find application due to their ability to improve the performance of the drilling fluids and oil well cement. The magnetic properties of these NPs provide additional advantages of their separation from drilling fluids. The possibility of separating NPs from drilling fluids to reuse them can be significant concerning the economy as well as the safety and environmental benefits of drilling operations. IONPs have been added to water-based drilling fluids as a multifunctional additive to improve performance. For instance, IONPs improved the gel-forming ability of clay particles as they increased the viscosity of bentonite-based fluids. Furthermore, NPs lower fluid loss at LPLT conditions, where the low concentration of NPs in the system performs better than the high concentration [108]. The ability of IONPs to increase the shear stress values of drilling fluids is reported by *Barry et al. (2015)* [109]. Moreover, a

lower concentration of 0.5wt.% in the drilling fluids reduces the fluid loss by 27% and 23.4% for NPs with the size of 3nm and 30nm NPs, respectively. *Vryzas et al. (2016)* [110, 111] research the possibility of improvement in filtration and rheological parameters of Na-bentonite drilling fluids with novel magnetite NPs. The results indicate that NPs can increase yield stress and apparent viscosity of fluids. Furthermore, 0.5 wt.% NPs at HPHT provide a 40% reduction in fluid loss. Moreover, studies done by *Mahmoud et al. (2018)* [112, 113] show that IONPs enhance the gel formation and yield strength of drilling fluids. Further, NPs produced filter cake with better packing characteristics, reducing fluid loss. Including IONPs in drilling fluids in the presence and absence of salt improves the filtration and rheological characteristics. However, better performance was shown by NPs in the absence of salt [114]. Drilling fluids having commercial IONPs and SiO_2 NPs were investigated by *Mahmoud et al. (2016, 2017)* [22, 87] to control formation damage at HPHT. Different concentrations of NPs were tested in this study with a 7 wt.% suspension of Ca-bentonite as a base fluid. Findings from this work illustrate that adding IONPs to the drilling fluids impacted yield point and plastic viscosity. On the other hand, the addition of silica NPs reduces the yield point at elevated temperatures. Furthermore, the aging test at 177 °C and 16 hrs shows that SiO_2 NPs have better rheological stability than IONPs. Filtration experiments at HPHT, i.e., 300 psi and 121 °C, confirm that NPs contributed to the 42.7% reduction in the filtrate volume. Additionally, filter cake thickness is increased by 17.32% compared to the base fluid. The addition of 0.5 wt.% NPs to drilling fluids provide the best performance.

SiO_2 NPs find application in the oil and gas industry, such as enhanced oil recovery, drilling fluids, and oil well cement, due to their unique properties such as biocompatibility, ease of surface modification, and large surface area [115, 116]. Numerous researchers have tested SiO_2 NPs as an additive in drilling fluids. SiO_2 NPs can alter drilling fluid's rheological, lubrication, and filtration parameters [7]. In addition, SiO_2 NPs are used to prevent water intrusion into formation by several studies as NPs physically block the pore entry [117–121]. *Riley et al. (2012a)* [122] and *Cai et al. (2012)*

[118] demonstrate that SiO_2 NPs in drilling fluids can modify the rheological parameters of water-based drilling fluids at 80 °C. The addition of SiO_2 NPs reduces the yield point and increases the plastic viscosity due to the increase in solid contents of drilling fluids. While studies show that 0.5 wt.% SiO_2 NPs increase the yield point and plastic viscosity under low pressure and temperature conditions [91, 123]. Another work shows the ability of SiO_2 NPs to reduce the plastic viscosity of water-based drilling fluids [105]. Studies show contradictory results for silica NPs when it comes to reduction in fluid loss. *Novara et al. (2021)* [124] show that SiO_2 NPs in the fresh water-based drilling fluids at 0.05wt.% and 0.01wt.% concentration decrease the fluid loss by 8.2% and 6.9%, respectively. Moreover, in case of salt water, 0.05wt.% NPs provide 11.2%, and 0.01wt.% show a 12.5% decrease in fluid loss. However, *Vryzas et al. (2015)* [125] shows an increase in fluid loss values for 0.5-1wt.% SiO_2 NPs, while *Cheraghian et al. (2018)* [126] show that 0.01g SiO_2 NPs in drilling fluids decrease the fluid loss. Another investigation by *Ragab and Noah (2014)* [127] demonstrates that 20-30wt.% SiO_2 NPs reduce fluid loss by 30% compared to the base fluid. Rheological properties and fluid loss of the drilling fluids containing conventional drilling fluids like bentonite, polymer, and KCl were enhanced by adding SiO_2 NPs. This nano-based formulation also contributed towards the formation of well-textured and thin mud cake. Cost analysis of this system proved the economic benefit of the nano-based drilling fluids. *Salih et al. (2016)*[128] identified that the optimum concentration for SiO_2 NPs should lie between 0.1-0.3wt.% to get better performance and drilling fluids properties. Moreover, these findings hinted at the effectiveness of SiO_2 NPs -based drilling fluids to minimize drilling & production issues. *Javeri et al. (2011)* [129] pointed out the effectiveness of SiO_2 NPs in controlling the formation damage by reducing mud cake thickness up to 34%. An investigation by *Kang et al. (2016)* [102] shows that SiO_2 NPs increase the plastic viscosity and yield point but reduce the API fluid loss. *Medhi et al. (2020)* [130] show the ability of silica NPs to reduce the fluid loss of drilling fluids by 31%. Moreover, studies also show the ability of silica NPs to reduce the coefficient of friction. For instance, *Mohamed et al. (2020)*

[131] added SiO_2 NPs in water-based drilling fluids and achieved a 25% reduction in friction.

Investigations done on the application of MWCNTs in drilling fluids show that nanotubes can modify the rheological parameters [132–134], provide stability at HPHT conditions [135–139], impact shale-related parameters of drilling fluids [26, 140–142]. *Ismail et al. (2017)* [136] show the impact of MWCNT on the properties of synthetic drilling fluids. The nanotubes increase gel strength, yield point, and plastic viscosity of drilling fluids. Also, nanotubes showed a slight reduction in fluid loss at high temperature. Furthermore, *Passade-Boupat et al. (2013)* [143] reported the high-temperature stability of drilling fluids with CNTs. Work done by *Abbas et al. (2022)* [144] shows the ability of MWCNTs to improve the yield point, plastic viscosity, and gel strength of water-based drilling fluids at 25–150 °C due to the high surface area to volume ratio of nanotubes. *Sedaghatzadeh et al. (2012)* [145] shows that MWCNTs improve the hole-cleaning capacity of water-based drilling fluids by enhancing the plastic viscosity and yield point. Also, nanotube forms uniform mud cake and decrease spurt loss. Furthermore, *Sedaghatzadeh et al. (2016)* and *Fazelabdolabadi et al. (2015)* [100, 146] show that carbon nanotubes improve the quality of cake formed after fluid loss test and rheological parameters respectively of drilling fluids. *Amanullah and Ziad Al-Abdullatif (2014)* [147] and *Amanullah and Al-Tahini (2009)* [82] reported that MWCNTs could promote the gelling capacity and increase the water-based drilling fluid's viscosity. Besides, nanotubes also produce thin mud cake by reducing fluid loss. *Özkan. (2018)* [148] added 0.1wt.% nanotubes in water-based drilling fluids and improved the plastic & apparent viscosity and yield point. Also, nanotubes in drilling fluids reduce fluid loss by 7% compared to the base fluid. A combination of MWCNTs and SiO_2 NPs was used as an additive for drilling fluids by *Ismail et al. (2016)* [149]. A comparative study of the additives with the base fluid shows increased rheological properties like plastic viscosity and yield point of drilling fluids. The best results in fluid loss reduction were achieved by the low concentration of NPs combination (SiO_2 +MWCNTs), which is 0.00285wt.%. Furthermore, MWCNTs and SiO_2 NPs reduce the coefficient of friction by 44%

and 38%, respectively. Another investigation by *Ismail et al. (2018)* [150] shows that adding graphene and MWCNTs in water-based drilling fluids improves the rheological parameters, reduces fluid loss, and prevents shale swelling. In addition, MWCNTs improve the lubricating properties of drilling fluids and demonstrate a 38-59% decrease in friction values [150]. The capability of MWCNTs to alter the yield stress, viscosity, and other rheological parameters is also reported by other studies [151–153]. Moreover, *Samsuri, A, & Hamzah, A (2011)* [152] shows that MWCNTs form a thin, tight mud cake that contributes to low fluid loss values. *Kazemi-Beydokhti et al. (2018)* [132] show that a high concentration of nanotubes, i.e., 1.1wt.% in the drilling fluids, increases the fluid loss as the nanotube could not plug the pores in the cake structure and just deposited on the cake. The electrostatic interaction of the nanotube with clay increases the cohesive force and viscosity of the system. Studies show the ability of MWCNTs to reduce the coefficient of friction. There is a reduction of friction by 30% and 50% for 0.02wt.% and 0.38wt.% MWCNTs, respectively, in xanthan gum (XG)/KCl water-based drilling fluids [154].

Since the surface charge directly impacts the colloidal stability of NPs, the surface energy of NPs dictates the dissolution, aggregation, and bioaccumulation [155]. The ability of NPs to provide more reactive sites is due to their high surface area-to-volume ratio. This provides NPs ample opportunity to interact with various polymers and produce nanocomposites. Application of nanocomposites based on polymers in drilling fluids instils high thermal stability at HPHT conditions [14, 156]. *Jia et al. (2022)* [157] studied the impact of silica-based composite on the rheological parameters of drilling fluids and reported a reduction in plastic viscosity and an increase in yield point. Moreover, silica-based nanocomposite reduces fluid loss by 22% and improves viscosity, as indicated by *Oseh et al. (2019)* [158]. *Mao et al. (2015)* [14] show that the addition of silica-based nanocomposite to drilling fluids provides better filtration, pore-plugging capability, rheology, and lubricity. In another study, *Mao et al. (2015)* [159] produced a composite that is based on the hydrophobic polymer and SiO_2 NPs. This composite having core-shell construction is

fabricated by sol-gel and inverse micro-emulsion polymerizations. Findings from this study depict that this nanocomposite with 0.5 wt.% concentration when added to water-based drilling fluids, reduces the fluid losses by 69% at HPHT conditions. A fluid system based on nanocomposite can provide borehole stability and reservoir protection, as pointed out by the authors. *Sun et al. (2020)* [160] study the influence of surface-modified SiO_2 NPs on water-based drilling fluids. The polymer presence on the surface of NPs reduces the fluid loss by 97.01% due to polymer adsorption on the clay surface and network structure formation. This structure provides efficient plugging of pores in the filter cake. Furthermore, *Bia et al. (2020)* [161] and [162] investigate SiO_2 -based composite's performance on water-based drilling fluids. The interaction of sulfonic acid groups on SiO_2 NPs and edges of the clay minimizes the water passage and stabilizes the wellbore, and reduces the fluid loss. *Heydarzadeh Darzi et al. (2022)* [163] show that functional groups on MWCNTs promote their bonding with the bentonite particles as nanotubes improve the yield point and plastic viscosity values. While nanotubes do not impact fluid loss values, adding MWCNTs functionalized with carboxyl groups to 4% bentonite-based drilling fluids reduces the settling of barite at high temperatures and salt concentrations. Also, it decreases fluid loss by 30.2% [164]. Including MWCNTs with polyethylene glycol in water-based drilling fluids reduces the fluid loss and permeability of filter cake. Furthermore, yield stress, gel strength, and viscosity of drilling fluids increased with the addition of nanotubes [133]. Another study shows the impact of MWCNTs on the properties of water-based drilling fluids. The NPs provide additional sites for bonding with functional groups and improving plastic viscosity. Moreover, the electrostatic forces between nanotubes and drilling fluids additives increase the gel strength and yield point. The ability of the nanotube to minimize the permeability of filter cake reduces the fluid loss at high temperatures owing to the effective dispersion of MWCNTs in drilling fluids [165]. *Ma et al. (2020)* [137] tested functionalized MWCNTs to assess their thermal stability and salt tolerance. The higher stability and zeta potential of nanotubes kept them stable in a high salt solution. Electrostatic and steric repulsion due to the negative charge

on nanotubes promotes their stability at high temperatures in salt-based systems. *Abduo et al. (2016)* [166] introduced hydrophilic groups on the surface of MWCNTs and tested them in water and oil-based drilling fluids. The functionalized nanotubes improve the thermal stability of fluids up to 260 °C. One study shows increased viscosity of water-based drilling fluids by adding MWCNTs. However, combining polyethylene glycol (PEG) with MWCNTs reduces the plastic viscosity and yield point. This shows the presence of polymer with NPs can alter the viscosity of drilling fluids [167, 168]. *Kazemi-Beydokhti and Hajiabadi (2018)* [133] added MWCNTs functionalized with carboxyl groups and polyethylene glycol to drilling fluids to improve the distribution and stability of nanotubes in the fluid. Results show that 0.06wt.% nanotubes decrease the fluid loss and permeability of mud cake of drilling fluids. There was increase in gel strength, plastic viscosity, and yield stress with the addition of nanotubes in drilling fluids due to hydrogen bond formation between PEG and clay particles.

2.2 Application of NPs in Oil-Based Drilling Fluids

Studies have shown that small-sized materials can contribute to controlling gas hydrate formation [169], barite sag [36], and stabilizing the shale-based formations as well as improving wellbore stability [26, 102, 170–172]. The research is done to highlight the impact of NPs on oil-based drilling fluids. For example, *Agarwal et al. (2011)* [36] investigated the impact of SiO_2 and clay NPs on invert emulsion drilling fluids. This work shows the potential of clay NPs and a hybrid of clay and silica NPs in altering the viscosity of the invert emulsion drilling muds. Moreover, the work done by *Anoop et al. (2014)* [173] showed that the addition of 2.0 vol% of 20nm SiO_2 NPs to oil-based drilling fluids increased the viscosity at ambient conditions. Also, NPs kept the rheological parameters of the drilling fluids stable under HPHT conditions. *Nasser et al. (2016)* [151] reported an increase in oil-based fluid viscosity with graphite NPs under LPLT conditions. The ability of NPs to keep the rheological parameters stable and to

control the barite settling of drilling fluids at HPHT is also shown by *Wagle et al. (2015)* [174]. NPs also control the fluid loss of oil-based drilling fluids. Adding MWCNTs and graphene NPs to oil-based fluid reduces the HPHT fluid loss [175]. Furthermore, *Zang et al. (2015)* [171] investigated the ability of NPs to produce thin filter cake with low fluid loss. The study reported improved performance by adding 2 wt.% NPs in drilling fluids.

The effect of IONPs has been studied in oil-based drilling fluids. For instance, work performed by *Contreras et al. (2014, 2016)* [31, 176] confirms the potential of iron hydroxide NPs in improving the filtration properties of the drilling fluids. In these investigations, calcium and iron NPs with various concentrations and suitable lost circulation material (LCM) were tested. The study concluded that at LPLT and HPHT conditions, the performance of iron-based fluids in reducing the filtrate volume was better than the calcium NPs-based fluids. Iron oxide NPs can provide wellbore strengthening at HPHT conditions. The studies done by *Contreras et al. (2014, 2016)* also indicate the importance of drilling fluids filtration properties to attain wellbore strengthening at HPHT conditions [26, 172, 176]. Results from work done by *Zakaria et al. (2012)* [177] showed that iron-based NPs in drilling fluids reduce the filtrate volume by 70% under LPLT conditions.

2.3 Application of NPs in Oil Well Cement

NPs, as an additive in the cement slurry, can fine-tune the properties of cement. The exceptional properties of NPs grab the attention of the cement industry. A variety of NPs such as SiO_2 , IONPs, copper oxide, titanium dioxide, Al_2O_3 , and CNTs are incorporated into the cement slurry to alter the properties such as tensile & compressive strength [178], thickening time of slurry [179], fluid loss, viscosity, [178], flexural strength [180, 181], and permeability [182]. Moreover, NPs have shown an impact on the durability, control shrinkage, and corrosion resistance of cement [183]. NPs have been added to the oil well cement by many researchers to influence the properties of cement [48, 179, 183–187]. NPs facilitate the construction of a crystalline

structure that imparts flexibility and controls the micro-cracking in the cement structure [188]. The high surface area of NPs in the cement promotes the formation of C-S-H gel by providing a large surface area for nucleation reaction. The additional C-S-H gel improves the porosity and permeability of cement. Ample C-S-H gel in a cement matrix instead of $Ca(OH)_2$ crystals provides a denser structure [189]. Several studies show the impact of SiO_2 NPs on the properties of cement [179, 190–195]. A small amount of SiO_2 NPs in the cement improves the porosity, permeability, setting time, rheological, and mechanical properties. Moreover, silica NPs also improve the fluid loss from the cement slurry. Adding up to 1% silica NPs to the cement improves the yield stress from 22.6 Pa to 36.5 Pa [196]. Clay NPs in the cement slurry modify the temperature resistance and rheology. *Murtaza et al. (2019)* [197] show that the plastic viscosity of cement slurry increases by 73% with the clay NPs, while the yield point is reduced by adding NPs. Moreover, 1% inclusion of clay NPs in cement improves the compressive strength by 15% compared to 2% and 3% inclusion which only provide 5% and 11% increments, respectively. Another study shows the improvement in permeability and porosity of cement with the addition of clay NPs [198]. In addition, clay NPs also improve the compressive and tensile strength of cement [199]. *Jafariesfad et al. (2016)* [200] reported the impact of magnesium oxide (MgO) NPs on the short and long-term bulk shrinkage of cement. The study shows that MgO NPs can control the bulk shrinkage of cement. Moreover, *Li et al. (2021)* [201] added zinc oxide NPs to the cement slurry and delayed the setting time of the slurry as well as controlled the shrinkage of cement.

Many studies reported the application of Al_2O_3 NPs in cement [202–204] [205–208]. Al_2O_3 depicts high strength, chemical stability, and corrosion resistance, enabling its use as a building and refractory material. The application of Al_2O_3 NPs in construction provided contradictory observations. Some studies conclude that the addition of NPs has a significant effect on strength improvement [205, 208–210], while other stated no or slight effect of NPs on strength [203, 207, 211]. Moreover, *Vipulanandan et al. (2018)* [212] show that the reaction of alumina NPs with hydroxide in the slurry significantly enhances the

compressive strength. Also, *Deshpande and Patil (2017)* [213] report the significant improvement in the compressive strength of cement with the addition of alumina NPs. It was suggested that the lack of optimum concentration and uniform dispersion of NPs in the cement contributed to this contradicted behaviour [202, 207, 209, 214].

The presence of Al_2O_3 NPs in the cement reduces the portlandite content and forms mono-carbonate and mono-sulphate. The additional AFm phases increased in strength at later stages by decreasing the porosity and production of refined pore structure. The Al_2O_3 NPs slow dissolution in the highly alkaline cement slurry and provide strength improvement at later stages [215]. Al_2O_3 NPs in the cement increase compressive strength due to the formation of excessive C-S-H gel at the initial phase of the hydration reaction that also produces dense cement microstructure [216]. *Muzenski et al. (2019)* show a 30% increase in the compressive strength of cement with a 0.25% addition of Al_2O_3 nanofibers in cement-based material [217]. *Mohseni et al. (2015)* [218] studies the impact of Al_2O_3 NPs on the properties of cement. Adding Al_2O_3 NPs reduces the fluid loss of class G cement at high temperature. The strength retrogression of cement at high temperature is reduced by adding silica and alumina NPs, as reported by *Senff et al. (2010)* [219]. Therefore, NPs show a substantial increase in the strength of cement [219]. Alumina nanofiber was also tested in cement to enhance its properties. Alumina nanofibers in cement allow effective bond formation with cement hydrates. This facilitates the homogeneous spacing at the nanoscale that controls the crack growth by physically interrupting the propagation [220]. The alumina nanofibers act as a bridge embedded in the structure of C-S-H gel and provide reinforcement against stresses [217]. The nanofibers improve the compressive strength and tensile strength of class H cement. The effective dispersion of admixture in cement is essential to improve functional and structural properties. The efficient dispersion of nanofiber is significant, as ineffective dispersion leads to agglomeration. A high concentration of alumina nanofibers negatively impacts cement's compressive strength, micropores, and permeability. The possible reason is that the coagulation and flocculation of NPs impact C-S-H

formation and strength of cement [221]. It is reported in the study that the optimum concentration of ANF in cement is 0.1% BWOC [222]. The incorporation of Alumina nanofibers in cement not only improves durability but also enhances elasticity.

NPs based on carbon contributed to the improvement in cement properties owing to their unique mechanical, electrical, thermal, and chemical properties [223–225]. Plenty of research is done where nanofibers and nanotubes are added to the cement composites [226–229]. The interest in nanotubes and nanofibers is due to their outstanding Young’s modulus and tensile strength [230]. CNTs provide better strength and create a denser microstructure by acting as a filler in the cement. Moreover, *El-Gamal et al. (2017)* [223] reported the improvement of microstructure and mechanical properties of cement sheath by nanotubes. *Santra et al. (2012)* [178] suggest that to get effective reinforcement of CNTs in the cement slurry, several factors are essential such as the size and aspect ratio of CNTs, the functionality of CNTs, and the dispersion of CNTs in cement. A study by *Liu et al. (2019)* [231] states that early-stage cement strength fracture toughness is affected by MWCNTs in the cement matrix. Moreover, nanotubes, due to their filling mechanism, reduce the pore size and enhance the hydration rate. This results in better control of crack growth occurring at the nanoscale and improved mechanical strength [232]. Studies have suggested that the concentration of nanotubes in the cement slurry will dictate its performance. For example, one of the studies suggested that the optimum concentration should be 0.25% by weight of cement (BWOC) [233], while another indicates that 0.1% BWOC provides better performance [234].

Studies have shown an increase in the compressive strength of cement (construction) with the addition of 0.045 to 0.15% carbon nanotubes [235, 236]. Moreover, the study shows the ability of 0.1% carbon nanofibers to increase the compressive strength and crystallinity of concrete specimens. Moreover, carbon fibres also reduce the thermal deformation of concrete [237]. *Li et al. (2005, 2007)* [238, 239] showed the improvement in flexural and compressive strength of

cement with the addition of functionalized and not functionalized MWCNTs. Various studies show that low concentration (0.02-0.1wt.%) of MWCNTs in the cement improves the flexural strength and Young's modulus by 8-40% and 15-55%, respectively [240–242]. *Lu et al. (2019)* [232] shows that 0.05wt.% MWCNT in oil well cement enhances the compressive and flexural strength after 28 days by 37.50% and 45.79%. Also, nanotubes reduce the modulus of elasticity by 19.07%. The presence of MWCNT in cement improves the hydration process and provides strength and toughness by crack bridging and network filling. The work done by *Paula et al. (2014)* [185] shows that CNTs do not have a significant impact on the rheological properties of oil well cement owing to the presence of dispersant in the slurry. The CNTs in this work were directly grown on the cement using chemical vapor deposition. However, there was only a slight improvement in tensile strength, and no impact on the compressive strength of cement was observed in this work. *Khan et al. (2016)* [186] shows the impact of 0.1, 0.25, and 0.5% functionalize MWCNTs on the properties of class G cement. The results show an improvement in the compressive strength of cement with the addition of 0.5% nanotubes. While Ultrasonic Cement Analyser (UCA) results show the highest strength increase in the case of 0.1% nanotube, microstructure analysis shows the ability of nanotubes to act as a filler in the cement structure and decreases the porosity of the structure. *Santra et al. (2012)* [178] demonstrate the impact of silica, alumina, and CNTs on the properties of oil well cement. The cement slurries with CNTs show acceptable flowability and pumpability. However, the nanotubes without surfactant did not increase the mechanical properties of cement. While the addition of surfactant to disperse nanotubes improves both tensile and compressive strengths. Furthermore, silica NPs accelerate strength development. In contrast, alumina NPs slightly impact strength development due to the adsorption of water molecules on NPs that lowers the amount of water in the slurry and increases the portlandite precipitation. The addition of carbon nanotubes in the oil well cement under HPHT improves the compressive strength and reduces the thickening time and fluid loss [243]. The impact of carbon nanotubes on the properties of oil well

cement was studied by *Ghajari et al. (2014)* [244]. The study shows that 1wt.% of CNTs in the cement matrix increases the yield point and plastic viscosity. In addition, nanotubes reduced fluid loss by 70% and increased compressive strength by 73.8%. In comparison, a high level of CNTs in the cement matrix decreases compressive strength due to improper dispersion of CNTs in cement [244]. Application of 0.1 wt.% MWCNT-OH in the high-performance concrete resulted in an increase in flexural and compressive strength as well as impact resistance [245]. However, studies also show decreased flexural and compressive strength with functionalized MWCNT [246, 247]. There is a possibility of interaction between OH groups on the nanotube surface and the C-S-H cement product [248]. The functional groups present on the surface of nanotubes accelerate cement hydration. There is a considerable increase in the compressive strength of cement composites with the addition of a small amount of functionalized nanotubes [248]. Performance CNTs in cement is affected by poor dispersion of nanotubes in the cement matrix [249–251]. The presence of functional groups on the surface of nanotubes also facilitates their better dispersion in cement [251, 252]. However, some studies also pointed out the incompatibility of surfactant used to disperse nanotubes with the cementitious material during the hydration stage [253]. Also, some studies show disagreement over the strength improvement with CNTs [254, 255].

Since the agglomeration of NPs contributed to weaker zones in the cement, it is essential to ensure the dispersion of NPs in a suitable solvent to avoid the sticking of NPs [256]. Uniform dispersion of NPs in the cement slurry is crucial in achieving better performance. As the agglomeration of NPs contributed to the decrease in compressive strength due to the production of voids in the cement matrix [257, 258], surfactants are used to create stable dispersions of nanotubes. Studies have reported the addition of surfactants such as sodium dodecyl sulfate (SDS) and triton x-100 to disperse the nanotubes [259]. The surfactant creates electrostatic repulsion and weakens the van der Waals forces between nanotubes to form stable dispersions in water [232]. However, the hydration reaction of cement can be negatively impacted due to the presence of surfactant. Surfactants

in the cement paste can delay or cease the hydration process and ultimately impact the hardening of cement [260]. Studies observe that surfactant in the cement can produce air bubbles in the mixture, reducing the cement's compressive strength [261, 262]. Furthermore, lower concentration of NPs has a better performance compared to the use of large amounts, which ultimately may lead to non-reacted NPs in cement-based materials [192, 263–266]. Various studies stated that small amounts of carbon nanotubes in cement, i.e., 0.02-0.0025% contributed to an increase in the mechanical strength of cement-based materials [230, 262, 267]. At the same time, high silica concentration in class G cement decreases the compressive strength of cement [268]. Moreover, a high amount of MWCNTs in cement paste negatively impacts cement properties [262].

2.4 Application of NPs in Geopolymer

NPs also show the ability to influence various properties of geopolymer. Investigations are done by many researchers to study the impact of NPs on the workability of geopolymer [269–272], microstructure [270], [273], density and porosity [273–275], and chemical shrinkage [276]. Additionally, studies show the impact of NPs on the mechanical properties of geopolymers [270, 273, 277]. However, few studies address the effect of NPs on the properties of geopolymers for oil well cementing [278, 279]. Al_2O_3 plays a crucial role in geopolymer technology. The addition of Al_2O_3 decreases the Si/Al ratio and improves the flexibility of geopolymer with a higher degree of resistivity to corrosive chemicals [280]. In addition, Al_2O_3 can produce lightweight and sound-isolating geopolymer material [281, 282]. Furthermore, the hydroxyl group plays a role in the geopolymerization reaction. Therefore, the use of NPs functionalized with OH- groups involves the NPs in geopolymer reactions to further enhance the properties of geopolymers. Therefore, in this work, MWCNTs functionalized with a hydroxyl group and Al_2O_3 NPs have been added to rock-based geopolymer to improve its performance. Research work has been done on the impact of Al_2O_3 NPs and MWCNTs on different geopolymer systems. For instance, *Guo et*

al. (2014) [263] have added γ - Al_2O_3 to fly-ash based geopolymer. The results from Fourier-transform infrared spectroscopy (FT-IR) and scanning Electron Microscopy (SEM) analysis show that Al_2O_3 NPs produced a material structure with a narrow pore distribution as NPs modified the pore structure of the geopolymer. Moreover, 2.0 wt.% of Al_2O_3 NPs in fly ash-based geopolymer improved the compressive strength from 50 MPa to 56.8 MPa for neat geopolymer after 28 days. Another study done by *Chindaprasirt et al.* (2012) [283] depicts that adding Al_2O_3 NPs to high calcium fly-ash based geopolymer lowers the setting time of the slurry. *Phoo-Ngernkham et al.* (2014) [270] showed that high calcium fly ash geopolymer based on Al_2O_3 NPs produces a denser structure as NPs improve the geopolymer microstructure. Additionally, improved elastic modulus, compressive, and flexural strength of the geopolymer paste with NPs was reported.

Owing to the exceptional mechanical properties of nanotubes, MWCNTs have also been used in geopolymers to improve mechanical properties (i.e., compressive and tensile strengths as well as Young modulus). *Saafi et al.* (2013) [284] introduced MWCNTs to a low calcium fly ash-based geopolymer. MWCNTs having a concentration of 1 wt.% by weight of the geopolymer improved flexural strength and young modulus of the geopolymer. A lower concentration of the MWCNTs in the geopolymer matrix gave better results due to sufficient dispersion of the nanotubes in the slurry, as reported by *Saafi et al.* (2013) [284]. In addition, the influence of carbon nanotubes on the modulus of elasticity and compressive strength of fly ash-based geopolymer has been reported by *Rovnaník et al.* (2016) [285]. According to *Rovnaník et al.* (2016) [285], low concentration (0.15 wt.%) of MWCNTs in the mix design provides the best result for modulus of elasticity and compressive strength of the geopolymer. Published results by *Abbasi et al.* (2016) [286] show that carbon nanotubes in metakaolin-based geopolymers improve their strength. They concluded that adding 0.5% nanotubes had increased the geopolymer's flexural and compressive strength by 28% and 32%, respectively. Moreover, SEM analysis confirmed the ability of nanotubes to bridge the microcracks in the geopolymer structure

owing to the bonding of MWCNTs with the geopolymer.

Similar to cement, the agglomeration of NPs may have a negative impact on the properties of geopolymer or other cement-based materials. Therefore, achieving sufficient dispersion of NPs in the geopolymer slurry is vital to achieving uniform distribution of NPs in the geopolymer structure. In addition, it is crucial to add a low concentration of NPs in the mix design.

3 Nanoparticles Synthesis

This chapter presents the theory of NPs synthesis and methods to synthesize IONPs, and an overview of SiO_2 NPs, Al_2O_3 NPs, and the CNTs. In the end, a background of NPs surface modification is provided.

Desired end-product and functionality dictate the synthesis approach used to fabricate NPs. There are numerous methods to fabricate NPs, and they can be broadly classified into two processes that are top-down and bottom-up [287].

As shown in Figure 3.1 (modified from [288]), large particles are crushed into small pieces through mechanical processes such as ball milling during the top-down method.

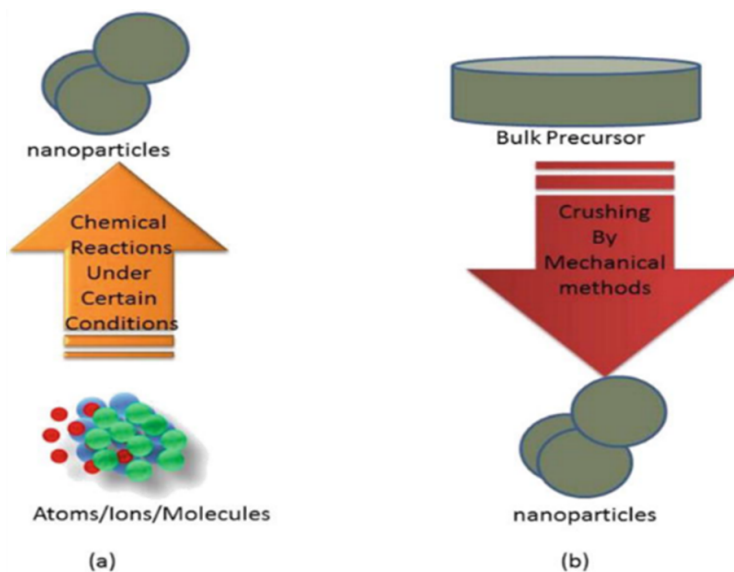


Figure 3.1: Top-down and Bottom-up approaches to synthesize NPs.

On the other hand, the bottom-up approach is the opposite of top-down. This approach synthesizes NPs from atomic and molecular levels to large particles involving chemical processes [288]. In the case

of the top-down method, there is a possibility of waste production during the fabrication process, and it is difficult to control the particle size leading to higher particle size distribution. While the bottom-up approach not only eliminates the wastage of precursor material but also provides NPs with narrow particle size distribution and gives better control over particle shape and size [287].

The bottom-up approach usually used to synthesize inorganic NPs is called crystallization. Crystallization transforms matter from a high-energy disordered state to a crystal phase with low free energy. The first crystallization step is nucleation, which represents the formation of a new phase in the bulk solution. The nucleation can be homogeneous or heterogeneous. In the case of homogeneous nucleation, the nuclei start to form in the bulk solution, while in heterogeneous nucleation, it form on a solid substrate such as impurities or foreign particles [287]. The driving force for nucleation is supersaturation, and the supersaturation can be generated in the solution by employing a process that can increase the concentration of material of interest above the solubility limit in the solution. An in-situ chemical reaction can be a way to increase the concentration of solute in the solution in a controlled manner. Metallic solids are usually produced by the process of reduction from their salts which generates supersaturated solutions. The solution is saturated once the solubility limit is passed, and this state of the system is called a metastable zone. The crystallization process can occur in a metastable zone. The rate of formation of nuclei N per unit time per unit volume can be expressed by the Arrhenius rate equation, as presented in Eq. 3.1,

$$\frac{dN}{dt} = A \exp\left(-\frac{\Delta G_{crit}}{k_B T}\right) \quad (3.1)$$

In Eq. 3.1, ΔG_{crit} is the thermodynamic parameter that defines the minimum energy barrier required to form a stable nucleus in the solution, and A represents the pre-exponential factor. When spherical particles undergo homogeneous nucleation, ΔG_{crit} can be presented as Eq. 3.2,

$$\Delta G_{crit} = \frac{16\pi\gamma^3v^2}{3(k_B T \ln S)^2} \quad (3.2)$$

In Eq. 3.2, γ represents the interfacial energy of the solid-liquid interface, while molecular volume is represented as v . Using Eq. 3.2, the final expression for nucleation rate can be generated as Eq. 3.3,

$$J = A \exp\left(-\frac{16\pi\gamma^3v^2}{3k_B^3 T^3 (\ln S)^2}\right) \quad (3.3)$$

Eq. 3.3 clearly illustrates that the parameters such as temperature, interfacial energy, and supersaturation influence the nucleation rate. The presence of surfaces such as primary particles, dislocations, and foreign particles made the overall surface energy for the formation of critical nuclei lower for the heterogeneous nucleation compared to the homogeneous nucleation. Therefore, the expression for the overall energy barrier for heterogeneous nucleation includes the factor ϕ , which accounts for the reduction in surface energy as indicated in Eq. 3.4.

$$\Delta G_{crit,heter} = \phi \Delta G_{crit,hom} \quad (3.4)$$

The factor ϕ depends on the contact angle θ , which measures the affinity between the two contacting surfaces. A strong bond between the nuclei and substrate contributes to lower values of θ , which means complete wetting [287].

As soon as stable nuclei is formed in the supersaturated solution, the nuclei growth starts with the addition of atoms, molecules, or ions on the crystal surface and the incorporation of these building units in the lattice sites. Nucleation and growth stages can be separated as a function of concentration and time, as shown in the LaMer diagram in Figure 3.2(modified from [289]).

Nucleation starts as the critical concentration is achieved. As the nuclei start to form, there is a reduction in the supersaturation,

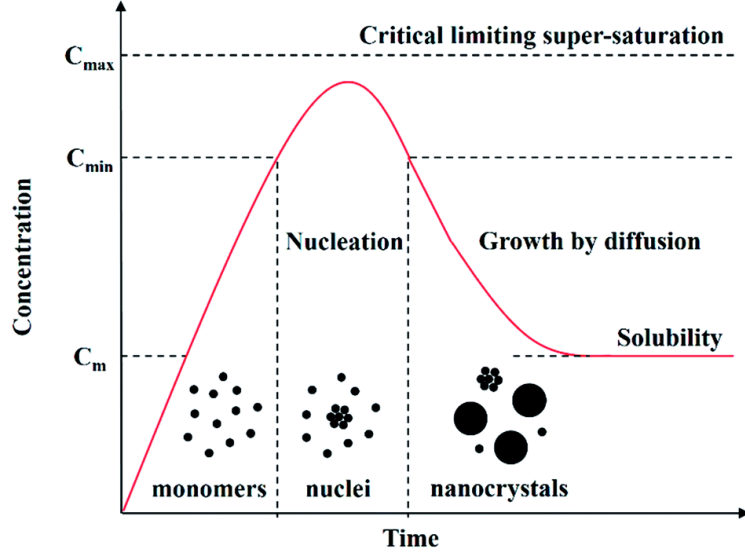


Figure 3.2: Mechanism of NPs nucleation and growth, illustrated by Lamer diagram.

as depicted in Figure 3.2. As the supersaturation is reduced to a critical value, there is no more formation of nuclei. However, there is a continuous reduction in the supersaturation as growth occurs until the solution reaches a saturation state, i.e., an equilibrium state [287]. Several theories explain the crystal growth mechanism. One of them is diffusion reaction theory which considers the involvement of two steps for crystal growth. The first step is the diffusion process, which involves transporting solute molecules from the bulk solution to the solid surface. In the second step, the arrangement of the solute molecules into a crystal lattice occurs by the first-order reaction. The growth process can be diffusion-controlled and reaction-controlled and can be represented by Eq. 3.5 and Eq. 3.6,

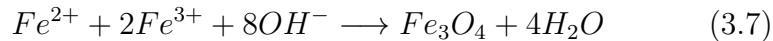
$$\frac{dm}{dt} = k_d A (C - C_i) \quad (3.5)$$

$$\frac{dm}{dt} = k_r A (C - C^*) \quad (3.6)$$

In the equations, m = mass of solid particle deposited in time t , k_d = coefficient of mass transfer based on diffusion, k_r = rate constant in case of surface reaction, A = surface area for the crystal, C_i = concentration of solute at the interface of crystal-solution C = concentration of solute in a supersaturated solution and C^* = equilibrium solubility. Crystal growth and nucleation are principal steps that influence the shape and size of the NPs [287]. As discussed in the literature study, the IONPs show the potential to improve the performance of water-based drilling fluids. Therefore, in this work, the IONPs were synthesized by two methods which will be described in the next section.

3.1 Co-Precipitation

NPs synthesis using the co-precipitation method is the most widely used route, owing to the simplicity of the experimental setup as well as the use of environmentally friendly and cost-effective precursors to produce the NPs at lab scale [290]. The process of synthesizing NPs by this method involves the use of precursors like ferric and ferrous salt in an aqueous solution. The aqueous solution with the ferrous and ferric ions is mixed with an alkaline solution at a moderate temperature to produce the NPs, as shown by the chemical reaction (Eq. 3.7) [291],



Although this method can provide a high yield of NPs and avoid using organic solvents, the mechanisms underlying the particle formation still need to be clearly understood, making it challenging to optimize the synthesis process using the co-precipitation method. The rapid particle formation during this method gives little time to characterize the initial precipitates [290]. However, some studies are available that try to study the growth kinetics by varying the pH and slowing down the reaction kinetics by employing the weak bases [292, 293]. The reaction parameters such as pH, temperature, ionic strength, and type of alkaline solution are vital as they dictate the properties like

morphology, size, and composition of the NPs. The NPs produced by this method have broad particle size distribution and are not very stable. Therefore, NPs are stabilized, and uniform particle size distribution is achieved using functionalized polymers or surfactants like polyethylene glycol, dodecylamine [294], and sodium oleate [295].

3.2 Thermal Decomposition

As mentioned above, co-precipitation is a simple process to produce hydrophilic NPs without the need to use a solvent. However, the NPs produced from this method have broad size distribution and variations in different batches with respect to size, shape, and other physio-chemical properties owing to limited control over the synthesis process. The thermal decomposition route can be employed to get better control over the shape and size of the particles and achieve uniform particle size distribution. Moreover, particles produced through this method are in the organic phase, i.e., hydrophobic, which finds application in oil-based drilling fluids. The method is based on decomposing iron precursors such as oleate and pentacarbonyl in an organic solvent at high temperature in the presence of a stabilizing agent [296, 297]. The better control over the size of particles compared to the prevalent co-precipitation method is due to the temporal separation of nucleation and growth events that facilitate narrow particle size distribution [298].

In this work, commercial NPs such as SiO_2 , Al_2O_3 , and MWCNTs were also used. The following section will provide a brief overview of these NPs.

3.3 Silica NPs

SiO_2 NPs are available in different forms, such as conventional SiO_2 NPs (non-porous), mesoporous SiO_2 NPs, and hollow or core-shell NPs. Mesoporous SiO_2 NPs are desired owing to their functionalization with various materials, tuneable pore size and volume, and high stability [115, 116]. SiO_2 NPs can be synthesized

in different sizes from 10-500nm, with physicochemical properties and shapes depending on the technique and synthesis parameters. Stober's method and microemulsion are the most common methods for synthesizing silica NPs. Stober's process involves the hydrolysis and condensation of silica precursors such as tetraethyl orthosilicate (TEOS) or sodium silicate solution in the presence of ammonium hydroxide, water, and alcohol [116]. Modifying the Stober process by adding surface-active agents like cetyltrimethyl ammonium (CTAB) and polymers can produce mesoporous SiO_2 NPs [299]. It is crucial to enhance the stability of silica NPs, and several strategies can improve the stability of SiO_2 NPs, such as electrostatic stabilization, the use of surfactants, and the functionalization of NPs. Out of these strategies, surface functionalization is a promising technique as the presence of large content of silanol groups on the surface of SiO_2 NPs facilitates the functionalization of NPs with various coupling agents like (3-mercaptopropyl) trimethoxysilane (MPTMS), 3-(aminopropyl) triethoxysilane (APTES) [300] and PEG [301]. Grafting silane on the surface of NPs provides steric stabilization and improves SiO_2 NPs stability in water [302]. Moreover, Surface modification with PEG improves the biocompatibility and colloidal stability of SiO_2 NPs [301, 302].

3.4 Aluminium Oxide NPs

Al_2O_3 NPs, also called alumina, finds application in numerous disciplines due to their superior properties such as mechanical strength, wear resistance, non-toxic, heat, and chemical stability [303–305]. Also, Al_2O_3 finds applications to produce composite materials and surface protective coatings [306]. Owing to the exceptional harness and toughness of Al_2O_3 NPs, they are added as a filler to high-performance materials to enhance their ductility, toughness, and resistance to scratch [307].

Several techniques, such as sol-gel, ball milling, laser ablation, precipitation, plasma arc, and hydrothermal, can be utilized to synthesize Al_2O_3 NPs [303, 306–308]. The arc discharge is one of the methods to synthesize Al_2O_3 NPs in this method, metal precursor

is vaporized by exposing it to the arc discharge between electrodes. Afterward, the metallic vapor is condensed by contacting with the cooling tube and form clusters. The nucleation process starts with cluster formation, followed by the growth of NPs [309, 310]. The NPs formed by this method are in the range of 20-60 nm. The small size of NPs contributes to the agglomeration of the particles due to high surface energies. The success of NPs for a particular application depends on effective dispersion in a fluid [310]. This work used stable dispersion of Al_2O_3 NPs in water to facilitate the proper mixing and reaction with cement and geopolymer materials.

3.5 Carbon Nanotubes

The discovery of carbon nanotubes is attributed to Dr. Sumo Iijima as he described in his paper *“the new type of carbon structure consisting of needle-like tubes”* where each needle consists of *“coaxial tubes of graphitic sheets, ranging in number from 2 up to about 50”* [311]. CNTs are allotropes of carbon (walls of carbon nanotubes are made of Sp^2 hybridized carbon atoms), and the two common structures of CNTs are single-wall carbon nanotubes (SWCNTs) and MWCNTs. SWCNTs are graphene sheets rolled up into a circular form. The diameter of SWCNTs is in the range of 0.4 to 4 nm. In comparison, MWCNTs are concentric tubes of graphene sheets. The number of walls or tubes for MWCNTs can be varied from 2 to less than a hundred. Moreover, MWCNTs have diameters in the range of 1nm and seldom increase above 100nm [312]. High-temperature techniques such as arc discharge and laser ablation were the early methods to produce carbon nanotubes. However, now comparatively low-temperature processes such as chemical vapor deposition have replaced these methods. Nanotubes synthesis by chemical vapor deposition is based on the decomposition of carbon-based gases in the presence of a catalyst at temperature around 700 °C to 900 °C. Gases such as methane, acetylene, and carbon monoxide are used as carbon sources. In addition, transition metals such as Fe, Co, and Ni are used as catalysts either in the form of a film or deposited NPs [312]. CNTs find application in various fields due to their exceptional

mechanical, electrical, and thermal properties. As mentioned in the introduction, various studies explored the possibility of using nanotubes to improve the performance of drilling fluids and oil well cement. This work used MWCNTs and MWCNTs functionalized with -OH and -COOH groups as additives in water-based drilling fluids, cement, and geopolymer. Surface modification of nanotubes aims to improve their stability in the solvent, especially in water, as unmodified MWNCTs can agglomerate due to Vander Waal forces. The surface-modified nanotubes can provide better dispersion and interaction with water-based fluids.

3.6 Surface Modification of NPs

As mentioned in the literature study, NPs are prone to agglomeration due to their high surface energies originating from a large surface-to-volume ratio. In order to minimize their high surface energies, NPs promote aggregate formation. IONPs especially have high chemical activity, which promotes their oxidation in the air leading to the loss of dispersibility of NPs. Therefore, surface functionalization of NPs is beneficial to improve their stability. The surface functionalization techniques can be either coating or grafting organic molecules, polymers, surfactants, and inorganic materials such as metal oxides, metal sulphides, or SiO_2 . The protecting layers or shells not only provide the required stability to the particles but also introduce the functional groups on the surface of NPs to promote further functionalization steps [313]. Surface coating or modification can be either in-situ or post-synthesis [314]. In the case of in-situ technique, functionalization is done during the synthesis process of NPs, for example, functionalization of IONPs with dextran [315]. However, the other technique (post-synthesis) involves the attachment of ligands on the surface of NPs after their production [316, 317]. There are various ligands, such as chitosan [318], polyethylene glycol, Na-citrate [319], and CTAB [320] which can be applied depending on the required functional groups and final use of particles. In the case of IONPs, coating with SiO_2 has received much interest due to the better biocompatibility, stability, and non-toxicity of SiO_2 NPs. In addition,

SiO_2 can provide better colloidal stability due to lower Vander Waals forces as compared to other metal oxides. Furthermore, SiO_2 can allow further conjugation of NPs with different functional groups. Therefore, in this work, the IONPs coated with silica (Fe-Si) were tested to take advantage of the improved properties of this core-shell nanocomposite. In addition, the surface of IONPs was coated with XG polymer to improve their physicochemical properties.

4 Materials and Methodology

This chapters cover the methodologies used for IONPs synthesis and surface modifications that were performed on IONPs and commercial SiO_2 NPs. It gives an overview of the in-house made and commercial NPs used in this work. It presents the drilling fluids, cement and geopolymer formulation. Further, the characterization techniques used in this work are elaborated. Finally, the results for in-house prepared and commercial NPs are presented.

4.1 Synthesis of Iron Oxide NPs

As described in the introduction, the co-precipitation method was used to synthesize hydrophilic IONPs [321]. First, to make 100 mL of 1M NH_4OH solution, 15.4 mL of 25% ammonia solution was added to 84.6 mL of de-ionized water. Separately, in 25 mL of distilled water, 2.0 g of $FeCl_2 \cdot 4H_2O$ and 5.4 g of $FeCl_3 \cdot 6H_2O$ were dissolved. Afterward, 10 mL of this rusty-colored solution was transferred to a burette. Then this rusty colored solution was added dropwise into 100 mL of 1 M NH_4OH solution under vigorous stirring. For stirring, a magnetic stirrer was used. A black-colored solution was formed by adding the iron solution to the ammonia solution. Afterward, with the completion of the reaction, the black-colored solution was transferred to conical centrifuge tubes. A strong magnet was placed under the conical centrifuge tubes to separate the particles magnetically, and the particles were washed several times with water. To harvest all the particles, the washing process was repeated. Almost clear fluid was obtained as NPs were drawn to a strong magnet after the first cleaning steps of particles with water. However, after several washes with de-ionized water, the separation of particles became difficult as less transparent fluid was obtained when a magnet was placed under the solution. It is crucial to stop the particles washing at this point to avoid the loss of particles. In the cases of IONPs synthesized by this method, the term Fe NPs is used throughout the results section.

The synthesis of hydrophobic IONPs is based on the thermal

decomposition of metal precursors, as explained in Chapter 3. This method was adapted from the previous work by *Bandyopadhyay et al. (2014)* [322]. To produce NPs, Iron pentacarbonyl ($Fe(CO)_5$) was used as a precursor. The required amount of Oleylamine (OAm) and Octadecene (ODE) was added to the round bottom flask and kept under an inert atmosphere with continuous stirring for 30 minutes at 120 °C. After 30 minutes, the temperature of the reaction solution was raised to 180 °C. After reaching 180 °C, a suitable amount of iron pentacarbonyl was injected into a hot reaction mixture using a syringe. The temperature was kept stable for 20 minutes to complete the reaction and formation of NPs. The solution was cooled to 20 °C afterward, and the supernatant was decanted. The IONPs were washed with the required amount of acetone and hexane to clean the particles. In the end, a magnet was used to harvest the IONPs, and the NPs were cleaned twice with acetone. After cleaning, the NPs were dispersed in a known volume of hexane for further use.

4.2 Coating of Xanthan Gum on Iron Oxide NPs and Fe-Si NPs

XG polymer was coated on the surface of IONPs by first adding 0.1 g of xanthan gum into 50 mL water to make a polymer solution. Afterward, 0.2 g of IONPs were added to this polymer solution, and the resulting mixture was left for shaking for 24 hrs. Afterward, the resulting solution was used to formulate the drilling fluids. The term Fe-XG is used for IONPs coated with XG throughout the text. In addition to Fe-XG, IONPs functionalized with silica (Fe-Si NPs) used in this work were provided by NTNU.

4.3 Silica NPs and Surface Modification

In this work, three types of SiO_2 NPs were used. SiO_2 NPs in powder form were purchased from Sigma Aldrich (Oslo, Norway). Surface modification of these SiO_2 NPs was done with silane to incorporate sodium sulphonate on the surface of NPs. NPs were functionalized

based on the method described by *Weston et al. (2015)* [323]. 5 g of SiO_2 NPs were dispersed in 200 ml toluene by probe sonication. 3 g of (3-Mercaptopropyl) trimethoxysilane 95% was added to this SiO_2 NPs dispersed in toluene. The solution was placed on stirring for 12 hrs at a temperature of 35 °C. After 12 hrs of reaction with silane, the NPs were separated from the solution by centrifugation and washed several times with the 30/70 (v/v) mixture of de-ionized water and isopropanol. After washing, NPs were dried for 24 hrs in a vacuum oven at 120 °C [323]. After that, the SiO_2 NPs having immobilized mercaptopropyl groups were oxidized using an aqueous 30% H_2O_2 solution. Here, dried NPs were added to the aqueous 30% H_2O_2 solution and the resulting solution was stirred with a magnetic stirrer for 24 hrs [324, 325]. This results in the formation of sulfonic acid groups on the surface of SiO_2 NPs. NPs were washed with water several times and dried. After every washing step particles were centrifuged. After that, the dried NPs were dispersed into 0.1 M *NaOH* solution and stirred for 24 hrs to convert the sulfonic acid moieties to sodium sulfonate. After 24 hrs, the particles were washed with de-ionized water and dried by putting them into the vacuum oven at around 35 °C for three days [325]. The third type of SiO_2 NPs was purchased from NYACOL Nano Technologies, Inc. (Ashland, MA, USA). NYACOL SiO_2 NPs were received as a 30 wt.% dispersion in de-ionized water, with proprietary coating on the surface of NPs to provide long-term stability. Term Si NPs is used for SiO_2 in powder form. The surface-modified SiO_2 NPs is called Si-C and NPs from NYACOL is called Si-N throughout the text.

4.4 MWCNTs

Three types of MWCNTs were used in this study, MWCNTs, MWCNTs functionalized with hydroxyl groups (MWCNT-OH), and MWCNTs functionalized with Carboxylic acids (MWCNT-COOH). The nanotube dispersions in anionic surfactant were purchased from US Research NPs, Inc (Houston, TX, USA). The abbreviations MW for MWCNTs, MW-OH for MWCNT-OH, and MW-COOH for MWCNT-COOH are used throughout the text.

4.5 Aluminium Oxide NPs

Al_2O_3 NPs used in this work were purchased from Alfa Aesar as a colloidal dispersion in 50% water with dispersant. NPs dispersion was used in cement and geopolymer formulation without further modification. These NPs are called AL NPs throughout the text.

4.6 Drilling fluids Formulation

This work prepared two types of drilling fluids, i.e., Bentonite and KCl-based. In order to achieve comparable viscosity and density of the fluids, the compositions for both bentonite and KCl fluids were designed based on previous work [326]. The compositions of the fluids are shown in Table 4.1 and Table 4.2.

Table 4.1: Composition of bentonite drilling fluids.(Paper I).

Material	Base Fluid	Base Fluid + NPs
Water	350 mL	350 mL
Soda ash	4.8 g	4.8 g
Xanthan gum	0.71 g	0.71 g
Bentonite	10.04 g	10.04 g
Barite	183 g	183 g
NPs in water	-	0.05, 0.1, 0.2 g

Table 4.2: Composition of KCl drilling fluids (Paper I).

Material	Base Fluid	Base Fluid + NPs
Water	350 mL	350 mL
Soda ash	0.75 g	0.75 g
Xanthan gum	1.5 g	1.5 g
KCl	24.80 g	24.80 g
Barite	175 g	175 g
Iron oxide NPs in water	-	0.05, 0.1, 0.2 g

The required concentration of NPs was added to both fluids to formulate fluids with NPs. The mixing of bentonite fluid was done by mixing soda ash, XG, and bentonite, with a Hamilton Beach mixer for 5 minutes and an additional 10 minutes mixing to dislodge any material attached to the walls of the mixing container. This was followed by mixing barite for 5 minutes and another 10 minutes to dislodge adhering materials to get the uniform mixing of components. In the end, NPs (0.0095 wt.% – 0.038 wt.%) were added to the fluid and mixed for 5 min to disperse NPs in the fluid system. To prepare Fe-XG NPs-based drilling fluids, Fe-XG was first mixed with water, and afterward, all components except barite were added and followed the same mixing procedure with 5 + 10 minutes. After adding barite, the same procedure of 5 + 10 minutes was followed. In the case of KCl-based fluids, bentonite is replaced with KCl while the mixing procedure remains the same.

An oil-based invert emulsion drilling fluid with oil to water ratio of 90/10 was mixed based on the formulation from MI-SWACO, a Schlumberger Company. Table 4.3 shows the details of additives and their percentages used to produce the drilling fluids. All the additives were mixed with the mixer for 5 minutes, excluding barite, which was mixed for 25 minutes. The uniform dispersion of NPs in the drilling fluids was attained by mixing 0.5wt.% and 1.0wt.% of NPs with fluids for 10-15 minutes.

4.7 Cement and Geopolymer Formulation

The most common and important binding material in oil wells is Ordinary Portland cement (OPC) [38]. The OPC is produced in a rotary kiln from a molten mixture of suitable ingredients. When cement is mixed with water, cement and other additives present in the cement blend, undergo a chemical reaction with the water, known as hydration of cement. As a result of hydration, the cement forms a gel structure and develops compressive strength. The reaction of minerals present in the clinker and produced phases after the solidification will dictate the properties of cement. Portland cement is classified based on mineral phases present in the cement. API

Table 4.3: Composition of oil-based drilling fluids (Paper II).

Product Name	Base Fluid (wt.%)	Base fluid + NPs (wt.%)
EDC 95/11	28.48	28.48
Onemul	1.43	1.43
Lime	1.43	1.43
Water	3.87	3.87
CaCl ₂	1.19	1.19
Versatrol M	0.57	0.57
Benton 128	0.4	0.4
Barite	62.62	62.62
IONPs in Hexane	-	0.5 and 1.0

standard classified Portland cement into six (class A, B, C, D, G, and H) different classes based on the operational conditions to which cement can be exposed [327]. The most commonly used classes in oil wells are G and H. These classes are available as moderate and high sulphate resistance, known as MSR and HSR. This work used API class G cement with HSR produced by Norcem as reference cement. Table 4.4 shows the composition of cement used in this work.

Table 4.4: Chemical composition of cement.

Chemical composition	wt. %
<i>MgO</i>	2.1
<i>SO₃</i>	2.1
<i>C₃S</i>	54
<i>C₃A</i>	2
<i>C₄AF + 2*C₃A</i>	15
<i>Na₂O</i>	0.6
<i>I.R</i>	0.2
<i>LOI</i>	1

In this work, the rock-based geopolymer was produced using granite as a precursor supplied by Velde Pukk AS. Granite is an igneous rock with the main components of quartz and feldspar. The particle

size of the granite powder used in this work was below $63 \mu m$, and it was used to produce geopolymer without any additional processing. However, to normalize the chemical composition of granite, a suitable amount of blast furnace slag and silica flour was added. Table 4.5 presents the chemical composition of the precursor. *Khalifeh et al. (2016)* [328] performed extensive work to develop rock-based geopolymer. Steel production contributes to the production of a by-product called ground granulated Blast Furnace Slag (GGBFS). The GGBFS is added to the precursor mix in a percentage so that the final calcium content of the mix design is less than 10 wt.%. MEROX, Sweden, provided the GGBFS with the product name Merit 5000 for this work. In order to fine-tune the Si/K_2O ratio, silica flour supplied by Halliburton was used.

Table 4.5: Chemical composition of geopolymer (Paper III).

Chemical composition	wt. %
<i>SiO₂</i>	65.77
<i>Al₂O₃</i>	10.04
<i>Fe₂O₃</i>	0.58
<i>CaO</i>	11.98
<i>MgO</i>	6.37
<i>Na₂O</i>	1.89
<i>K₂O</i>	1.78
<i>TiO₂</i>	0.91
<i>MnO</i>	0.01
<i>SrO</i>	0.01
<i>BaO</i>	0.01
<i>S₂-</i>	0.48
<i>LOI</i>	0.17
Total	99.99

4.7.1 Cement and Geopolymer Slurry Preparation

API class G cement with HSR from Norcem was mixed with water to achieve 44% BWOC according to API specification using an API

Waring blender [327]. In this mixing procedure, first solid was mixed with liquid by applying a rotation rate of 4000 ± 250 RPM for 15 seconds, followed by further shearing of slurry at 12000 ± 250 RPM. The required quantity of NPs was added in a liquid phase and mixed with the mixer. A similar mixing procedure was followed for geopolymer. Table 4.6 and Table 4.7 show the slurry mix designs. First, the pulverized granite rock was mixed with other industrial wastes to prepare a unique chemical composition. Moreover, the hardener solution was prepared by mixing deionized water with potassium silicate solutions. Then, suitable amounts of either AL NPs or MW-OH were added to the hardener and mixed with a high-shear rate mixer. Afterward, the hardener and NPs blend was mixed with the normalized geopolymeric precursors using the commercial Waring blender. The liquid-to-solid ratio (L/S) of the samples was 0.55. The cement and geopolymer slurries were conditioned with the atmospheric consistometer to achieve homogeneous slurries. The sample preparations were conducted according to *API RP 10B-2* [329].

Table 4.6: Composition of the AL NPs modified geopolymer (Paper III).

Component	Weight
Precursor	735
Hardener	324.45
Water	81.9
AL NPs	0.36

Table 4.7: Composition of the MW-OH modified geopolymer (Paper III).

Component	Weight
Precursor	735
Hardener	324.45
Water	81.9
MW-OH	0.18

4.8 Characterization Techniques and Test Methods

4.8.1 Scanning Transmission Electron Microscopy (STEM)

STEM is a combination of transmission and scanning electron microscopy employed to characterize NPs to obtain imaging and morphology of particles. In transmission electron microscopy, a high-energy beam of electrons is focused on a thin sample of the specimen to construct the image. In STEM fine electron probe in a raster pattern is scanned through the specimen, and several detectors detect the resulting scattering or transmission of electrons. The interaction of the electron beam and specimen atoms generates the serial signal stream. This is correlated with beam position to generate a virtual image of scanned material [330]. STEM images of IONPs were acquired using an S-5500 electron microscope operating at 30 kV voltage. NPs solutions were dropped on a Formvar carbon-coated copper grid to prepare TEM grids (Electron Microscopy Sciences, Hatfield, Pennsylvania, USA). To limit the aggregation of NPs due to evaporation at room temperature, it is important to wipe with Kimberly-Clark wipes immediately.

4.8.2 Scanning Electron Microscopy (SEM)

To get images of NPs and the presence of NPs in the filter cake as well as the structural makeup of cement and geopolymer samples, SEM analysis was done with a Supra 35VP electron microscope (Zeiss, Oberkochen, Germany). The cake specimen after the fluid loss test was used to analyse drilling fluids, while cement and geopolymer crushed samples after the UCS test were used for the analysis. It is crucial to prepare high-quality samples for analysis. Therefore, samples were coated with palladium to ensure that the surface of the samples was electronically conductive and there was no build-up or charging of electrons. In the case of SEM, the beam of an electron is scanned through the sample, and the interaction

of the electron beam and atoms in the sample generates different energy signals. The signals provide information about the sample's tomography, composition, and texture. The analysis was performed in the secondary analysis mode, which is the most common SEM mode. In this mode, a secondary electron detector detects the interaction between the surface atoms and the electron beam. In addition to SEM analysis, energy dispersive X-ray spectroscopy (EDS) was used to perform the elemental analysis of samples. The characteristic X-rays are produced when the primary electrons excite the electrons in the inner shells of sample atoms, and electrons from the outer shell replace these excited electrons as they move inward. This produces energy in the form of X-rays, which are detected by silicon crystals with lithium doping. Since there is a difference in the atomic structure of elements, the resulting energy and X-ray wavelength will vary for each element. Hence allowing the quantification and detection of elements. It is possible to detect X-rays from a single area or spot. Also, analysis can be done in an automated sequence enabling scanning of areas to map the presence of elements within a specific area.

4.8.3 Dynamic Light Scattering (DLS) and Zeta Potential

The principle of dynamic light scattering is based on measuring the radius of a hypothetical hard sphere that diffuses with a similar velocity as the particle of interest. The reported hydrodynamic size from the measurement indicates the size of hydrated particles. Therefore, the size measured by this technique differs from the dry size of particles, as the hydrodynamic size considers the associated water, and particles can behave differently when they are in solution. The collisions between particles in the suspension promote Brownian motion. The intensity of light scattered by these particles undergoes time-based fluctuation due to this random motion. The auto-correlation functions containing the diffusion coefficient of particles can be used to measure these time-based fluctuations. The estimation of the average diffusion coefficient can be made from these auto-correlations. This diffusion coefficient can be used to calculate the hydrodynamic sizes using the Stokes-Einstein equation. Therefore,

DLS from the diffusion behavior of suspended particles in the solution can provide particle size and particle size distributions by measuring the time-based fluctuations in the intensity of light scattered [287].

The charged particles in the solution and counter ions surrounding the charged particles close to the surface make the electrical double layer. Zeta potential can be defined as the potential at a shear plane, that is, a meeting point of a diffuse layer and a slipping plane. This is the distance from the particle surface where motion between the immobilized layer and mobile fluid starts. Electrophoretic mobilities of particles are used to calculate the zeta potential by applying the Helmholtz-Smoluchowski equation. In this study, the Zetasizer Nano-ZS instrument from Malvern was used to measure the sizes and zeta potential of NPs. All the measurements were performed in aqueous solutions.

4.8.4 Viscosity

A Couette coaxial cylinder rotational viscometer from OFITE model 900 was used to measure viscosity parameters of drilling fluids at atmospheric pressure and different temperature, i.e., 22 °C, 50 °C, and 80 °C. Dial readings at different rotational speeds were recorded in ascending and descending order. In this work, the modified Herschel-Bulkley model was used as it reasonably estimates the behaviour of drilling fluids for a wide range of shear rates [331]. Eq. 4.1 presents the Herschel-Bulkley model,

$$\tau = \tau_y + K(\dot{\gamma})^n \quad (4.1)$$

In this equation, τ is the shear stress, $\dot{\gamma}$ is the shear rate, τ_y is yield stress, while n and k are flow and consistency factors. Recently, *Saasen and Ytrehus. (2020)* [331] stated that the Herschel-Bulkley model might provide an inaccurate estimation of drilling fluids viscosity as the dependency of consistency index k on the flow index n limits the comparison of the model for different drilling fluids. Also, different values of k and n can give similar flow curves.

Therefore, *Saasen and Ytrehus* modified the model by rearranging the parameters. This model with dimensionless shear rate is presented in Eq. 4.2 as,

$$\tau = \tau_y + \tau_s \left(\frac{\dot{\gamma}}{\dot{\gamma}_s} \right)^n \quad (4.2)$$

In Eq. 4.2 $\tau_s = \tau - \tau_y$ at $\dot{\gamma} = \dot{\gamma}_s$, where τ_s and $\dot{\gamma}_s$ are surplus shear stress and shear rate, respectively, while yield stress τ_y was estimated using the Zamora and Power approach where $\tau_y = 2\tau_3 - \tau_6$. Yield stress from this approach provides values with reasonable accuracy for hydraulic calculation. The shear rate of 170.31/s was used as the surplus shear rate. Moreover, to calculate low shear curvature exponent (n_{ls}) and high shear curvature exponent (n_{hs}), shear stress (τ_x) at shear rates ($\dot{\gamma}_x$) of 51.11 1/s and 1022 1/s were selected, and Eq. 4.3 was used for calculation,

$$n = \frac{\ln\left(\frac{\tau_x - \tau_y}{\tau_s}\right)}{\ln\left(\frac{\dot{\gamma}_x}{\dot{\gamma}_s}\right)} \quad (4.3)$$

In the case of cement and geopolymer, the slurries were conditioned up to 50 °C in the atmospheric consistometer, and afterward, rheological behavior was measured using Fann 35 viscometer. After reaching 50 °C, the slurry was conditioned for 20 minutes to attain a uniform temperature. The Casson model was used to calculate the yield stress and plastic viscosity. Casson model is a two-parameter model, and it provided a good fit in the case of measured shear stress and shear strain values of cement-based materials. The Casson model depicts more accurate results at both high and low shear rates [332]. The model is shown in Eq. 4.4 and Eq. 4.5 [38],

$$\tau^{0.5} = \tau_c^{0.5} + \mu_c^{0.5} \dot{\gamma}^{0.5} \quad \text{For } \tau \geq \tau_c \quad (4.4)$$

$$\gamma = 0 \quad \text{For } \tau < \tau_c \quad (4.5)$$

Where,

τ represent shear stress (Pa)

τ_c is the Casson yield stress (Pa)

μ_c is the Casson plastic viscosity (Pa.s)

$\dot{\gamma}$ is the shear rate (sec^{-1})

4.8.5 Fluid loss

LPLT 300 API filter press (FANN, Houston, TX 77032, USA) was used to measure the fluid loss of water-based drilling fluids at ambient temperature and 0.7 MPa (100 psi). The test was conducted according to the API standard, *API Recommended Practice 13B-1* [333]. High temperature and high-pressure fluid loss test was performed to measure the static fluid loss from oil-based drilling fluids, geopolymer, and cement samples. In the case of geopolymer and cement slurries, these were conditioned in an atm consistometer before the measurements. The achieved differential pressure was 5.2 MPa, and the slurries were passed through the 850 μm sieve. In the case of oil-based drilling fluids, the test was performed at 100 °C and a pressure of 3.5 MPa. In both cases, the pressure was applied by using carbon dioxide cartridges. The tests were performed according to API standards [329, 334].

4.8.6 Mechanical Friction

CSM tribometer was used to measure the coefficient of friction of water and oil-based drilling fluids. The 13cr Steel ball with a 6mm diameter and plate surface was used to perform the test. Moreover, the normal load of 5N was applied for a distance of 10m at a rate of 3cm/s to conduct the test. All the tests were done at ambient temperature and atmospheric pressure, with repeated measurements to report average values.

4.8.7 Viscoelasticity

MCR 302 rheometer (Anton Paar) was used to conduct amplitude sweep tests for water and oil-based drilling fluids with a constant frequency of 10 rad/s with varying strains of 0.0005% to 1000%. The test was done to measure the viscoelastic properties of drilling fluids.

4.8.8 Barite Sag Test for Oil-Based Drilling Fluids

To estimate the barite settling under static conditions, aging of the oil-based drilling fluids at 100 °C for 16 hrs was done. The measured densities at the top (ρ_{top}) and bottom (ρ_{bottom}) were used to calculate the sag factor, as shown in Eq. 4.6 [335],

$$(Sag\ factor)_{static} = \frac{\rho_{bottom}}{\rho_{top} + \rho_{bottom}} \quad (4.6)$$

The known volume of drilling fluids was obtained using the syringe, and the mass of that volume was used to calculate the density using $\rho = m/v$. The viscometer sag test was used to calculate the dynamic sagging [21]. The sagging shoe was placed at the bottom of a heating cup in this test. The drilling fluids were mixed for some time at 600 rpm to avoid the settling of particles. After that, for $MW_{initial}$, 20mL of drilling fluids sample was obtained. Afterward, 140mL of drilling fluids was heated at 50 °C. The sagging test was then performed on the heated drilling fluids at 100 RPMs for 30 minutes. After 30 minutes, 20mL of the sample was taken from the sag shoe and called MW_{final} . To calculate the dynamic sag Eq. 4.7 was used,

$$(Sag\ factor)_{dynamic} = \frac{MW_{final}}{2(MW_{initial})} \quad (4.7)$$

4.8.9 Temperature and Pressure Conditions for Cement and Geopolymer Tests

Testing of the cement and geopolymer samples was done at 50 °C and 70 °C in this work with the ramp-up rate of 1 °C/min. The

selected pressure for the consistency, uniaxial compressive strength, and ultrasonic cement analyzer was 14 MPa. Even though oil wells can experience harsher conditions with respect to temperature and pressure, the selected conditions can still be a good starting point to test the application of NPs in cementitious materials under downhole conditions.

4.8.10 Consistency

Pressurized and atmospheric consistometer recommended by *API RP 10B-2* standard [329] were used to check the pumpability and effect of pressure on the pumpability of the slurries. For atmospheric and pressurized consistency measurements, OFITE model 60 and 2040, respectively, were used. The slurries were added to the dedicated cell for the equipment to perform the test. In the pressurized consistometer, the selected pressure rate was 1.7MPa/min.

4.8.11 Uniaxial Compressive Strength

The required amount of slurries were mixed and conditioned for 30 minutes in an atmospheric consistometer and transferred to cylindrical plastic molds. The samples were cured in the autoclave using water as a curing medium. The autoclave was pressurized to 14 MPa using an ISCO pump and put into the oven at 70 °C. The cylindrical molds with a height/length ratio of 2 are recommended for annular cement integrity simulations. After curing for the required time, the autoclaves were removed from the oven, and samples were cooled to ambient temperature. Afterward, plastic molds were removed, and both sides of cylindrical samples were cut to attain a flat surface for compressive strength measurement. A Toni Technik-H mechanical tester linked to TestXpert v7.11 software was used to measure the unconfined compressive strength of the samples. The test was conducted at a 35 MPa/min loading rate according to the *API RP 10B-2* standard [329]. The samples were loaded between parallel plates, and the loading was on the surface of the cylindrical plugs. The testing procedure is according to *NS-EN 196-1* standard [336, 337], and the compressive strength is given by Eq. 4.8,

$$\sigma_c = \frac{F}{A} \quad (4.8)$$

In the equation, σ_c is uniaxial stress measured in MPa, F is the maximum recorded force (N), and A is the contact area of the specimen (mm^2). The slope of the axial stress-strain curve in the elastic region was used to calculate the modulus of elasticity.

4.8.12 Indirect Tensile Strength Measurement

Compared to steel, rock and cement-like structures show weak tensile strength. Hence, the indirect method is used to measure the tensile strength of these materials. Usually, a Brazilian test measures the indirect tensile strength of cement-based materials. In this work, the samples were cured using the same procedure as the UCS test, and cylindrical samples were cut into disk shapes. The tests were conducted following the procedure described in *NS-EN 12390-6:2009* standard [338]. The samples were placed vertically between parallel curved jaws, and a loading rate of 50 N/s was applied according to *ASTM D3967-16* [339] until the failure. The test was performed by using Zwick/Z020 mechanical testing machine with TestXpertII software to record the applied force. The tensile strength was calculated by using Eq. 4.9 [339],

$$\sigma_t = \frac{2F}{\pi DL} \quad (4.9)$$

In Eq. 4.9 σ_t represents the tensile stress in MPa, F is the maximum force applied on the sample (N), D is the diameter of the sample (mm), and L is the length of the specimen (mm). The unit of the tensile strength is N/mm^2 .

4.8.13 Sonic Strength Development

The 4265-HT Chandler Ultrasonic Cement Analyser (UCA) was used to measure the sonic strength of the cement and geopolymer materials

at 70 °C. The slurries were conditioned in the consistometer and poured into the UCA cell. The cell is equipped with transducers at both ends, which enables UCA to compute the transit time of sonic waves through the sample. In the case of cement samples, the transit time is converted to compressive strength by applying a pre-defined algorithm. Since the transit time of waves varies for different materials, it is required to develop a new algorithm to estimate the values for new materials. Hence to facilitate geopolymer customized algorithm feature was used from UCA. The algorithm was generated using uniaxial compressive strength (UCS) results at different times and corresponding transit times. A polynomial equation was generated by plotting measured compressive strength and transit time and put into the UCA software to calculate the sonic compressive strength.

4.8.14 X-ray Diffraction (XRD)

XRD is a widely employed technique to study the material structure and crystallinity at an atomic level. In this technique incident, an X-ray beam is applied to the sample and elastically scattered in specific directions. The angle of incident X-ray θ produces a reflection pattern based on Bragg's law, presented in Eq. 4.10,

$$2d \sin \theta = n\lambda \quad (4.10)$$

The reflection pattern is related to the lattice constants or parameters of crystals. In Eq. 4.10, d is the distance between the atomic planes, λ is the wavelength of incident X-rays, and n is a positive integer. As the angle of incident X-rays is increased stepwise, the constructive interference of the X-rays scattered in the atomic planes creates peaks. The identification of minerals present in the sample is based on the reflection pattern. The variation in the peak intensities is dependent on the crystal structure. This work obtained XRD patterns of cement and geopolymer samples using Bruker D8 Advance Eco diffractometer (having Cu-K α radiation source, $\lambda = 1.5406 \text{ \AA}$, 40kV, and 25mA). The X-ray patterns were recorded in the 2θ range of 5–70° at the

step of $1^\circ/\text{min}$.

4.9 Iron Oxide NPs

Figures 4.1 a and b show the STEM image and particle size of Fe NPs synthesized by the co-precipitation method. The co-precipitation method does not require high temperature and very long reaction time and provides high particle yield. However, this method does not permit precise control over the shape and particle size, resulting in particles with broad particle size distribution. The average particle size of the NPs formed by this method was 11 ± 2 nm.

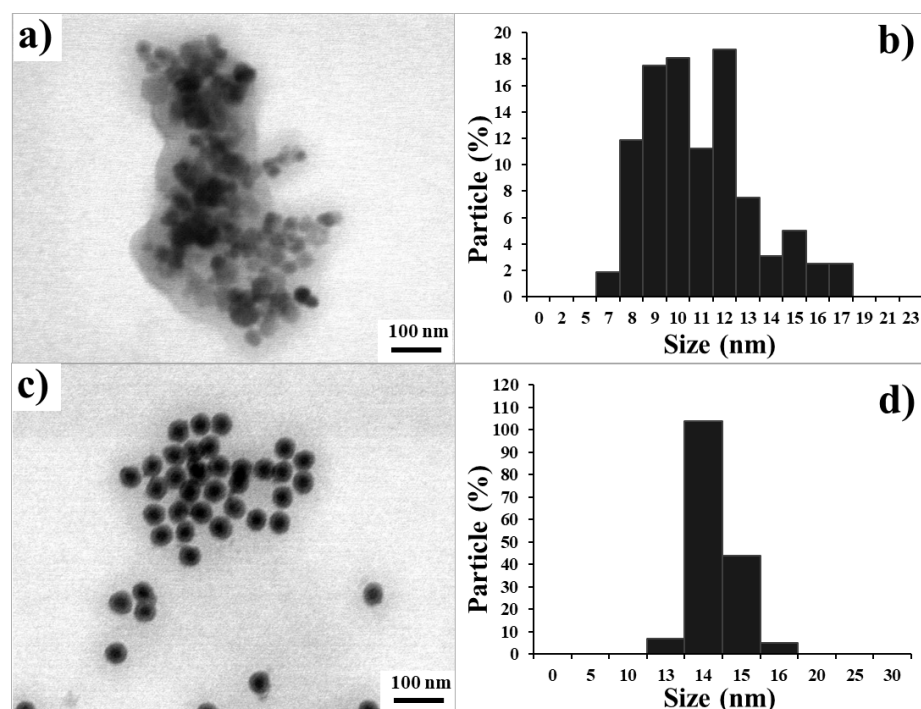
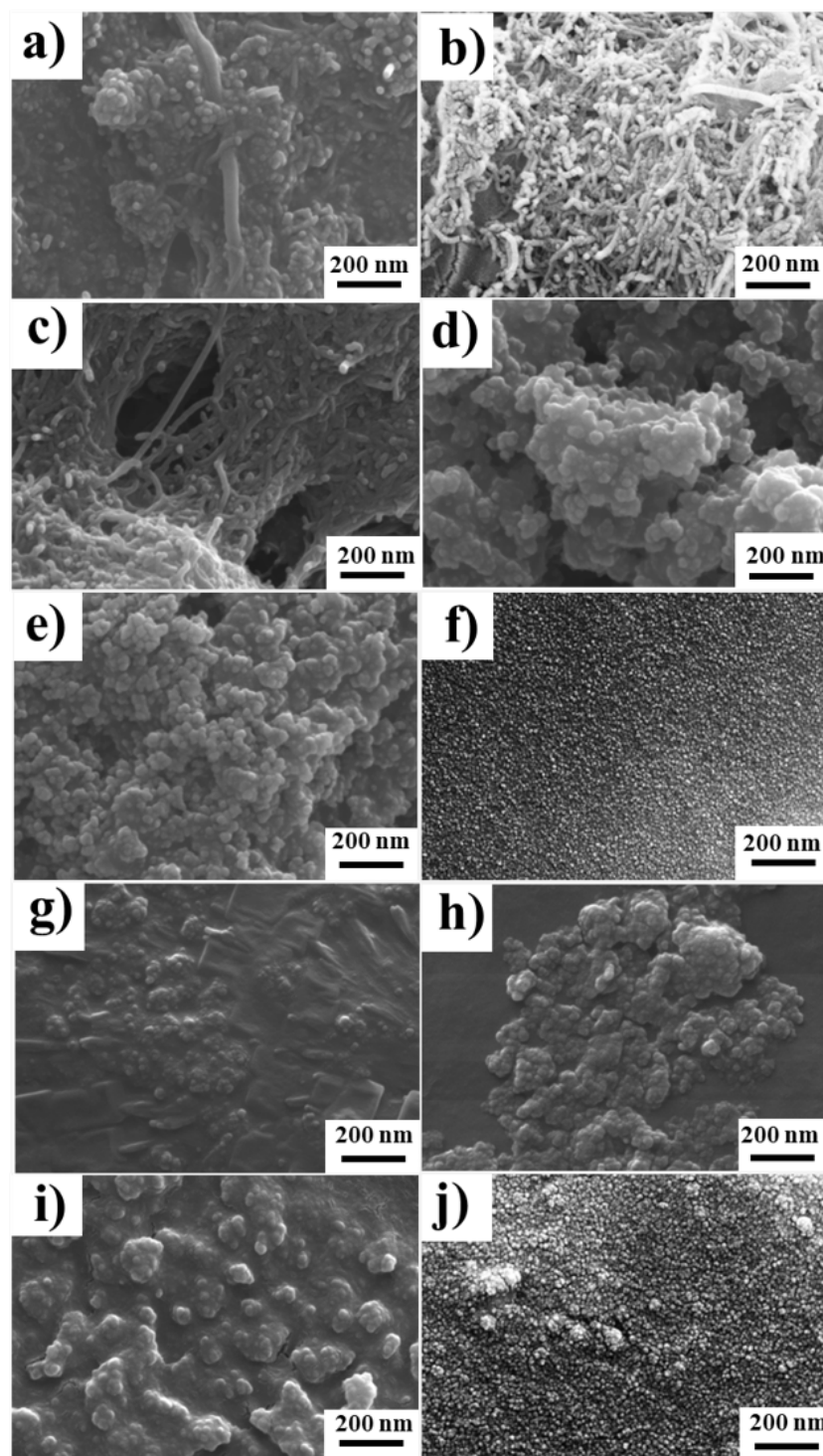


Figure 4.1: a) STEM image of IONPs produced by co-precipitation method b) Size distribution of NPs c) STEM image of IONPs produced by thermal decomposition method d) Size distribution of NPs (Paper I, Paper II).

The hydrophobic NPs produced by the thermal decomposition method show spherical morphology, as indicated in Figure 4.1 c. The NPs show narrow size distribution, with most particles in the size range of 14nm. Figure 4.1 d shows the histogram size distribution for the particles.

4.10 Commercial and Surface Modified NPs

Figure 4.2 shows the SEM images of the commercial NPs and surface-modified NPs. Figures 4.2 a-c) show the MW, MW-OH, and MW-COOH. To get the stable dispersions of nanotubes in water, they were dispersed in a non-ionic surfactant with aromatic groups using ultrasonication and centrifugation. The nanotubes were manufactured by the CVD method, with outside and inside diameters of 20-30 nm and 5-10 nm, respectively. Moreover, the lengths of the tubes are 10-30 μm . In the case of MW-OH, the OH content is 1.76 wt.%, while for MW-COOH, the COOH content is 1.23 wt.% as provided by the manufacturer. Figure 4.2 d-f presents the SiO_2 NPs. The Si NPs shown in Figure 4.2 d have a spherical morphology and porous structure with particle size in the range of 5-20 nm, as provided by the supplier. The surface-modified NPs, i.e., Si-C shown in Figure 4.2 e, improve the stability of Si NPs. Moreover, Figure 4.2 f shows Si-N NPs; the size of NPs, provided by the manufacturer is 27nm. Figure 4.2 g, and i show the SEM image of IONPs and IONPs coated with XG and silica, respectively. The surface modification increases the size of NPs. AL NPs are shown in Figure 4.2 j, the particle size of dry powder, as provided by the supplier, is around 45nm. As indicated in Figure 4.2 j particles show spherical morphology.



⁶⁰
Figure 4.2: SEM images of NPs a) MW b) MW-OH c) MW-COOH d) Si NPs e) Si-C NPs f) Si-N NPs g) Fe NPs h) Fe-XG NPs i) Fe-Si j) Al NPs (Paper IV).

The hydrodynamic sizes and surface charges of NPs at 25 °C and 50 °C are given in Table 4.8 and Table 4.9.

Table 4.8: Size and zeta potential of NPs at 25 °C (Paper I, IV).

NPs	Size (nm)	Zeta Potential (mV)
MWCNT	161.8 ± 1.9	-26.2 ± 1.0
MWCNT-OH	158.1 ± 1.5	-30.1 ± 0.5
MWCNT-COOH	174.6 ± 2.7	-28.8 ± 0.4
Si NPs	217.3 ± 11.9	-36.1 ± 2.5
Si-C NPs	395.1 ± 29.4	-34.9 ± 2.2
Si-N NPs	36.8 ± 0.5	-35.8 ± 1.7
Fe NPs	273.5 ± 5.9	-31.3 ± 0.3
Fe-XG NPs	487.6 ± 8.6	-39.2 ± 0.6
Fe-Si NPs	634.7 ± 102.5	-37.3 ± 1.4
AL NPs	126.33 ± 5.11	18.70 ± 0.53

Table 4.9: Size and zeta potential of NPs at 50 °C (Paper I, IV).

NPs	Size (nm)	Zeta Potential (mV)
MWCNT	189.8 ± 8.8	-27.5 ± 0.4
MWCNT-OH	216.2 ± 21.1	-29.3 ± 0.8
MWCNT-COOH	184.1 ± 12.7	-31.3 ± 0.5
Si NPs	676.8 ± 123.7	-15.4 ± 0.7
Si-C NPs	852.3 ± 161.2	-27.9 ± 1.2
Si-N NPs	46.1 ± 2.7	-26.5 ± 0.6
Fe NPs	381.2 ± 19.6	-20.8 ± 0.2
Fe-XG NPs	673.6 ± 65.5	-34.8 ± 0.4
Fe-Si NPs	1856.3 ± 161.2	-24.4 ± 0.4
AL NPs	168.73 ± 6.07	4.49 ± 0.16

Since DLS measured the particle's hydrodynamic radius, there is a difference in the sizes measured by SEM (measures the dry radius of NPs) and DLS. The surface modification increases the size of NPs in the case of Si-C, Fe-XG, and Fe-Si. In addition, there is

an increase in the zeta potential of Fe-XG and Fe-Si, owing to the better stability of NPs compared to bare NPs. There is an increase in size and decrease in zeta potential at 50 °C for all the NPs except MWCNT, indicating the agglomeration of NPs at higher temperature. However, the surface-modified NPs show better stability even at higher temperatures (see Table 4.9). AL NPs show positive surface charge; however, these particles also show a low loss in stability at high temperature, as indicated in the table. This might impact the application of these particles at high temperature.

5 Application of NPs in Water Based Drilling Fluids.

This chapter discusses the main findings of water-based drilling fluids with three different types of NPs and surface-modified NPs. The results in this chapter are based on papers I and IV. Also, unpublished work is discussed in the chapter.

5.1 Rheological Parameters of Drilling Fluids with NPs

5.1.1 Shear Stress Measurement

Iron NPs

Figures 5.1 a, b, and c present the effect of Fe, Fe-XG, and Fe-Si NPs on shear stress values at different shear rates of water-based bentonite drilling fluids. There is an increase in the shear stress values at higher temperature for the base fluids, which is more significant at lower shear rates. This phenomenon is due to the flocculation of bentonite, owing to the interparticle interaction. The edge-to-face (EF) and face-to-face (FF) interactions of bentonite particles caused the agglomeration, ultimately increasing the shear stress values. Adding 0.0095wt.% Fe NPs cause a further increase in the shear stress due to the possible interaction of NPs with the positively charged edges of the bentonite platelets and with the barium ions present in the fluid system. However, the increased NPs concentration to 0.019wt.% decreases the shear stress values due to electrostatic repulsion between NPs and other additives in the fluid system. Further, an increase in the NPs concentration to 0.038wt.% causes an increase in the shear stress values due to the agglomeration of NPs. Surface modification of Fe NPs with XG increases the stability of NPs, which causes the reduction in shear stress values at a low shear rate.

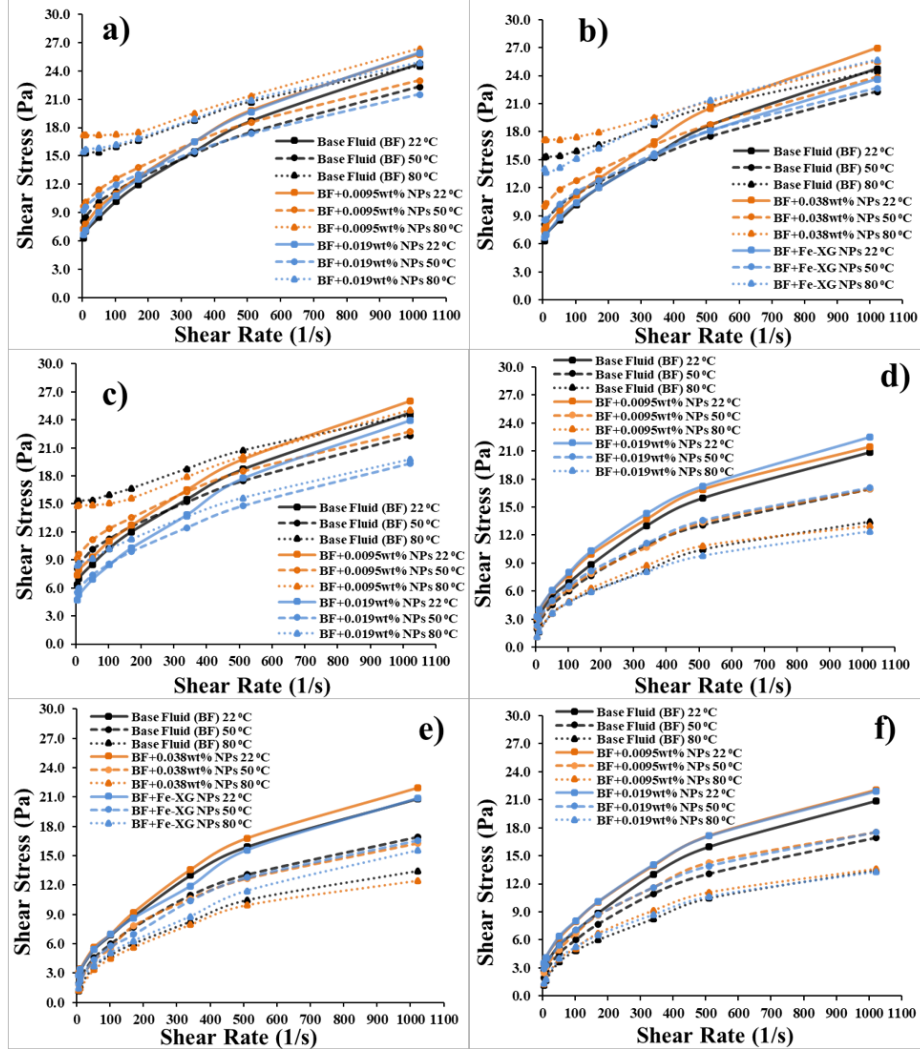


Figure 5.1: Impact of Fe, Fe-XG, and Fe-Si NPs on shear stress of water-based drilling fluids a) Bentonite drilling fluids with 0.0095wt.% and 0.019wt.% Fe NPs b) Bentonite drilling fluids with 0.038wt.% Fe and Fe-XG NPs c) Bentonite drilling fluids with 0.0095wt.% and 0.019wt.% Fe-Si NPs d) KCl drilling fluids with 0.0095wt.% and 0.019wt.% Fe NPs e) KCl drilling fluids with 0.038wt.% Fe and Fe-XG NPs f) KCl drilling fluids with 0.0095wt.% and 0.019wt.% Fe-Si NPs (Paper I).

Previous studies also show a similar trend in the case of Fe NPs in water-bentonite suspension [340]. The addition of NPs to the base fluid increases the viscosity and shear stress due to an aggregation of Fe NPs. However, surface modification of NPs minimizes the aggregation, as shown in this work, where surface modification with polymer shows a similar trend. Fe-Si NPs lower the shear stress values of base fluid, where a higher concentration of 0.019wt.% significantly reduces the values. The presence of silica on the surface of Fe NPs inhibits the flocculation of bentonite. Silica particles adsorb on the clay and form a layer on the clay's surface, preventing water contact with the clay.

Figures 5.1 d, e, and f show the shear stress values for the KCl-based fluids with NPs. High salt concentrations make these fluid systems dispersive, which also causes a decrease in shear stress values at higher temperature. The addition of Fe NPs to these fluids does not have a significant impact on the shear stress values. There is only a slight increase in shear stress values for both 0.0095wt.% and 0.019wt.% NPs at 22 °C and 50 °C. However, at 80 °C NPs do not alter the shear stress values of the base fluid. Although, the coating of XG on the NPs surface shows slight improvement, which can be attributed to the NPs stability due to the polymer's presence on the surface. In addition, the polymer interacts better with the potassium ions in the fluid system. For Fe-Si NPs, there is an increase in shear stress values for both 0.0095wt.% and 0.019wt.% at 22 °C, 50 °C, and 80 °C. This shows that silica particles interact with the potassium and XG polymer in the drilling fluids.

SiO₂ NPs

SiO₂ NPs addition to the bentonite fluids reduces the shear stress values for all three types of NPs at 22 °C, 50 °C, and 80 °C see Figures 5.2 a, b and c.

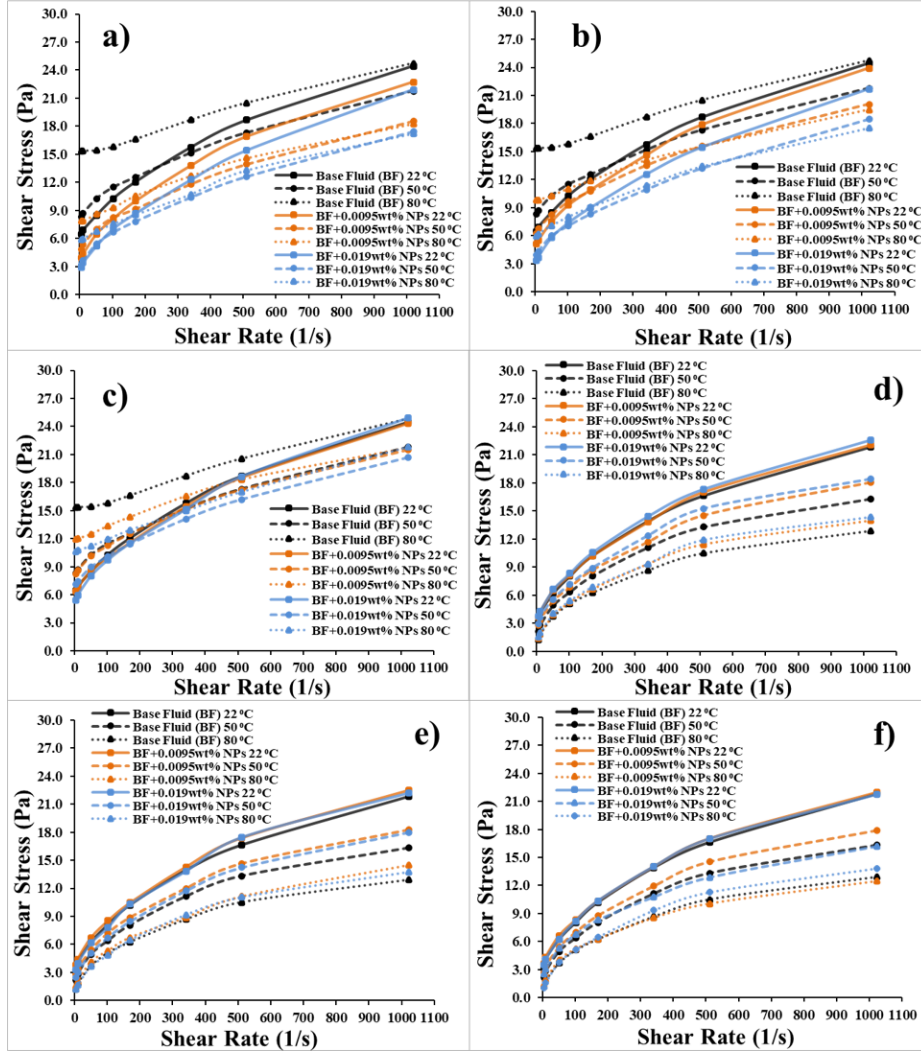


Figure 5.2: Impact of SiO_2 NPs on shear stress of water-based drilling fluids a) Bentonite drilling fluids with 0.0095wt.% and 0.019wt.% Si NPs b) Bentonite drilling fluids with 0.0095wt.% and 0.019wt.% Si-C NPs c) Bentonite drilling fluids with 0.0095wt.% and 0.019wt.% Si-N NPs d) KCl drilling fluids with 0.0095wt.% and 0.019wt.% Si NPs e) KCl drilling fluids with 0.0095wt.% and 0.019wt.% Si-C NP f) KCl drilling fluids with 0.0095wt.% and 0.019wt.% Si-N NPs.

Si and Si-C show more reduction as compared to Si-N. This indicates that surface modification of NPs can provide different functionalities to the NPs, which ultimately fine-tunes the interaction of NPs with the fluid system. Moreover, for KCl fluids with silica NPs shows similar behaviour as shown by Fe-Si NPs, and NPs increase the shear stress values owing to the better interaction of the XG polymer with the silane group and sodium sulphonate on the surface of Si and Si-C NPs, respectively see Figures 5.2 c, d and f. Furthermore, Si-N NPs show less increment compared to the other two NPs.

Nanotubes

Figures 5.3 a, b, and c show the impact of MWCNTs on the shear stress values of water-based bentonite drilling fluids. There is no change in shear stress values with the addition of MW at 22 °C. However, at higher temperature, i.e., at 50 °C and 80 °C, the nanotubes significantly increase the shear stress values, especially at 80 °C. The adsorption of nanotubes on the bentonite surface contributed to this behaviour. This is also confirmed by the SEM images shown in the section 5.4. MW-OH and MW-COOH show similar behaviour to MW.

The results for KCl fluids indicate that low concentrations of MW increase the shear stress values owing to better interaction with polymer and other additives present in the fluid system, see Figures 5.3 d, e, and f. However, a further increase in the concentration forms two phases in the fluid system since the fluids show zero shear stress values at lower shear rates. The high surfactant in the system contributed towards the settling of barite, which forms two phases and separates the solid and liquid. However, the addition of MW-OH and MW-COOH does not form two phases at higher concentrations owing to functional groups on the surface of nanotubes. The functional groups provide better stability to the fluids even at higher temperature.

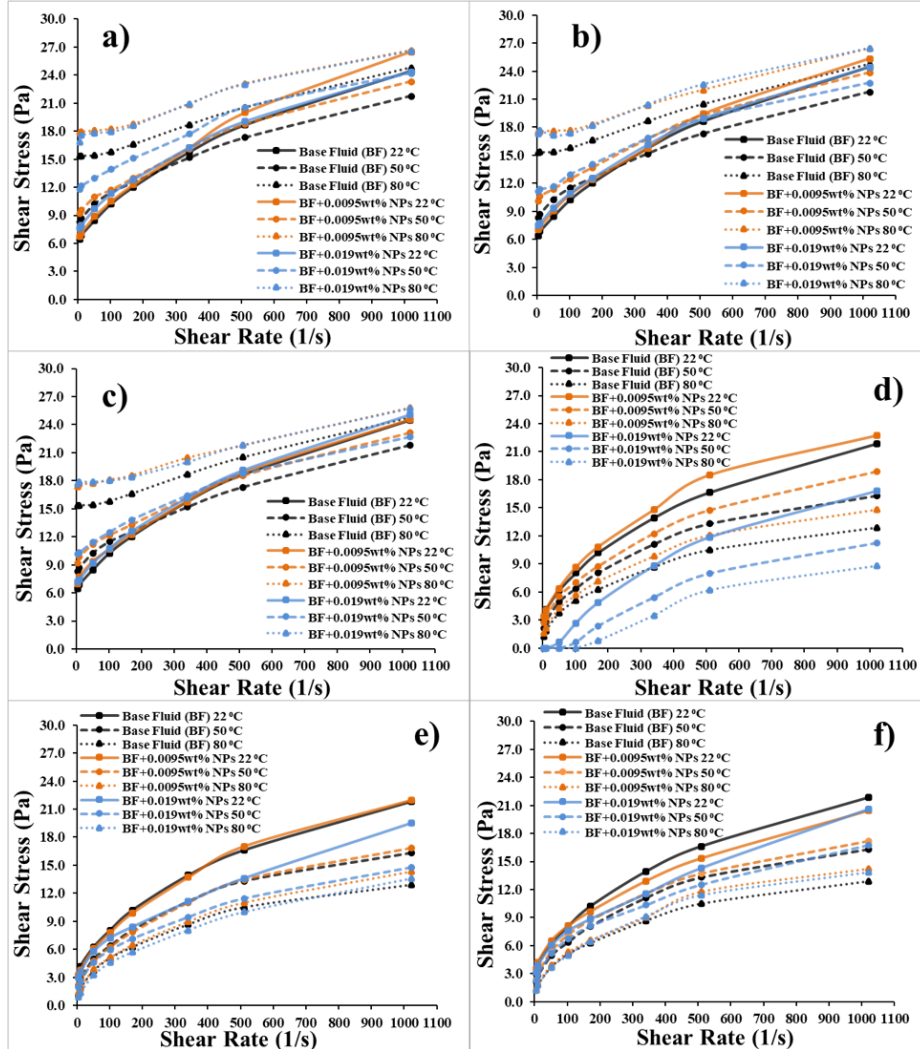


Figure 5.3: Impact of MWCNTs on shear stress of water-based drilling fluids a) Bentonite drilling fluids with MW b) Bentonite drilling fluids with MW-OH c) Bentonite drilling fluids with MW-COOH d) KCl drilling fluids with MW e) KCl drilling fluids with MW-OH f) KCl drilling fluids with MW-COOH.

5.1.2 Gel Strength

Iron NPs

Adding 0.0095wt.% Fe NPs increases the 10 sec and 10 min gel strength of bentonite fluids, as shown in Figures 5.4 a, b.

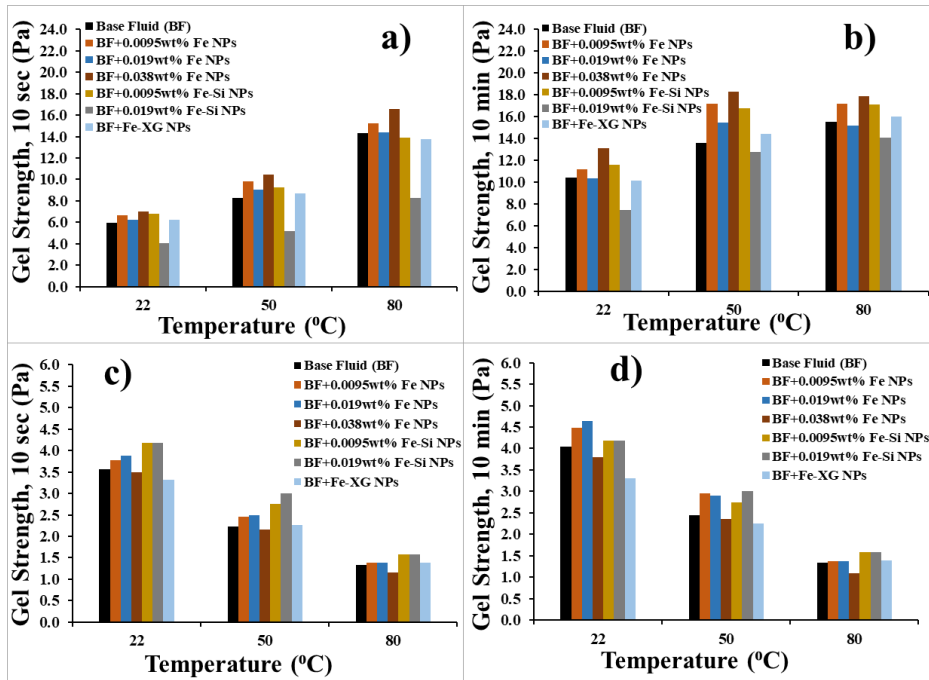


Figure 5.4: Impact of Fe, Fe-XG and Fe-Si NPs on gel strength of water-based drilling fluids a) 10 sec gel strength of bentonite drilling fluids b) 10 min gel strength of bentonite drilling fluids c) 10 sec gel strength of KCl drilling fluids d) 10 min gel strength of KCl drilling fluids (Paper I).

At low concentrations, the NPs attached to the bentonite edges and contributed to the gel formation. Further, an increase in NPs concentration to 0.019wt.% reduces the gel strength, and fluid shows a similar gel strength as base fluid. This shows that increasing the NPs in the fluid system minimizes the gel formation by deflocculating the bentonite. However, adding more NPs in the fluid again increases

the gel strength due to NPs agglomerates attached to the bentonite and other additives in the drilling fluids. Gel strength results for Fe-XG also confirm a polymer's ability to stabilize the NPs and reduce the gel strength of base fluid. Coating of silica on Fe NPs increases the 10 min gel strength of the base fluid for 0.0095wt.% NPs. However, an increase in the NPs concentration to 0.019wt.% shows a reduction in the gel strength. This again confirms the ability of silica to disperse the bentonite and control the excessive gel formation.

The results for KCl fluids are shown in Figures 5.4 c, d. There is an increase in base fluid's 10 s and 10 min gel strength with the addition of 0.0095wt.% and 0.019wt.% NPs at 22 °C and 50 °C. However, there is no change in the gel strength of base fluids at higher temperature due to the reduced stability of NPs at high temperature and the presence of high salt concentration. Increasing the concentration to 0.038wt.% also reduces the gel strength. However, surface modification with silica increases both 10 s and 10 min gel strength at all temperatures. Silica improves the stability of Fe NPs and creates a gel structure with other additives present in the fluid. While polymer coating on Fe NPs, i.e., Fe-XG, slightly improves the gel strength at 80 °C due to better stability of Fe-XG at higher temperature.

SiO₂ NPs

Si and Si-C NPs reduce the 10 s and 10 min gel strength of bentonite fluids at 22 °C, 50 °C, and 80 °C for both 0.0095wt.% and 0.019wt.% NPs, see Figures 5.5 a, b. NPs show a more significant reduction in 10 s gel strength at low temperature. However, bentonite fluids regain their strength after 10 minutes and at higher temperature by minimizing the impact of NPs. Still, NPs can decrease the gel formation at 80 °C for both Si and Si-C NPs. However, Si-N NPs do not show this trend and increase the 10 min gel strength at 80 °C, indicating the ability of surface groups on Si-N NPs to facilitate the gel formation with bentonite.

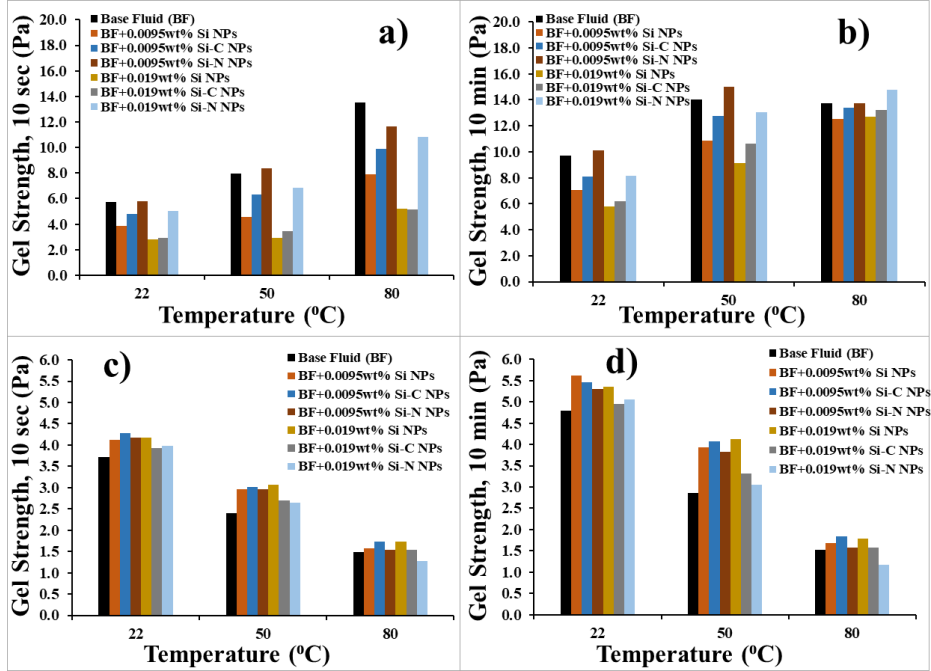


Figure 5.5: Impact of SiO_2 NPs on gel strength of water-based drilling fluids a) 10 sec gel strength of bentonite drilling fluids b) 10 min gel strength of bentonite drilling fluids c) 10 sec gel strength of KCl drilling fluids d) 10 min gel strength of KCl drilling fluids.

SiO_2 NPs show an opposite trend in KCl fluids as 0.0095wt.% of NPs shows improvement in gel strength of base fluid as depicted in Figures 5.5 c, d. All the fluids show a sharp decrease in the gel strength at 80 $^{\circ}C$ due to high salt concentration in the system. Although 0.0095wt.% Si-C and 0.019wt.% Si NPs increase the 10 min gel strength by 20% and 17%, respectively, compared to base fluid at 80 $^{\circ}C$. The presence of silane and sodium sulfonate groups on the surface of Si and Si-C NPs, respectively, forms a gel structure with potassium and XG in the fluid. On the contrary 0.019wt.% Si-N NPs reduce the gel strength of base fluid due to higher electrostatic repulsion creating phase separation in the fluid.

Nanotubes

The addition of MW, MW-OH, and MW-COOH improves the gel-forming ability of bentonite fluids (Figures 5.6 a, b).

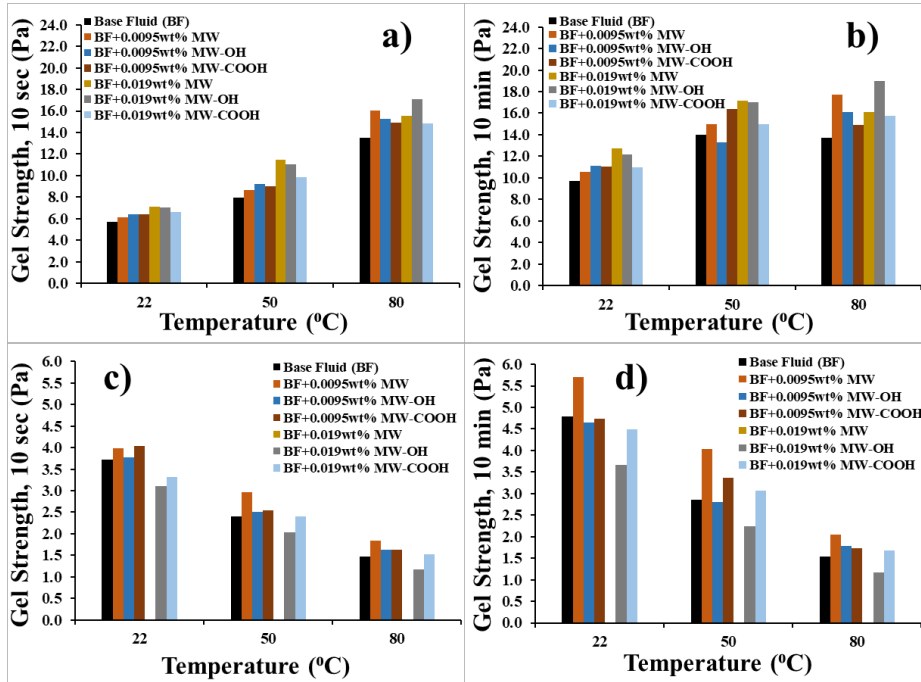


Figure 5.6: Impact of MWCNTs on gel strength of water-based drilling fluids a) 10 sec gel strength of bentonite drilling fluids b) 10 min gel strength of bentonite drilling fluids c) 10 sec gel strength of KCl drilling fluids d) 10 min gel strength of KCl drilling fluids.

Nanotube adsorption on the surface of bentonite forms a network structure that further increases the gel strength. At 80 °C, MW and MW-OH show more increase in gel strength compared to the MW-COOH. The large particle size of MW-COOH might have contributed to a comparatively weaker gel structure. However, the results show that MWCNTs could further enhance bentonite’s gel strength, which might be relevant in applications requiring higher gel strength to hold the cuttings.

Similar to Bentonite fluids, 0.0095wt.% MW, MW-OH, and MW-COOH improve the gel strength of KCl fluids, especially at 80 °C. Further, an increase in the nanotube concentration in the fluids disrupts the stability of colloidal dispersion by suppressing the electric double layer, especially in the case of MW phase separation, giving no values for gel strength see Figures 5.6 c, d. At the same time, MW-OH and MW-COOH show a decrease in gel strength at 22 °C and 50 °C but keep the drilling fluids suspension stable. In addition, MW-COOH slightly improves the gel strength of base fluid at 50 °C and 80 °C; this shows that the nature of the functional group attached to the nanotube's surface can influence their behaviour in drilling fluids.

5.1.3 Low and High Shear Curvature Exponents

Iron NPs

As mentioned above, the flocculation of bentonite platelets at high temperature creates strong gel structures. Therefore, for these types of fluids increase in shear stress is measured while lowering the shear rate, specifically for lower shear rates. Hence, there is an increase in yield stress values, and flow index n becomes greater than unity showing shear thickening behaviour. This work aims to demonstrate the impact of NPs; therefore, using these values is still applicable. Also, the aim was to demonstrate the ability of NPs to facilitate the shear thinning behaviour of drilling fluids.

The impact of Fe NPs on n_{ls} and n_{hs} (flow index or shear curvature for low and high shear) values of bentonite fluids are presented in Figures 5.7 a, b. Adding 0.0095wt.% and 0.019wt.% Fe NPs promote the shear thinning behaviour and reduce the values of n_{ls} , with 0.019wt.% keeping the values lower than 1 at 80 °C. However, increased NPs concentration in the drilling fluids increases the n_{ls} at 80 °C. Moreover, 0.0095wt.% and 0.038wt.% increase the n_{hs} values of the base fluid while 0.019wt.% NPs slightly reduce the n_{hs} . Similar to Fe NPs, the addition of 0.019wt.% Fe-Si also reduces the n_{ls} of base fluid, while Fe-XG increases the value. Moreover, 0.019wt.% of Fe-Si and

Fe-XG reduces the n_{hs} values of the base fluids at 80 °C. However, 0.0095wt.% and 0.038wt.% NPs in the drilling fluids increase the n_{hs} . Results for Fe NPs show that the optimum concentration to reduce curvature exponent is 0.019wt.%, while at high concentrations, agglomeration of NPs increases the n_{ls} and n_{hs} . Silica on the surface of NPs forms a layer on the bentonite particles and neutralizes the positive charge of bentonite, reducing n_{ls} and n_{hs} .

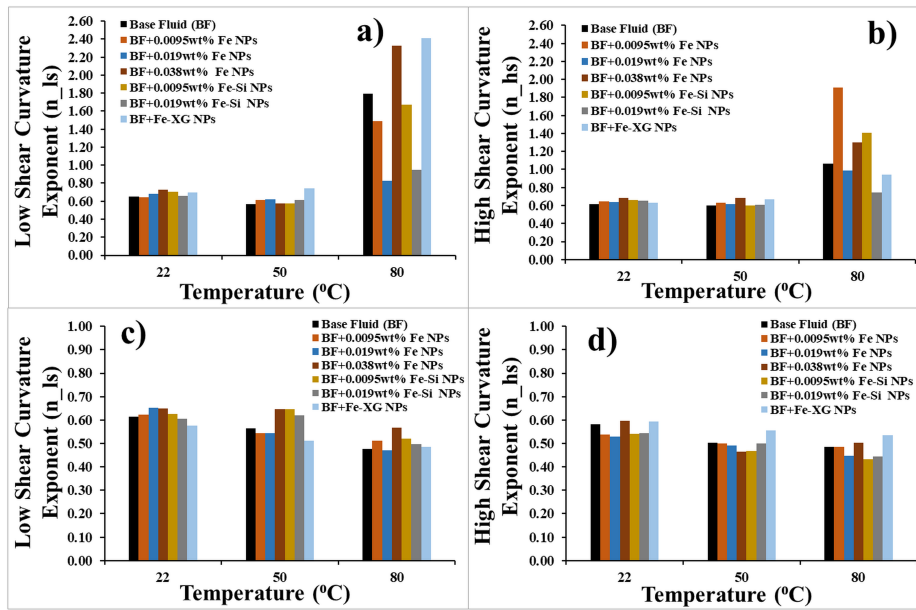


Figure 5.7: Impact of Fe, Fe-XG and Fe-Si NPs on n_{ls} and n_{hs} of water-based drilling fluids a) n_{ls} of bentonite drilling fluids b) n_{hs} of bentonite drilling fluids c) n_{ls} of KCl drilling fluids d) n_{hs} of KCl drilling fluids (Paper IV).

There is a minor effect of Fe NPs on the n_{ls} and n_{hs} values of KCl drilling fluids, as shown in Figures 5.7 c, d. The most significant impact is shown by 0.038wt.% Fe NPs in the fluid, with an increment of 19% in n_{ls} value at 80 °C. While Fe-Si also slightly increases the n_{ls} at 50 °C and 80 °C.

SiO₂ NPs

SiO₂ NPs do not have a significant impact on n_{ls} and n_{hs} values of bentonite drilling fluids at 22 °C and 50 °C; Figures 5.8 a, b. In contrast at 80 °C, 0.0095wt.% and 0.019wt.% NPs decrease the n_{ls} and n_{hs} of base fluids. The 0.019wt.% of Si-C NPs reduces the n_{ls} by 64%. Similar to Fe-Si NPs, SiO₂ NPs also control the shear thickening behaviour of bentonite drilling fluids owing to the neutralization of positive charge on bentonite platelets by SiO₂ NPs, inhibiting the temperature-induced flocculation of drilling fluids.

In the case of KCl drilling fluids NPs show a minor effect on the n_{ls} and n_{hs} values of the fluids (Figures 5.8 c, d). Again, NPs show impact at higher temperature by enhancing the n_{ls} for 0.019wt.% Si and Si-C NPs. Although there is a high amount of KCl salt in the system, NPs still provide slight increments in n_{ls} and n_{hs} values due to improved colloidal stability at high temperature.

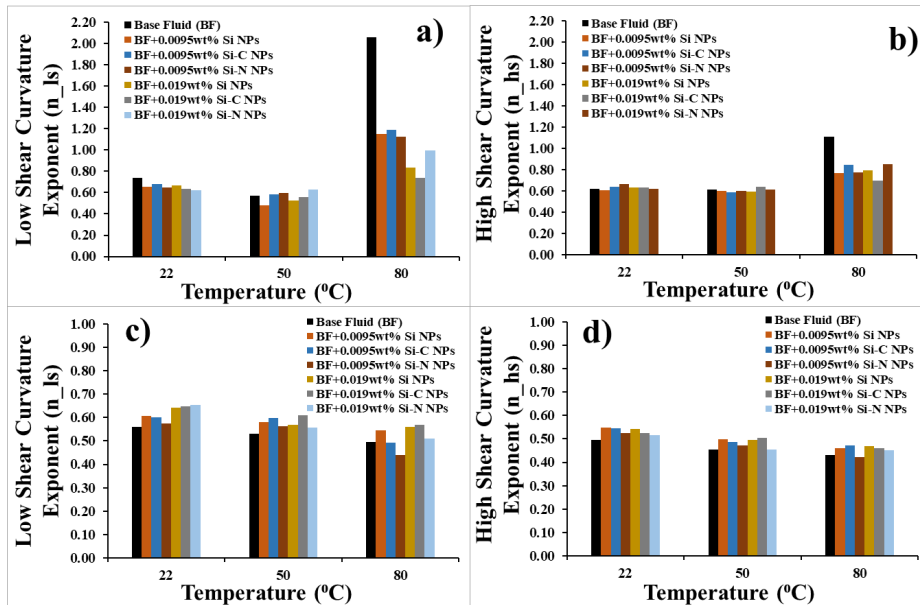


Figure 5.8: Impact of SiO₂ NPs on n_{ls} and n_{hs} of water-based drilling fluids a,b) n_{ls} and n_{hs} of bentonite drilling fluids c,d) n_{ls} and n_{hs} of KCl drilling fluids (Paper IV).

Nanotubes

Like other NPs, nanotubes also impact the bentonite drilling fluids at 80 °C. 0.019wt.% MW achieved an 84% decrease in n_{ls} , while a lower concentration of 0.0095wt.% of MW-OH and MW-COOH reduced the n_{ls} values by 38% and 67%, respectively, at 80 °C. Moreover, 0.0095wt.% MW and MW-OH increase the n_{hs} of base fluid but increasing the MW concentration in the drilling fluids reduces the n_{hs} values (Figures 5.9 a, b). The nanotubes demonstrate the ability to keep the n_{ls} values lower than 1 by disrupting the gel structures of bentonite. The presence of surfactant provides the uniform dispersion of nanotubes in the drilling fluids, minimizing bentonite agglomeration.

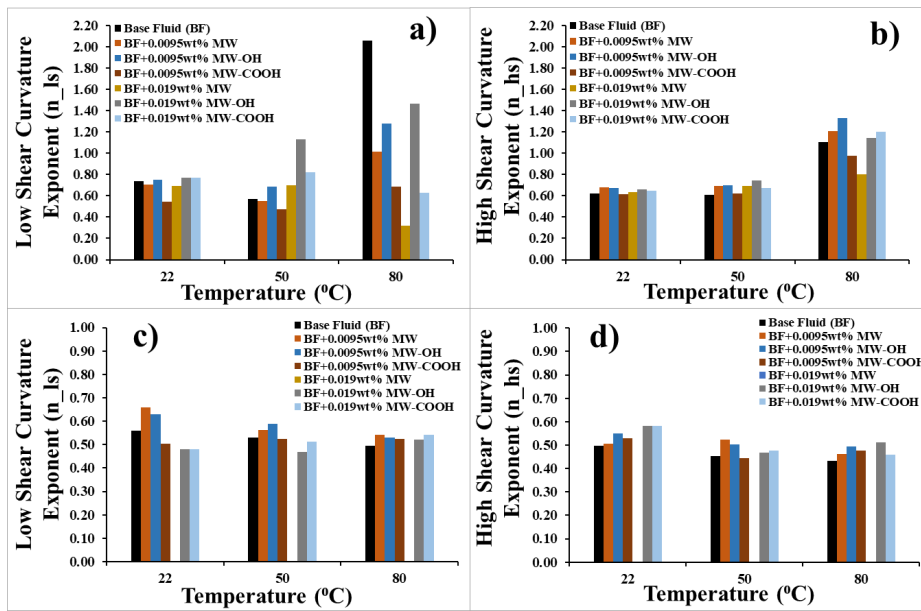


Figure 5.9: Impact of MWCNTs on n_{ls} and n_{hs} of water-based drilling fluids a,b) n_{ls} and n_{hs} of bentonite drilling fluids c,d) n_{ls} and n_{hs} of KCl drilling fluids (Paper IV).

As stated previously, the high concentration of nanotubes in the KCl drilling fluids forms two phases in the system due to the settling of drilling fluids additives. Therefore, in the case of 0.019wt.% MW in

the drilling fluids did not show the shear stress values at lower stress, see Figures 5.9 c, d. However, 0.019wt.% of MW-OH and MW-COOH kept the dispersions stable, but high nanotube concentrations only slightly increased n_{ls} values at 80 °C. Results for nanotubes depict that low concentration provides the desired performance compared to the high particle loading in the drilling fluids.

5.1.4 Yield and Surplus Stress

Iron NPs

Yield stress results for Fe NPs in the bentonite drilling fluids (Figure 5.10 a) show that 0.0095wt.% and 0.038wt.% Fe NPs increment the yield stress of base fluid by 13%, while 0.019wt.% do not alter the yield stress at 80 °C. In addition, Fe-XG slightly decreases the yield stress at 80 °C. Similarly, 0.019wt.% Fe-Si also reduces the yield stress but shows a more prominent reduction of 46%. Since 0.0095wt.% and 0.038wt.% Fe NPs increase yield stress, they reduce the surplus stress at 80 °C, see Figure 5.10 b. While 0.019wt.% Fe and Fe-Si, as well as Fe-XG, increases the surplus stress. Higher surplus stress can be beneficial when low pump pressure is required to start the flow of drilling fluids, as higher values of surplus stress at specific shear rates will achieve high flow rates.

The KCl drilling fluids with only a high concentration of Fe NPs, i.e., 0.038wt.%, increase the yield stress of fluids by 63% at 80 °C; see Figure 5.10 c. Furthermore, Fe-Si shows an increment in the yield stress, and 0.019wt.% NPs increase yield stress by 90% and 56% at 50 °C and 80 °C, respectively. While Fe-XG lowers the yield stress of base fluid at 22 °C, 50 °C, and 80 °C. Surplus stress results show that only 0.038wt.% Fe NPs reduce the surplus stress by 14% at 80 °C as shown in Figure 5.10 d. High salt concentration in the drilling fluids minimizes the stability of NPs, at lower concentration. While excessive agglomeration of Fe NPs may have promoted the increase in yield stress at 80 °C for 0.038wt.% Fe NPs in the base fluid.

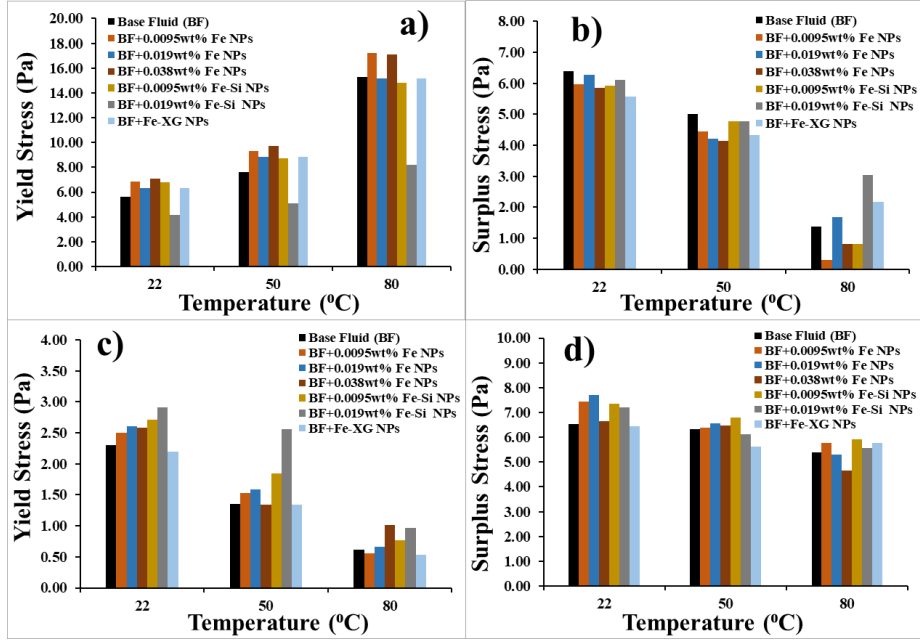


Figure 5.10: Yield stress and surplus stress of water-based drilling fluids with Fe, Fe-XG and Fe-Si NPs a) Yield stress of bentonite drilling fluids b) Surplus stress of bentonite drilling fluids c) Yield stress of KCl drilling fluids d) Surplus stress of KCl drilling fluids (Paper IV).

SiO₂ NPs

Figure 5.11 a, show the yield stress values of bentonite drilling fluids and fluids with *SiO₂* NPs. Si NPs and Si-C show a significant reduction in yield stress of base fluids at 22 °C, 50 °C, and 80 °C. Si and Si-C show almost 60% reduction in yield stress at 80 °C. While Si-N only shows a 31% reduction in yield stress at 80 °C. There is a substantial increase in surplus stress values of base fluid with the addition of Si, Si-C, and Si-N NPs, with Si-C showing the highest increase of 159% as shown in Figure 5.11 b. Yield stress results indicate that *SiO₂* NPs can reduce the strong gelling tendency of base fluids at high temperature by forming weaker structures at low shear rates, this can avoid potential wellbore instability issues.

Lower yield stress provides high surplus stress that allows lower pump pressure to start the flow of drilling fluids.

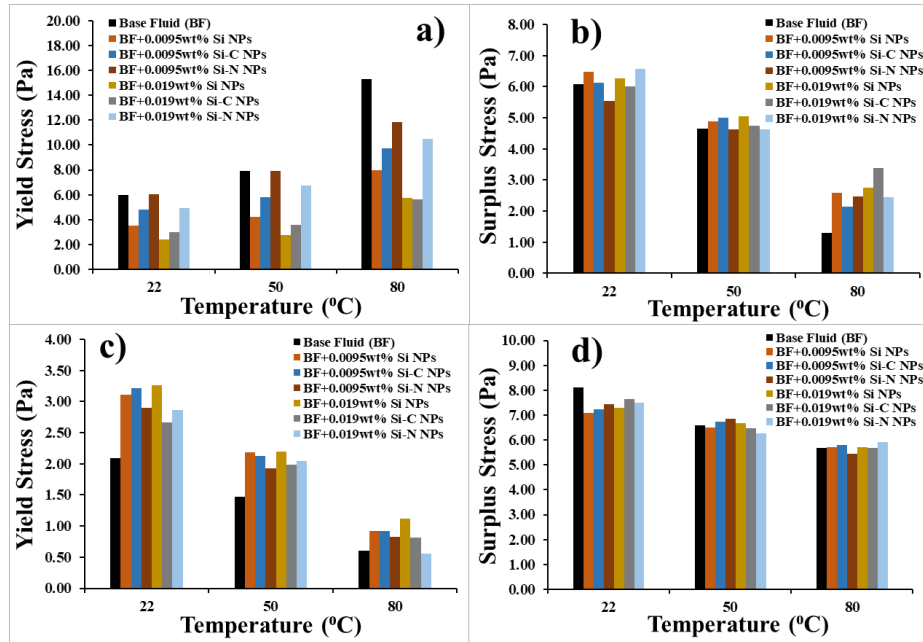


Figure 5.11: Yield stress and surplus stress of water-based drilling fluids with Si, Si-C and Si-N NPs a,b) Yield and surplus stress of bentonite drilling fluids c,d) Yield stress and surplus stress of KCl drilling fluids (Paper IV).

SiO_2 NPs attain higher yield stress for KCl drilling fluids, as indicated in Figure 5.11 c. Around 87% increase in yield stress of base fluid is achieved by the Si NPs at 80 °C. NPs show a minor impact on the surplus stress values of the base fluid, see Figure 5.11 d. The ability of SiO_2 NPs to stabilize the KCl drilling fluids at a lower shear rate enables the increase in yield stress.

Nanotubes

All three types of nanotubes increase the yield stress values of bentonite drilling fluids, see Figure 5.12 a. At high temperature, 0.0095wt.% MW increases the yield stress of base fluid by 16%.

However, 0.0095wt.% MW and MW-OH reduce the surplus stress of base fluids at 50 °C and 80 °C. While 0.019wt.% MW significantly increases the surplus stress at 80 °C (Figure 5.12 b). Results for nanotubes indicate that the adsorption of tubes on bentonite at a low shear rate enables the high yield stress.

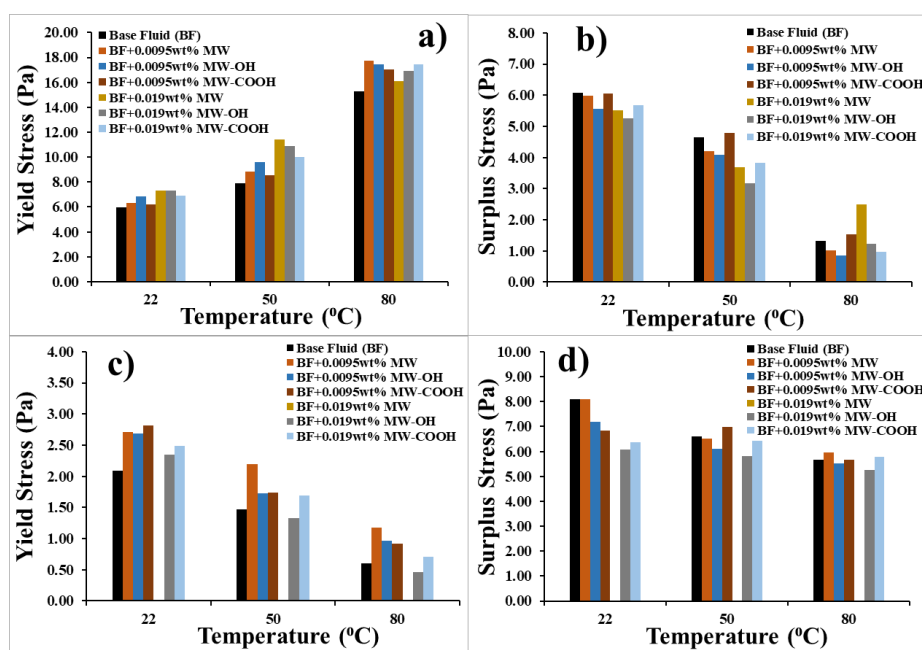


Figure 5.12: Yield stress and surplus stress of water-based drilling fluids with MW, MW-OH, MW-COOH a,b) Yield and surplus stress of bentonite drilling fluids c,d) Yield stress and surplus stress of KCl drilling fluids (Paper IV).

Results for KCl drilling fluids show that 0.0095wt.% MW, MW-OH, and MW-COOH increase the yield stress of base fluid at 22 °C, 50 °C, and 80 °C. However, increasing the concentration of MW in KCl drilling fluids provides no yield stress due to phase separation. Even though the presence of functional groups on MW-OH and MW-COOH provides yield stress values, there is still a decrease compared to the base fluid. Nanotubes show a slight impact on surplus stress values of the base fluid (Figure 5.12 c, d).

5.1.5 Viscoelastic Properties

Iron NPs

Viscoelastic properties of the drilling fluids can give further insight into the internal gel structure of fluids under dynamic conditions. Storage modulus can describe the energy stored by a material when the shear is applied, while loss modulus defines the energy lost by the material with the application of shear. The following section will show the impact of NPs on the viscoelastic properties of water-based drilling fluids.

Yield stress from viscoelastic data can be estimated from the plot between shear stress and strain rate. The stress at which the deviation from the linear viscoelastic region (LVE) range occurs is taken as yield stress. In addition, the point where storage and loss modulus become equal is called the flow point. The measurements were performed at 22 °C. Fe NPs show an increase in the base fluid's yield stress and flow points. For yield stress, 0.0095wt.% Fe NPs show the highest increase, followed by 0.038wt.% NPs and Fe-XG. However, 0.019wt.% reduces the base fluid's yield stress and flow point, as indicated in Table 5.1.

Table 5.1: Yield stress and flow point (Oscillatory) for bentonite drilling fluids (Paper I).

Samples	Yield Stress (Pa)	Flow Point (Pa)
Base fluid (BF)	4.60	8.46
BF + 0.0095wt.% Fe NPs	5.60	9.30
BF + 0.019wt.% Fe NPs	4.90	9.48
BF + 0.038wt.% Fe NPs	5.20	8.91
BF + 0.0095wt.% Fe-Si NPs	4.80	9.07
BF + 0.019wt.% Fe-Si NPs	3.30	7.74
BF + Fe-XG NPs	5.10	9.38

Table 5.2 shows the values for KCl drilling fluids, the addition of Fe NPs to the drilling fluids reduced the yield stress and flow point values

Table 5.2: Yield stress and flow point (Oscillatory) for KCl drilling fluids (Paper I).

Samples	Yield Stress (Pa)	Flow Point (Pa)
Base fluid (BF-1)	2.00	4.90
BF + 0.0095wt.% Fe NPs	2.00	4.63
BF + 0.019wt.% Fe NPs	1.90	4.39
BF + 0.0095wt.% Fe-Si NPs	2.40	4.91
BF + 0.019wt.% Fe-Si NPs	2.40	5.03
Base fluid (BF-2)	1.60	4.30
BF + 0.038wt.% Fe NPs	1.40	3.72
BF + Fe-XG NPs	2.00	4.59

due to the formation of weaker gel structures. In contrast, Fe-XG shows a slight increment in values owing to the gel-forming ability of the polymer. Moreover, Fe-Si also demonstrates improvement in yield stress and flow point.

SiO₂ NPs

SiO₂ NPs ability to control the gelation of bentonite influences the yield stress and flow point values of bentonite drilling fluids. All three types show a similar trend and decrease the values of the base fluid. An increase in NPs concentration in the fluids further reduces the values, where Si NPs showed the highest reduction. Although NPs decrease the yield flow point of base fluids, Si-C and Si-N show less reduction, especially at high concentrations, due to functional groups on the surface of NPs enabling gel formation with the bentonite, as indicated in Table 5.3. KCl drilling fluids with *SiO₂* NPs show increased yield stress and flow point values, see Table 5.4. The addition of 0.019wt.% provides the highest increase, while Si-C and Si-N demonstrate similar increases in yield stress values.

Table 5.3: Yield stress and flow point (Oscillatory) for bentonite drilling fluids.

Samples	Yield Stress (Pa)	Flow Point (Pa)
Base fluid (BF)	4.80	8.47
BF + 0.0095wt.% Si NPs	3.00	5.72
BF + 0.0095wt.% Si-C NPs	3.00	6.41
BF + 0.0095wt.% Si-N NPs	4.60	8.36
BF + 0.019wt.% Si NPs	2.10	4.22
BF + 0.019wt.% Si-C NPs	2.30	4.58
BF + 0.019wt.% Si-N NPs	3.90	7.53

Table 5.4: Yield stress and flow point (Oscillatory) for KCl drilling fluids.

Samples	Yield Stress (Pa)	Flow Point (Pa)
Base fluid (BF)	2.10	5.22
BF + 0.0095wt.% Si NPs	2.30	5.11
BF + 0.0095wt.% Si-C NPs	2.50	4.89
BF + 0.0095wt.% Si-N NPs	2.50	5.18
BF + 0.019wt.% Si NPs	2.90	5.71
BF + 0.019wt.% Si-C NPs	2.40	5.00
BF + 0.019wt.% Si-N NPs	2.40	5.04

Nanotubes

Table 5.5 and Table 5.6 show the results for nanotubes. Based on the previous results, only low concentrations of nanotubes were used for viscoelastic properties. Nanotubes increase the yield stress and flow points of the base fluid in the case of both bentonite and KCl drilling fluids, except for 0.0095wt.% MW-OH in KCl drilling fluids, which slightly decreases the flow point of the base fluid. MW-COOH provides slightly more increase in yield stress and flow point values of KCl drilling fluids owing to better interaction of carboxylic acid with the additives in the fluid system.

Table 5.5: Yield stress and flow point (Oscillatory) for bentonite drilling fluids.

Samples	Yield Stress (Pa)	Flow Point (Pa)
Base fluid (BF)	4.80	8.47
BF + 0.0095wt.% MW	6.00	9.54
BF + 0.0095wt.% MW-OH	6.00	9.62
BF + 0.0095wt.% MW-COOH	5.70	9.50

Table 5.6: Yield stress and flow point (Oscillatory) for KCl drilling fluids.

Samples	Yield Stress (Pa)	Flow Point (Pa)
Base fluid (BF)	2.10	5.22
BF + 0.0095wt.% MW	2.70	5.38
BF + 0.0095wt.% MW-OH	2.50	5.06
BF + 0.0095wt.% MW-COOH	3.00	5.60

5.2 Mechanical Friction

Iron NPs

It is important to keep the torque and drag during the drilling operation to a minimum level. Therefore, to achieve this, lubrication provided by the drilling fluid is crucial. The mechanical friction between the string and hole/casing depends on the fluid which is present in the well. Improving the lubricating properties of drilling fluids will permit smooth casing running operation and allow drilling longer distances.

The presence of bentonite in water-based drilling fluids increases mechanical friction. NPs addition to these fluids can reduce the coefficient of friction as depicted in Figures 5.13 a, b. The addition of

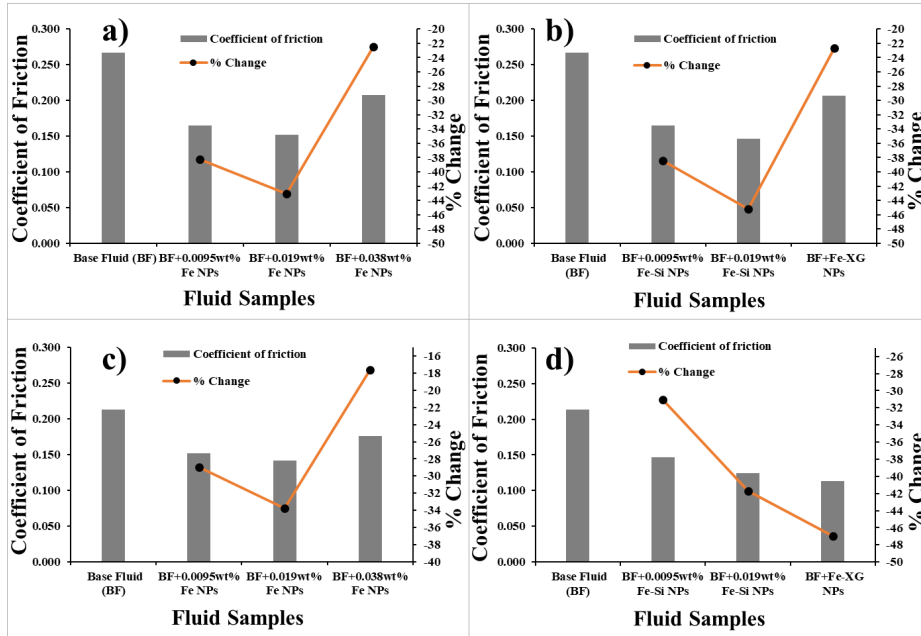


Figure 5.13: Friction values of water-based drilling fluids a, b) Bentonite-based fluids with NPs c, d) KCl-based fluids with NPs (Paper I).

0.019wt.% Fe and Fe-Si demonstrate the highest decrease in friction. The possible reason for this behaviour is the ability of NPs to form a lubricating film around the surface of micro-sized additives present in the fluid. However, an increase in NPs concentration slightly increases the friction compared to a lower concentration, owing to the agglomeration of NPs. Polymer presence on the surface of NPs also contributed to a slighter decrease in friction of base fluids.

The absence of bentonite in the KCl drilling fluids permits the low friction values for these fluids, as indicated in Figures 5.13 c, d. Even though KCl drilling fluids show low friction values, NPs can still further decrease the friction coefficient. In this case, 0.019wt.% Fe and Fe-Si and Fe-XG NPs showed a significant decrease in friction.

SiO₂ NPs

Since *SiO₂* NPs reduce the excessive gelation of bentonite drilling fluids, they show a decrease in friction values of the fluids, especially at high concentrations, see Figures 5.14 a, b. Surface-modified NPs, i.e., Si-C and Si-N, show more reduction compared to the Si NPs. The small size of Si-N NPs enables the NPs to enter the contact zone between the rough surfaces.

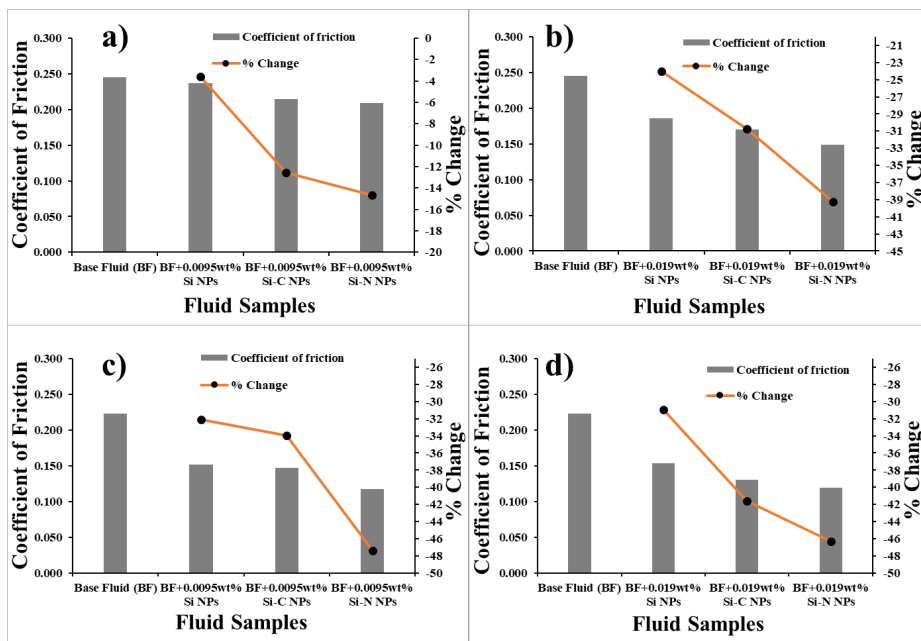


Figure 5.14: Friction values of water-based drilling fluids with *SiO₂* NPs a,b) Bentonite drilling fluids with NPs c,d) KCl drilling fluids with NPs.

In the case of KCl drilling fluids, NPs show a similar trend and decrease the friction of base fluids. Again, the ability of NPs to form a lubricating film around the additives present in the fluid contributed to this behaviour. NPs act as a fluid and fill the microscopic spaces between the rough surfaces in the fluid, see Figures 5.14 c, d.

Nanotubes

MWCNTs are known for their lubricating properties. In bentonite drilling fluids, nanotubes are physically adsorbed on the bentonite and other additives in drilling fluids and lower the friction values of the base fluid. Nanotubes provide a lubricating coating on rough surfaces and reduce friction, especially at lower concentrations. Uniform and stable dispersion of nanotubes in surfactant contributed to effective interaction with the drilling fluids. A high amount of nanotubes in the fluids may cause slight agglomeration of nanotubes, which minimizes the lubricating effect (Figures 5.15 a, b). Similar behaviour is observed for KCl drilling fluids, as shown in Figures 5.15 c, d, where MW shows the highest reduction in friction of the base fluids.

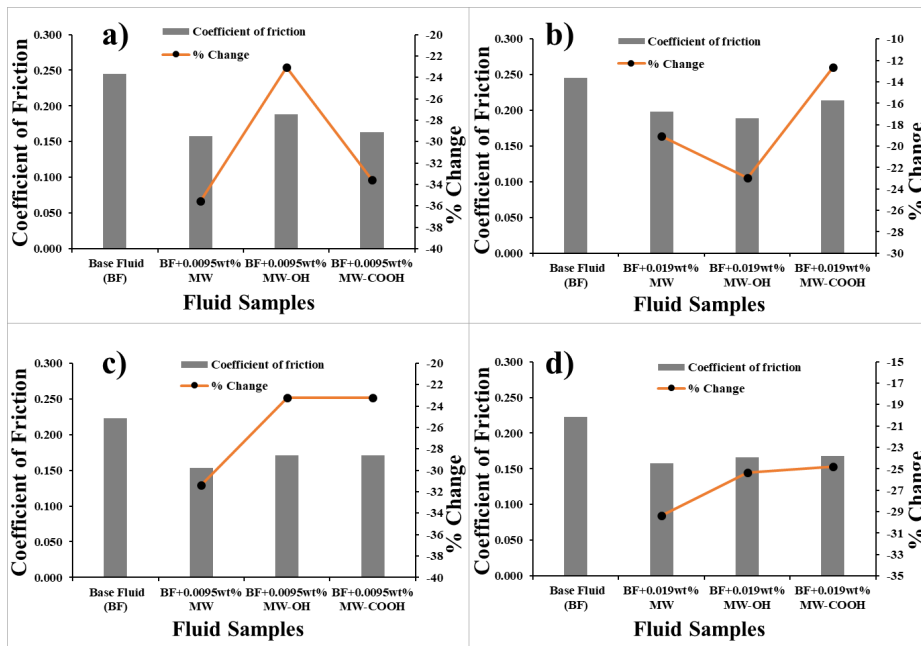


Figure 5.15: Friction values of water-based drilling fluids with MWCNTs a,b) Bentonite drilling fluids with nanotubes c,d) KCl drilling fluids with nanotubes.

5.3 Fluid Loss

Iron NPs

The drilling fluids additive and solid particles that construct the filter cake are crucial in controlling the fluid loss to the formation. Proper control of fluid loss to the formation is essential to improve the quality of drilling fluids. The following section presents the ability of NPs to control the fluid loss of water-based drilling fluids.

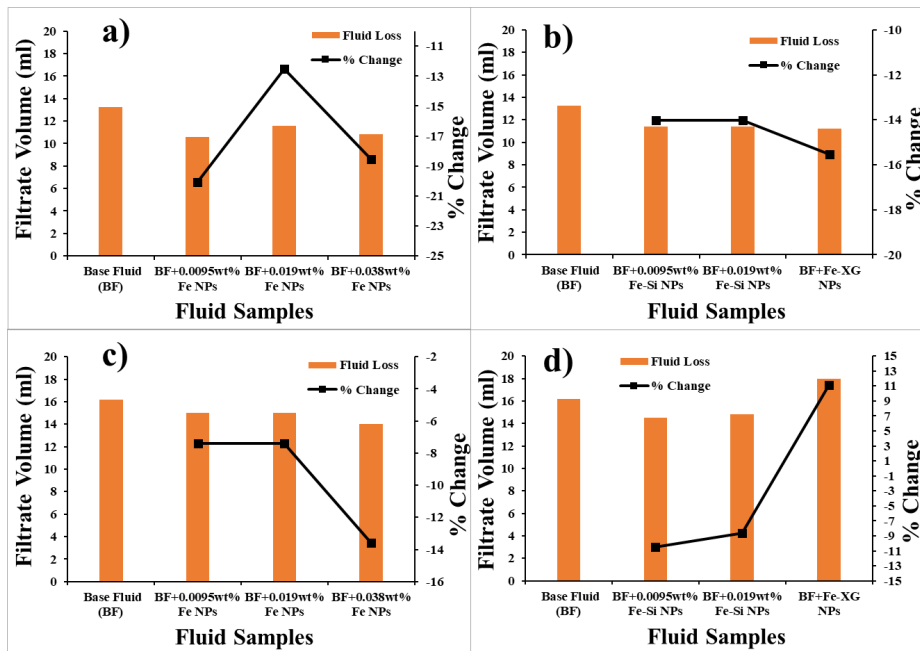


Figure 5.16: Filtrate volume of water-based drilling fluids after fluid loss test a,b) Bentonite-based fluids with NPs c, d) KCl-based fluids with NPs (Paper I).

The fluid loss results for the bentonite drilling fluids and fluids with NPs are shown in Figures 5.16 a, b. Fe NPs with different concentrations show similar reductions in the fluid loss values. The lowest percentage of NPs (0.0095wt.%) in the fluids resulted in the highest decrease in fluid loss. Polymer coating on Fe NPs, i.e., Fe-XG, also shows a 16% decrease in fluid loss. The possible reason for a

reduction in fluid loss is the ability of NPs to fill the micropores in the filter cake, as confirmed by the SEM analysis. Even though the Fe-Si NPs reduce the viscosity of the bentonite drilling fluids, they still demonstrate a decrease in fluid loss owing to the filling of pores in the filter cake. However, the decrease in fluid loss is less compared to 0.0095wt.% Fe NPs, which explains that the presence of silica on Fe NPs creates electrostatic repulsion with bentonite particles.

Figures 5.16 c, d shows the impact of NPs on KCl drilling fluids. Higher concentration of Fe NPs in the fluid shows the most considerable reduction of 14% compared to other concentrations. This shows that at room temperature and high pressure, more particles in the fluid allow better filling of pores in the filter cake that controls fluid flow. Fe-Si NPs also show a similar decrease in fluid loss, attributed to the increase in viscosity of the fluids with NPs that construct more compact filter cake. However, in the case of Fe-XG, there is an increase in fluid loss due to weaker gel formation of Fe-XG with KCl drilling fluids.

SiO₂ NPs

SiO₂ NPs in the bentonite drilling fluids show a reduction in the fluid loss values of the base fluid. Si-N with 0.0095wt.% shows a 14% reduction in fluid loss values of the drilling fluids (Figures 5.17 a, b). However, an increase in NPs percentage in the drilling fluids provides a slighter decrease in fluid loss owing to a decrease in the viscosity of the fluids.

SiO₂ NPs show a minor reduction in fluid loss values of KCl drilling fluids see Figures 5.17 c, d. This may be due to weak interparticle interaction of NPs with the additives in the drilling fluids that disrupt at high pressure. Here again, Si-N provides the highest reduction of 13%, showing the ability of finer particles to fill the pores in the cake structure.

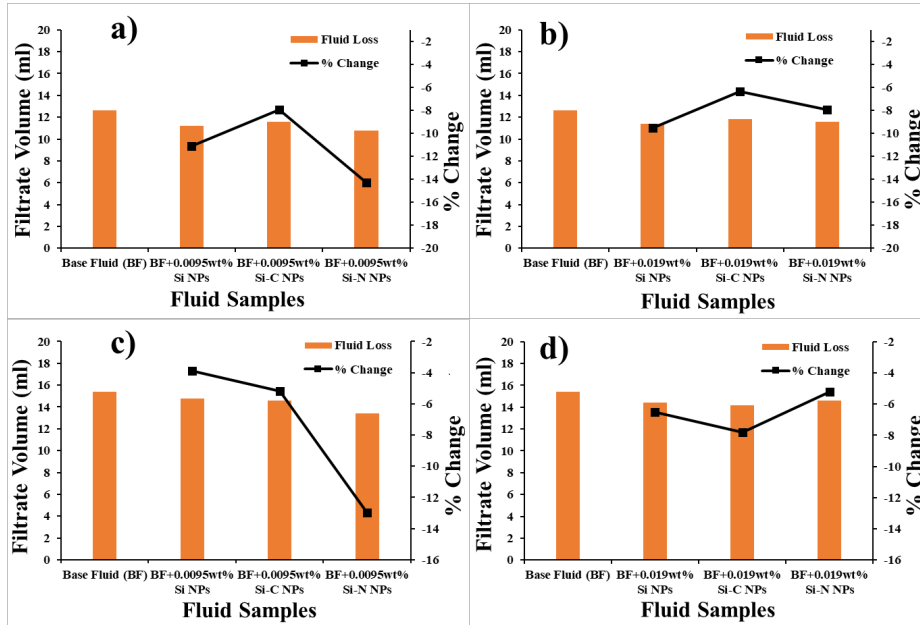


Figure 5.17: Fluid loss of water-based drilling fluids a,b) Bentonite drilling fluids with NPs c,d) KCl drilling fluids with NPs.

Nanotubes

Adsorption of nanotubes on bentonite and KCl slightly decreases fluid loss values of both bentonite and KCl drilling fluids by filling the micropores in filter cake, see Figures 5.18 a, b. The slight decrease is due to the non-significant bridging of the gaps in the cake structure by nanotubes. MW-COOH with 0.0095wt.% in bentonite drilling fluids reduces the fluid loss by 10%.

However, for KCl drilling fluids, MW-COOH increases the fluid loss, showing the ability of carboxyl acid groups on the surface of MW-COOH to create a weaker structure with KCl salt. Even though MW-COOH improves the gel strength of fluid still, high pressure disrupts the structure of the filter cake, causing more fluid loss. Nevertheless, for MW and MW-OH, the fluid loss decreases by 9% for KCl drilling fluids, which shows the ability of these nanotubes to maintain the gel strength even under pressure.

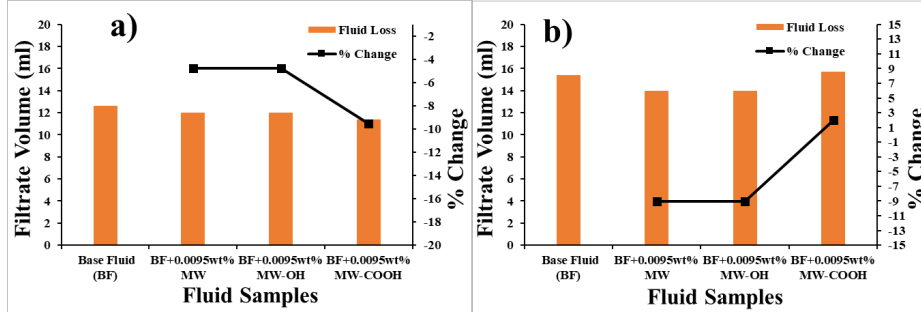


Figure 5.18: Fluid loss of water-based drilling fluids a,b) Bentonite drilling fluids with nanotubes c,d) KCl drilling fluids with nanotubes.

5.4 Microscale Analysis of Filter Cake

Iron NPs

SEM images of filter cake formed after the fluid loss test of bentonite drilling fluids with and without NPs are shown in Figures 5.19 a-f. The SEM image with Fe NPs, Figures 5.19 c, d confirms the presence of NPs in the cake as pointed by the arrow. The ability of NPs to fill the voids in the cake structure is the possible reason for the reduction of fluid loss. In the case of Fe-XG, as shown in Figure 5.19 e, f, the particles are deposited on the clay platelets. Long chains of XG provide better sealing ability, and the particles bridge the pore spaces in the cake structure. However, SEM analysis confirms the agglomeration of particles even for Fe-XG. This hinders the ability of NPs to minimize fluid loss further.

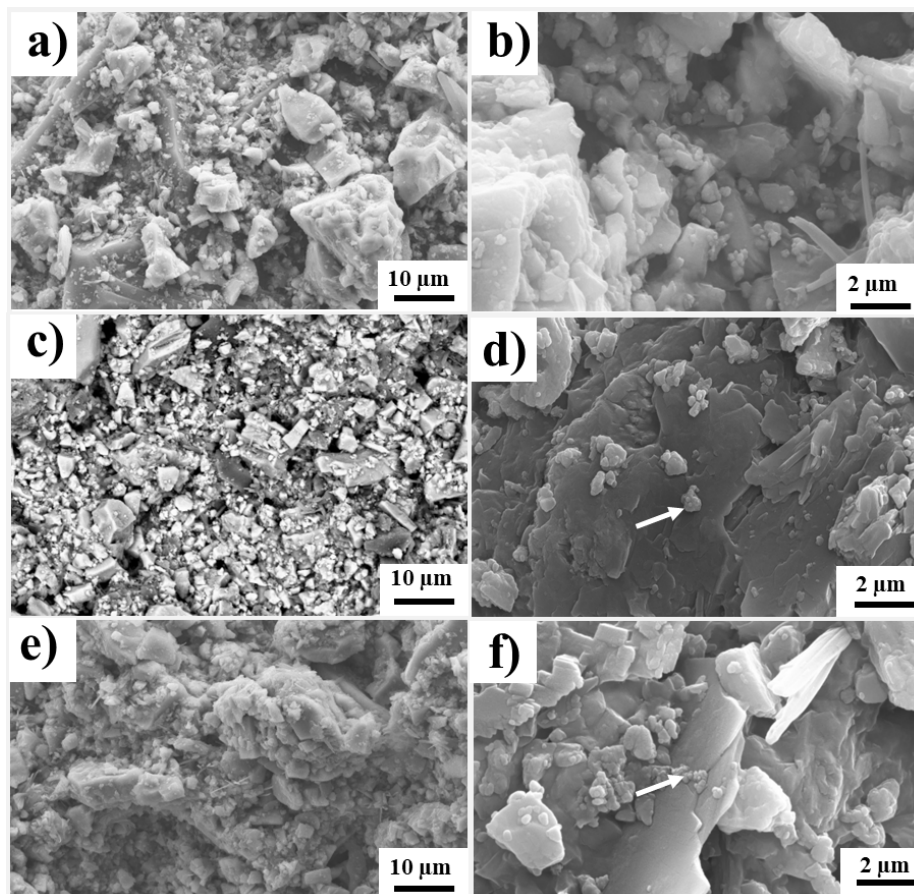


Figure 5.19: SEM images of filter cake of bentonite drilling fluids a,b) Structure of filter cake for base fluid c,d) Structure of filter cake for Fe NPs e,f) Structure of filter cake for Fe-XG (Paper I).

Fe-Si NPs also adsorbed on the cake structure and facilitate fluid loss reduction by filling the cake structure's micropores compared to base fluid, as presented in Figures 5.20 a-d.

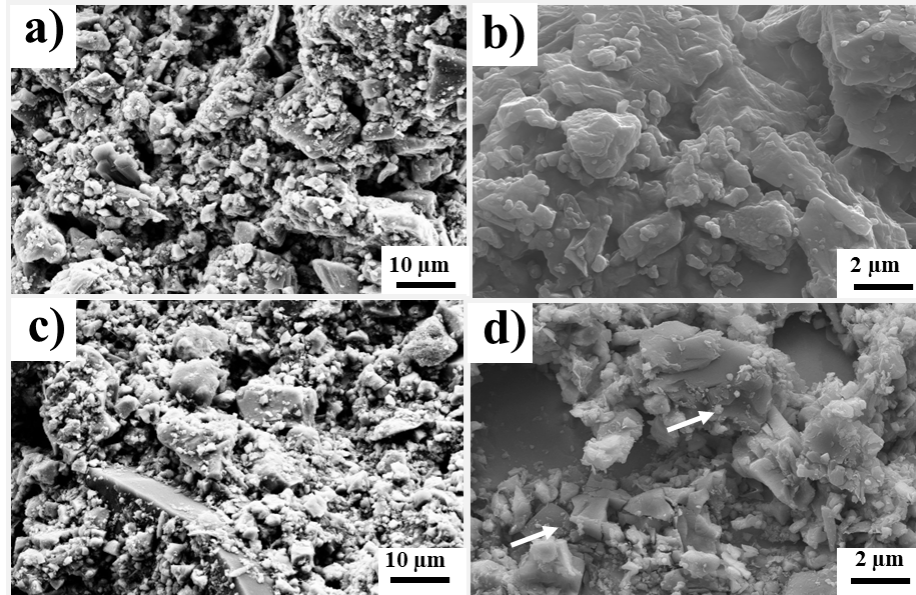


Figure 5.20: SEM images of filter cake of bentonite drilling fluids a,b) Structure of filter cake for base fluid c,d) Structure of filter cake for Fe-Si NPs.

Similarly, for KCl drilling fluids, SEM images confirm the presence of NPs in the cake structure, see Figures 5.21 c-f. Although NPs fill the voids in the cake structure and are adsorbed on the salt surface, the cake structure with NPs still has large pores in the structure, contributing to high fluid loss values. Moreover, for Fe-XG, the high fluid loss values might be due to the deposition of NPs on a salt surface that inhibits the ability to block the pores in the cake structure. Moreover, salt dissociation induces flocculation, and large agglomerates of Fe-XG formed which created voids in the structure, as shown in Figures 5.21 e, f.

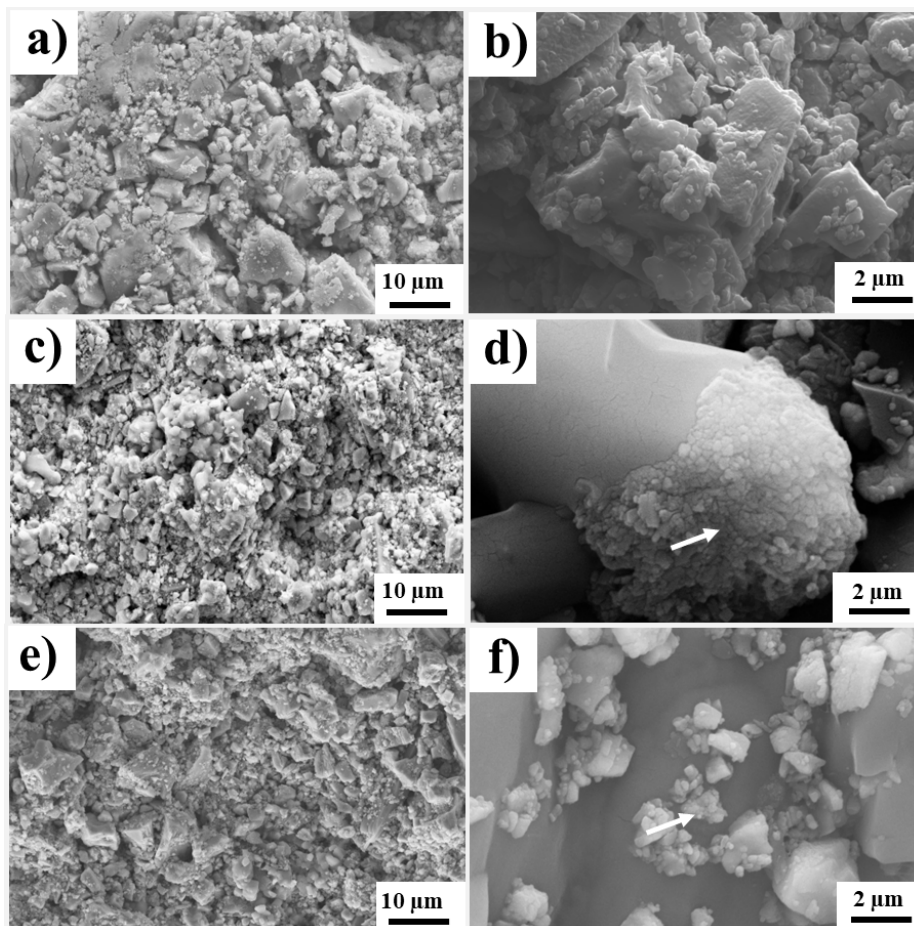


Figure 5.21: SEM images of filter cake of KCl drilling fluids a,b) Structure of filter cake for base fluid c,d) Structure of filter cake for Fe NPs e,f) Structure of filter cake for Fe-XG (Paper I).

Fe-Si NPs could bridge the gaps in the cake structure formed by KCl drilling fluids, as indicated in Figures 5.22 c, d. NPs deposited on the surface of the cake fill the empty spaces in the cake structure, lowering the fluid loss values.

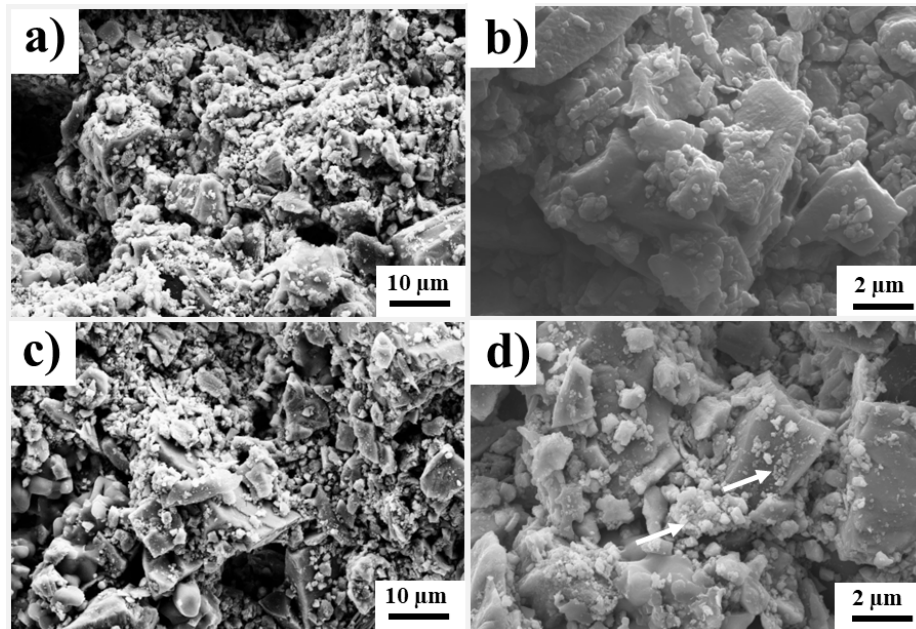


Figure 5.22: SEM images of filter cake of KCl drilling fluids a,b) Structure of filter cake for base fluid c,d) Structure of filter cake for Fe-Si NPs.

SiO₂ NPs

Figures 5.23 a-h show the SEM images for the filter cake formed by bentonite drilling fluids and drilling fluids with *SiO₂* NPs. Images for all three types of *SiO₂* NPs show that although NPs fill the voids in the cake structure, there are still pores present in the cake structure. This inhibits the further reduction in fluid loss. The ability of Si-N to provide a higher decrease in fluid loss is due to the more compact structure formed by the NPs, see Figures 5.23 g, h.

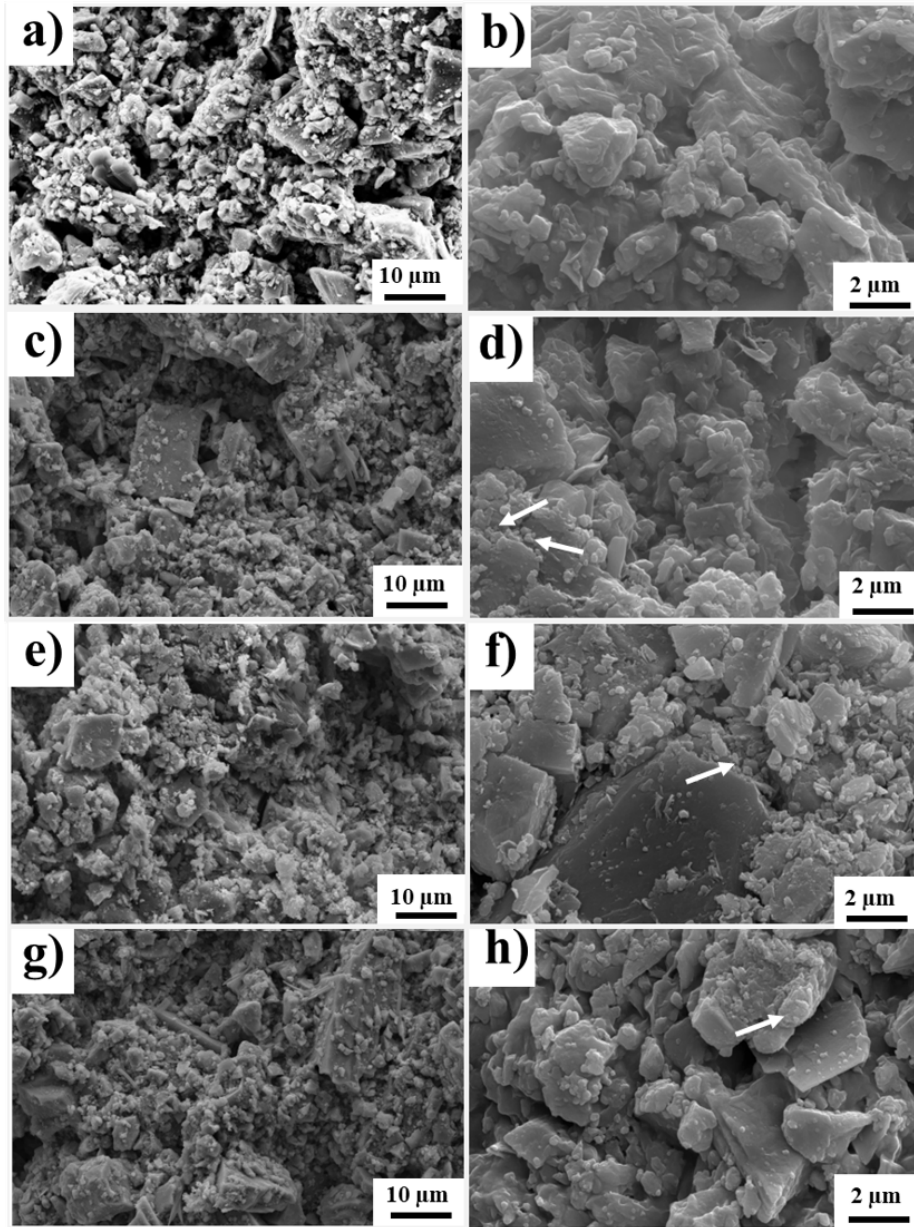


Figure 5.23: SEM images of filter cake of bentonite drilling fluids a,b) Base fluid c,d) Si NPs e,f) Si-C NPs g,h) Si-N NPs.

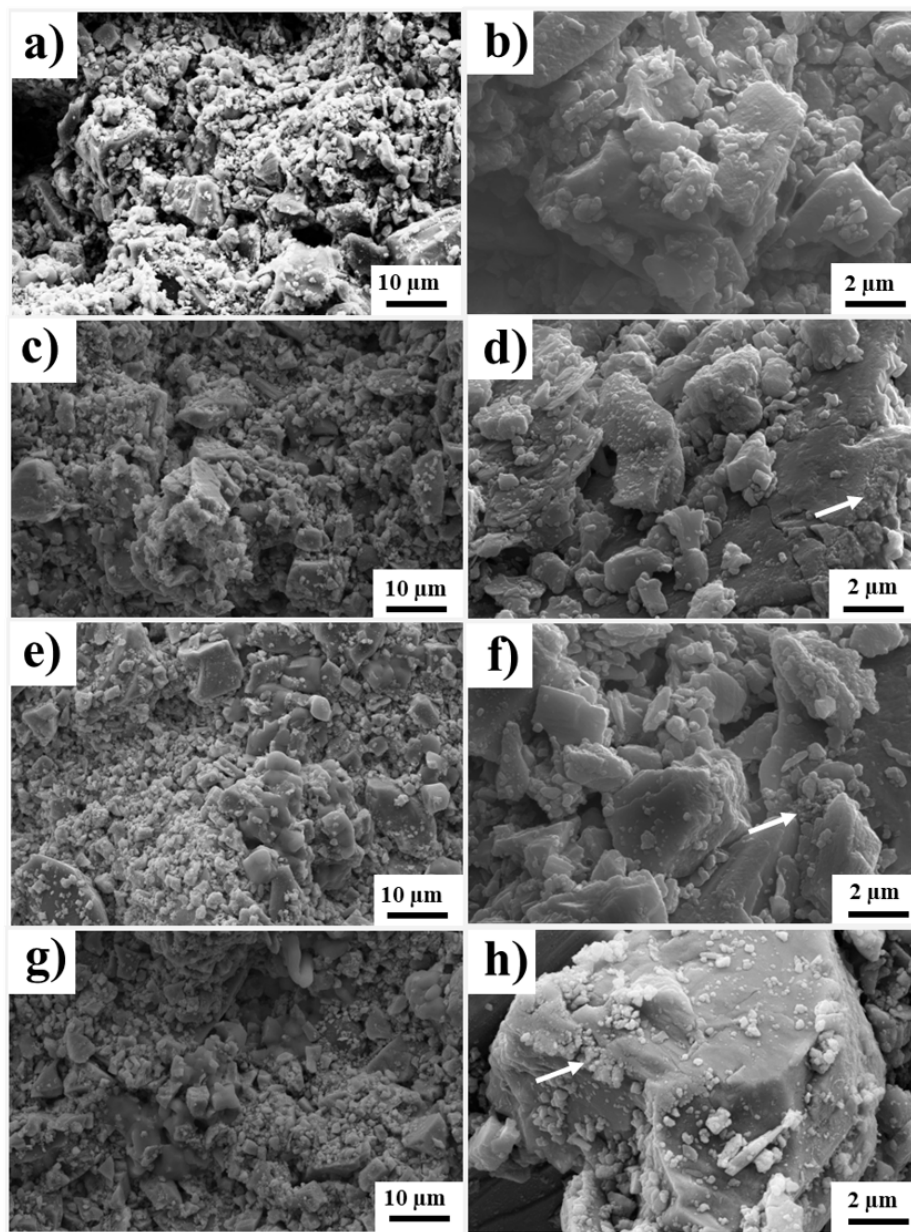


Figure 5.24: SEM images of filter cake of KCl drilling fluids a,b) Structure of filter cake for base fluid c,d) Structure of filter cake with Si NPs fluid e,f) Structure of filter cake with Si-C NPs g,h) Structure of filter cake with Si-N NPs.

Furthermore, for KCl drilling fluids, again NPs deposited on the cake structure, and SEM images confirmed the presence of NPs throughout the cake structure. However, in the case of Si NPs and Si-C, the NPs could not construct a compact cake structure, as indicated in Figures 5.24 c-f. In contrast, Si-N NPs form a comparatively compact structure, and there is a uniform distribution of NPs on the surface cake, which explains the ability of Si-N NPs to provide a higher decrease in fluid loss (Figures 5.24 g, h).

Nanotubes

SEM images for bentonite drilling fluids filter cake with nanotubes confirm the presence of tube structures in the cake; see Figures 5.25 a-h. Nanotubes are deposited on the clay surface present in the cake structure. However, owing to the large size of the tubes, they cannot significantly reduce the fluid loss. MW-COOH bridge gap in the cake structure, which may be a reason for more decrease in fluid loss compared to other nanotubes.

Nanotubes are present in the cake structure of KCl drilling fluids. Again, nanotubes deposited on the cake structure and interacted with the KCl salt without filling the voids in the microstructure, as presented in Figures 5.26 a-h. Still, the decrease in fluid loss by MW and MW-OH is due to the bridging of voids in the structure by nanotubes.

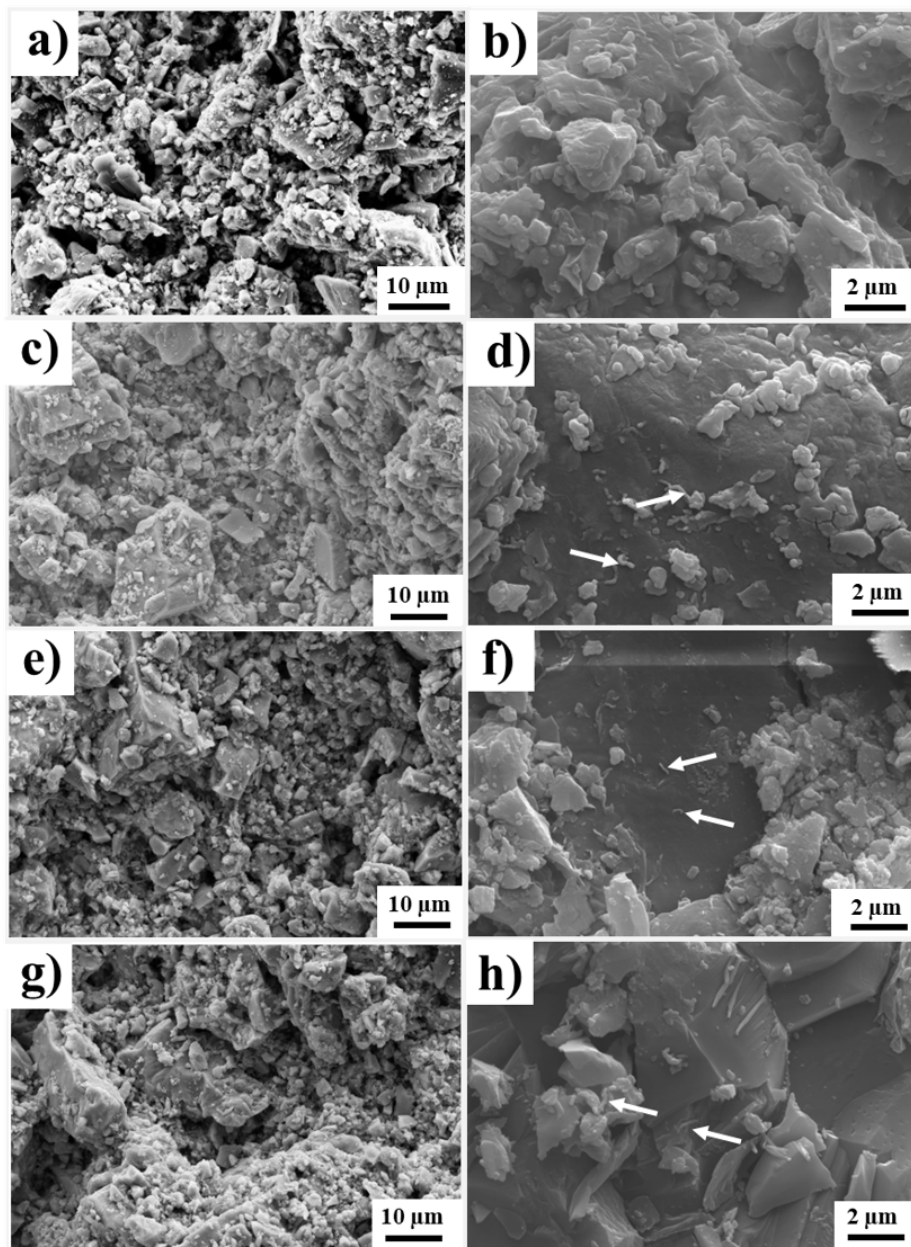


Figure 5.25: SEM images of filter cake of bentonite drilling fluids
a,b) Base fluid c,d) MW e,f) MW-OH g,h) MW-COOH.

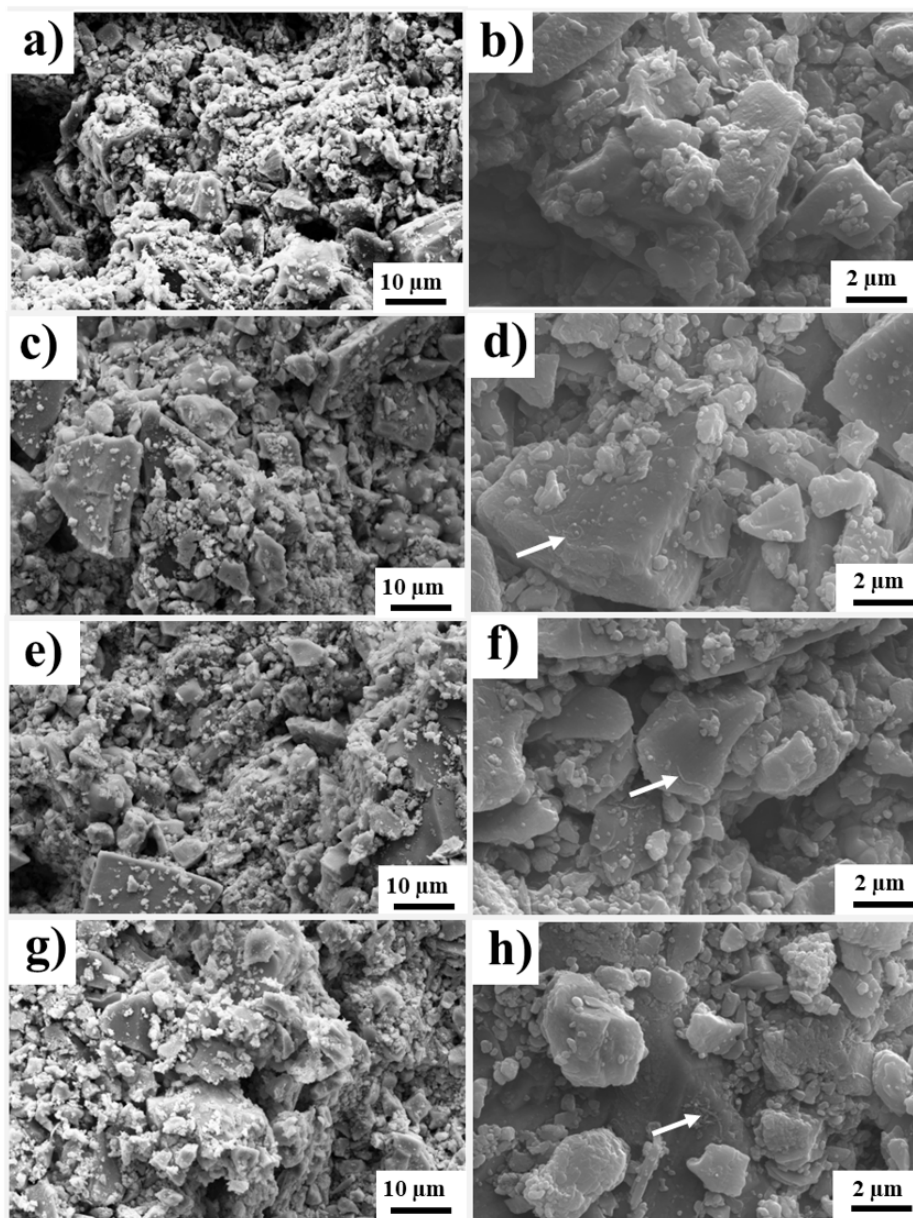


Figure 5.26: SEM images of filter cake of KCl drilling fluids a,b) Base fluid c,d) MW e,f) MW-OH g,h) MW-COOH.

5.5 Energy Dispersive X-ray Spectroscopy

Iron NPs

EDS analysis for filter cake formed by bentonite drilling fluid with Fe NPs shows the high amount of Fe NPs present throughout the cake structure compared to base fluid, as shown in Figures 5.27 a-f. Figures 5.27 c, d show that Fe NPs are uniformly distributed in the cake structure. However, the Fe-XG NPs are not uniformly distributed in the cake structure as depicted in Figures 5.27 e, f. This may be possibly due to the coating of XG on the surface of NPs.

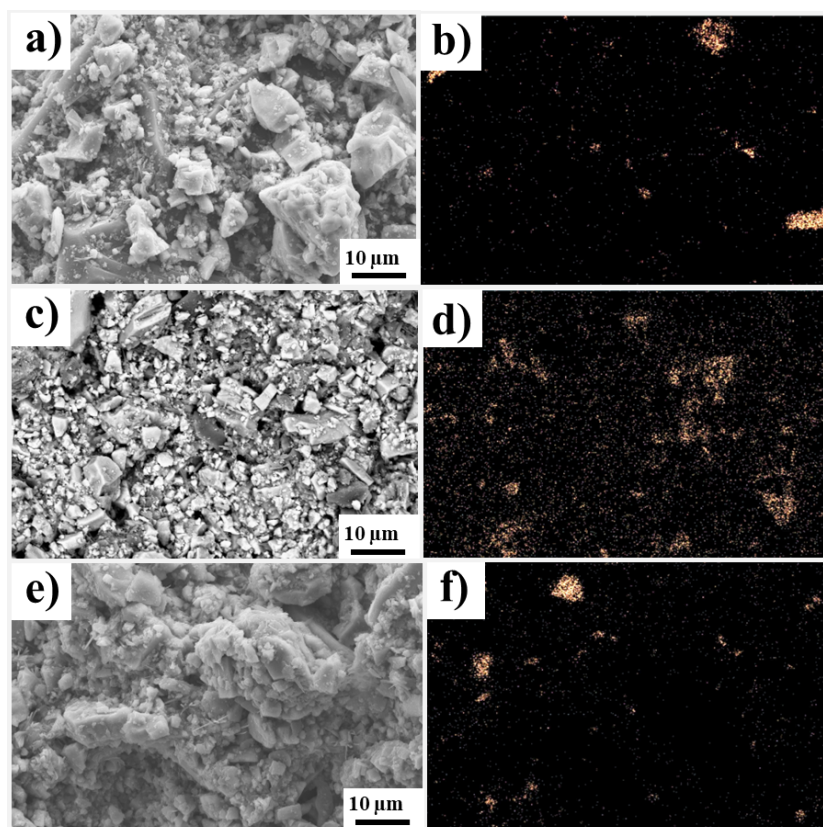


Figure 5.27: EDS analysis of filter cake formed by bentonite drilling fluids a,b) Base fluid c,d) Base fluid with Fe NPs e,f) Base fluid with Fe-XG NPs (Paper I).

Also, the agglomeration of Fe-XG can be a reason for this behaviour. Surface modification of Fe NPs with silica i.e., Fe-Si NPs provides better distribution of NPs in the cake structure as presented in Figures 5.28 c, d, as compared to the base fluid.

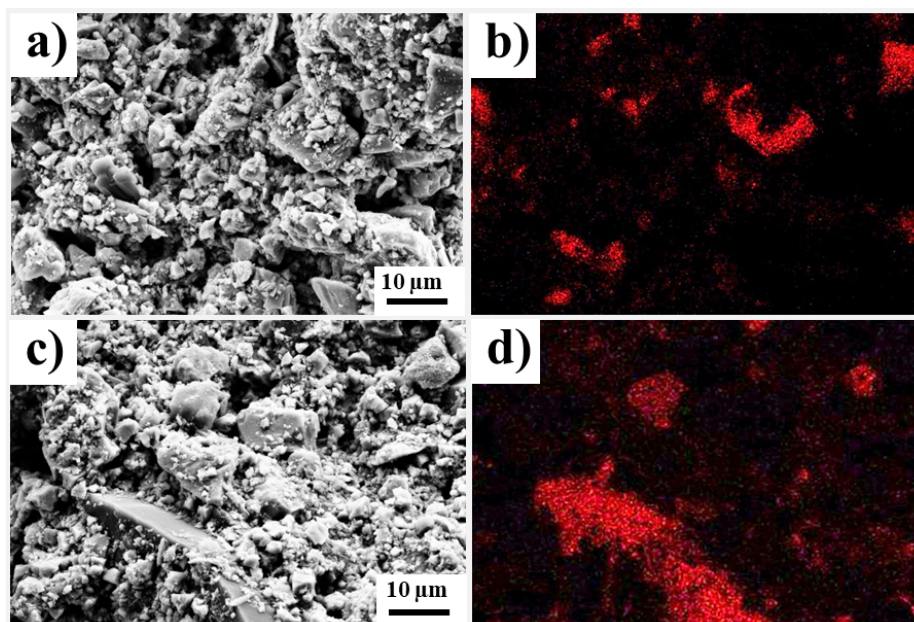


Figure 5.28: EDS analysis of filter cake formed by bentonite drilling fluids a,b) Base fluid c,d) Base fluid with Fe-Si NPs.

In the case of KCl drilling fluids, although the Fe NPs are present in the cake structure as the content of Fe is higher for fluids with NPs, still the NPs are not distributed throughout the cake structure possibly due to agglomeration of NPs. Hence there is less reduction in fluid loss. Similar behaviour can be observed for Fe-XG, as shown in Figures 5.29 c-f.

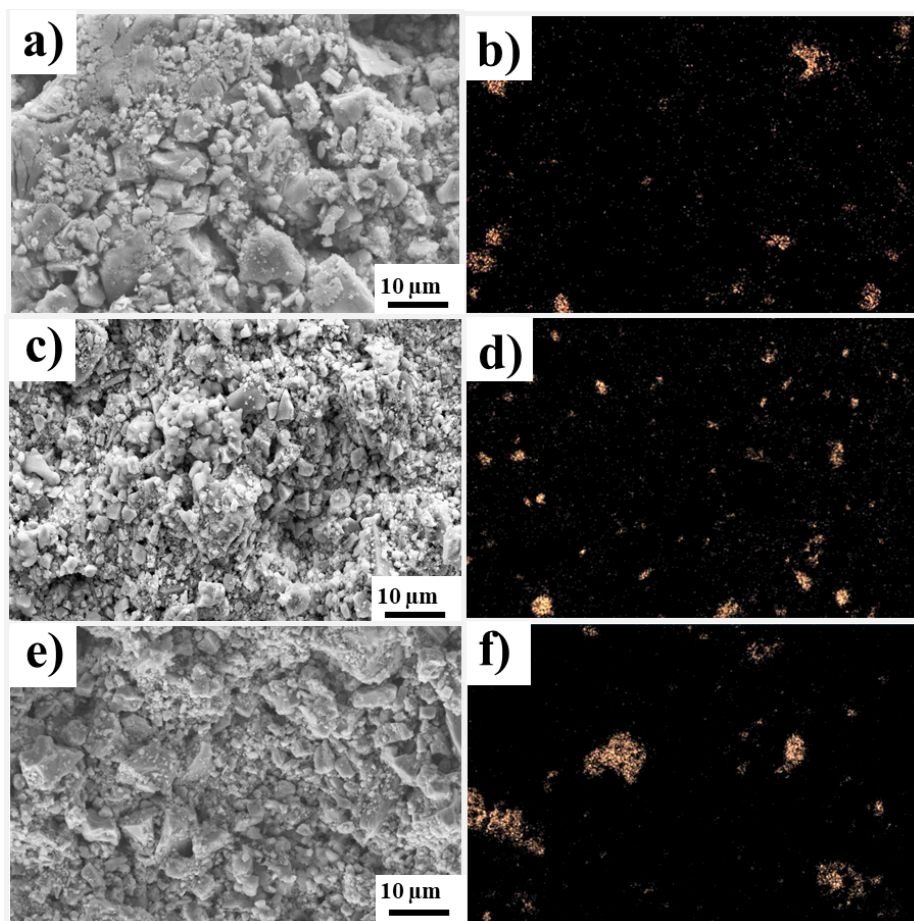


Figure 5.29: EDS analysis of filter cake formed by KCl drilling fluids a,b) Base fluid c,d) Base fluid with Fe NPs e,f) Base fluid with Fe-XG NPs (Paper I).

For Fe-Si NPs, there is a high amount of SiO_2 in the cake structure with NPs; see Figures 5.30 c, d. The presence of SiO_2 in the base fluid is due to bentonite. The difference between Figures 5.30 b and d shows the ability of NPs to create a more compact structure by dispersing throughout the cake structure.

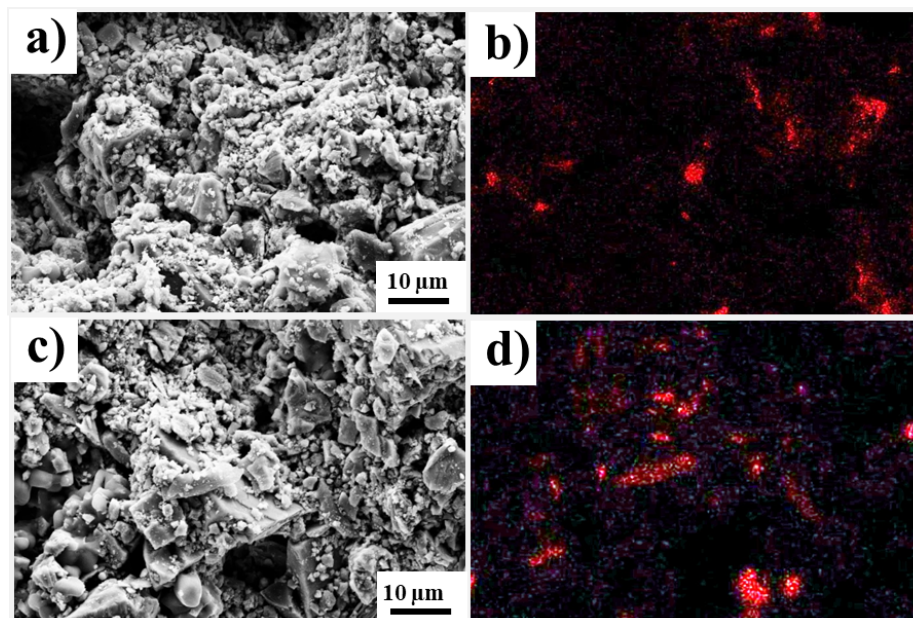


Figure 5.30: EDS analysis of filter cake formed by KCl drilling fluids a,b) Base fluid c,d) Base fluid with Fe-Si NPs.

SiO₂ NPs

SiO₂ NPs are deposited on the filter cake surface formed by bentonite drilling fluids, as shown in Figures 5.31 c-h. Compared to base fluid, the *SiO₂* NPs filled the voids by being uniformly distributed throughout the cake structure.

In the case of KCl fluids, the results show that NPs are not uniformly distributed in the cake structure. They are deposited on the salt surface or other additives in the fluid system, as shown in Figures 5.32 c-h.

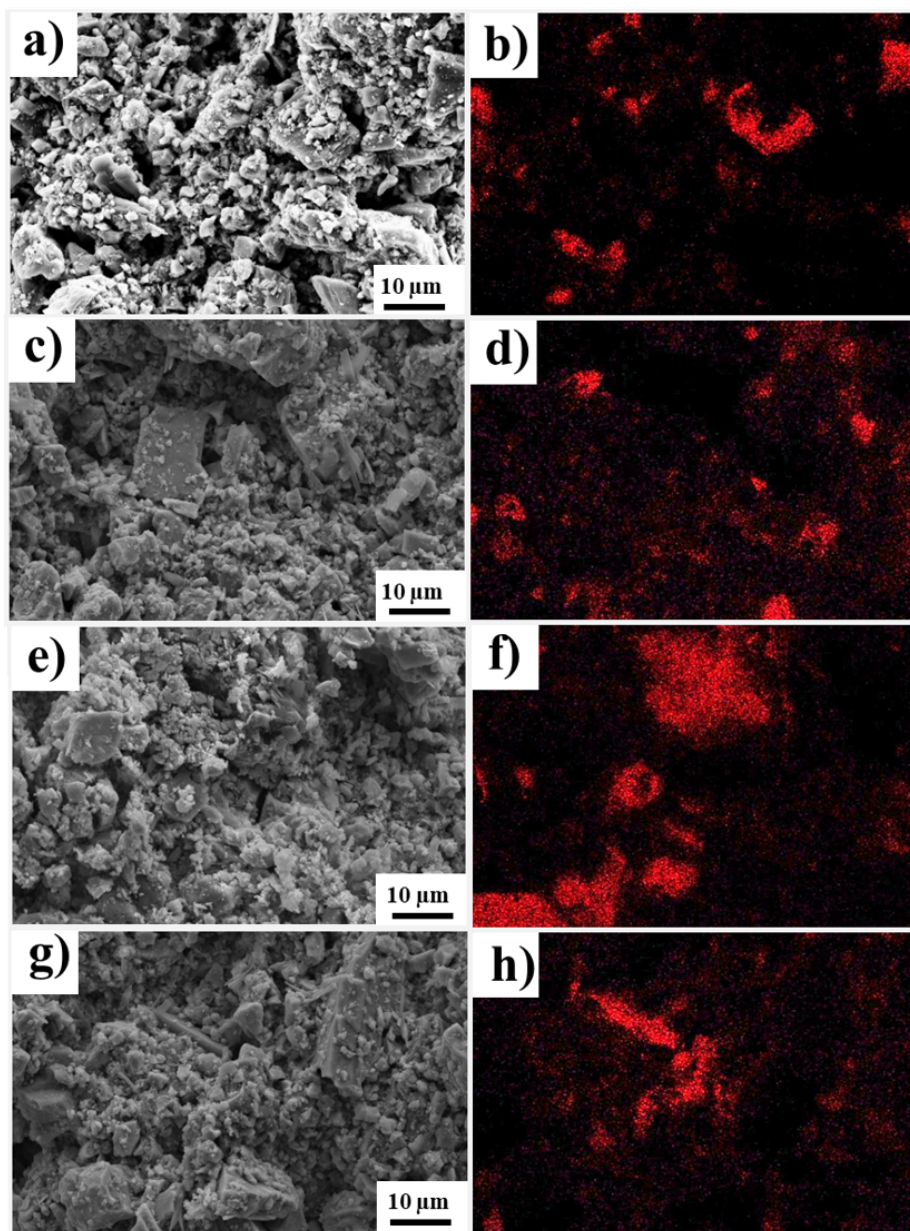


Figure 5.31: EDS analysis of filter cake formed by bentonite drilling fluids a,b) Base fluid c,d) Base fluid with Si NPs e,f) Base fluid with Si-C NPs g,h) Base fluid with Si-N NPs.

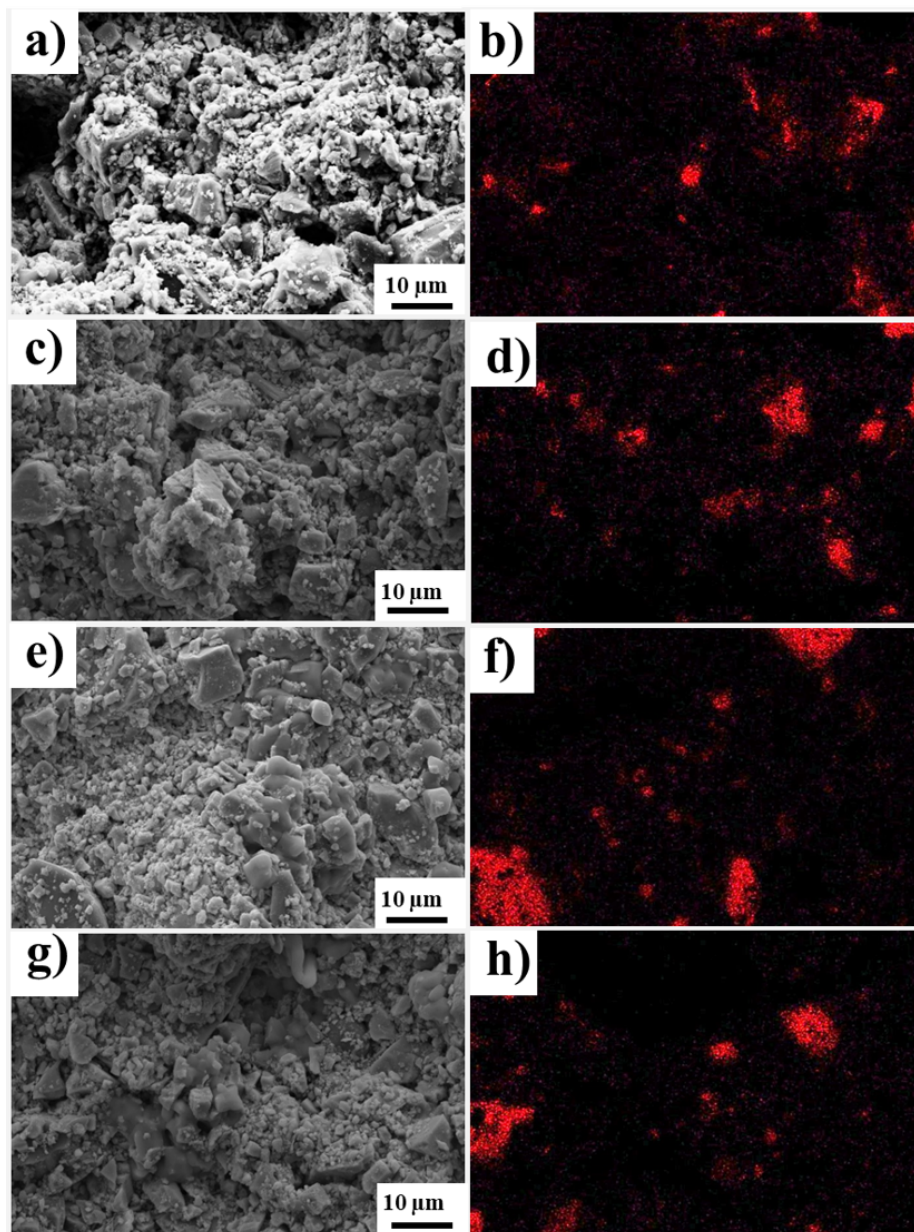


Figure 5.32: EDS analysis of filter cake formed by KCl drilling fluids a,b) Base fluid c,d) Base fluid with Si NPs e,f) Base fluid with Si-C NPs g,h) Base fluid with Si-N NPs.

Nanotubes

Even though nanotubes are distributed throughout the filter cake structure formed by bentonite and KCl drilling fluids, as indicated in Figures 5.33 a-h and Figures 5.34 a-h, there are still large voids in the cake structure. Hence, the nanotubes do not lead to a very large reduction in the fluid loss values. Moreover, the ability of nanotubes to trap large amounts of fluid due to their hollow tube structure, which they released under high pressure contributed to the low reduction in fluid loss. However, MW-COOH still reduces the fluid loss for bentonite fluids by 10%. While MW and MW-OH in the cake structure of KCl drilling fluids bridged the gaps more effectively, which explains the better reduction in fluid loss values, see Figures 5.34 c-h.

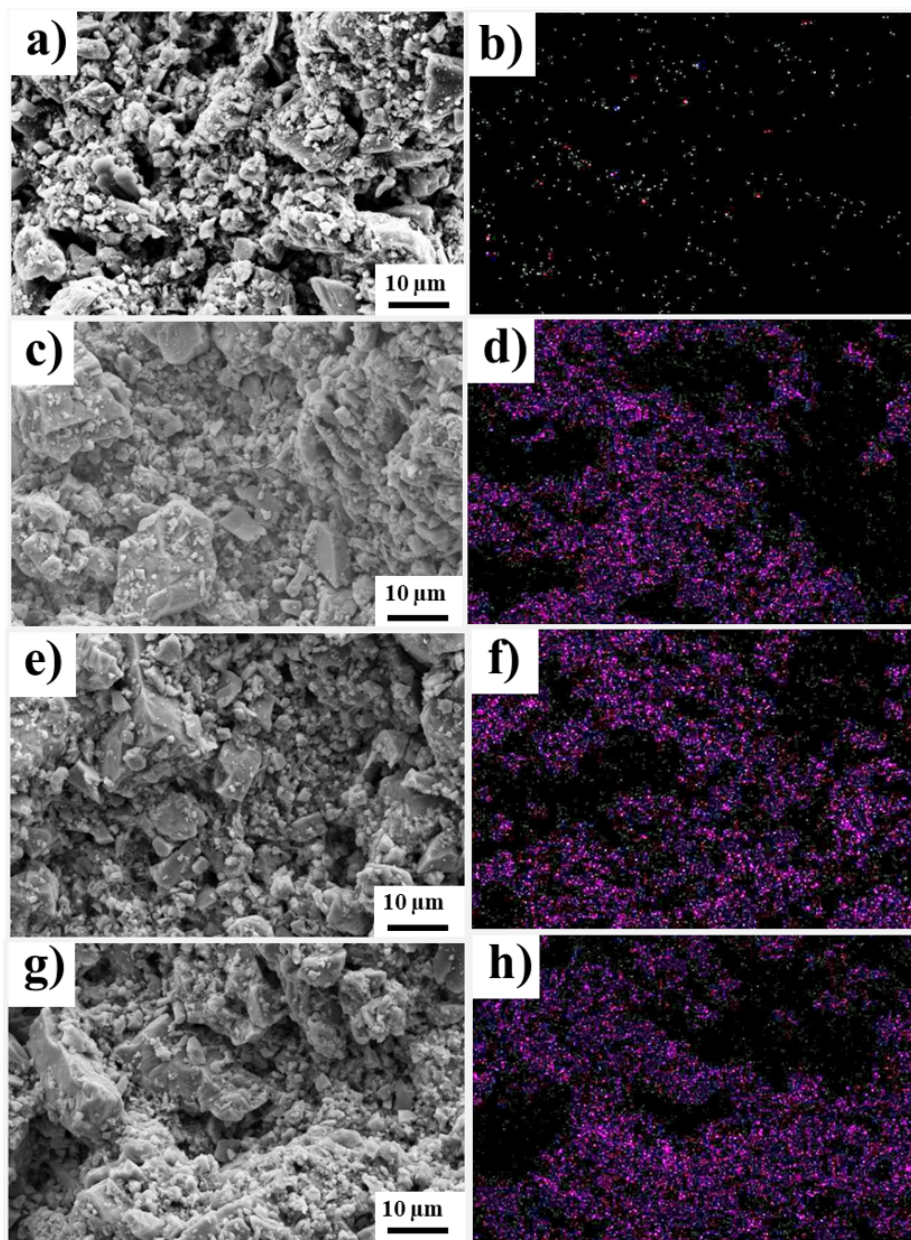


Figure 5.33: EDS analysis of filter cake formed by bentonite drilling fluids a,b) Base fluid c,d) Base fluid with MW e,f) Base fluid with MW-OH g,h) Base fluid with MW-COOH.

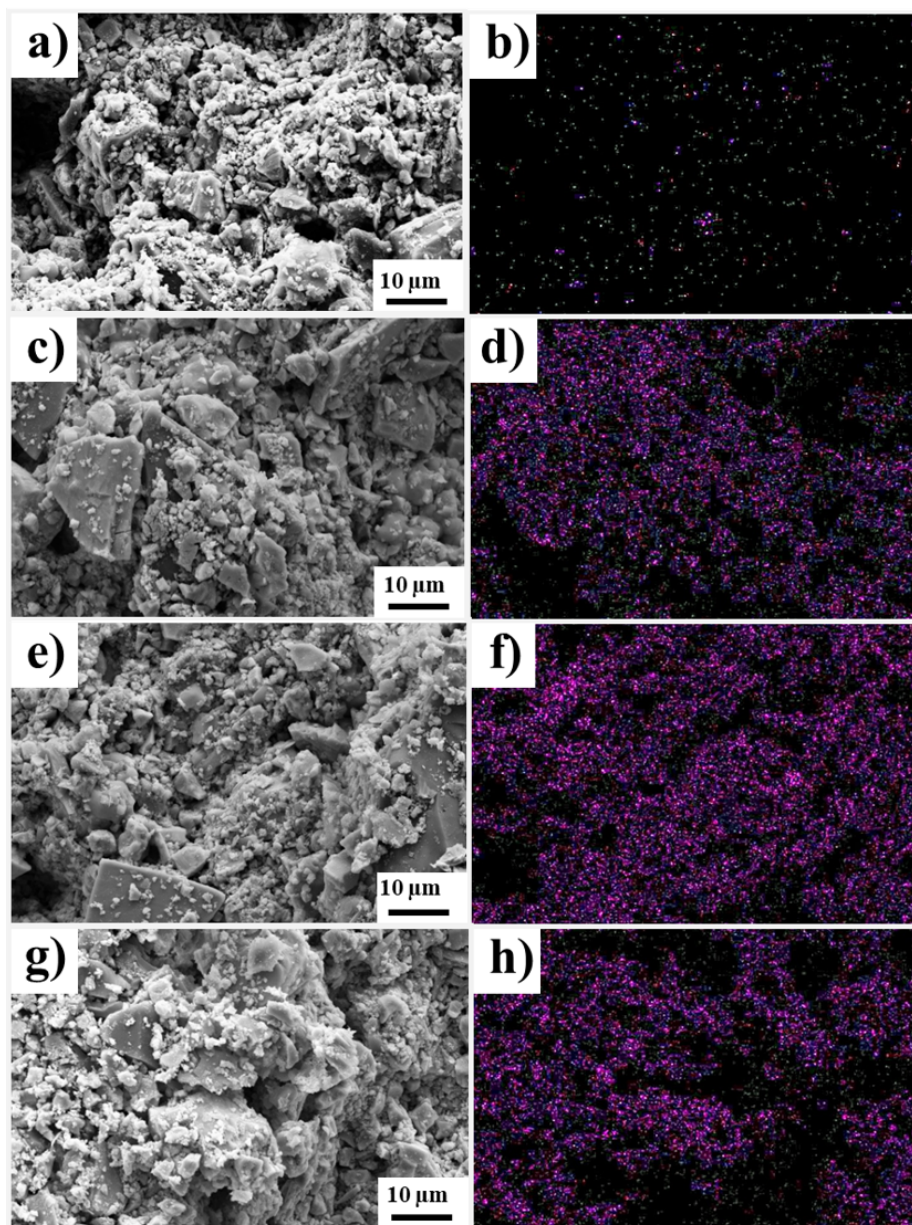


Figure 5.34: EDS analysis of filter cake formed by KCl drilling fluids a,b) Base fluid c,d) Base fluid with MW e,f) Base fluid with MW-OH g,h) Base fluid with MW-COOH.

6 Application of IONPs in Oil-Based Drilling Fluids.

This chapter covers the results from the impact of IONPs on the rheological parameters, mechanical friction, and fluid loss properties of oil-based drilling fluids. The results are based on the paper II.

6.1 Rheological Parameters of the Drilling Fluids

The shear stress of the oil-based drilling fluids with 0.5wt.% and 1wt.% NPs at various shear rates is presented in Figure 6.1.

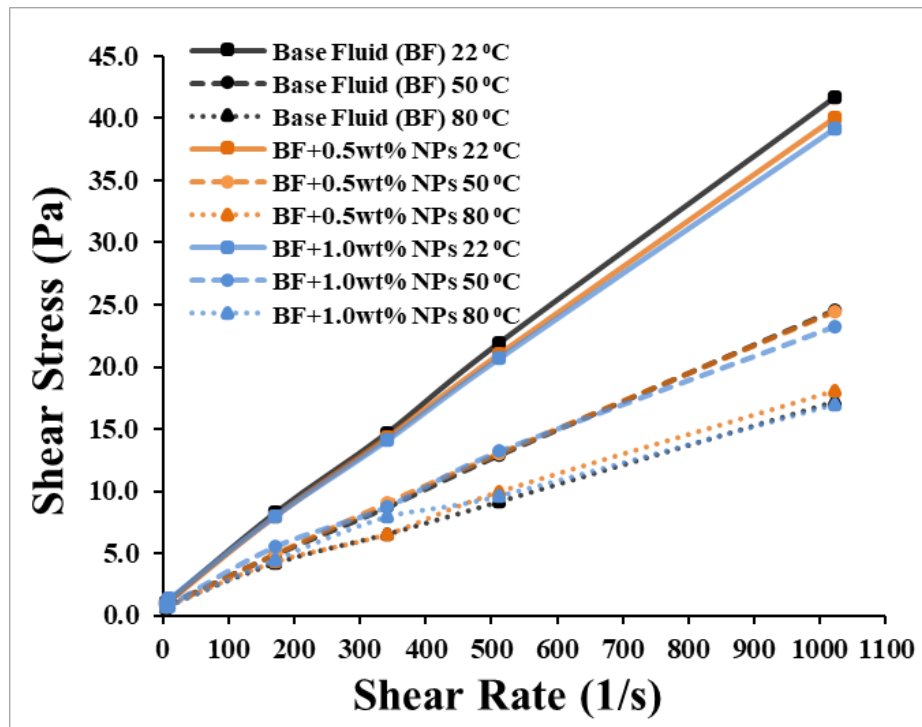


Figure 6.1: Effect of temperature and IONPs on shear stress at different shear rates for oil-based drilling fluids (Paper II).

The measurements were done at ambient and high temperature under atmospheric pressure. The results show that NPs do not significantly impact the shear stress values of the base fluid. Moreover, as shown in Paper II, the apparent viscosity of drilling fluids decreases with the shear rate, confirming the shear-thinning behavior of fluids. IONPs increase the viscosity of drilling fluids at high temperature, especially at lower shear rate values (Paper II).

6.1.1 Gel Strength

Figures 6.2 a, b show the 10 s and 10 min gel strength of drilling fluids with and without NPs. Adding 0.5wt.% Fe NPs to the fluid increase the 10 s gel strength by 6% and 14% at 50 °C and 80 °C, respectively. Moreover, 10 minutes of gel strength increased by 4.5% and 14.3% for 0.5wt.% NPs. However, a higher concentration of NPs destabilizes the system compared to the base fluid. This shows that the lower concentration of NPs effectively changes the base fluid's gel properties. The ability of fine particles to keep the fluids stable at low shear is the possible reason for improving the gel strength (Paper II).

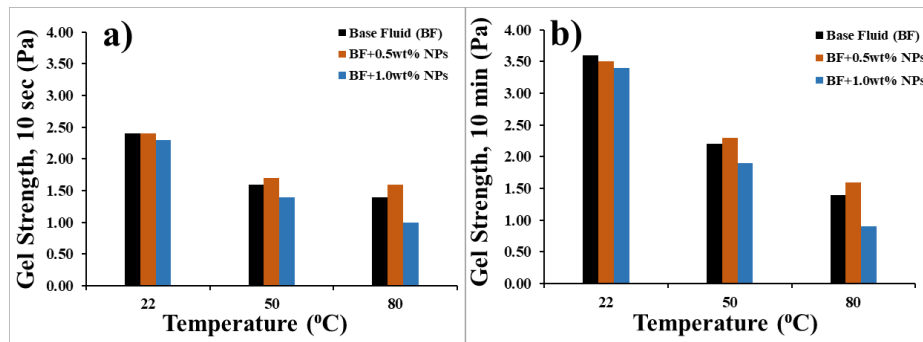


Figure 6.2: Gel strength a) 10 sec and b) 10 min of drilling fluids and drilling fluids with 0.5 wt.% IONPs and 1.0 wt.% IONPs at different temperatures (Paper II).

6.1.2 Yield and Surplus Stress

Figure 6.3 a shows the Herschel–Bulkley (HB)-Yield stress for the base Oil-based mud (OBM) and OBM with IONPs. The addition of NPs to the base fluid decreases the yield stress at 22 °C, as shown in Figure 6.3. However, at a higher temperature (80 °C), there is an increase in yield stress values for NPs-based fluids compared to the base fluid. The increase was significant both for the 0.5 wt.% and 1.0 wt.% concentrations, as shown in Figure 6.3 (Paper II).

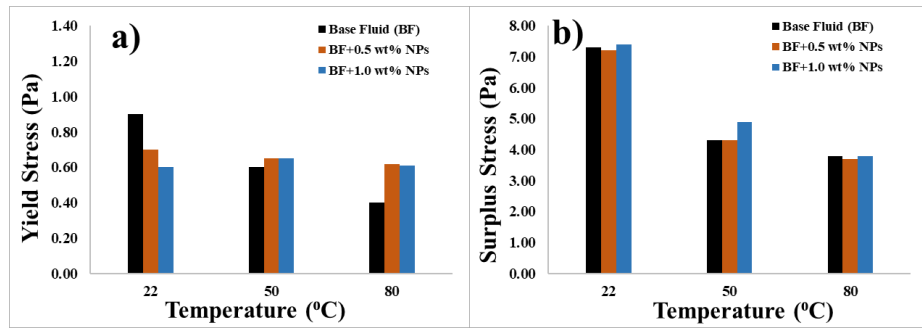


Figure 6.3: Effect of temperature on a) Yield and b) Surplus stress of oil-based drilling fluids and drilling fluids with IONPs (Paper II).

6.1.3 Low and High Shear Curvature Exponents

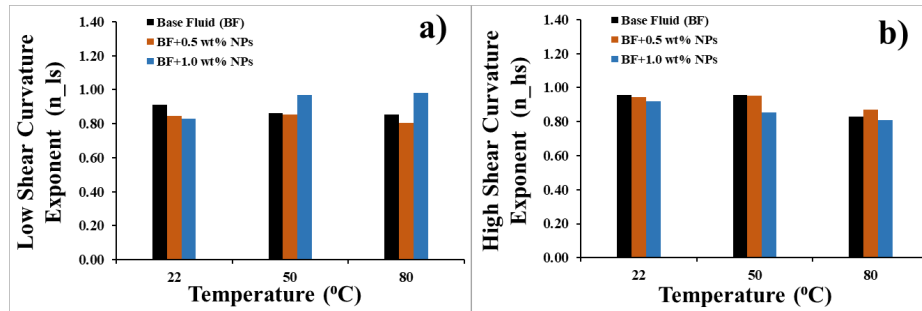


Figure 6.4: a) n_{ls} and b) n_{hs} of oil-based drilling fluids and drilling fluids with IONPs (Paper II).

Figures 6.4 a and b show that NPs do not significantly affect n_{ls} and n_{hs} respectively. Fluid with 0.5 wt.% NPs shows a minor increase in n_{hs} value at 80 °C compared to the base fluid (Paper II).

6.1.4 Barite Sagging

Although the reference drilling fluid shows an acceptable sag factor of 0.53 [335], NPs still further reduce the sag factor. Using 0.5wt.% NPs in the drilling fluids provide more reduction than high concentration, see Figure 6.5. Barite sagging under dynamic conditions is vital since drilling fluids will be exposed to dynamic and static conditions. Since 0.5wt.% concentration provides better performance under static conditions, only low concentration was used to perform a test under dynamic conditions. As shown in Figure 6.5, there is a reduction in sagging under dynamic conditions for fluid with NPs (Paper II).

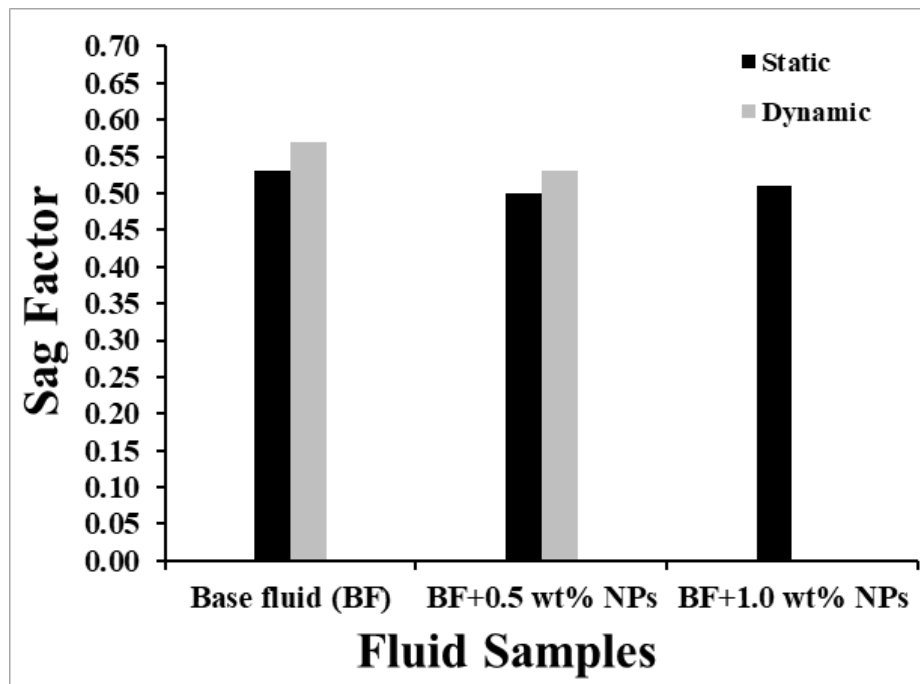


Figure 6.5: Static and dynamic barite sagging of oil based drilling fluids and drilling fluids with NPs (Paper II).

6.2 Friction Measurement

Oil-based drilling fluids show lower mechanical friction values than water-based drilling fluids [341]. Still, further reduction in friction values can be beneficial to lower the torque and drag during drilling. Similar to gel strength and barite sagging results, low concentration of NPs in drilling fluids provides more reduction in friction values, see Figure 6.6. The possible reason for the decrease in the coefficient of friction is due to the formation of a lubricating film by NPs between the ball and plate surface, as also observed in the case of water-based fluids. Small-sized NPs act as fluid in the system, minimizing friction (Paper II).

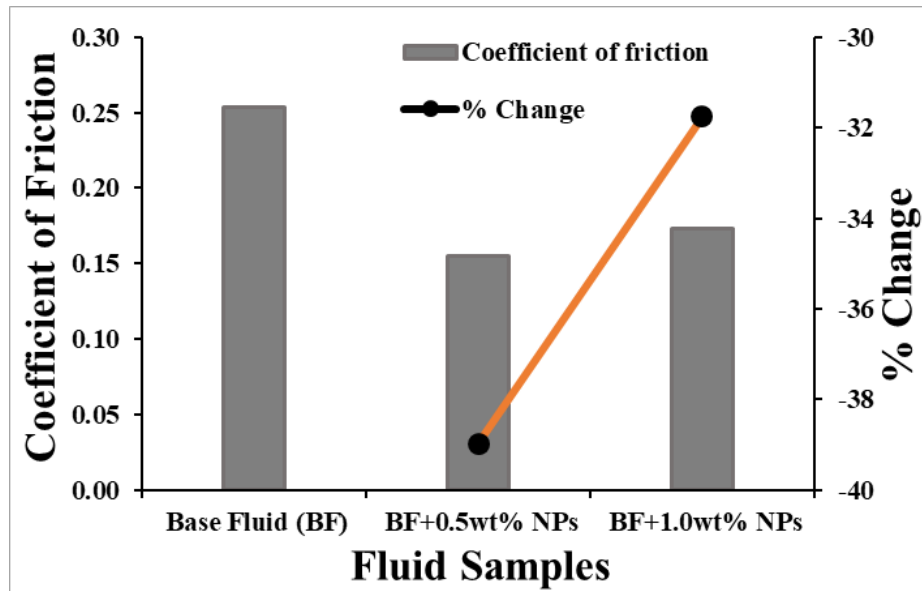


Figure 6.6: Impact of NPs on the coefficient of friction of oil-based drilling fluids (Paper II).

6.3 Effect of NPs on the Fluid Loss and Filter Cake

As mentioned in the introduction, control of fluid loss to the formation is one of the important parameters to define the quality of drilling fluids. The properties of filter cake formed by the drilling fluids are vital to limit fluid loss. Figure 6.7 shows the fluid loss test results at high temperature and pressure. The filtration and fluid loss rate is substantially decreasing with the addition of 0.5wt.% Fe NPs in the drilling fluids. A test was done with 0.5% hexane to confirm the ability of NPs to reduce fluid loss rather than hexane. Results show that the significant contribution to decreasing fluid loss is from the NPs. The addition of NPs to drilling fluids seals the pores in the structure and reduces fluid loss [342] (Paper II).

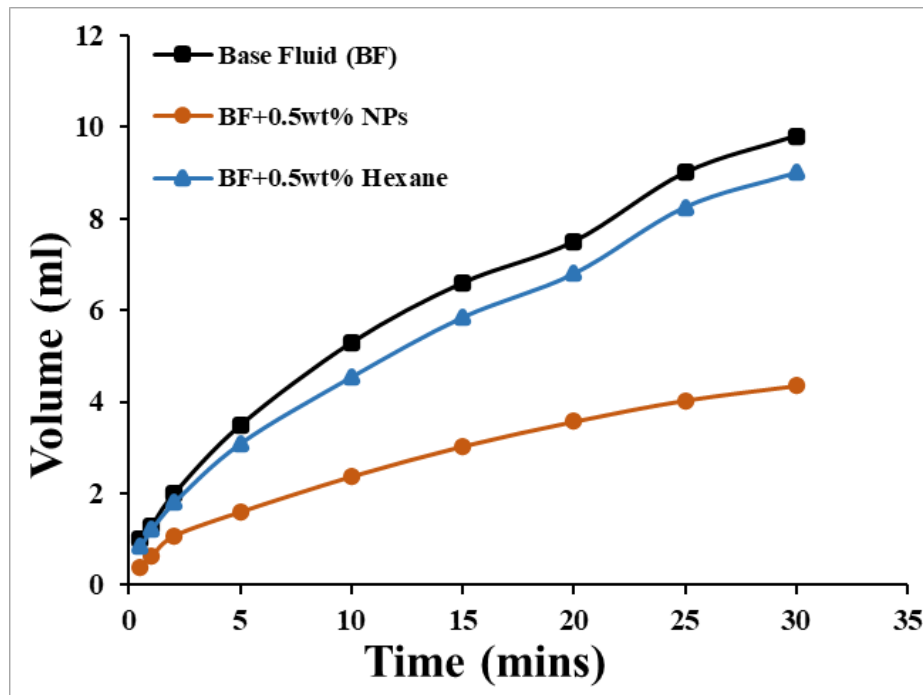


Figure 6.7: Filtrate volume after fluid loss test for oil-based drilling fluids with IONPs (Paper II).

Since the properties of filter cake, such as thickness and permeability, are crucial in limiting fluid loss, calculating these properties can provide insight into the quality of filter cake. The filter volume is directly proportional to the square root of time if the effect of the filter paper resistance factor is negligible [4]. Eq. 6.1 presents the relation, and it is valid for the high temperature and pressure tests,

$$V_f = \sqrt{\frac{2k_{mc}\Delta P}{\mu_f} \left(\frac{f_{sc}}{f_{sm}} - 1 \right)} A\sqrt{t} \quad (6.1)$$

In the above equation, the permeability of the filter cake and differential pressure are represented by k_{mc} and Δp , respectively. Further, the volume fraction of solids in the filter cake and drilling fluids are represented by f_{sc} and f_{sm} , respectively. Here, A is the area of the filter, μ_f is the viscosity of the filtrate and t is the time. Since it was not possible to continuously measure the filter cake thickness during the test, a relation between the filter cake height and fluid volume is used instead, i.e., Eq. 6.2. This equation is valid in case of static filtration [4],

$$h_{mc} = \frac{V_f}{A \left(\frac{f_{sc}}{f_{sm}} - 1 \right)} \quad (6.2)$$

Eq. 6.1 and Eq. 6.2 can be used to estimate the permeability of the filter cake by using the corresponding cumulative volume (V_{f30}),

$$k_{mc} = 0.5\mu_f \frac{h_{mc}V_{f30}}{30A\Delta P} \quad (6.3)$$

Table 6.1 presents the calculated and measured results. The results show that 0.5wt.% NPs reduce the cake thickness and permeability by 55% and 88%, respectively. This ultimately led to a reduction of 70% in fluid loss. These results show that NPs in the drilling fluids can produce fluid that can perform better under high temperature and pressure.

Table 6.1: Filter cake properties and filter volume (Paper II).

Samples	K_{mc} (%)	h_{mc} (%)	V_f (%)
Drilling fluids + 0.5wt.% Hexane	-15	-6.55	-2
Drilling fluids + 0.5wt.% NPs	-87.7	-54.58	-70

A filter cake with high thickness can cause the drill string sticking, due to an increase in contact between the filter cake and the drill string [343]. The force required to free the pipe depends on the coefficient of friction, differential pressure, and contact area of the pipe in the hole wall. Since NPs lower friction and contact area, this reduces the drill string sticking problem during drilling operations [344]. In addition, impermeable filter cake also contributes to lower fluid losses to the formation in cases where well pressure is close to the fracture gradient (Paper II).

7 Application of Nanotubes and AL NPs in Cement and Geopolymer

This chapter presents the results from paper III and unpublished work for the application of NPs in cement. The chapter discusses the impact of NPs on the properties of cement and geopolymer materials.

7.1 Rheological Properties

The rheology of cement is an essential element in the design, evaluation, and execution of cementing operations. Viscous data of cementitious materials can predict a material's flow properties at different conditions, such as during mixing and pumping. Various parameters like temperature, pressure, solid content, type of hardener or fluid, and conditioning duration can influence the viscous properties of the slurry.

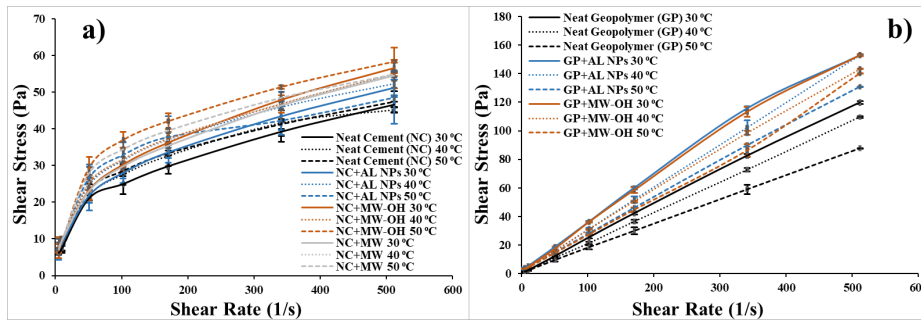


Figure 7.1: Effect of temperature and NPs on the rheological behaviour of a) Cement b) Geopolymer (Paper III).

The viscous properties of cement and the impact of NPs are presented in Figure 7.1 a. Cement slurry shows non-Newtonian behaviour, and the addition of NPs shows the same trend. NPs addition to cement slurry, show higher shear stress values, with MW-OH showing the highest increase. This indicates that NPs addition to cement makes slurry more viscous due to the high surface area of NPs. In the case of AL NPs, there is a decrease in shear stress values at high

temperatures at high shear rates. This behaviour may be due to the formation of a weaker gel structure that disrupts at higher shear rates. NPs also increase the apparent viscosity of cement slurry, and MW-OH depicts the highest increase due to functional groups providing better interaction with cement slurry.

The rheological properties of the neat geopolymer also show non-Newtonian (Bingham Plastic) behaviour. The addition of NPs shows similar trends but with higher shear stress values for the same shear rate. Hence, NPs also increase the viscosity of geopolymer, as indicated in Figure 7.1 b. As discussed by *Hodne et al. (2001)* [345], adding micro-sized silica particles increased the viscosity of the cement slurry. A similar trend is observed in this study; adding NPs to the slurry increases the solid content. Moreover, the high surface area of NPs makes slurry more cohesive and viscous.

The slurry containing MW-OH shows a change in shear stress values at high shear rates as the temperature increases from 40 °C to 50 °C. The reason for the behaviour remains unknown. However, shear rates greater than 250 1/s are not usually experienced in the field scale, except in the case of the Bottom Hole Assembly [346]. Figures 7.2 a, b show the apparent viscosity of the slurries at different temperatures. It can be seen that NPs have increased the apparent viscosity. Moreover, for all slurries, there is a decrease in viscosity with an increase in shear rate showing shear thinning behaviour.

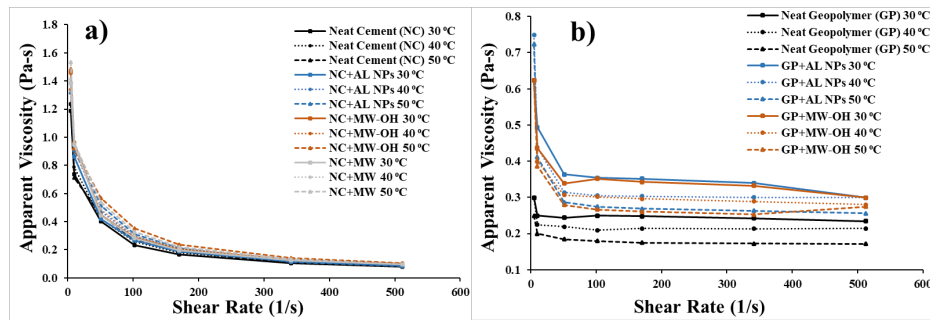


Figure 7.2: Apparent viscosity of a) neat cement with NPs and b) geopolymer modified with AL NPs, and MW-OH (Paper III).

Table 7.1: Casson Yield stresses and Casson plastic viscosities of cement (Paper III).

Samples	Yield Stress (Pa)	Plastic Viscosity (Pa-s)
Neat Cement (NC) 30 °C	6.13	0.04
Neat Cement (NC) 40 °C	6.89	0.04
Neat Cement (NC) 50 °C	6.60	0.05
NC+AL NPs 30 °C	6.96	0.05
NC+AL NPs 40 °C	7.61	0.05
NC+AL NPs 50 °C	8.74	0.04
NC+MW-OH 30 °C	7.35	0.05
NC+MW-OH 40 °C	7.55	0.05
NC+MW-OH 50 °C	8.67	0.06
NC+MW 30 °C	7.29	0.05
NC+MW 40 °C	7.83	0.05
NC+MW 50 °C	8.82	0.05

Table 7.2: Casson Yield stresses and Casson plastic viscosities of geopolymer (Paper III).

Samples	Yield Stress (Pa)	Plastic Viscosity (Pa-s)
Neat Geopolymer (GP) 30 °C	0.015	0.23
Neat Geopolymer (GP) 40 °C	0.009	0.21
Neat Geopolymer (GP) 50 °C	0.014	0.17
GP+AL NPs 30 °C	0.36	0.29
GP+AL NPs 40 °C	0.22	0.27
GP+AL NPs 50 °C	0.34	0.23
GP+MW-OH 30 °C	0.25	0.29
GP+MW-OH 40 °C	0.21	0.26
GP+MW-OH 50 °C	0.15	0.24

Table 7.1 and Table 7.2 show the values for yield stress and plastic viscosity for neat cement and geopolymer mixed with NPs, respectively. Yield stress and plastic viscosity of cement-based materials are crucial for displacement and the pumpability of the slurry. Higher yield stress and plastic viscosity values of the cement and geopolymer mix with NPs thicken the system and control the segregation of materials by providing better cohesion. This increase in viscosity does not affect the pumpability of the slurry, as indicated by the setting time results. However, it can impact pump pressures and friction in the well, causing more significant downhole pressures when circulating (Paper III).

7.2 Fluid-Loss Test

The formation in contact with the cement slurry during its placement acts as a filter that permits fluid flow while retaining the particles and forming a filter cake. The excessive fluid loss to the formation can contribute to wellbore control problems, such as maintaining the hydrostatic pressure due to the loss of liquid phase from the slurry. The decrease in hydrostatic pressure below the formation pore pressure can allow the penetration of formation fluids in the annuli resulting in channels within the cement sheath. In addition, incomplete hydration of cement can occur due to the loss of the liquid phase from the slurry, as this liquid phase can contribute to the solidification reaction. Moreover, high fluid loss can make slurry more viscous, which can cause more considerable pressure losses and the requirement of higher pumping pressure during operation. This high pump pressure can induce fractures in the formation. Therefore, additives are used in the cement slurry to avoid high fluid losses.

Fluid loss results for neat cement and cement with NPs are shown in Figure 7.3 a. Since the additives are not present in the cement slurry, it shows high fluid loss values. Moreover, the addition of NPs even further increases fluid loss. This might be due to the delay in the gelation of cement slurry by NPs at high pressure and temperature. The NPs adsorbed water during the hydration process and released it at high pressure, increasing fluid loss. An increase in fluid loss for

nanotubes shows the ability of nanotubes to trap large amounts of fluid due to hollow tube structure. The results are in accordance with the pumpability results where NPs contributed to longer pumping time.

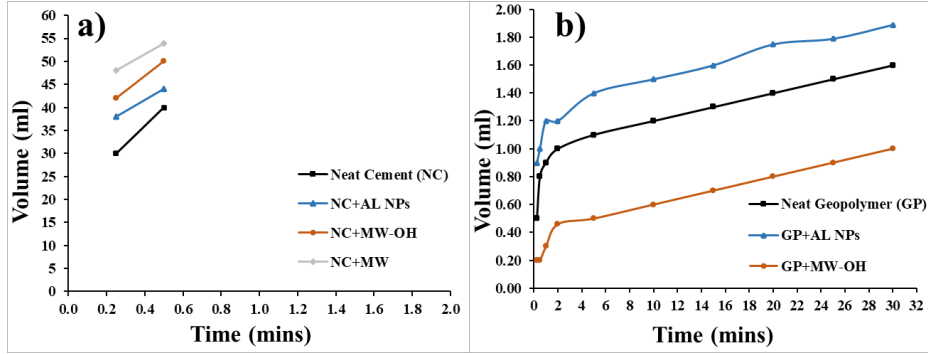


Figure 7.3: Impact of AL NPs and nanotubes on static fluid loss of a) cement and b) geopolymeric slurries (Paper III).

There is no hydration reaction involved in the geopolymerization process and it requires less amount of water. Therefore, lower values of fluid loss are associated with the geopolymer. However, hardener loss may result in loss of hydrostatic pressure or incomplete reaction. Our measurements confirmed the lower fluid loss values with geopolymer after 30 minutes, as shown in Figure 7.3 b. The mix containing AL NPs showed an increase in fluid loss values. The possible reason might be a delay in the hardening of slurry with AL NPs. Moreover, attachment of MW-OH to the oligomers results in a considerable decrease in fluid loss values of geopolymer, as shown in Figure 7.3 b (Paper III).

7.3 Pumpability

It is crucial to know the pumpability and workability of the cement slurry to estimate the duration for which the slurry is pumpable before the gelation occurs. Temperature ramp-up rate and bottom-hole circulating temperature (BHCT) depend on the specific well. As mentioned before in this work, 50 °C was selected as BHCT. The

typical upper limit for consistency above which the slurry is not pumpable is 70 Bearden units of consistency (Bc). Figures 7.4 a-c shows the consistency at atmospheric and high-pressure results for neat cement with and without NPs.

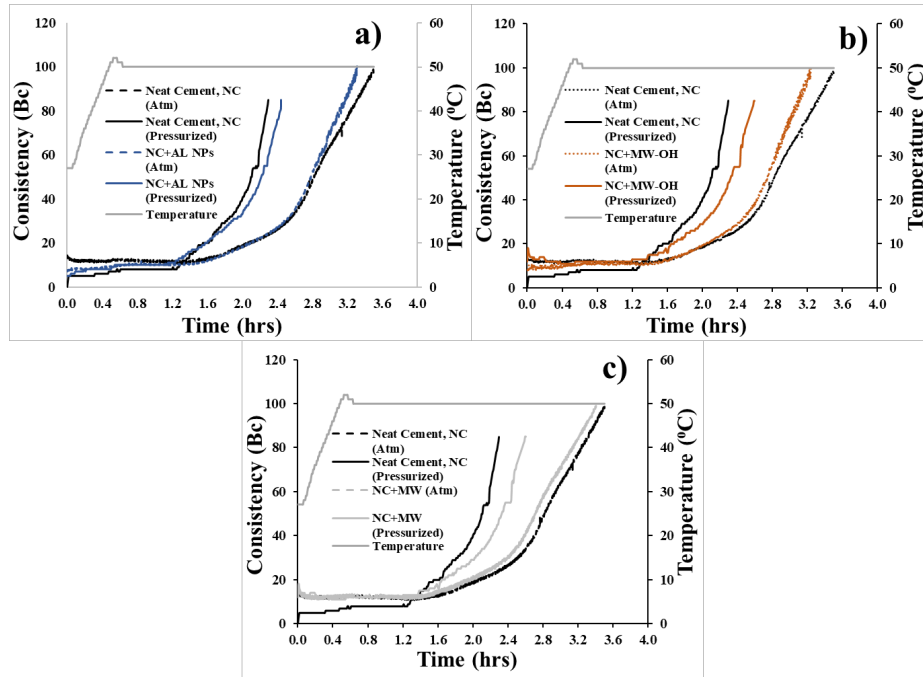


Figure 7.4: a) Effect of AL NPs on setting time of the cement slurry b) Effect of MW-OH on setting time of the cement slurry c) Effect of MW on setting time of the cement slurry.

High pressure reduces the pumping time by accelerating the gelation of cement. All the materials show this trend; however, NPs delay the gelation at high pressure. This indicates that high pressure influences the reaction between cement and NPs and delays the hydration of cement, especially in the case of nanotubes. The retardation effect of NPs on cement hydration is due to the ability of NPs to hinder water contact with cement [347–349]. Also, in the case of nanotubes, chemical retardation is caused by the surface groups on NPs such as OH due to electrostatic interaction with Ca^+ , causing complexation

of Ca^{+} . [348–350]. However, at atmospheric pressure, NPs slightly reduce the setting time owing to the ability of NPs to accelerate the reaction rate.

It is crucial to control the setting time of geopolymer slurry for its application in an oil field. Borax-based retarders are suggested to prolong the geopolymer setting; however, they decrease the material's mechanical strength. NPs can be used to increase the pumpability of the geopolymer slurries by acting as a retarder. Figures 7.5 a, b show that adding NPs significantly increases the available pumping time of the geopolymers. A possible scenario for this phenomenon could be that the NPs act as a shield between the aluminosilicate precursor and hardener and decrease the dissolution rate of alumina-silicates [351]. NPs delay the gelation step and prolong the setting of the geopolymer slurry. Also, the addition of NPs to the geopolymer slurry promotes the electrostatic repulsion between similar charges in the slurry system. Furthermore, as the NPs are dispersed in surfactants, they might act as retarders and delay the setting time of the geopolymer slurries. The inclusion of the NPs prolonged the pumping time to 3 hours; see Figures 7.5 a and b. This work shows that pressure does not have a significant impact on pumping time, which is in accordance with a previous investigation done by *Khalifeh et al. (2019a)* [352] on neat geopolymers (Paper III).

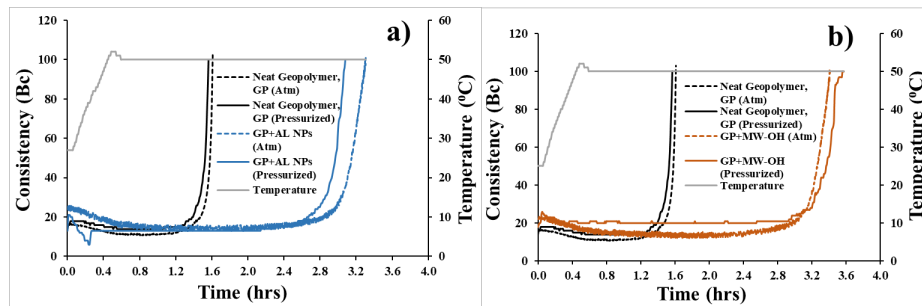


Figure 7.5: a) Effect of AL NPs on setting time of the geopolymer slurry b) Effect of MW-OH on setting time of the geopolymer slurry (Paper III).

7.4 Mechanical Properties

7.4.1 Uniaxial Compressive Strength (UCS)

The unconfined compressive strength tests were performed after the specimens aged 12hr, 24hr, 3, 7, and 28 days. For each curing time, three specimens were crushed, and the average strength values were reported to represent the unconfined compressive strength. Even though the cement and geopolymer specimens were cured in autoclaves, the mechanical destructive tests were conducted at ambient conditions. Figure 7.6 a, presents the compressive strength data for the neat cement and cement with NPs. The inclusion of NPs in the cement does not significantly impact the strength of cement until 3 days, except for MW. This confirms the ability of NPs to delay the gelation of cement. This confirms the ability of NPs to delay the gelation of cement. However, after 28 days, the cement shows strength retrogression, but NPs incorporation in the matrix provides thermal stability. NPs in the cement create strong structures by eliminating weak zones within the cement structure. Nanotubes show better compressive strength than other samples; owing to the high mechanical strength of tubes, MW shows the highest strength after 28 days.

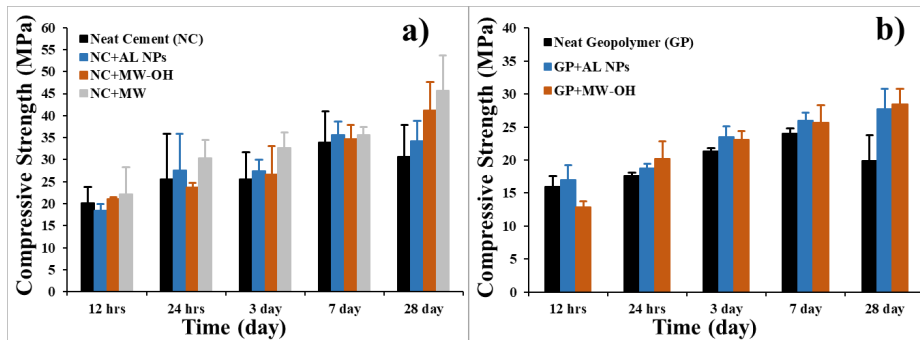


Figure 7.6: Unconfined compressive strength for a) Neat cement with AL NPs and nanotubes b) Neat geopolymer with AL NPs and MW-OH (Paper III).

The addition of MW-OH and AL NPs to the geopolymer contributed

to an increase in compressive strength, as indicated in Figure 7.6 b. The integration of NPs in the material structure facilitates this behaviour. Owing to the fineness of NPs, the chemical reactivity increases and ultimately produces structures with higher strength and durability. Moreover, NPs in the geopolymeric slurry might provide additional nucleation sites for the aluminosilicate reaction, creating a denser, more homogeneous geopolymer paste. Furthermore, the increase in compressive strength is due to the elimination of weaker zones and narrow pore distribution within the geopolymer matrices. In the case of MW-OH, the presence of hydroxyl groups on the surface of the MW generated additional OH- groups in the slurry by reacting with a geopolymer or forming a hydrogen bond. The interaction between MW-OH and geopolymer incorporates the MW throughout the geopolymer structure, as confirmed by the microstructure analysis. It can ultimately construct nanotubes reinforced geopolymer with higher mechanical properties such as compressive strength. *Li et al. (2013) [353]* have shown similar behaviour. This work shows that creating a hydrogen bond between geopolymer and N-Carboxymethyl chitosan by adding carboxymethyl chitosan into fly ash-based geopolymer enhances the mechanical properties (Paper III).

7.4.2 Modulus of Elasticity

Young's modulus (E) of cement and formation rock determines the tensile strength requirements of oil well cement [354, 355]. The failure of cement sheath integrity depends on the downhole stress induced by changes in pressure and temperature throughout the well life-cycle [356]. Moreover, the flexibility of cement material is vital and required in several cases to control the damage, as higher tensile and compressive strengths of the material may not provide the optimum solution [354]. The piston displacement measurements from the uniaxial compressive strength test were employed to calculate Young's modulus by using the slope of the stress-strain curve in its linear range, owing to the limitations of using a tri-axial cell. Still, the relative elasticities remain comparable even though the real elasticity is higher than the estimated values. Incorporating

nanotubes in the cement structure decreases Young's modulus after 1 day, while AL NPs show similar values to cement, as indicated in Figure 7.7 a. Moreover, after 7 days, there is a minor improvement in Young's modulus of cement with AL NPs, while for both nanotubes, values still decrease. After 28 days, there is an increase in Young's modulus of cement with NPs compared to the neat cement, owing to the decrease in compressive strength of cement.

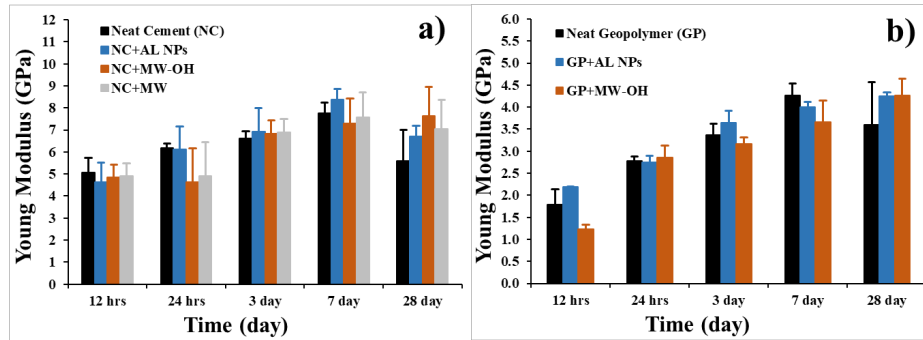


Figure 7.7: Estimated Young's modulus values a) Neat cement with NPs b) Neat geopolymer with NPs (Paper III).

NPs inclusion to the geopolymer does not significantly increase Young's modulus values, as depicted in Figure 7.7 b. However, owing to an increase in unconfined compressive strength for geopolymer with NPs, there is a minor increase in Young's modulus values after 28 days. Low Young's modulus values with higher tensile and compressive strength benefit oil well-cementing applications. The natural flexibility of the nanotube structure and functionalization with $-OH$ groups instil more flexibility in the geopolymer structure. The higher unconfined compressive strength attained by geopolymer with AL NPs in the first 3 days is translated into an increase in the Young modulus values. Figure 7.6 b shows that the AL NPs-based geopolymer system attained most of its strength in 3 days, and after that, there is a slow increase in the strength (Paper III).

7.4.3 Compressive Strength to Young Modulus Ratios

The flexibility and compressive strengths are both crucial to define the mechanical properties of cementitious materials. The higher flexibility of the material minimizes the requirement of high strength as it can deal with external stress more effectively compared to the material with slightly better strength but lower flexibility. The ratio of compressive strength and Young's modulus (UCS/YM) is a qualitative parameter that can define the material's performance under a compression load, as high ratios indicate better performance. The presence of NPs in the cement structure improves the ratio after 1 day. However, after 7 days, only nanotubes slightly improved the ratio as there is an increase in Young's modulus for the AL NPs-based cement. After 28 days, MW incorporation in the cement structure provides the highest ratio increase due to the high compressive strength and comparatively low Young's modulus of the MW-based cement see Figure 7.8 a.

The higher compressive strength and lower Young's modulus of geopolymer incorporated with NPs provided higher values for the ratio of unconfined compressive strength to Young's modulus. Even though there is a decrease in the value after 28 days due to increased compressive strength and Young's modulus, the ratio was still slightly better in the case of NPs-based geopolymer systems, as presented in Figure 7.8 b (Paper III).

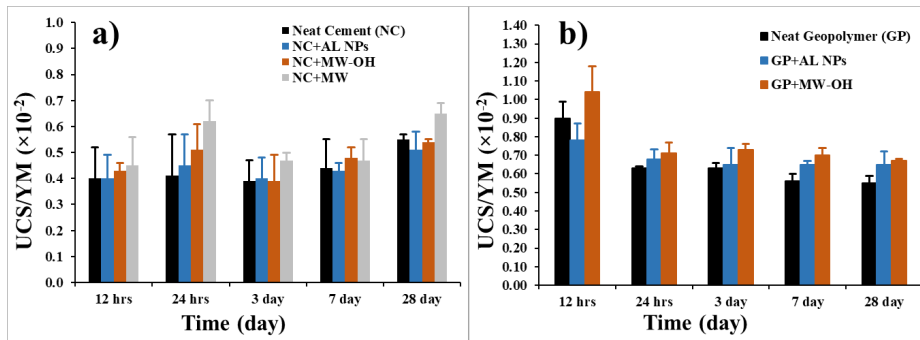


Figure 7.8: Ratio of unconfined compressive strength to Young's modulus a) Cement samples b) Geopolymer samples (Paper III).

7.4.4 Tensile Strength (TS)

The tensile strength of barrier materials is crucial. Low values can contribute to loss of zonal isolation and damage the cement integrity as cement sheath can suffer radial loads that cause tangential and radial cracks. There is a decrease in the tensile strength of cement with NPs after 7 days; see Figure 7.9 a, This again shows that NPs delay the hydration and gelation of cement, which ultimately influences the strength development of cement. However, after 28 days, there is a decrease in the tensile strength of the cement. Even though cement suffers from loss in tensile strength, MW-OH and MW provide better strength owing to the stability of nanotubes at high temperatures. In contrast, AL NPs still show low tensile strength indicating that the concentration of NPs in the slurry may not be enough to work as a filler and avoid strength loss at high temperatures.

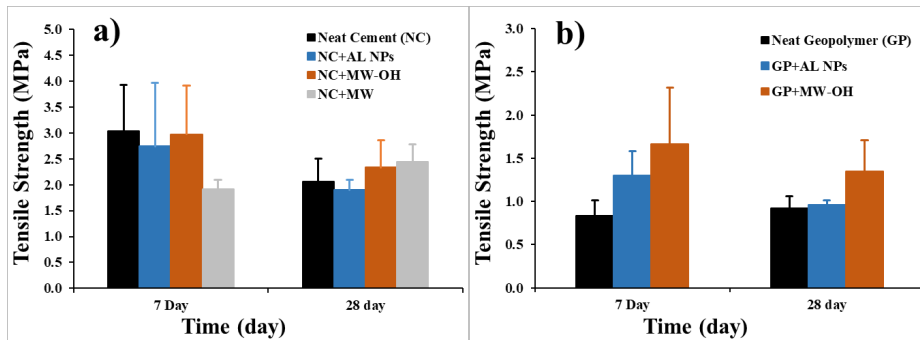


Figure 7.9: Indirect tensile strength a) Neat cement with NPs b) Neat geopolymer with NPs (Paper III).

In order to use geopolymer as an alternative material for well cementing applications, it is vital to increase the tensile strength due to their lower tensile strength. This work shows that NPs can be a promising candidate to enhance the tensile strength of the neat geopolymer. MW-OH and AL NPs have shown significant improvement in the tensile strength of geopolymer after 7 days; see Figure 7.9 b. There was a 123% increase in tensile strength with the MW-OH additive, while the AL NPs led to a 68% improvement after 7

days. Modification of geopolymer with NPs provides greater stability to geopolymer against tensile failures. However, the results for longer curing time show no significant increase in the tensile strength compared to neat geopolymer. In fact, after 28 days, samples with nano-additives showed a decrease in tensile strength values compared to 7 days. Still, for MW-OH, after 28 days, tensile strength values were better than for the neat geopolymer, as shown in Figure 7.9 b. The possible reason for this phenomenon might be the use of a new batch of materials for 28 days tensile strength test (Paper III).

7.4.5 Tensile Strength to Young's Modulus Ratios

As mentioned above, the required tensile strength for cement depends on Young's modulus of adjacent formation and should be lower. If this is not the case, there is a possibility of the formation of radial cracks and debonding of cement from its interface with the formation. Therefore, a lower Young's modulus of material can maintain zonal isolation even though the value for tensile strength is low. Again, a ratio of tensile strength to Young's modulus (TS/YM) defines the performance of different materials under load. It is beneficial to have a high strength to Young's modulus ratio to minimize mechanical damage to the cement sheath [357]. NPs addition to the cement does not significantly affect the ratio; only MW slightly improves the ratio after 28 days, as shown in Figure 7.10 a.

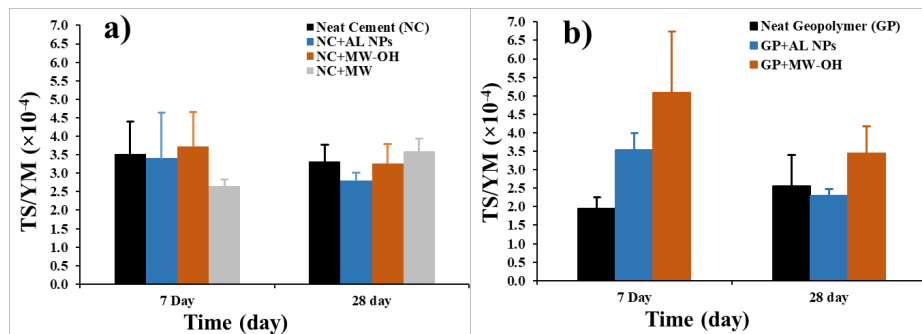


Figure 7.10: Ratio of average tensile strength to Young's modulus of a) Cement samples b) Geopolymer (Paper III).

This substantial increase in tensile strength to Young's modulus ratio for geopolymer samples with NPs, especially in the case of MW-OH after 7 days, could be attributed to the high tensile strength and relatively lower Young's modulus. However, the increase was not substantial for NP-based samples after 28 days compared to the neat geopolymer. Geopolymer with AL NPs, shows a slight decrease in ratio, while for MW-OH, the ratio still showed improvement, as indicated in Figure 7.10 b (Paper III).

7.5 Sonic Strength

The ultrasonic cement analyser measures the strength of barrier material by measuring the transit time of sonic waves through the material at high temperature and pressure. The chemistry and structure of the material under investigation can affect wave transmission and transit time. The instrument's software uses an algorithm based on an experimental database and converts the transit time to the compressive strength of cement. Since the algorithm uses the data from previous experiments, it reasonably estimates the compressive strength of neat cement. However, a new algorithm is required to estimate the compressive strength in the case of alternative barrier materials. This thesis used compressive strength data from UCS and plotted against corresponding transit time to generate empirical correlation. Figures 7.11 a-d presents the sonic strength and transit time of cement and cement modified with NPs. Results show that all the materials achieved strength after 1 day. Adding MW and MW-OH slightly improves the strength of the cement, which is as per the compressive strength results. However, the difference in UCS and UCA compressive strength values is due to the use of a predefined algorithm for cement-based materials.

The sonic strength results for geopolymer modified with NPs indicate that the maximum strength was developed on the first day see Figures 7.12 a, b. The results also show that in static conditions, i.e., for UCA, the geopolymers set faster than in the dynamic situation, as shown in consistency results (compare Figure 7.5 and Figure 7.12). The possible reason is the gelation delay due to continuous slurry

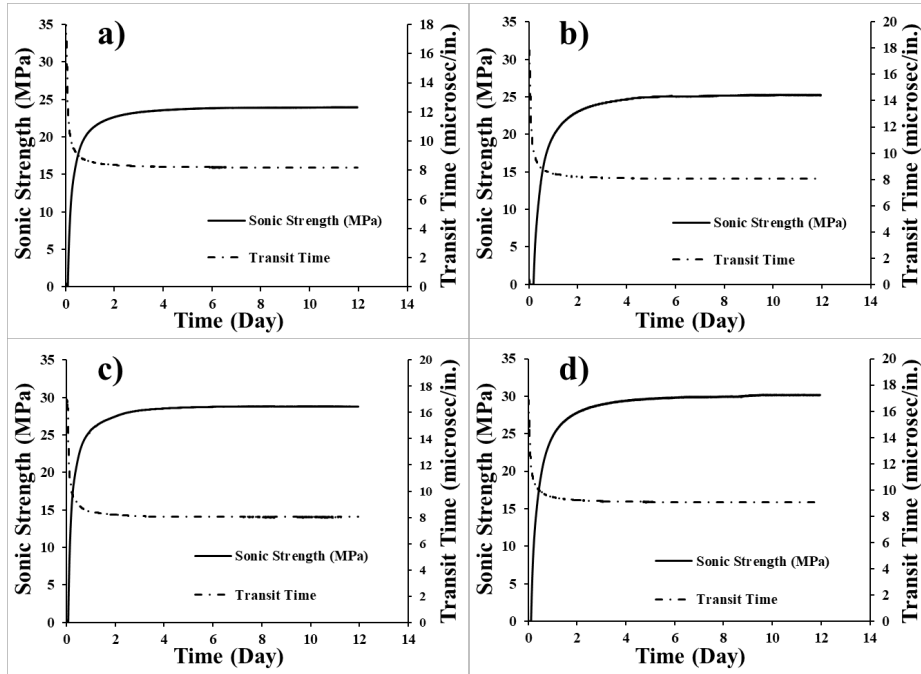


Figure 7.11: a) Sonic Strength development of cement b) Modified with AL NPs c) Modified with MW-OH c) Modified with MW.

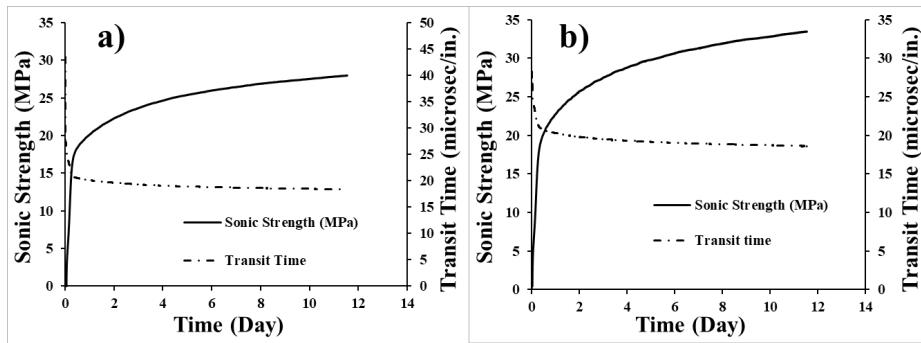


Figure 7.12: Sonic Strength development of a) Geopolymer modified with AL NPs b) Modified with MW-OH (Paper III).

mixing. The temperature increase at the start to 70 °C contributed to high transit time values due to a reduction in the viscosity of the slurries, as also indicated in Figure 7.1 and Figure 7.2 [358].

Moreover, a study done by *Liu. (2017)* [66] shows that additives added to the mix design can influence the transit time. Therefore, in this work, NPs addition to the geopolymer influences the transit time (Paper III).

7.6 X-ray Diffraction

The X-ray diffraction technique provides insight into the crystallography and phases formed by the materials. XRD analysis also provides information about the possible phase changes due to the addition of additives in cement-based materials. The crushed specimens from 7 days UCS test were further grinded to form a powder to perform the analysis. XRD analysis for cement-based samples is represented in Figure 7.13.

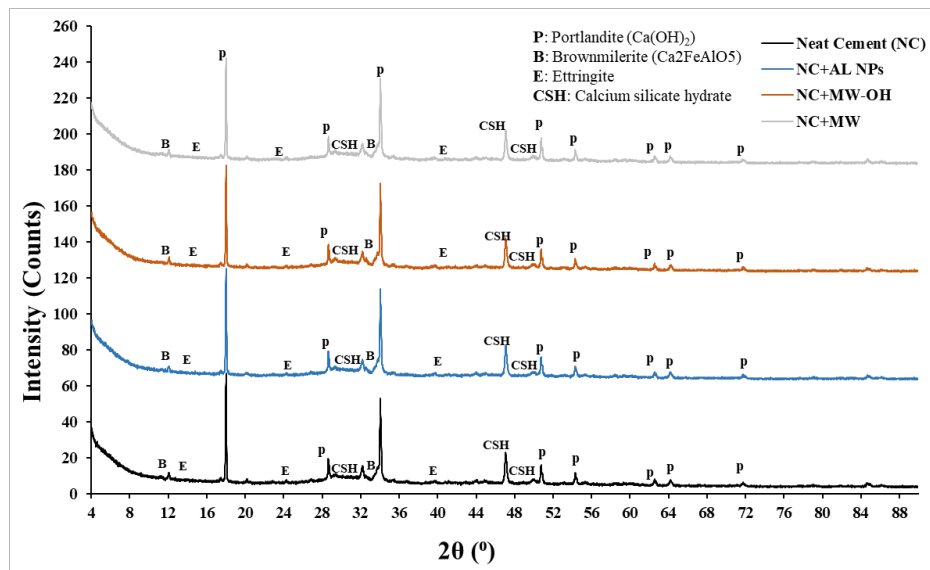


Figure 7.13: XRD pattern for the neat cement and cement with AL NPs and nanotubes.

Neat cement and cement modified with NPs show similar peaks. The main phases present in the cement structure are portlandite, calcium silicate hydrate, and a small amount of ettringite and brownmillerite.

Even though the addition of NPs shows similar peaks, there is a decrease in the intensity of peaks for portlandite. This shows that NPs convert the calcium hydroxide to form calcium silicate gels, especially in the case of MW nanotubes. This improves the strength of the cement structure, as confirmed by compressive strength results, see Figure 7.13.

XRD analysis for geopolymer showed that the main phases in the structure are quartz (SiO_2), microcline ($K(AlSi_3O_8)$), albite $Na(AlSi_3O_8)$, oligoclase $((Ca, Na)(Al, Si)_4O_8)$, clinoptilolite-Na $((Na, K, Ca)_{2-3}Al_3(Al, Si)_2Si_{13}O_{36}12H_2O)$ and illite ($K_{0.65}Al_{2.0}[Al_{0.65}Si_{3.35}O_{10}](OH)_2$) as presented in Figure 7.14.

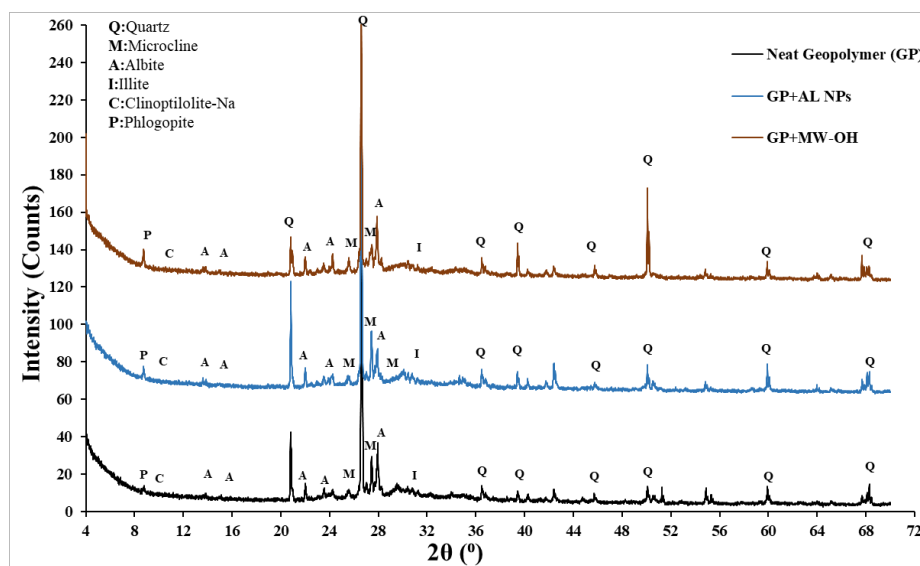


Figure 7.14: XRD pattern for the neat geopolymer and geopolymer with AL NPs and MWCNT-OH indicating additional peaks and peak shifts for geopolymer with NPs (Paper III).

Similar phases are also present in the NPs-based geopolymer structures. Moreover, X-ray analysis shows that the presence of NPs in the geopolymer slurries contributed to the formation of additional phases due to the ability of NPs to take part in the reaction. The stable NPs dispersions might be the reason for the effective reaction

between NPs and other additives to produce geopolymer slurries. Furthermore, functional groups on the MW-OH promote the reaction with oligomers and produce additional phases (Paper III).

7.7 Microstructure Analysis

The SEM analysis was done on the samples from one week UCS test. Figure 7.15 shows the image of the neat cement. The hydration reaction of Portland cement forms calcium hydroxide and calcium silica hydrates (C-S-H) gels.

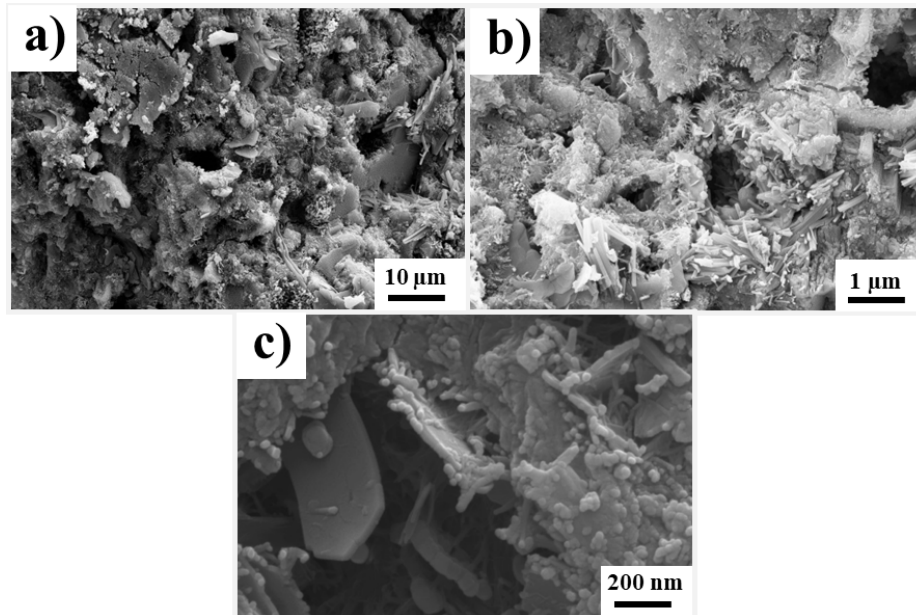


Figure 7.15: SEM images of the neat cement a) Overview of the structure b, c) Internal structure.

The honeycomb C-S-H and hexagonal plates of portlandite are present in the cement structure after seven days, as shown in Figures 7.15 a-c. In addition, needle-shaped structures indicate the presence of ettringite. Big pores are present in the structure of neat cement, which shows the absence of dense structures. In the case of AL NPs, a similar structure is formed. However, the NPs in the structure act

as a filler and take part in the hydration reaction, see Figures 7.16 a-c.

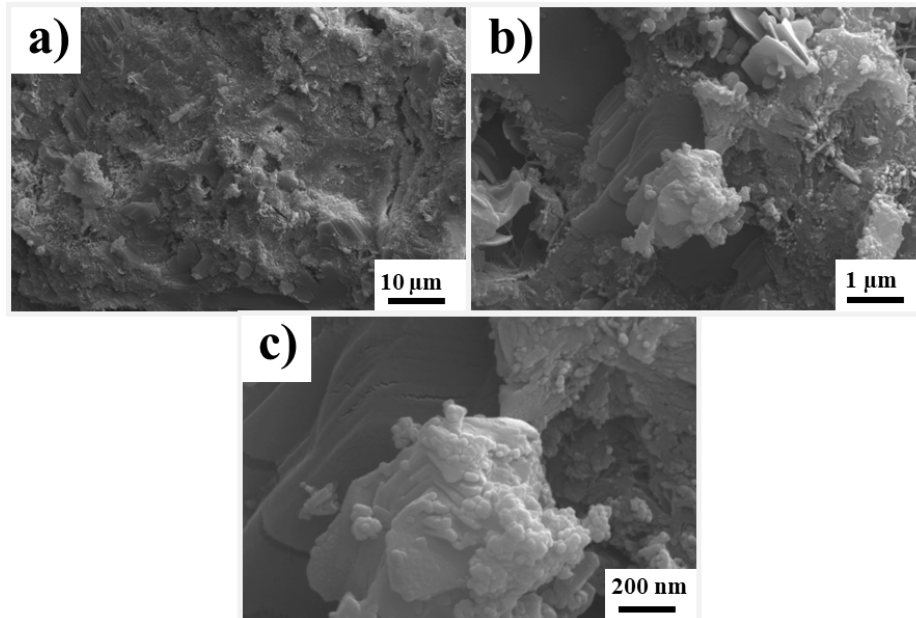


Figure 7.16: SEM images of cement with AL NPs a) Overview of the structure b) Internal structure showing AL NPs and cement c) AL NPs presence in the structure of cement.

In addition, SEM images confirm the presence of MW and MW-OH in the cement structure. The nanotubes can bridge the gaps in the cement structure that contributed to the improved compressive strength, as shown in Figures 7.17 a-c and Figures 7.18 a-c.

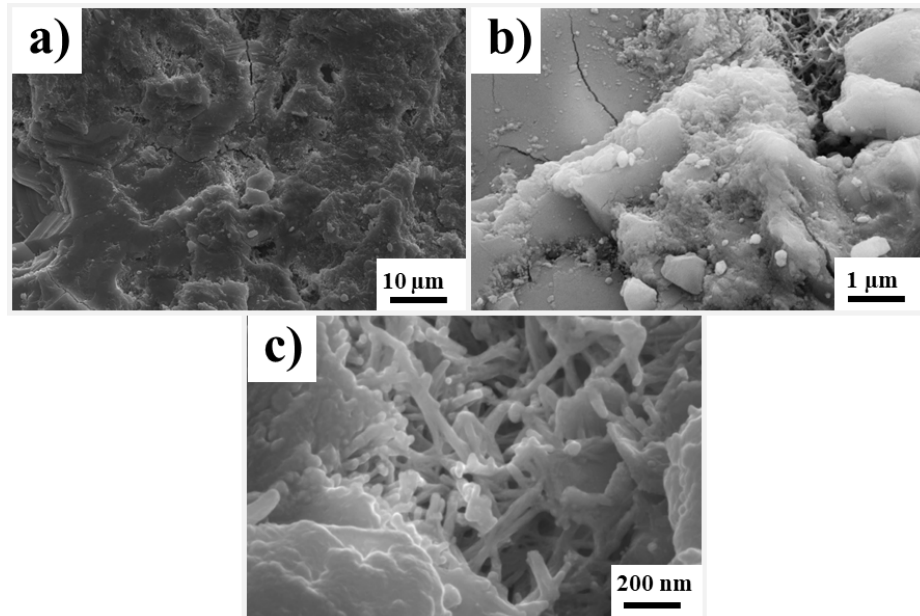


Figure 7.17: SEM images of cement with MW-OH a) Overview of the structure b) Internal structure showing MW-OH and geopolymer c) MW-OH presence in the structure of geopolymer.

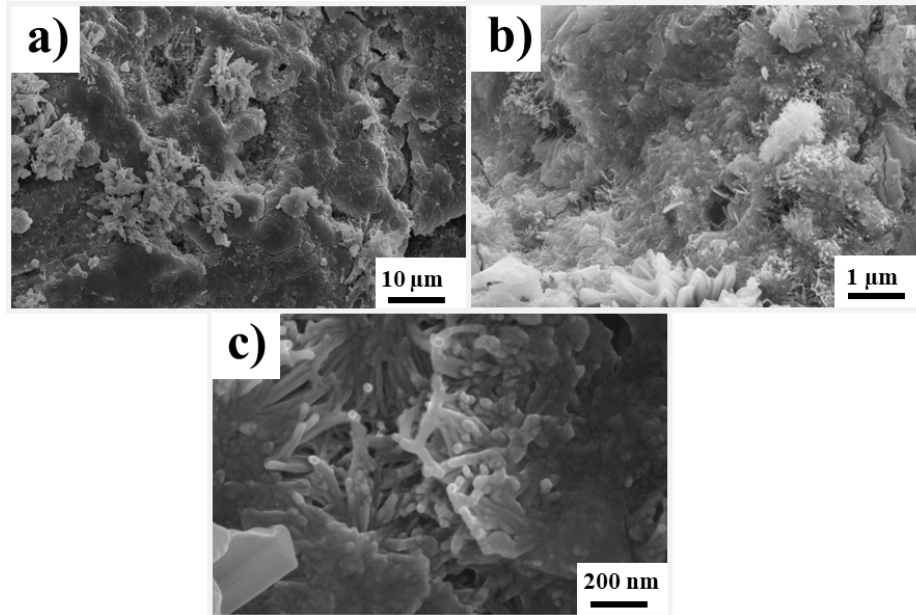


Figure 7.18: SEM images of cement with MW a) Overview of the structure b) Internal structure showing MW and cement c) MW presence in the structure of cement.

Microstructure analysis also confirms the contribution of NPs in the geopolymerization process. Geopolymers with AL NPs produced dense and compact microstructure with better interlocking morphology than neat geopolymers, see Figures 7.19 a-c and Figures 7.20 a-c. Owing to the low Si/Al ratio, the geopolymer with AL NPs formed a highly ordered structure, as indicated in Figure 7.20. *Yong et al. (2007)* [359] also reported similar behaviour of ordered structure with the higher chemical interaction with a decrease in Si/Al. The compact and homogeneous structure with the addition of NPs is due to their ability to fill the gaps in the geopolymer structure, as reported by other studies [360, 361]. The filling effect and strong bond formation contribute to the higher strength of the geopolymer, as confirmed by the results for compressive strength.

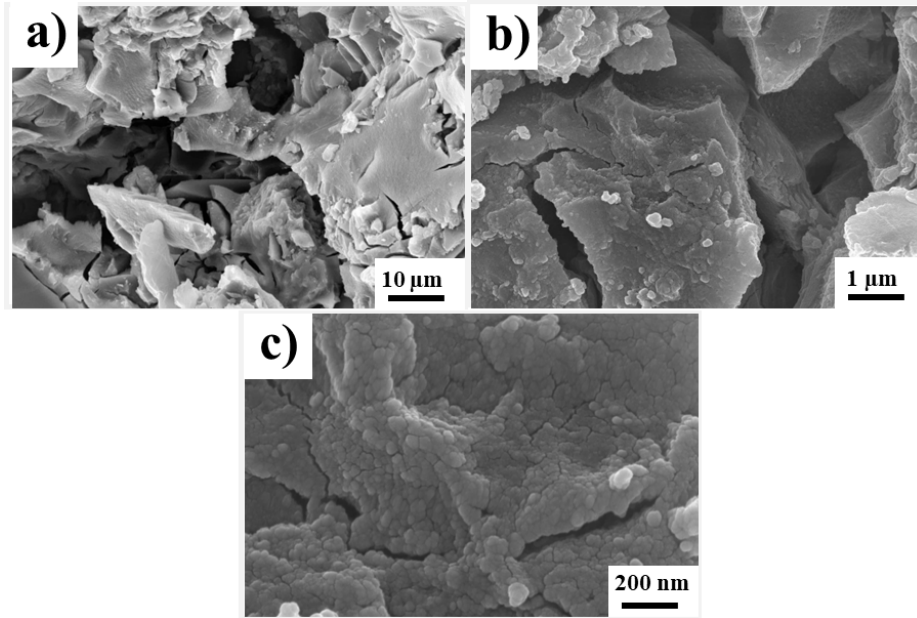


Figure 7.19: SEM images of the neat geopolymer a) Overview of the structure b, c) Internal structure (Paper III).

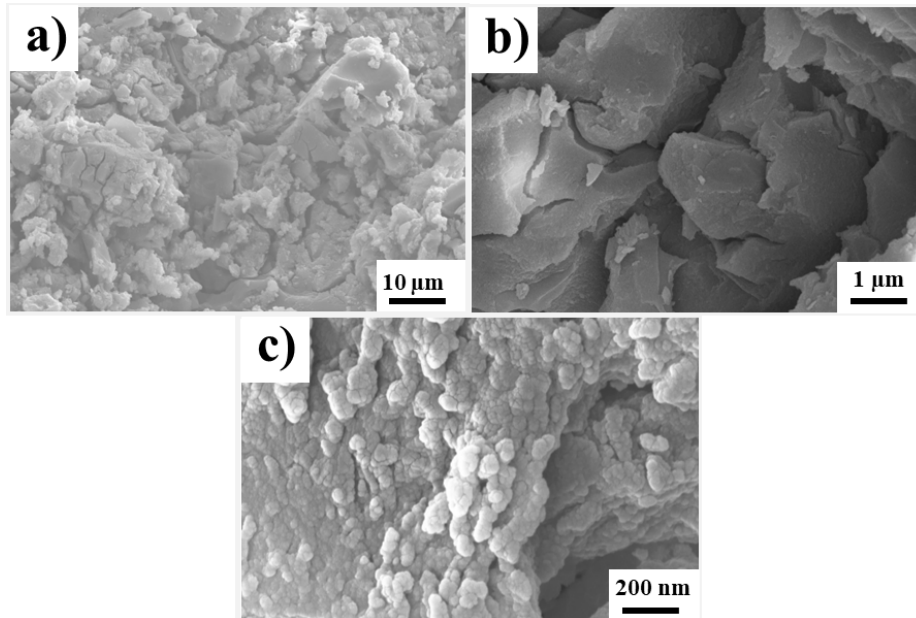


Figure 7.20: SEM images of geopolymer with AL NPs a) Overview of the structure b) Internal structure showing AL NPs and geopolymer c) AL NPs presence in the structure of geopolymer (Paper III).

Similarly, for MW-OH-based geopolymer, the uniform distribution of nanotubes throughout the geopolymer structure produced compact structures, as presented in Figures 7.21 a-c. MW-OH creates bonds with the products formed during the geopolymerization reaction, as shown in Figures 7.21 b, c. In addition, nanotubes can bridge the microcracks in the structure of the geopolymer. As mentioned above, the samples used for SEM analysis are from the UCS test. Therefore, there are cracks present in the structure (Paper III).

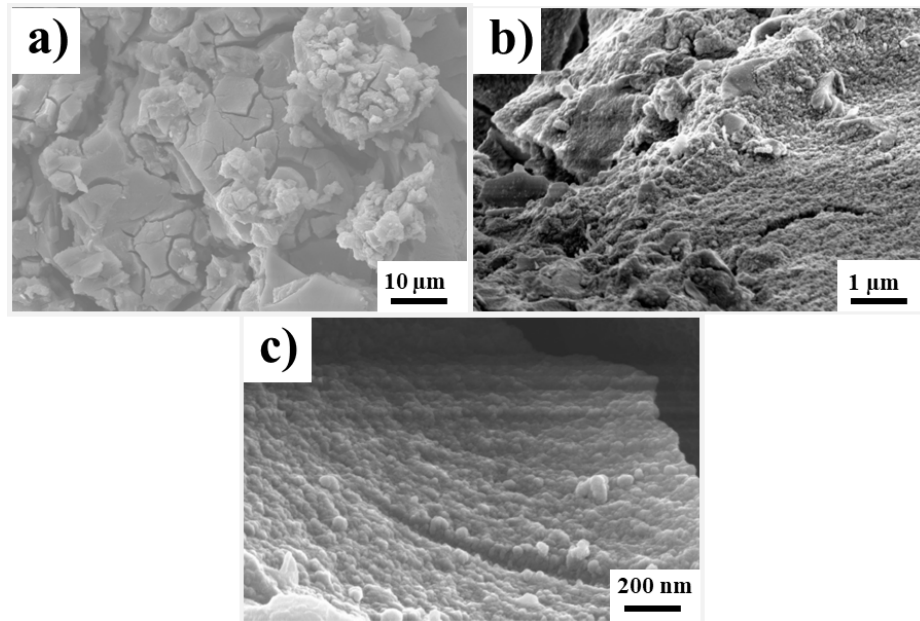


Figure 7.21: SEM images of Geopolymer with MW-OH a) Overview of the structure b) Internal structure showing MW-OH and geopolymer c) MW-OH presence in the structure of geopolymer (Paper III).

8 Conclusions and future work

8.1 Conclusions

This experimental work has investigated how different types of NPs can change the properties of drilling fluids, cement, and geopolymers. Both commercial and in-house prepared NPs have been applied. Different characterization techniques and tests were used to quantify the particle's effect on modifying fluid and material properties. Below, the main findings for water-based drilling fluids, oil-based drilling fluids, cement, and geopolymers are summarised.

Water-Based Drilling Fluids,

Bentonite Drilling Fluids:

- Results suggest that the addition of IONPs (Fe, Fe-XG and Fe-Si), SiO_2 (Si, Si-C, and Si-N), and MWCNTs (MW, MW-OH, MW-COOH) NPs in the bentonite drilling fluids can modify the rheological parameters of the fluid.
- Fe NPs and MWCNTs increase bentonite drilling fluid's gel strength and yield stress. In comparison, surface modification of Fe NPs with polymer (Fe-XG) and silica (Fe-Si) reduces the gel strength. Moreover, SiO_2 NPs also reduce the gel-forming ability of bentonite fluids. Addition of 0.019wt.% Si NPs reduce the gel strength by 8%. In addition, Si, Si-C, and Si-N reduce the yield stress by 62%, 63%, and 31%, respectively. This indicates that surface modification can fine-tune the properties based on the functional groups on the surface of NPs.
- Furthermore, adding NPs to the bentonite drilling fluids promotes the shear thinning behaviour by controlling the excessive gel formation of bentonite fluid at low shear rates.
- The gel strength and yield stress increase by Fe NPs and MWCNTs can enhance the suspension and cutting carrying capacity of drilling fluids, hence improving the transport

of cuttings. However, excessively high values can lead to problems such as increased pumping pressure, difficulties in fluid circulation, and poor hole cleaning. As shown in this work, surface modification of NPs with polymer or silica and the use of SiO_2 NPs can resolve this issue.

- NPs addition to bentonite drilling fluids reduces the mechanical friction values. 0.019wt.% of Fe NPs and 0.0095wt.% MWCNTs in the drilling fluids provide the highest reduction of 43% and 36%, respectively. While, in the case of SiO_2 NPs, surface modified, i.e., Si-N, shows a 39% reduction in friction values. Reduced mechanical friction will lead to reduced torque and drag which again can make it possible to make longer wells and avoid exceeding the operational limits of drilling equipment.
- Fluid loss results suggest that NPs provide reduction for bentonite-based fluids. NPs filled the pores in the filter cake and controlled the fluid flow, as confirmed by the microscale analysis of the filter cake. 0.0095wt.% Fe NPs show the highest decrease of 20%. While, for MWCNTs, MW-COOH reduces the fluid loss by 10%, and Si-N shows a 14% reduction in fluid loss in the case of SiO_2 NPs. Several advantages, such as wellbore stability, reduced formation damage, improved hole cleaning, cost saving, and environmental benefits, are associated with reduced fluid loss.

KCl Drilling Fluids:

- In KCl-based drilling fluids, adding a small concentration of Fe NPs does not significantly impact the gel strength values of the fluid. However, 0.038wt.% Fe NPs reduce the gel strength at high temperature. In contrast, surface modification of Fe with silica (Fe-Si) provides a 22% increase in the gel strength of fluid at 80 °C. Moreover, 0.0095wt Si-C also shows an increase in gel strength. Also, 0.0095wt.% MW shows the most increase in gel strength in the case of MWCNTs. Yield stress results show that 0.038wt.% Fe NPs and 0.019wt.% Fe-Si NPs in drilling fluids increase the yield stress. Also, Si, Si-C, and Si-N NPs

increase the yield stress of the KCl fluid. The results show the potential of NPs to improve the cutting carrying capacity of KCl drilling fluids.

- All types of NPs significantly reduce the mechanical friction values of KCl drilling fluids. Again, low friction values of drilling fluids can reduce the torque and drag which can make it possible to reach longer in the well and avoid exceeding operational limits of drilling.
- In the case of KCl-based fluid, there was no significant reduction in fluid loss owing to the non-uniform distribution of NPs. Also, NPs adsorbed in the cake structure without filling the pores. 0.038wt.% Fe NPs showed the most significant decrease. Also, 0.0095wt.% Fe-Si shows a 10% decrease, and for SiO_2 NPs, Si-N reduces the fluid loss by 13%. In the case of MWCNTs, MW, and MW-OH reduces the fluid loss by 9%.

Oil-Based Drilling Fluids,

The results from this work suggested that IONPs can improve the stability of oil-based drilling fluids at high temperature by keeping the emulsion stable.

- Hydrophobic IONPs are designed to be stable at high temperature, without significant degradation, ensuring their effectiveness in drilling fluids.
- At higher temperatures, 0.5wt.% NPs increase the gel strength of oil-based drilling fluids by 14%. Since elevated temperature can cause gel strength to decrease, which impacts the ability of fluid to suspend solids and maintain stability, NPs act as a bridging agent between colloidal solids in the drilling fluids. They can create a network within the fluid, enhancing the gel-like structure.
- Moreover, 0.5wt.% IONPs in drilling fluids improve the yield stress at high temperature by 55%. The stable dispersion of NPs in the drilling fluids contributed to this increase.

- The higher gel strength and yield stress improve a fluid's resistance to the settling and sagging of barite particles. Therefore, NPs improve barite particle suspension and prevent segregation and settling. IONPs reduced the sag factor both under static and dynamic conditions. For dynamic conditions, the NPs reduced the barite sagging tendency of the base fluid to the safe sag factor limit of 0.53.
- IONPs exhibit lubricating properties and reduce the mechanical friction of oil-based drilling fluids by 39% for 0.5wt.% concentration in the fluid. This lubricating effect of NPs can help minimize torque and drag.
- The oil-based drilling fluid's fluid loss has also been reduced by 70% with NPs. Additionally, a thin filter cake was formed by the IONPs-based drilling fluids. Reduced filter cake thickness and filtrate volume are associated with the reduced permeability of the filter cake. Reducing fluid loss is vital for maintaining wellbore stability, and preventing formation damage.
- Moreover, results from this study also indicate that a low concentration of NPs provides better performance. Therefore, using a low concentration of NPs is recommended to achieve a uniform distribution of NPs in the drilling fluids.

Cement and Geopolymer,

- NPs increase the viscosity of the cement and geopolymer slurries, which can impact the displacement of the slurries; however, NPs increase the pumping time of slurries at high pressure. Especially in the case of geopolymer, the pumping time increases significantly.
- Adding NPs to the cement increases the fluid loss, and the increase is more significant in the case of nanotubes. High fluid loss can cause several issues, such as formation damage, potential channelling in cement sheath, and incomplete hydration. In the case of geopolymer, MW-OH decreased the fluid loss. However, AL NPs increase fluid loss compared to

neat geopolymer.

- Compressive strength results show that AL NPs, MW-OH, and MW increase neat cement's strength after 28 days by 11%, 34%, and 49%, respectively. For geopolymer, both AL NPs and MW-OH increased the compressive strength of the neat geopolymer by 39% and 43%, respectively, after 28 days.
- NPs show a slight increase in Young's modulus values of cement after 28 days, while geopolymer with NPs does not show a significant increase in Young's modulus values compared to the neat geopolymer after 28 days.
- After 28 days, only MW showed an increase in the ratio of UCS and YM of neat cement compared to other NPs. Adding AL NPs and MW-OH to geopolymer slightly increases the UCS and YM ratio after 28 days.
- Tensile strength results show that nanotubes (MW-OH and MW) increase neat cement's tensile strength by 13% and 19%, respectively, after 28 days. For geopolymer, both AL NPs and MW-OH-based mixtures showed improvement after 7 days. However, after 28 days, the increase is not very significant in the case of AL NPs, while the MW-OH-based mixture still showed improvement compared to the neat geopolymer.
- NPs addition to the cement does not show any improvement in the TS to YM ratio after 28 days. Only MW shows a slight increase of 8%. The incorporation of NPs produced a more flexible geopolymer structure until 7 days, with a significant increase in the TS to YM ratio compared to neat geopolymer. However, after 28 days, the TS to YM ratio for AL NPs slightly decreases compared to neat geopolymer, while the MW-OH ratio is improved compared to neat geopolymer.
- UCA results confirm that maximum strength development occurs at the early stages of curing for cement and geopolymer systems with NPs.
- The XRD analysis confirmed the formation of new phases for

geopolymers with NPs, which indicated the chemical reaction of NPs with geopolymers. While for cement with NPs, there was a change in the intensity of peaks due to phase conversions.

- SEM analysis confirmed the presence of AL NPs, MW-OH, and MW in the cement structure. For geopolymer, there is the formation of dense and compact microstructure with the NPs.
- This study indicates that NPs can produce cement and geopolymer material with improved mechanical strength and flexibility for a short curing period. However, NPs might lose these properties for more extended curing periods and should be investigated in future studies. Also, it is critical to reduce the fluid loss for cement slurries and should be investigated further.

The main findings of this research work are:

- Increasing gel strength and yield stress with NPs can improve the drilling fluid's ability to suspend cuttings, support the wellbore, and provide effective hole cleaning.
- The excessive gel formation of bentonite-based drilling fluids can be avoided by choosing the proper NPs or by altering the functionality of NPs. This can avoid potential wellbore instability problems such as poor hole cleaning and high pumping pressure.
- NPs facilitate shear thinning behavior in drilling fluids. Shear thinning allows the efficient flow of fluid through the drill bit and drill string, facilitating effective pumping. This helps to avoid the cutting settling in the wellbore, minimizing the risk of a stuck pipe.
- NPs improve the lubricating properties of drilling fluids, which can improve drilling efficiency, prevent stuck pipe incidents, extend tool life, and enhance wellbore stability.
- The ability of NPs to reduce the fluid loss of drilling fluid can provide several advantages during drilling operations, such as

wellbore stability, reduced formation damage, improved hole cleaning, cost savings, and environmental benefits.

- NPs control barite settling and can solve fluid density control, hole cleaning, and wellbore stability issues. Moreover, reducing barite sagging can provide better pumpability of the drilling fluid.
- Increasing the compressive strength of cement and geopolymer with NPs can offer a more robust and durable sheath around the casing. This can enhance the integrity of the wellbore, minimizing the risk of casing failure and leaks.
- An increase in YM of cement with NPs indicates greater stiffness and resistance to deformation.
- Cement and geopolymer with NPs are less prone to deformation until compressive loads as NPs increase the UCS to YM ratio.
- NPs can improve the ability of cement and geopolymer to withstand axial loads or stretching forces without undergoing deformation and breaking by improving tensile strength.
- Due to the improved TS to YM ratio, cement, and geopolymer with NPs are less prone to brittle failure under tensile stresses.

8.2 Future Work

The potential future work on the application of drilling fluids and cement can be,

- Laboratory and field scale testing of NPs in commercial water-based drilling fluids to assess their suitability for large-scale application.
- Cost analysis of adding NPs to the drilling fluids to assess the cost-saving potential of adding NPs to the drilling fluids.
- Health, safety, and environmental considerations should be considered when working with NPs in drilling fluids.

Conclusions and future work

- Microscale analysis of filter cake formed by the oil-based drilling fluids with NPs.
- Long-term assessment of mechanical properties of cement and geopolymer with NPs.
- Contamination of cement and geopolymer with drilling fluid and studying the impact on NPs in preserving the properties of cement and geopolymer.
- Since the viscosity of cement slurry can impact the quality of the cement sheath formed around the casing. Moreover, it can impact cement bonding with the casing and the wellbore. The impact of NPs on the viscosity of cement and geopolymer should be investigated further.
- This work shows that NPs can contribute to increased fluid loss of cement. Therefore, future studies should consider minimizing the fluid loss from cement by testing different NPs.
- The impact of NPs on the bonding of cement with the casing and formation needs further investigation.

References

- [1] Ryen Caenn, Henry CH Darley, and George R Gray. *Composition and properties of drilling and completion fluids*. Gulf professional publishing, 2011.
- [2] N Berthezene, J-C De Hemptinne, A Audibert, and J-F Argillier. Methane solubility in synthetic oil-based drilling muds. *Journal of Petroleum Science and Engineering*, 23(2): 71–81, 1999.
- [3] George V Chilingarian and Paul Vorabutr. *Drilling and drilling fluids*. 1983.
- [4] Adam T Bourgoyne, Keith K Millheim, Martin E Chenevert, Farrile S Young, et al. *Applied drilling engineering*, volume 2. Society of Petroleum Engineers Richardson, 1986.
- [5] Ryen Caenn and George V Chillingar. Drilling fluids: State of the art. *Journal of petroleum science and engineering*, 14(3-4): 221–230, 1996.
- [6] Mehran Sadeghalvaad and Samad Sabbaghi. The effect of the tio₂/polyacrylamide nanocomposite on water-based drilling fluid properties. *Powder Technology*, 272:113–119, 2015.
- [7] Abdul Hazim Abdullah, Syahrir Ridha, Dzeti Farhah Mohshim, Mohammad Yusuf, Hesam Kamyab, Shwetank Krishna, and Mohd Azuwan Maoinsar. A comprehensive review of nanoparticles in water-based drilling fluids on wellbore stability. *Chemosphere*, page 136274, 2022.
- [8] Shu He, Lixi Liang, Yinjin Zeng, Yi Ding, Yongxue Lin, and Xiangjun Liu. The influence of water-based drilling fluid on mechanical property of shale and the wellbore stability. *Petroleum*, 2(1):61–66, 2016.
- [9] Russell T Ewy and E Keith Morton. Wellbore-stability performance of water-based mud additives. *SPE Drilling & Completion*, 24(03):390–397, 2009.

REFERENCES

- [10] Sidharth Gautam, Chandan Guria, and Vinay K Rajak. A state of the art review on the performance of high-pressure and high-temperature drilling fluids: Towards understanding the structure-property relationship of drilling fluid additives. *Journal of Petroleum Science and Engineering*, 213:110318, 2022.
- [11] J Abdo and MD Haneef. Clay nanoparticles modified drilling fluids for drilling of deep hydrocarbon wells. *Applied Clay Science*, 86:76–82, 2013.
- [12] Hanyi Zhong, Zhengsong Qiu, Weian Huang, Dong Sun, Daoming Zhang, and Jie Cao. Synergistic stabilization of shale by a mixture of polyamidoamine dendrimers modified bentonite with various generations in water-based drilling fluid. *Applied Clay Science*, 114:359–369, 2015.
- [13] Xiangchao Shi, Lei Wang, Jianhua Guo, Qiang Su, and Xiao Zhuo. Effects of inhibitor kcl on shale expansibility and mechanical properties. *Petroleum*, 5(4):407–412, 2019.
- [14] Hui Mao, Zhengsong Qiu, Zhonghou Shen, and Weian Huang. Hydrophobic associated polymer based silica nanoparticles composite with core-shell structure as a filtrate reducer for drilling fluid at ultra-high temperature. *Journal of Petroleum Science and Engineering*, 129:1–14, 2015.
- [15] Xin Zhao, Zhengsong Qiu, Mingliang Wang, Weian Huang, and Shifeng Zhang. Performance evaluation of a highly inhibitive water-based drilling fluid for ultralow temperature wells. *Journal of Energy Resources Technology*, 140(1):012906, 2018.
- [16] Hanyi Zhong, Guangcheng Shen, Zhengsong Qiu, Yongxue Lin, Lijun Fan, Xiaodong Xing, and Jia Li. Minimizing the hthp filtration loss of oil-based drilling fluid with swellable polymer microspheres. *Journal of Petroleum Science and Engineering*, 172:411–424, 2019.
- [17] Vikrant Wagle, Abdullah S Al-Yami, and Ali AlSafran.

REFERENCES

- Designing invert emulsion drilling fluids for hthp conditions. In *SPE Kingdom of Saudi Arabia Annual Technical Symposium and Exhibition*. OnePetro, 2018.
- [18] Ahmet Ay, T Sagberg, KR Gyland, Arne Askø, Ole Henrik Jordal, and Ørjan Døssland. Use of specially treated micronized barite fluid system with wellbore strengthening approach to drill extremely depleted reservoir-hpht kvitebjørn field, offshore norway. In *SPE Norway Subsurface Conference?*, page D011S004R001. SPE, 2016.
- [19] Salem Basfar, Abdelmjeed Mohamed, Salaheldin Elkatatny, and Abdulaziz Al-Majed. A combined barite–ilmenite weighting material to prevent barite sag in water-based drilling fluid. *Materials*, 12(12):1945, 2019.
- [20] Rolv Rommetveit, Kjell Kåre Fjelde, Bjarne Aas, Norman F Day, Eric Low, and David H Schwartz. Hpht well control; an integrated approach. In *Offshore Technology Conference*, pages OTC–15322. OTC, 2003.
- [21] Mario Zamora and Reginald Bell. Improved wellsite test for monitoring barite sag. In *proceedings of the AADE 2004 drilling fluids conference, Houston, TX, USA*, pages 6–7, 2004.
- [22] Omar Mahmoud, Hisham A Nasr-El-Din, Zisis Vryzas, and Vassilios C Kelessidis. Characterization of filter cake generated by nanoparticle-based drilling fluid for hp/ht applications. In *SPE International Conference on Oilfield Chemistry?*, page D021S006R006. SPE, 2017.
- [23] Wenhao He, Asadollah Hayatdavoudi, Keyong Chen, Kaustubh Sawant, Qin Zhang, and Chi Zhang. Enhancement of plastering effect on strengthening wellbore by optimizing particle size distribution of wellbore strengthening materials. *Journal of Energy Resources Technology*, 141(12):122905, 2019.
- [24] Svein Syltøy, Svein Erik Eide, Steinar Torvund, Per Cato Berg, Tore Larsen, Helge Fjeldberg, Knut Steinar Bjørkevoll, John McCaskill, Ole Iacob Prebensen, and Eric Low. Highly

REFERENCES

- advanced multitechnical mpd concept extends achievable hpht targets in the north sea. In *SPE/IADC Managed Pressure Drilling and Underbalanced Operations Conference and Exhibition?*, pages SPE-114484. SPE, 2008.
- [25] Trent Jacobs. Pushing the frontier through wellbore strengthening. *Journal of Petroleum Technology*, 66(11):64–73, 2014.
- [26] Oscar Contreras, Geir Hareland, Maen Husein, Runar Nygaard, and Mortadha Alsaba. Wellbore strengthening in sandstones by means of nanoparticle-based drilling fluids. In *SPE deepwater drilling and completions conference*. OnePetro, 2014.
- [27] Franco Federici, Thierry Bossi, Christian Parisi, Luigi Merli, Daniele Moro, Pierangelo Pirovano, and Giuseppe Li Bassi. Method for reducing filtrate loss from oil based drilling fluids, February 24 2015. US Patent 8,962,533.
- [28] Claas H Van Der Zwaag, Tor Henry Omland, and Tore Vandbakk. Dynamic filtration: Seepage losses on tyrihans. In *SPE International Symposium and Exhibition on Formation Damage Control*. OnePetro, 2012.
- [29] Johannes Fink. *Petroleum engineer’s guide to oil field chemicals and fluids*. Gulf Professional Publishing, 2021.
- [30] JJ Azar and GR Samuel. Drilling engineering [e-book]. oklahoma, 2007.
- [31] Oscar Contreras, Geir Hareland, Maen Husein, Runar Nygaard, and Mortadha Alsaba. Application of in-house prepared nanoparticles as filtration control additive to reduce formation damage. In *SPE International Symposium and Exhibition on Formation Damage Control*. OnePetro, 2014.
- [32] AK Mohamed, SA Elkatatny, MA Mahmoud, RA Shawabkeh, and AA Al-Majed. The evaluation of micronized barite as a weighting material for completing hpht wells. In *SPE Middle*

REFERENCES

- East Oil and Gas Show and Conference*, page D031S027R005. SPE, 2017.
- [33] Chesnee Lae Davis, Philip Wayne Livanec, and William Walter Shumway. Additive to enhance sag stability of drilling fluid, March 17 2020. US Patent 10,590,323.
- [34] Salem Basfar, Salaheldin Elkatatny, Mohamed Mahmoud, Muhammad Shahzad Kamal, Mobeen Murtaza, and Theo Stanitzek. Prevention of barite sagging while drilling high-pressure high-temperature (hpht) wells. In *SPE Kingdom of Saudi Arabia Annual Technical Symposium and Exhibition*. OnePetro, 2018.
- [35] Salaheldin Elkatatny. Mitigation of barite sagging during the drilling of high-pressure high-temperature wells using an invert emulsion drilling fluid. *Powder technology*, 352:325–330, 2019.
- [36] Sushant Agarwal, Phuoc Tran, Yee Soong, Donald Martello, and Rakesh K Gupta. Flow behavior of nanoparticle stabilized drilling fluids and effect of high temperature aging. In *AADE national technical conference and exhibition*, volume 2011, pages 1–6, 2011.
- [37] Li-Ming Zhang and Dai-Yi Yin. Preparation of a new lignosulfonate-based thinner: introduction of ferrous ions. *Colloids and Surfaces A: Physicochemical and Engineering Aspects*, 210(1):13–21, 2002.
- [38] Dominique Guillot et al. Well cementing second edition. 2006.
- [39] NORSOK Standard. Well integrity in drilling and well operations. *D-010, rev, 4*, 2013.
- [40] Mesfin Belayneh and Bernt S Aadnøy. Effect of nano and micro sized particle additives on the mechanical strength of cement plug. In *International Conference on Offshore Mechanics and Arctic Engineering*, volume 56581, page V010T11A015. American Society of Mechanical Engineers, 2015.
- [41] B Vignes and B Aadnøy. Well-integrity issues offshore norway.

REFERENCES

- spe prod oper 25 (2): 145–150. *Society of Petroleum Engineers*, 2010.
- [42] Petroleum Safety Authority Norway. Trends in risk level in the norwegian petroleum activity, 2019. <https://www.ptil.no/contentassets/9f8d7613b06a4c989d6751b8eab0a6fd/rnnp-2019-summary-report.pdf>.
- [43] Petroleum Safety Authority Norway. Trends in risk level in the petroleum activity, summary report 2021, 2021. https://www.ptil.no/contentassets/104669d9b3fd4c17a630d5e671607594/sammendragsrapp_2021_engelsk.pdf.
- [44] Theresa L Watson and Stefan Bachu. Evaluation of the potential for gas and co2 leakage along wellbores. *SPE Drilling & Completion*, 24(01):115–126, 2009.
- [45] Torbjørn Vrålstad, Arild Saasen, Erling Fjær, Thomas Øia, Jan David Ytrehus, and Mahmoud Khalifeh. Plug & abandonment of offshore wells: Ensuring long-term well integrity and cost-efficiency. *Journal of Petroleum Science and Engineering*, 173:478–491, 2019.
- [46] Chad Shenold and Catalin Teodoriu. Development of a structured workflow for enhanced well cement integrity: lessons learned and the way ahead. *Journal of Natural Gas Science and Engineering*, 36:824–836, 2016.
- [47] Alexandre Lavrov and Malin Torsæter. Physics and mechanics of primary well cementing. 2016.
- [48] Narjes Jafariesfad, Mette Rica Geiker, Yi Gong, Pål Skalle, Zhiliang Zhang, and Jianying He. Cement sheath modification using nanomaterials for long-term zonal isolation of oil wells. *Journal of Petroleum Science and Engineering*, 156:662–672, 2017.
- [49] Akshar Thakkar, Aakash Raval, Shishir Chandra, Manan Shah, and Anirbid Sircar. A comprehensive review of the application

REFERENCES

- of nano-silica in oil well cementing. *Petroleum*, 6(2):123–129, 2020.
- [50] G Carette and VM Malhotra. Early-age strength development of concrete incorporating fly ash and condensed silica fume. *Special Publication*, 79:765–784, 1983.
- [51] VM Mahotra. Use of mineral admixtures for specialized concretes. *Concrete International*, 6(4):19–24, 1984.
- [52] Rolf F Feldman and Huang Cheng-yi. Properties of portland cement-silica fume pastes ii. mechanical properties. *Cement and Concrete Research*, 15(6):943–952, 1985.
- [53] G Radenti and L Ghiringhelli. Cementing materials for geothermal wells. *Geothermics*, 1(3):119–123, 1972.
- [54] Abdullah S Al-Yami. An overview of different chemicals used in designing cement slurries for oil and gas wells. In *SPE Kuwait oil and gas show and conference*, pages SPE–175259. SPE, 2015.
- [55] Catalin Teodoriu, Christian Kosinowski, Mahmood Amani, Jerome Schubert, and Arash Shadravan. Wellbore integrity and cement failure at hph conditions. *International Journal of Engineering*, 2(2):2305–8269, 2013.
- [56] Raj Kiran, Catalin Teodoriu, Younas Dadmohammadi, Runar Nygaard, David Wood, Mehdi Mokhtari, and Saeed Salehi. Identification and evaluation of well integrity and causes of failure of well integrity barriers (a review). *Journal of Natural Gas Science and Engineering*, 45:511–526, 2017.
- [57] Saeed Salehi, Mohammad Jamal Khattak, Nasir Ali, C Ezeakacha, and Fatemeh K Saleh. Study and use of geopolymer mixtures for oil and gas well cementing applications. *Journal of Energy Resources Technology*, 140(1):012908, 2018.
- [58] Shu-Yuan Pan, Yi-Hung Chen, Liang-Shih Fan, Hyunook Kim, Xiang Gao, Tung-Chai Ling, Pen-Chi Chiang, Si-Lu Pei, and Guowei Gu. Co₂ mineralization and utilization by alkaline solid

REFERENCES

- wastes for potential carbon reduction. *Nature Sustainability*, 3(5):399–405, 2020.
- [59] FN Costa and DV Ribeiro. Reduction in co2 emissions during production of cement, with partial replacement of traditional raw materials by civil construction waste (ccw). *Journal of Cleaner Production*, 276:123302, 2020.
- [60] Jan Skocek, Maciej Zajac, and Mohsen Ben Haha. Carbon capture and utilization by mineralization of cement pastes derived from recycled concrete. *Scientific Reports*, 10(1):1–12, 2020.
- [61] Javier Farfan, Mahdi Fasihi, and Christian Breyer. Trends in the global cement industry and opportunities for long-term sustainable ccu potential for power-to-x. *Journal of Cleaner Production*, 217:821–835, 2019.
- [62] Paul Carragher and Jeff Fulks. Well abandonment solutions utilizing bismuth and thermite. In *Abu Dhabi International Petroleum Exhibition and Conference*, page D021S031R004. SPE, 2018.
- [63] Mahmoud Khalifeh, Helge Hodne, Arild Saasen, and Torbjorn Vralstad. Techniques and materials for north sea plug and abandonment operations. In *Offshore Technology Conference*, pages OTC–23915. OTC, 2013.
- [64] Khalifeh Mahmoud, Saasen Arild, Vralstad Torbjorn, and H Helge. Potential utilization of class c fly ash-based geopolymer in oil well cementing operations. *Cement and Concrete Composites*, 53:10–17, 2014.
- [65] Mahmoud Khalifeh, Arild Saasen, Helge Hodne, Rune Godøy, and Torbjørn Vralstad. Geopolymers as an alternative for oil well cementing applications: A review of advantages and concerns. *Journal of Energy Resources Technology*, 140(9):092801, 2018.

REFERENCES

- [66] Xiangyu Liu. *Mud-to-cement conversion of synthetic-based drilling muds using geopolymers*. PhD thesis, 2017.
- [67] Saeed Salehi, Jamal Khattak, Fatemeh K Saleh, and Stanley Igbojekwe. Investigation of mix design and properties of geopolymers for application as wellbore cement. *Journal of Petroleum Science and Engineering*, 178:133–139, 2019.
- [68] Joseph Davidovits. Mineral polymers and methods of making them, September 14 1982. US Patent 4,349,386.
- [69] Joseph Davidovits. Geopolymers: inorganic polymeric new materials. *Journal of Thermal Analysis and calorimetry*, 37(8): 1633–1656, 1991.
- [70] Peter Duxson, Ana Fernández-Jiménez, John L Provis, Grant C Lukey, Angel Palomo, and Jannie SJ van Deventer. Geopolymer technology: the current state of the art. *Journal of materials science*, 42:2917–2933, 2007.
- [71] Joseph Davidovits. *Geopolymer, green chemistry and sustainable development solutions: proceedings of the world congress geopolymer 2005*. Geopolymer Institute, 2005.
- [72] Konstantinos A Komnitsas. Potential of geopolymer technology towards green buildings and sustainable cities. *Procedia Engineering*, 21:1023–1032, 2011.
- [73] B Singh, G Ishwarya, M Gupta, and SK Bhattacharyya. Geopolymer concrete: A review of some recent developments. *Construction and building materials*, 85:78–90, 2015.
- [74] Kang Gao, Kae-Long Lin, DeYing Wang, Hau-Shing Shiu, Chao-Lung Hwang, and Ta-Wui Cheng. Effects of nano-sio₂ on setting time and compressive strength of alkaliactivated metakaolin-based geopolymer. *The Open Civil Engineering Journal*, 7(1), 2013.
- [75] S Salehi, N Ali, MJ Khattak, and H Rizvi. Geopolymer composites as efficient and economical plugging materials in

REFERENCES

- peanuts price oil market. In *SPE Annual Technical Conference and Exhibition?*, page D021S032R007. SPE, 2016.
- [76] MCM Nasvi, PG Ranjith, J Sanjayan, and H Bui. Effect of temperature on permeability of geopolymer: A primary well sealant for carbon capture and storage wells. *Fuel*, 117:354–363, 2014.
- [77] Mahmoud Khalifeh, Jelena Todorovic, Torbjørn Vrålstad, Arild Saasen, and Helge Hodne. Long-term durability of rock-based geopolymers aged at downhole conditions for oil well cementing operations. *Journal of Sustainable Cement-Based Materials*, 6 (4):217–230, 2017.
- [78] Mahmoud Khalifeh, Arild Saasen, Torbjørn Vrålstad, Helge B Larsen, and Helge Hodne. Cap rock restoration in plug and abandonment operations; possible utilization of apelite-based geopolymers for permanent zonal isolation and well plugging. In *SPE Offshore Europe Conference and Exhibition*. OnePetro, 2015.
- [79] Maria DM Paiva, Emílio CCM Silva, Dulce MA Melo, Antônio E Martinelli, and José F Schneider. A geopolymer cementing system for oil wells subject to steam injection. *Journal of Petroleum Science and Engineering*, 169:748–759, 2018.
- [80] Munawar Khalil, Badrul Mohamed Jan, Chong Wen Tong, and Mohammed Ali Berawi. Advanced nanomaterials in oil and gas industry: Design, application and challenges. *Applied energy*, 191:287–310, 2017.
- [81] Mortadha T Alsaba, Mohammed F Al Dushaishi, and Ahmed K Abbas. A comprehensive review of nanoparticles applications in the oil and gas industry. *Journal of Petroleum Exploration and Production Technology*, 10:1389–1399, 2020.
- [82] Md Amanullah and Ashraf M Al-Tahini. Nano-technology-its significance in smart fluid development for oil and gas field

REFERENCES

- application. In *SPE Saudi Arabia Section Technical Symposium*. OnePetro, 2009.
- [83] Biswajit Mukherjee, Niladri Shekhar Dey, Ruma Maji, Priyanka Bhowmik, Pranab Jyoti Das, and Paramita Paul. Current status and future scope for nanomaterials in drug delivery. In *Application of nanotechnology in drug delivery*. IntechOpen, 2014.
- [84] Jianguo Xu, Zhengsong Qiu, Weian Huang, and Xin Zhao. Preparation and performance properties of polymer latex sdnl in water-based drilling fluids for drilling troublesome shale formations. *Journal of Natural Gas Science and Engineering*, 37:462–470, 2017.
- [85] CNR Rao and AK Cheetham. Science and technology of nanomaterials: current status and future prospects. *Journal of Materials Chemistry*, 11(12):2887–2894, 2001.
- [86] AARI Aftab, Abdul Razak Ismail, ZH Ibupoto, H Akeiber, and MGK Malghani. Nanoparticles based drilling muds a solution to drill elevated temperature wells: A review. *Renewable and Sustainable Energy Reviews*, 76:1301–1313, 2017.
- [87] Omar Mahmoud, Hisham A Nasr-El-Din, Zisis Vryzas, and Vassilios C Kelessidis. Nanoparticle-based drilling fluids for minimizing formation damage in hp/ht applications. In *SPE international conference and exhibition on formation damage control*. OnePetro, 2016.
- [88] Zisis Vryzas and Vassilios C Kelessidis. Nano-based drilling fluids: A review. *Energies*, 10(4):540, 2017.
- [89] J Abdo and M Danish Haneef. Nano-enhanced drilling fluids: pioneering approach to overcome uncompromising drilling problems. 2012.
- [90] J Abdo, H AL-Sharji, and E Hassan. Effects of nano-sepiolite on rheological properties and filtration loss of water-based drilling fluids. *Surface and Interface Analysis*, 48(7):522–526, 2016.

REFERENCES

- [91] Saeed Ghanbari, Ezatallah Kazemzadeh, Mohammad Soleymani, and Abbas Naderifar. A facile method for synthesis and dispersion of silica nanoparticles in water-based drilling fluid. *Colloid and Polymer Science*, 294:381–388, 2016.
- [92] Rajat Jain, Vikas Mahto, and VP Sharma. Evaluation of polyacrylamide-grafted-polyethylene glycol/silica nanocomposite as potential additive in water based drilling mud for reactive shale formation. *Journal of Natural Gas Science and Engineering*, 26:526–537, 2015.
- [93] Allan Katende, Natalie V Boyou, Issham Ismail, Derek Z Chung, Farad Sagala, Norhafizuddin Hussein, and Muhamad S Ismail. Improving the performance of oil based mud and water based mud in a high temperature hole using nanosilica nanoparticles. *Colloids and surfaces a: physicochemical and engineering aspects*, 577:645–673, 2019.
- [94] Muhammed Awais Alvi, Mesfin Belayneh, Arild Saasen, and Bernt S Aadnøy. The effect of micro-sized boron nitride bn and iron trioxide fe₂o₃ nanoparticles on the properties of laboratory bentonite drilling fluid. In *SPE Norway one day seminar*. OnePetro, 2018.
- [95] Muhammad Awais Ashfaq Alvi, Mesfin Belayneh, Arild Saasen, Kjell Kåre Fjelde, and Bernt S Aadnøy. Effect of mwcnt and mwcnt functionalized-oh and-cooh nanoparticles in laboratory water based drilling fluid. In *International Conference on Offshore Mechanics and Arctic Engineering*, volume 51296, page V008T11A069. American Society of Mechanical Engineers, 2018.
- [96] AARI Aftab, AR Ismail, S Khokhar, and Zafar Hussain Ibupoto. Novel zinc oxide nanoparticles deposited acrylamide composite used for enhancing the performance of water-based drilling fluids at elevated temperature conditions. *Journal of Petroleum Science and Engineering*, 146:1142–1157, 2016.
- [97] Norasazly Mohd Taha and Sean Lee. Nano graphene application

REFERENCES

- improving drilling fluids performance. In *International petroleum technology conference*, page D021S013R005. IPTC, 2015.
- [98] Kunlin Song, Qinglin Wu, Meichun Li, Suxia Ren, Lili Dong, Xiuqiang Zhang, Tingzhou Lei, and Yoichi Kojima. Water-based bentonite drilling fluids modified by novel biopolymer for minimizing fluid loss and formation damage. *Colloids and Surfaces A: Physicochemical and Engineering Aspects*, 507:58–66, 2016.
- [99] Jay Karen Maria William, Swaminathan Ponmani, Robello Samuel, R Nagarajan, and Jitendra S Sangwai. Effect of cuo and zno nanofluids in xanthan gum on thermal, electrical and high pressure rheology of water-based drilling fluids. *Journal of Petroleum Science and Engineering*, 117:15–27, 2014.
- [100] Babak Fazelabdolabadi, Abbas Ali Khodadadi, and Mostafa Sedaghatzadeh. Thermal and rheological properties improvement of drilling fluids using functionalized carbon nanotubes. *Applied Nanoscience*, 5:651–659, 2015.
- [101] Sedigheh Sadegh Hassani, Azadeh Amrollahi, Alimorad Rashidi, Mohammad Soleymani, and Saeede Rayatdoost. The effect of nanoparticles on the heat transfer properties of drilling fluids. *Journal of Petroleum Science and Engineering*, 146:183–190, 2016.
- [102] Yili Kang, Jiping She, Hao Zhang, Lijun You, and Minggu Song. Strengthening shale wellbore with silica nanoparticles drilling fluid. *Petroleum*, 2(2):189–195, 2016.
- [103] Charles O Nwaoji, Geir Hareland, Maen Husein, Runar Nygaard, and Mohammad Ferdous Zakaria. Wellbore strengthening-nano-particle drilling fluid experimental design using hydraulic fracture apparatus. In *SPE/IADC Drilling Conference and Exhibition*, pages SPE–163434. SPE, 2013.
- [104] Mukul M Sharma, Rui Zhang, Martin E Chenevert, Lujun Ji, Quan Guo, and Jim Friedheim. A new family of nanoparticle

REFERENCES

- based drilling fluids. In *SPE Annual Technical Conference and Exhibition?*, pages SPE–160045. SPE, 2012.
- [105] Jose Aramendiz and Abdulmohsin Imqam. Water-based drilling fluid formulation using silica and graphene nanoparticles for unconventional shale applications. *Journal of Petroleum Science and Engineering*, 179:742–749, 2019.
- [106] Subramanian Natarajan, Kannan Harini, Gnana Prakash Gajula, Bruno Sarmiento, Maria Teresa Neves-Petersen, and Viruthachalam Thiagarajan. Multifunctional magnetic iron oxide nanoparticles: Diverse synthetic approaches, surface modifications, cytotoxicity towards biomedical and industrial applications. *BMC Materials*, 1(1):1–22, 2019.
- [107] Gang Liu, Jinhao Gao, Hua Ai, and Xiaoyuan Chen. Applications and potential toxicity of magnetic iron oxide nanoparticles. *Small*, 9(9-10):1533–1545, 2013.
- [108] Youngsoo Jung, You-Hwan Son, Jung-Kun Lee, Tran X Phuoc, Yee Soong, and Minking K Chyu. Rheological behavior of clay–nanoparticle hybrid-added bentonite suspensions: specific role of hybrid additives on the gelation of clay-based fluids. *ACS applied materials & interfaces*, 3(9):3515–3522, 2011.
- [109] Matthew M Barry, Youngsoo Jung, Jung-Kun Lee, Tran X Phuoc, and Minking K Chyu. Fluid filtration and rheological properties of nanoparticle additive and intercalated clay hybrid bentonite drilling fluids. *Journal of Petroleum Science and Engineering*, 127:338–346, 2015.
- [110] Zisis Vryzas, Omar Mahmoud, Hisham Nasr-El-Din, Vassilis Zaspalis, and Vassilios C Kelessidis. Incorporation of fe₃o₄ nanoparticles as drilling fluid additives for improved drilling operations. In *International Conference on Offshore Mechanics and Arctic Engineering*, volume 49996, page V008T11A040. American Society of Mechanical Engineers, 2016.
- [111] Z Vryzas, V Zaspalis, L Nalbantian, O Mahmoud, HA Nasr-El-Din, and VC Kelessidis. A comprehensive approach

REFERENCES

- for the development of new magnetite nanoparticles giving smart drilling fluids with superior properties for hp/ht applications. In *International petroleum technology conference*, page D031S053R001. IPTC, 2016.
- [112] Omar Mahmoud, Hisham A Nasr-El-Din, Zisis Vryzas, and Vassilios C Kelessidis. Using ferric oxide and silica nanoparticles to develop modified calcium bentonite drilling fluids. *SPE Drilling & Completion*, 33(01):12–26, 2018.
- [113] Omar Mahmoud, Hisham A Nasr-El-Din, Zisis Vryzas, and Vassilios C Kelessidis. Effect of ferric oxide nanoparticles on the properties of filter cake formed by calcium bentonite-based drilling muds. *SPE Drilling & Completion*, 33(04):363–376, 2018.
- [114] Alireza Rezaei, Vahid Nooripoor, and Khalil Shahbazi. Applicability of fe 3 o 4 nanoparticles for improving rheological and filtration properties of bentonite-water drilling fluids in the presence of sodium, calcium, and magnesium chlorides. *Journal of Petroleum Exploration and Production Technology*, 10:2453–2464, 2020.
- [115] Alexander Liberman, Natalie Mendez, William C Trogler, and Andrew C Kummel. Synthesis and surface functionalization of silica nanoparticles for nanomedicine. *Surface science reports*, 69(2-3):132–158, 2014.
- [116] Vanitha Selvarajan, Sybil Obuobi, and Pui Lai Rachel Ee. Silica nanoparticles—a versatile tool for the treatment of bacterial infections. *Frontiers in chemistry*, 8:602, 2020.
- [117] Taner Sensoy, Martin E Chenevert, and Mukul M Sharma. Minimizing water invasion in shale using nanoparticles. In *SPE Annual Technical Conference and Exhibition?*, pages SPE–124429. SPE, 2009.
- [118] Jihua Cai, Martin E Chenevert, Mukul M Sharma, and Jim Friedheim. Decreasing water invasion into atoka shale using

REFERENCES

- nonmodified silica nanoparticles. *SPE Drilling & Completion*, 27(01):103–112, 2012.
- [119] Chang Min Jung, Rui Zhang, Martin Chenevert, and Mukul Sharma. High-performance water-based mud using nanoparticles for shale reservoirs. In *SPE/AAPG/SEG Unconventional Resources Technology Conference*, pages URTEC–1581549. URTEC, 2013.
- [120] Meghan Riley, Emanuel Stamatakis, Steve Young, Katerine Price Hoelscher, Guido De Stefano, Lou Ji, Quan Guo, and Jim Friedheim. Wellbore stability in unconventional shale—the design of a nano-particle fluid. In *SPE oil and gas India conference and exhibition*. OnePetro, 2012.
- [121] Norazwan Wahid, Muhammad Aslam Yusof, and Nor Hazimastura Hanafi. Optimum nanosilica concentration in synthetic based mud (sbm) for high temperature high pressure well. In *SPE/IATMI Asia Pacific Oil & Gas Conference and Exhibition*. OnePetro, 2015.
- [122] Meghan Riley, Emanuel Stamatakis, Steve Young, K Price-Hoelscher, and Guido De Stefano. Drilling unconventional shales with innovative water-based mud—part ii: Mud formulations and performance. In *2012 AADE Fluids Technical Conference and Exhibition*, 2012.
- [123] Railson CS da Luz, Marcus VG Paixão, and Rosangela de C Balaban. Nanosilica-chitosan hybrid materials: preparation, characterization and application in aqueous drilling fluids. *Journal of Molecular Liquids*, 279:279–288, 2019.
- [124] Rizky Novara, Roozbeh Rafati, and Amin Sharifi Haddad. Rheological and filtration property evaluations of the nano-based muds for drilling applications in low temperature environments. *Colloids and Surfaces A: Physicochemical and Engineering Aspects*, 622:126632, 2021.
- [125] Zisis Vryzas, Omar Mahmoud, Hisham A Nasr-El-Din, and Vassilios C Kelessidis. Development and testing of novel drilling

REFERENCES

- fluids using Fe_2O_3 and SiO_2 nanoparticles for enhanced drilling operations. In *International petroleum technology conference*. OnePetro, 2015.
- [126] Goshtasp Cheraghian, Qinglin Wu, Masood Mostofi, Mei-Chun Li, Masoud Afrand, and Jitendra S Sangwai. Effect of a novel clay/silica nanocomposite on water-based drilling fluids: Improvements in rheological and filtration properties. *Colloids and Surfaces A: Physicochemical and Engineering Aspects*, 555: 339–350, 2018.
- [127] AM Salem Ragab and A Noah. Reduction of formation damage and fluid loss using nano-sized silica drilling fluids. *Petroleum Technology Development Journal*, 2:75–88, 2014.
- [128] AH Salih, TA Elshehabi, and HI Bilgesu. Impact of nanomaterials on the rheological and filtration properties of water-based drilling fluids. In *SPE Eastern regional meeting*, pages SPE–184067. SPE, 2016.
- [129] Saket M Javeri, Zishaan W Haindade, and Chaitanya B Jere. Mitigating loss circulation and differential sticking problems using silicon nanoparticles. In *SPE/IADC Middle East Drilling Technology Conference and Exhibition*. OnePetro, 2011.
- [130] Srawanti Medhi, Satyajit Chowdhury, Dharmender Kumar Gupta, and Aryab Mazumdar. An investigation on the effects of silica and copper oxide nanoparticles on rheological and fluid loss property of drilling fluids. *Journal of Petroleum Exploration and Production Technology*, 10:91–101, 2020.
- [131] Abdulrahman Mohamed, Abdel-Sattar A Dahab, and Eissa Shokir. Enhancement of water-based mud rheology and lubricity using silica nanoparticles. *Petroleum & Coal*, 62(4), 2020.
- [132] Amin Kazemi-Beydokhti, Seyed Hasan Hajiabadi, and Ali Sanati. Surface modification of carbon nanotubes as a key factor on rheological characteristics of water-based drilling muds. *Iranian Journal of Chemistry and Chemical Engineering*, 37(4):1–14, 2018.

REFERENCES

- [133] Amin Kazemi-Beydokhti and Seyed Hasan Hajiabadi. Rheological investigation of smart polymer/carbon nanotube complex on properties of water-based drilling fluids. *Colloids and surfaces A: physicochemical and engineering aspects*, 556: 23–29, 2018.
- [134] Seyed Hasan Hajiabadi, Hamed Aghaei, Mina Kalateh-Aghamohammadi, Ali Sanati, Amin Kazemi-Beydokhti, and Feridun Esmaeilzadeh. A comprehensive empirical, analytical and tomographic investigation on rheology and formation damage behavior of a novel nano-modified invert emulsion drilling fluid. *Journal of Petroleum Science and Engineering*, 181:106257, 2019.
- [135] AARI Aftab, AR Ismail, and ZH Ibupoto. Enhancing the rheological properties and shale inhibition behavior of water-based mud using nanosilica, multi-walled carbon nanotube, and graphene nanoplatelet. *Egyptian journal of petroleum*, 26(2): 291–299, 2017.
- [136] Abdul Razak Ismail, WR Wan Sulaiman, MZ Jaafar, A Aftab, A Razi, and Z Ibupoto. The application of mwcnt to enhance the rheological behavior of drilling fluids at high temperature. *Malaysian Journal of Fundamental and Applied Sciences*, 12(3):95–98, 2016.
- [137] Lan Ma, Pingya Luo, Yi He, Liyun Zhang, Yi Fan, and Zhenju Jiang. Improving the stability of multi-walled carbon nano-tubes in extremely environments: Applications as nano-plugging additives in drilling fluids. *Journal of Natural Gas Science and Engineering*, 74:103082, 2020.
- [138] Majid Sajjadian, Vali Ahmad Sajjadian, and Alimorad Rashidi. Experimental evaluation of nanomaterials to improve drilling fluid properties of water-based muds hp/ht applications. *Journal of Petroleum Science and Engineering*, 190:107006, 2020.
- [139] Azeem Rana, Ibrahim Khan, and Tawfik A Saleh. Advances

REFERENCES

- in carbon nanostructures and nanocellulose as additives for efficient drilling fluids: trends and future perspective—a review. *Energy & Fuels*, 35(9):7319–7339, 2021.
- [140] Roozbeh Rafati, Sean Robert Smith, Amin Sharifi Haddad, Rizky Novara, and Hossein Hamidi. Effect of nanoparticles on the modifications of drilling fluids properties: A review of recent advances. *Journal of Petroleum Science and Engineering*, 161:61–76, 2018.
- [141] Azeem Rana, Ibrahim Khan, Shahid Ali, Tawfik A Saleh, and Safyan A Khan. Controlling shale swelling and fluid loss properties of water-based drilling mud via ultrasonic impregnated swcnts/pvp nanocomposites. *Energy & Fuels*, 34(8):9515–9523, 2020.
- [142] Nasiru Salahu Muhammed, Teslim Olayiwola, Salaheldin Elkatatny, Bashirul Haq, and Shirish Patil. Insights into the application of surfactants and nanomaterials as shale inhibitors for water-based drilling fluid: A review. *Journal of Natural Gas Science and Engineering*, 92:103987, 2021.
- [143] Nicolas Passade-Boupat, Cathy Rey, and Mathieu Naegel. Drilling fluid containing carbon nanotubes, June 25 2013. US Patent 8,469,118.
- [144] Muhammad Adeem Abbas, Asif Zamir, Khaled Abdalla Elraies, Syed Mohammad Mahmood, Navid Aslfattahi, R Saidur, Maqsood Ahmad, and Muhammad Hammad Rasool. Characterization of nano based drilling fluid for shale swelling inhibition. *Petroleum Science and Technology*, 40(22):2710–2736, 2022.
- [145] Mostafa Sedaghatzadeh, Abbasali Khodadadi, and Mohammad Reza Tahmasebi Birgani. An improvement in thermal and rheological properties of water-based drilling fluids using multiwall carbon nanotube (mwcnt). *Iranian Journal of Oil and Gas Science and Technology*, 1(1):55–65, 2012.

REFERENCES

- [146] Mostafa Sedaghatzadeh, Khalil Shahbazi, Mohammad Hossein Ghazanfari, and Ghasem Zargar. The impact of nanoparticles geometry and particle size on formation damage induced by drilling nano-fluid during dynamic filtration. *Journal of Nano Research*, 43:81–97, 2016.
- [147] Md Amanullah and Ziad Al-Abdullatif. Drilling, drill-in and completion fluids containing nanoparticles for use in oil and gas field applications and methods related thereto, September 16 2014. US Patent 8,835,363.
- [148] Abdullah ÖZKAN. Effect of multi-walled carbon nanotubes on the water-based drilling muds. *Muş Alparslan Üniversitesi Fen Bilimleri Dergisi*, 6(2):591–594, 2018.
- [149] AR Ismail, A Aftab, ZH Ibupoto, and N Zolkifile. The novel approach for the enhancement of rheological properties of water-based drilling fluids by using multi-walled carbon nanotube, nanosilica and glass beads. *Journal of Petroleum Science and Engineering*, 139:264–275, 2016.
- [150] AR Ismail, MSA Rashid, and B Thameem. Application of nanomaterials to enhanced the lubricity and rheological properties of water based drilling fluid. In *IOP Conference Series: Materials Science and Engineering*, volume 380, page 012021. IOP Publishing, 2018.
- [151] Jamal Nasser, Anna Jesil, Tariq Mohiuddin, Majid Al Ruqeshi, Geetha Devi, and Shahjahan Mohataram. Experimental investigation of drilling fluid performance as nanoparticles. *World Journal of Nano Science and Engineering*, 2013, 2013.
- [152] Ariffin Samsuri and Amir Hamzah. Water based mud lifting capacity improvement by multiwall carbon nanotubes additive. *Journal of Petroleum and Gas Engineering*, 2(5):99–107, 2011.
- [153] Mohamad Amin Halali, Cyrus Ghotbi, Kouros Tahmasbi, and Mohammad Hossein Ghazanfari. The role of carbon nanotubes in improving thermal stability of polymeric fluids: Experimental

REFERENCES

- and modeling. *Industrial & Engineering Chemistry Research*, 55(27):7514–7534, 2016.
- [154] Afiya Akram, Muhammad Awais Ashfaq Alvi, and Mesfin Belayneh. The impact of mwent on xg polymer/salt treated laboratory water based drilling fluid. *Int. J. Nano Sci. Nanotechnol*, 9(1):1–8, 2018.
- [155] Kevin W Powers, Scott C Brown, Vijay B Krishna, Scott C Wasdo, Brij M Moudgil, and Stephen M Roberts. Research strategies for safety evaluation of nanomaterials. part vi. characterization of nanoscale particles for toxicological evaluation. *Toxicological Sciences*, 90(2):296–303, 2006.
- [156] Haokun Shen, Kaihe Lv, Xianbin Huang, Jingping Liu, Yingrui Bai, Jintang Wang, and Jinsheng Sun. Hydrophobic-associated polymer-based laponite nanolayered silicate composite as filtrate reducer for water-based drilling fluid at high temperature. *Journal of Applied Polymer Science*, 137(18):48608, 2020.
- [157] Xiangru Jia, Xionghu Zhao, Bin Chen, Saviour Bassey Egwu, and Zhiyang Huang. Polyanionic cellulose/hydrophilic monomer copolymer grafted silica nanocomposites as hthp drilling fluid-loss control agent for water-based drilling fluids. *Applied Surface Science*, 578:152089, 2022.
- [158] Jeffrey O Oseh, MNA Mohd Norddin, Issham Ismail, Afeez O Gbadamosi, Augustine Agi, and Hakim N Mohammed. A novel approach to enhance rheological and filtration properties of water-based mud using polypropylene-silica nanocomposite. *Journal of Petroleum Science and Engineering*, 181:106264, 2019.
- [159] Hui Mao, Zhengsong Qiu, Zhonghou Shen, Weian Huang, Hanyi Zhong, and Wenhao Dai. Novel hydrophobic associated polymer based nano-silica composite with core-shell structure for intelligent drilling fluid under ultra-high temperature and

REFERENCES

- ultra-high pressure. *Progress in Natural Science: Materials International*, 25(1):90–93, 2015.
- [160] Jinsheng Sun, Xiaofeng Chang, Fan Zhang, Yingrui Bai, Kaihe Lv, Jintang Wang, Xinyu Zhou, and Bo Wang. Salt-responsive zwitterionic polymer brush based on modified silica nanoparticles as a fluid-loss additive in water-based drilling fluids. *Energy & Fuels*, 34(2):1669–1679, 2020.
- [161] Xiaodong Bai, Tao Ning, Xuepeng Zhang, Yuqian Xu, Xuemei Yong, Yumei Luo, and Song Zhou. Preparation and characterization of new expansible composite microspheres for use with water-based drilling fluids. *Polymers for Advanced Technologies*, 31(12):2955–2966, 2020.
- [162] Xiaodong Bai, Xingyuan Zhang, Tao Ning, Yumei Luo, and Song Zhou. Preparation, characterization and properties of sio 2 expansible composite microspheres for water-based drilling fluid. *Journal of Inorganic and Organometallic Polymers and Materials*, 30:1172–1183, 2020.
- [163] Hamid Heydarzadeh Darzi, Mahdieh Fouji, Reyhaneh Ghorbani Heidarabad, Hamed Aghaei, Seyed Hasan Hajiabadi, Pavel Bedrikovetsky, and Hassan Mahani. Carbon-based nanocomposites: Distinguishing between deep-bed filtration and external filter cake by coupling core-scale mud-flow tests with computed tomography imaging. *Journal of Natural Gas Science and Engineering*, 105:104707, 2022.
- [164] Jing-Ping Liu, Xian-Fa Zhang, Wen-Chao Zhang, Kai-He Lv, Yin-Rui Bai, Jin-Tang Wang, Xian-Bin Huang, Jia-Feng Jin, and Jin-Sheng Sun. Carbon nanotube enhanced water-based drilling fluid for high temperature and high salinity deep resource development. *Petroleum Science*, 19(2):916–926, 2022.
- [165] Abdul Ismail, Tan Seong, Aziah Buang, Wan Rosli, and Wan Rosli Wan Sulaiman. Improve performance of water-based drilling fluids using nanoparticles. 09 2014.
- [166] MI Abduo, AS Dahab, Hesham Abuseda, Abdulaziz M

REFERENCES

- AbdulAziz, and MS Elhossieny. Comparative study of using water-based mud containing multiwall carbon nanotubes versus oil-based mud in hpht fields. *Egyptian Journal of Petroleum*, 25(4):459–464, 2016.
- [167] Koorosh Tookallo. Analyzing effects of various kinds of multi-wall carbo nanotubes (mwcnt) on performance of water base mud (wbm). *COJ Rev. Res*, 1(2), 2018.
- [168] Koorosh Tookaloo, Javad Heidarian, Mohammad Soleymani, Alimorad Rashidi, and Mahdi Nazarisaram. Analyzing effects of multi-wall carbon nanotubes (mwcnt) & polyethylene glycol (peg) on performance of water base mud (wbm) in shale formation. *The Open Petroleum Engineering Journal*, 11(1), 2018.
- [169] Tianle Liu, Guosheng Jiang, Ping Zhang, Jiabin Sun, Huicui Sun, Ren Wang, and Mingming Zheng. A new low-cost drilling fluid for drilling in natural gas hydrate-bearing sediments. *Journal of Natural Gas Science and Engineering*, 33:934–941, 2016.
- [170] S Taraghikhah, M Kalhor Mohammadi, and K Tahmasbi Nowtaraki. Multifunctional nanoadditive in water based drilling fluid for improving shale stability. In *International petroleum technology conference*, page D021S011R003. IPTC, 2015.
- [171] Jie Zhang, Long Li, Shuangwei Wang, Jianhua Wang, Henglin Yang, Zhiliang Zhao, Jinzhi Zhu, and Zhen Zhang. Novel micro and nano particle-based drilling fluids: Pioneering approach to overcome the borehole instability problem in shale formations. In *SPE Asia Pacific Unconventional Resources Conference and Exhibition*, pages SPE–176991. SPE, 2015.
- [172] Oscar Contreras, Geir Hareland, Maen Husein, Runar Nygaard, and Mortadha Alsaba. Experimental investigation on wellbore strengthening in shales by means of nanoparticle-based drilling

REFERENCES

- fluids. In *SPE Annual Technical Conference and Exhibition?*, pages SPE–170589. SPE, 2014.
- [173] Kanjirakat Anoop, Reza Sadr, Mohammed Al-Jubouri, and Mahmood Amani. Rheology of mineral oil-sio₂ nanofluids at high pressure and high temperatures. *International Journal of thermal sciences*, 77:108–115, 2014.
- [174] Vikrant Wagle, Abdullah S Al-Yami, and Ziad AlAbdullatif. Using nanoparticles to formulate sag-resistant invert emulsion drilling fluids. In *SPE/IADC Drilling Conference and Exhibition*, page D011S005R006. SPE, 2015.
- [175] Tarek M Madkour, Samar Fadl, MM Dardir, and Mohamed A Mekewi. High performance nature of biodegradable polymeric nanocomposites for oil-well drilling fluids. *Egyptian Journal of Petroleum*, 25(2):281–291, 2016.
- [176] Oscar Contreras, Mortadha Alsaba, Geir Hareland, Maen Husein, and Runar Nygaard. Effect on fracture pressure by adding iron-based and calcium-based nanoparticles to a nonaqueous drilling fluid for permeable formations. *Journal of Energy Resources Technology*, 138(3):032906, 2016.
- [177] Mohammad F Zakaria, Maen Husein, and Geir Hareland. Novel nanoparticle-based drilling fluid with improved characteristics. In *SPE international oilfield nanotechnology conference and exhibition*, pages SPE–156992. SPE, 2012.
- [178] Ashok Santra, Peter J Boul, and Xueyu Pang. Influence of nanomaterials in oilwell cement hydration and mechanical properties. In *SPE international oilfield nanotechnology conference and exhibition*, pages SPE–156937. SPE, 2012.
- [179] V Ershadi, T Ebadi, AR Rabani, L Ershadi, and H Soltanian. The effect of nanosilica on cement matrix permeability in oil well to decrease the pollution of receptive environment. *International Journal of Environmental Science and Development*, 2(2):128, 2011.

REFERENCES

- [180] Hui Li, Hui-gang Xiao, and Jin-ping Ou. A study on mechanical and pressure-sensitive properties of cement mortar with nanophase materials. *Cement and Concrete research*, 34(3):435–438, 2004.
- [181] B Safi, H Aknouche, H Mechakra, D Aboutaleb, and KJIC Bouali. Incorporation mode effect of nano-silica on the rheological and mechanical properties of cementitious pastes and cement mortars. In *IOP Conference Series: Earth and Environmental Science*, volume 143, page 012015. IOP Publishing, 2018.
- [182] Celik Ozyildirim and Caroline Zegetosky. Exploratory investigation of nanomaterials to improve strength and permeability of concrete. *Transportation research record*, 2142(1):1–8, 2010.
- [183] M Murtaza, MK Rahman, and AA Al-Majed. Effect of nanoclay on mechanical and rheological properties of oil well cement slurry under hpht environment. In *International Petroleum Technology Conference*, page D031S047R003. IPTC, 2016.
- [184] Xueyu Pang, Peter J Boul, and Walmy Cuello Jimenez. Nanosilicas as accelerators in oilwell cementing at low temperatures. *SPE Drilling & Completion*, 29(01):98–105, 2014.
- [185] Júnia Nunes de Paula, José Márcio Calixto, Luiz Orlando Ladeira, Péter Ludvig, Tarcizo Cruz C Souza, José Marcelo Rocha, and Aline A Vargas de Melo. Mechanical and rheological behavior of oil-well cement slurries produced with clinker containing carbon nanotubes. *Journal of Petroleum Science and Engineering*, 122:274–279, 2014.
- [186] WA Khan, MK Rahman, MA Mahmoud, and P Sarmah. Mwcnt for enhancing mechanical properties of oil well cement for hpht applications. In *SPE/IADC Middle East Drilling Technology Conference and Exhibition*, page D033S018R003. SPE, 2016.
- [187] Ming Li, Shuang Deng, Fei Meng, Jianzhang Hao, and Xiaoyang

REFERENCES

- Guo. Effect of nanosilica on the mechanical properties of oil well cement at low temperature. *Magazine of Concrete Research*, 69(10):493–501, 2017.
- [188] Robin De la Roi, Christophe Egyed, and Jean-Paul Lips. Nano-engineered oil well cement improves flexibility and increases compressive strength: A laboratory study. In *SPE International Oilfield Nanotechnology Conference and Exhibition*, pages SPE–156501. SPE, 2012.
- [189] Shivshambhu Kumar, Achinta Bera, and Subhash N Shah. Potential applications of nanomaterials in oil and gas well cementing: Current status, challenges and prospects. *Journal of Petroleum Science and Engineering*, 213:110395, 2022.
- [190] Chengwen Wang, Xin Chen, Xiaotong Wei, and Ruihe Wang. Can nanosilica sol prevent oil well cement from strength retrogression under high temperature? *Construction and Building Materials*, 144:574–585, 2017.
- [191] Paratibha Aggarwal, Rahul Pratap Singh, and Yogesh Aggarwal. Use of nano-silica in cement based materials—a review. *Cogent Engineering*, 2(1):1078018, 2015.
- [192] Mathialagan Sumesh, U Johnson Alengaram, Mohd Zamin Jumaat, Kim Hung Mo, and Mohammed Fouad Alnahhal. Incorporation of nano-materials in cement composite and geopolymer based paste and mortar—a review. *Construction and Building Materials*, 148:62–84, 2017.
- [193] Mohammadmehdi Choolaei, Ali Morad Rashidi, Mehdi Ardjmand, Amir Yadegari, and Hamid Soltanian. The effect of nanosilica on the physical properties of oil well cement. *Materials Science and Engineering: A*, 538:288–294, 2012.
- [194] Rahul Patil and Abhimanyu Deshpande. Use of nanomaterials in cementing applications. In *SPE international oilfield nanotechnology conference and exhibition*, pages SPE–155607. SPE, 2012.

REFERENCES

- [195] Chun Huh, Hugh Daigle, Valentina Prigiobbe, and Masa Prodanovic. *Practical Nanotechnology for Petroleum Engineers*. CRC Press, 2019.
- [196] R Yu, P Spiesz, and HJH Brouwers. Effect of nano-silica on the hydration and microstructure development of ultra-high performance concrete (uhpc) with a low binder amount. *Construction and Building Materials*, 65:140–150, 2014.
- [197] Mobeen Murtaza, Mohamed Mahmoud, Salaheldin Elkatatny, Abdulaziz Al Majed, Weiqing Chen, and Abul Jamaluddin. Experimental investigation of the impact of modified nano clay on the rheology of oil well cement slurry. In *International Petroleum Technology Conference*, page D011S014R004. IPTC, 2019.
- [198] Mobeen Murtaza, Mohammad Kalimur Rahman, Abdulaziz Abdulla Al Majed, Zeeshan Tariq, and Mohamed Mahmoud. Scratch test for strength and toughness of oil well cement with nanoclay as an additive. In *Abu Dhabi International Petroleum Exhibition & Conference*. OnePetro, 2019.
- [199] Zeeshan Tariq, Mobeen Murtaza, and Mohamed Mahmoud. Effects of nanoclay and silica flour on the mechanical properties of class g cement. *ACS omega*, 5(20):11643–11654, 2020.
- [200] Narjes Jafariesfad, Yi Gong, Mette Rica Geiker, and Pål Skalle. Nano-sized mgo with engineered expansive property for oil well cement systems. In *SPE Bergen one day seminar*. OnePetro, 2016.
- [201] Xiaoying Li, Jun Li, Zhongyuan Lu, and Jiakun Chen. Properties and hydration mechanism of cement pastes in presence of nano-zno. *Construction and Building Materials*, 289:123080, 2021.
- [202] Mohamed Heikal, MN Ismail, and NS Ibrahim. Physico-mechanical, microstructure characteristics and fire resistance

REFERENCES

- of cement pastes containing al₂o₃ nano-particles. *Construction and Building Materials*, 91:232–242, 2015.
- [203] Salim Barbhuiya, Shaswata Mukherjee, and Hamid Nikraz. Effects of nano-al₂o₃ on early-age microstructural properties of cement paste. *Construction and Building Materials*, 52:189–193, 2014.
- [204] Raje Gowda, H Narendra, BM Nagabushan, Dinesh Rangappa, and R Prabhakara. Investigation of nano-alumina on the effect of durability and micro-structural properties of the cement mortar. *Materials Today: Proceedings*, 4(11):12191–12197, 2017.
- [205] Ali Nazari, Shadi Riahi, Shirin Riahi, Seyedeh Fatemeh Shamekhi, and A Khademno. Influence of al₂o₃ nanoparticles on the compressive strength and workability of blended concrete. *Journal of American Science*, 6(5):6–9, 2010.
- [206] Ali Nazari and Shadi Riahi. Improvement compressive strength of concrete in different curing media by al₂o₃ nanoparticles. *Materials Science and Engineering: A*, 528(3):1183–1191, 2011.
- [207] Zhenhua Li, Huafeng Wang, Shan He, Yang Lu, and Miao Wang. Investigations on the preparation and mechanical properties of the nano-alumina reinforced cement composite. *Materials Letters*, 60(3):356–359, 2006.
- [208] Igor Campillo, A Guerrero, JS Dolado, A Porro, Jose A Ibáñez, and S Goñi. Improvement of initial mechanical strength by nanoalumina in belite cements. *Materials Letters*, 61(8-9):1889–1892, 2007.
- [209] Ali Nazari, Shadi Riahi, Shirin Riahi, Seyedeh Fatemeh Shamekhi, and A Khademno. Mechanical properties of cement mortar with al₂o₃ nanoparticles. *Journal of American Science*, 6(4):94–97, 2010.
- [210] VV Vikulin, MK Alekseev, and IL Shkarupa. Study of the effect of some commercially available nanopowders on the strength of

REFERENCES

- concrete based on alumina cement. *Refractories and Industrial Ceramics*, 52(4):288–290, 2011.
- [211] Payam Hosseini, Reza Hosseinpourpia, Arash Pajum, Mohammad Mahdi Khodavirdi, Hamed Izadi, and Ali Vaezi. Effect of nano-particles and aminosilane interaction on the performances of cement-based composites: An experimental study. *Construction and Building Materials*, 66:113–124, 2014.
- [212] C Vipulanandan, A Mohammed, and AS Ganpatye. Smart cement performance enhancement with nanoal₂o₃ for real time monitoring applications using vipulanandan models. In *Offshore technology conference*, page D041S056R007. OTC, 2018.
- [213] Abhimanyu Deshpande and Rahul Patil. Applications of nanotechnology in oilwell cementing. In *SPE Middle East Oil and Gas Show and Conference*, page D041S039R002. SPE, 2017.
- [214] Nima Farzadnia, Abang Abdullah Abang Ali, and Ramazan Demirboga. Characterization of high strength mortars with nano alumina at elevated temperatures. *Cement and Concrete Research*, 54:43–54, 2013.
- [215] Qiyu Shao, Keren Zheng, Xuejin Zhou, Jin Zhou, and Xiaohui Zeng. Enhancement of nano-alumina on long-term strength of portland cement and the relation to its influences on compositional and microstructural aspects. *Cement and Concrete Composites*, 98:39–48, 2019.
- [216] Karla P Bautista-Gutierrez, Agustín L Herrera-May, Jesús M Santamaría-López, Antonio Honorato-Moreno, and Sergio A Zamora-Castro. Recent progress in nanomaterials for modern concrete infrastructure: Advantages and challenges. *Materials*, 12(21):3548, 2019.
- [217] Scott Muzenski, Ismael Flores-Vivian, and Konstantin Sobolev. Ultra-high strength cement-based composites designed with aluminum oxide nano-fibers. *Construction and Building Materials*, 220:177–186, 2019.

REFERENCES

- [218] Ehsan Mohseni, Bahareh Mehdizadeh Miyandehi, Jian Yang, and Mohammad Ali Yazdi. Single and combined effects of nano-sio₂, nano-al₂o₃ and nano-tio₂ on the mechanical, rheological and durability properties of self-compacting mortar containing fly ash. *Construction and Building Materials*, 84:331–340, 2015.
- [219] Luciano Senff, Dachamir Hotza, Wellington L Repette, Victor M Ferreira, and João A Labrincha. Mortars with nano-sio₂ and micro-sio₂ investigated by experimental design. *Construction and Building Materials*, 24(8):1432–1437, 2010.
- [220] Libya Ahmed Sbia, Amirpasha Peyvandi, Parviz Soroushian, and Anagi M Balachandra. Optimization of ultra-high-performance concrete with nano-and micro-scale reinforcement. *Cogent Engineering*, 1(1):990673, 2014.
- [221] Phillip D McElroy, Hossein Emadi, and Daniel Unruh. Permeability and elastic properties assessment of alumina nanofiber (anf) cementitious composites under simulated wellbore cyclic pressure. *Construction and Building Materials*, 239:117867, 2020.
- [222] Phillip D McElroy, Hossein Emadi, Marshall C Watson, and Lloyd Heinze. Hydration products and mechanical properties investigations of nanofiber additives in cement wellbore environments. In *SPE Western Regional Meeting*. onepetro, 2021.
- [223] SMA El-Gamal, FS Hashem, and MS Amin. Influence of carbon nanotubes, nanosilica and nanometakaolin on some morphological-mechanical properties of oil well cement pastes subjected to elevated water curing temperature and regular room air curing temperature. *Construction and Building Materials*, 146:531–546, 2017.
- [224] Youli Lin and Hongjian Du. Graphene reinforced cement composites: A review. *Construction and Building Materials*, 265:120312, 2020.
- [225] Neil Neuberger, Hertanto Adidharma, and Maohong Fan.

REFERENCES

- Graphene: A review of applications in the petroleum industry. *Journal of Petroleum Science and Engineering*, 167:152–159, 2018.
- [226] Li Li, Virgilio C Boncan, Andreas Brandl, and Andrew K Jordan. Fundamental investigation of mechanical properties of additives and class h cement under downhole conditions. In *SPE/IATMI Asia Pacific Oil & Gas Conference and Exhibition*. OnePetro, 2015.
- [227] LI Ming, Liu Meng, YANG Yuanyi, Li Zaoyuan, and Guo Xiaoyang. Mechanical properties of oil well cement stone reinforced with hybrid fiber of calcium carbonate whisker and carbon fiber. *Petroleum Exploration and Development*, 42(1): 104–111, 2015.
- [228] Arnon Chaipanich, Rattiyakorn Rianyai, and Thanongsak Nochaiya. The effect of carbon nanotubes and silica fume on compressive strength and flexural strength of cement mortars. *Materials Today: Proceedings*, 4(5):6065–6071, 2017.
- [229] Shawgi Ahmed, Chinedum Peter Ezeakacha, and Saeed Salehi. Improvement in cement sealing properties and integrity using conductive carbon nano materials: from strength to thickening time. In *SPE annual technical conference and exhibition*. onepetro, 2018.
- [230] Florence Sanchez and Konstantin Sobolev. Nanotechnology in concrete—a review. *Construction and building materials*, 24(11): 2060–2071, 2010.
- [231] Jintao Liu, Jiali Fu, Tongyuan Ni, and Yang Yang. Fracture toughness improvement of multi-wall carbon nanotubes/graphene sheets reinforced cement paste. *Construction and Building Materials*, 200:530–538, 2019.
- [232] Shichao Lu, Xiaoyan Wang, Zhaorui Meng, Qingchun Deng, Fangfang Peng, Chengcheng Yu, Xu Hu, Yi Zhao, Yangchuan Ke, and Fengzhong Qi. The mechanical properties, microstructures and mechanism of carbon nanotube-reinforced

REFERENCES

- oil well cement-based nanocomposites. *RSC advances*, 9(46): 26691–26702, 2019.
- [233] Mohamed O Mohsen, Ramzi Taha, Ala Abu Taqa, and Ahmed Shaat. Optimum carbon nanotubes' content for improving flexural and compressive strength of cement paste. *Construction and Building Materials*, 150:395–403, 2017.
- [234] Laura Silvestro and Philippe Jean Paul Gleize. Effect of carbon nanotubes on compressive, flexural and tensile strengths of portland cement-based materials: A systematic literature review. *Construction and Building Materials*, 264:120237, 2020.
- [235] Andrzej Cwirzen, Karin Habermehl-Cwirzen, AG Nasibulin, EI Kaupinen, PR Mudimela, and Vesa Penttala. Sem/afm studies of cementitious binder modified by mwcnt and nano-sized fe needles. *Materials characterization*, 60(7):735–740, 2009.
- [236] Andrzej Cwirzen, Karin Habermehl-Cwirzen, and Vesa Penttala. Surface decoration of carbon nanotubes and mechanical properties of cement/carbon nanotube composites. *Advances in cement research*, 20(2):65–73, 2008.
- [237] Antanas Laukaitis, Jadvyga Kerienė, Modestas Kligys, Donatas Mikulskis, and Lina Lekūnaitė. Influence of mechanically treated carbon fibre additives on structure formation and properties of autoclaved aerated concrete. *Construction and building materials*, 26(1):362–371, 2012.
- [238] Geng Ying Li, Pei Ming Wang, and Xiaohua Zhao. Mechanical behavior and microstructure of cement composites incorporating surface-treated multi-walled carbon nanotubes. *Carbon*, 43(6):1239–1245, 2005.
- [239] Geng Ying Li, Pei Ming Wang, and Xiaohua Zhao. Pressure-sensitive properties and microstructure of carbon nanotube reinforced cement composites. *Cement and Concrete Composites*, 29(5):377–382, 2007.

REFERENCES

- [240] Surendra P Shah, MS Konsta-Gdoutos, ZS Metaxa, and P Mondal. Nanoscale modification of cementitious materials. In *Nanotechnology in Construction 3: Proceedings of the NICOM3*, pages 125–130. Springer, 2009.
- [241] Maria S. Konsta-Gdoutos, Zoi S. Metaxa, and Surendra P. Shah. Highly dispersed carbon nanotube reinforced cement based materials. *Cement and Concrete Research*, 40(7):1052–1059, 2010. ISSN 0008-8846. doi: <https://doi.org/10.1016/j.cemconres.2010.02.015>. URL <https://www.sciencedirect.com/science/article/pii/S0008884610000542>.
- [242] Maria S. Konsta-Gdoutos, Zoi S. Metaxa, and Surendra P. Shah. Multi-scale mechanical and fracture characteristics and early-age strain capacity of high performance carbon nanotube/cement nanocomposites. *Cement and Concrete Composites*, 32(2):110–115, 2010. ISSN 0958-9465. doi: <https://doi.org/10.1016/j.cemconcomp.2009.10.007>. URL <https://www.sciencedirect.com/science/article/pii/S0958946509001632>.
- [243] Mirza Talha Baig, Muhammad Kalimur Rahman, and Abdulaziz Al-Majed. Application of nanotechnology in oil well cementing. In *SPE Kuwait Oil and Gas Show and Conference*, page D031S011R001. SPE, 2017.
- [244] Ali Ghajari, Hamid Soltanian, and Seyyed Alireza Mortazavi. An improvement to physical properties of heavy-weight oil well cements using carbon nanotubes. *Journal of Petroleum Science and Technology*, 4(2):10, 2014.
- [245] Saeed Sahranavard, Hasan Haji-Kazemi, and Sedighe Abbasi. Effect of multi-walled carbon nanotubes on mechanical properties of high-performance mortar. *Magazine of Concrete Research*, 66(18):948–954, 2014.
- [246] Sekhar Chandra Ray, Chih-Wen Pao, Huang-Ming Tsai, Huang-Chin Chen, Yu-Shin Chen, Shang-Lun Wu, Dah-Chin Ling, I-Nan Lin, Way-Faung Pong, Sanju Gupta, et al. High-temperature annealing effects on multiwalled carbon nanotubes:

REFERENCES

- electronic structure, field emission and magnetic behaviors. *Journal of Nanoscience and Nanotechnology*, 9(12):6799–6805, 2009.
- [247] YA Kim, T Hayashi, M Endo, Y Kaburagi, T Tsukada, J Shan, K Osato, and S Tsuruoka. Synthesis and structural characterization of thin multi-walled carbon nanotubes with a partially faceted cross section by a floating reactant method. *Carbon*, 43(11):2243–2250, 2005.
- [248] Oxana V Kharissova, L Torres Martínez, and B Kharisov. Recent trends of reinforcement of cement with carbon nanotubes and fibers. *Advances in Carbon Nanostructures*, pages 137–160, 2016.
- [249] Xiao-Lin Xie, Yiu-Wing Mai, and Xing-Ping Zhou. Dispersion and alignment of carbon nanotubes in polymer matrix: a review. *Materials science and engineering: R: Reports*, 49(4):89–112, 2005.
- [250] SL Colston, D O’connor, P Barnes, EL Mayes, S Mann, H Freimuth, and W Ehrfeld. Functional micro-concrete: The incorporation of zeolites and inorganic nano-particles into cement micro-structures. *Journal of Materials Science Letters*, 19:1085–1088, 2000.
- [251] Jie Liu, Michael J Casavant, Michael Cox, DA Walters, P Boul, Wei Lu, AJ Rimberg, KA Smith, Daniel T Colbert, and Richard E Smalley. Controlled deposition of individual single-walled carbon nanotubes on chemically functionalized templates. *Chemical physics letters*, 303(1-2):125–129, 1999.
- [252] Weijie Huang, Yi Lin, Shelby Taylor, Jay Gaillard, Apparao M Rao, and Ya-Ping Sun. Sonication-assisted functionalization and solubilization of carbon nanotubes. *Nano Letters*, 2(3):231–234, 2002.
- [253] Ardavan Yazdanbakhsh, Zachary Grasley, Bryan Tyson, and Rashid K Abu Al-Rub. Distribution of carbon nanofibers and

REFERENCES

- nanotubes in cementitious composites. *Transportation Research Record*, 2142(1):89–95, 2010.
- [254] Arnon Chaipanich, Thanongsak Nochaiya, Watcharapong Wongkeo, and Pincha Torkittikul. Compressive strength and microstructure of carbon nanotubes–fly ash cement composites. *Materials Science and Engineering: A*, 527(4-5):1063–1067, 2010.
- [255] Inkyu Rhee and Young-Sook Roh. Properties of normal-strength concrete and mortar with multi-walled carbon nanotubes. *Magazine of Concrete Research*, 65(16):951–961, 2013.
- [256] Mostafa Jalal, Esmaeel Mansouri, Mohammad Sharifipour, and Ali Reza Pouladkhan. Mechanical, rheological, durability and microstructural properties of high performance self-compacting concrete containing sio2 micro and nanoparticles. *Materials & Design*, 34:389–400, 2012.
- [257] Mostafa Seifan, Shaira Mendoza, and Aydin Berenjian. Mechanical properties and durability performance of fly ash based mortar containing nano-and micro-silica additives. *Construction and Building Materials*, 252:119121, 2020.
- [258] Ghasan Fahim Huseien, Hussein K Hamzah, Abdul Rahman Mohd Sam, Nur Hafizah A Khalid, Kwok Wei Shah, Dan Paul Deogrescu, and Jahangir Mirza. Alkali-activated mortars blended with glass bottle waste nano powder: Environmental benefit and sustainability. *Journal of cleaner production*, 243:118636, 2020.
- [259] Baoguo Han and Xun Yu. Effect of surfactants on pressure-sensitivity of cnt filled cement mortar composites. *Frontiers in Materials*, 1:27, 2014.
- [260] Rashid K Abu Al-Rub, Bryan M Tyson, Ardavan Yazdanbakhsh, and Zachary Grasley. Mechanical properties of nanocomposite cement incorporating surface-treated and untreated carbon nanotubes and carbon nanofibers. *Journal of nanomechanics and micromechanics*, 2(1):1–6, 2012.

REFERENCES

- [261] Hongyu Shao, Binmeng Chen, Bo Li, Shengwen Tang, and Zongjin Li. Influence of dispersants on the properties of cnts reinforced cement-based materials. *Construction and Building Materials*, 131:186–194, 2017.
- [262] Dainius Leonavičius, Ina Pundienė, Giedrius Girskas, Jolanta Pranckevičienė, Modestas Kligys, and Agnė Kairytė. The effect of multi-walled carbon nanotubes on the rheological properties and hydration process of cement pastes. *Construction and Building Materials*, 189:947–954, 2018.
- [263] Xiaolu Guo, Wenpei Hu, and Huisheng Shi. Microstructure and self-solidification/stabilization (s/s) of heavy metals of nano-modified cfa–mswifa composite geopolymers. *Construction and building materials*, 56:81–86, 2014.
- [264] Ahmed Abdulhamid Mahmoud, Salaheldin Elkatatny, Abdulmalek Ahmed S, and Mohamed Mahmoud. Nanoclay content influence on cement strength for oil wells subjected to cyclic steam injection and high-temperature conditions. In *Abu Dhabi International Petroleum Exhibition & Conference*. OnePetro, 2018.
- [265] Ahmed Abdulhamid Mahmoud, Salaheldin Elkatatny, Abdulmalek Ahmed, and Rahul Gajbhiye. Influence of nanoclay content on cement matrix for oil wells subjected to cyclic steam injection. *Materials*, 12(9):1452, 2019.
- [266] HM Khater and HA Abd el Gawaad. Characterization of alkali activated geopolymer mortar doped with mwcnt. *Construction and building materials*, 102:329–337, 2016.
- [267] Jonathan M Makar and Gordon W Chan. Growth of cement hydration products on single-walled carbon nanotubes. *Journal of the American Ceramic Society*, 92(6):1303–1310, 2009.
- [268] Chengwen Wang, Xin Chen, Wei Zhou, Yonghong Wang, Yucheng Xue, and Faqiang Luo. Working mechanism of nano-sio₂ sol to alleviate the strength decline of oil well cement under high temperature. *Natural Gas Industry B*, 6(5):517–523, 2019.

REFERENCES

- [269] Mahmoud M Hassaan, Hisham M Khater, Medhat S El-Mahllawy, and Abdeen M El Nagar. Production of geopolymer composites enhanced by nano-kaolin material. *Journal of advanced ceramics*, 4:245–252, 2015.
- [270] Tanakorn Phoo-ngernkham, Prinya Chindaprasirt, Vanchai Sata, Sakonwan Hanjitsuwan, and Shigemitsu Hatanaka. The effect of adding nano-sio₂ and nano-al₂o₃ on properties of high calcium fly ash geopolymer cured at ambient temperature. *Materials & Design*, 55:58–65, 2014.
- [271] Erich D Rodríguez, Susan A Bernal, John L Provis, Jordi Paya, José M Monzo, and María Victoria Borrachero. Effect of nanosilica-based activators on the performance of an alkali-activated fly ash binder. *Cement and Concrete Composites*, 35(1):1–11, 2013.
- [272] Kang Gao, Kae-Long Lin, DeYing Wang, Chao-Lung Hwang, Hau-Shing Shiu, Yu-Min Chang, and Ta-Wui Cheng. Effects sio₂/na₂o molar ratio on mechanical properties and the microstructure of nano-sio₂ metakaolin-based geopolymers. *Construction and building materials*, 53:503–510, 2014.
- [273] H Assaedi, FUA Shaikh, and It Meng Low. Effect of nano-clay on mechanical and thermal properties of geopolymer. *Journal of Asian Ceramic Societies*, 4(1):19–28, 2016.
- [274] Partha Sarathi Deb, Prabir Kumar Sarker, and Salim Barbhuiya. Sorptivity and acid resistance of ambient-cured geopolymer mortars containing nano-silica. *Cement and Concrete Composites*, 72:235–245, 2016.
- [275] Hasan Suliman G Assaedi, Faiz Shaikh, and Marcella Low. Utilization of nanoclay to reinforce flax fabric-geopolymer composites. *International Journal of Chemical, Molecular, Nuclear, Materials and Metallurgical Engineering*, 9(12):1327–1335, 2015.
- [276] LY Yang, ZJ Jia, YM Zhang, and JG Dai. Effects of nano-tio₂

REFERENCES

- on strength, shrinkage and microstructure of alkali activated slag pastes. *Cement and Concrete Composites*, 57:1–7, 2015.
- [277] Sudipta Naskar and Arun Kumar Chakraborty. Effect of nano materials in geopolymer concrete. *Perspectives in science*, 8: 273–275, 2016.
- [278] Syahrir Ridha and Utami Yerikania. The strength compatibility of nano-sio₂ geopolymer cement for oil well under hpht conditions. *Journal of Civil Engineering Research*, 5(4A):6–10, 2015.
- [279] Mahmoud Khalifeh, Saeed Salehi, Aleksandra Jamrozik, Raymos Kimanzi, and Saeid Abdollahpour. Nano-modified rock-based geopolymers as supplement to portland cement for oil well cementing. In *International Conference on Offshore Mechanics and Arctic Engineering*, volume 58875, page V008T11A034. American Society of Mechanical Engineers, 2019.
- [280] John L Provis and Jan Stephanus Jakob Van Deventer. *Geopolymers: structures, processing, properties and industrial applications*. Elsevier, 2009.
- [281] Ailar Hajimohammadi, Tuan Ngo, and Priyan Mendis. How does aluminium foaming agent impact the geopolymer formation mechanism? *Cement and Concrete Composites*, 80: 277–286, 2017.
- [282] C Leiva, Y Luna-Galiano, C Arenas, B Alonso-Fariñas, and C Fernández-Pereira. A porous geopolymer based on aluminum-waste with acoustic properties. *Waste Management*, 95:504–512, 2019.
- [283] Prinya Chindaprasirt, Pre De Silva, Kwesi Sagoe-Crentsil, and Sakonwan Hanjitsuwan. Effect of sio₂ and al₂o₃ on the setting and hardening of high calcium fly ash-based geopolymer systems. *Journal of Materials Science*, 47:4876–4883, 2012.
- [284] Mohamed Saafi, Kelly Andrew, Pik Leung Tang, David McGhon, Steven Taylor, Mahubur Rahman, Shangtong Yang,

REFERENCES

- and Xiangming Zhou. Multifunctional properties of carbon nanotube/fly ash geopolymeric nanocomposites. *Construction and Building Materials*, 49:46–55, 2013.
- [285] Pavel Rovnaník, Hana Šimonová, Libor Topolář, Pavel Schmid, and Zbyněk Keršner. Effect of carbon nanotubes on the mechanical fracture properties of fly ash geopolymer. *Procedia Engineering*, 151:321–328, 2016.
- [286] Saloumeh Mesgari Abbasi, Hamidreza Ahmadi, Gholamreza Khalaj, and Bahar Ghasemi. Microstructure and mechanical properties of a metakaolinite-based geopolymer nanocomposite reinforced with carbon nanotubes. *Ceramics International*, 42(14):15171–15176, 2016.
- [287] Sulalit Bandyopadhyay. *Fabrication and application of nanomaterials*. McGraw-Hill Education, 2019.
- [288] Jitendra Pal Singh, Manish Kumar, Aditya Sharma, Ganesh Pandey, Keun Hwa Chae, and Sangsul Lee. Bottom-up and top-down approaches for mgo. *Sonochemical Reactions*, 2020.
- [289] Jin Chang and Eric R Waclawik. Colloidal semiconductor nanocrystals: controlled synthesis and surface chemistry in organic media. *RSC Advances*, 4(45):23505–23527, 2014.
- [290] Maximilian O Besenhard, Alec P LaGrow, Aden Hodzic, Manfred Kriechbaum, Luca Panariello, Giorgio Bais, Katerina Loizou, Spyridon Damilos, M Margarida Cruz, Nguyen Thi Kim Thanh, et al. Co-precipitation synthesis of stable iron oxide nanoparticles with naoh: New insights and continuous production via flow chemistry. *Chemical Engineering Journal*, 399:125740, 2020.
- [291] Alec P LaGrow, Maximilian O Besenhard, Aden Hodzic, Andreas Sergides, Lara K Bogart, Asterios Gavriilidis, and Nguyen Thi Kim Thanh. Unravelling the growth mechanism of the co-precipitation of iron oxide nanoparticles with the aid of synchrotron x-ray diffraction in solution. *Nanoscale*, 11(14):6620–6628, 2019.

REFERENCES

- [292] Cristina Blanco-Andujar, Daniel Ortega, Quentin A Pankhurst, and Nguyen Thi Kim Thanh. Elucidating the morphological and structural evolution of iron oxide nanoparticles formed by sodium carbonate in aqueous medium. *Journal of Materials Chemistry*, 22(25):12498–12506, 2012.
- [293] Taebin Ahn, Jong Hun Kim, Hee-Man Yang, Jeong Woo Lee, and Jong-Duk Kim. Formation pathways of magnetite nanoparticles by coprecipitation method. *The journal of physical chemistry C*, 116(10):6069–6076, 2012.
- [294] M Aslam, Elise A Schultz, Tao Sun, Thomas Meade, and Vinayak P Dravid. Synthesis of amine-stabilized aqueous colloidal iron oxide nanoparticles. *Crystal growth & design*, 7(3):471–475, 2007.
- [295] Jing Sun, Shaobing Zhou, Peng Hou, Yuan Yang, Jie Weng, Xiaohong Li, and Mingyuan Li. Synthesis and characterization of biocompatible fe₃o₄ nanoparticles. *Journal of biomedical materials research Part A*, 80(2):333–341, 2007.
- [296] Jongnam Park, Kwangjin An, Yosun Hwang, Je-Geun Park, Han-Jin Noh, Jae-Young Kim, Jae-Hoon Park, Nong-Moon Hwang, and Taeghwan Hyeon. Ultra-large-scale syntheses of monodisperse nanocrystals. *Nature materials*, 3(12):891–895, 2004.
- [297] Taeghwan Hyeon, Su Seong Lee, Jongnam Park, Yunhee Chung, and Hyon Bin Na. Synthesis of highly crystalline and monodisperse maghemite nanocrystallites without a size-selection process. *Journal of the American Chemical Society*, 123(51):12798–12801, 2001.
- [298] Asha N Sharma, Dan Luo, and M Todd Walter. Hydrological tracers using nanobiotechnology: proof of concept. *Environmental science & technology*, 46(16):8928–8936, 2012.
- [299] Si-Han Wu, Chung-Yuan Mou, and Hong-Ping Lin. Synthesis of mesoporous silica nanoparticles. *Chemical Society Reviews*, 42(9):3862–3875, 2013.

REFERENCES

- [300] Samuel Sterman and James G Marsden. Silane coupling agents. *Industrial & Engineering Chemistry*, 58(3):33–37, 1966.
- [301] Jesse V Jokerst, Tatsiana Lobovkina, Richard N Zare, and Sanjiv S Gambhir. Nanoparticle pegylation for imaging and therapy. *Nanomedicine*, 6(4):715–728, 2011.
- [302] Anisha A D’souza and Ranjita Shegokar. Polyethylene glycol (peg): a versatile polymer for pharmaceutical applications. *Expert opinion on drug delivery*, 13(9):1257–1275, 2016.
- [303] Zhaohan Li, Parker R Wray, Magel P Su, Qiaomiao Tu, Himashi P Andaraarachchi, Yong Jin Jeong, Harry A Atwater, and Uwe R Kortshagen. Aluminum oxide nanoparticle films deposited from a nonthermal plasma: Synthesis, characterization, and crystallization. *ACS omega*, 5(38):24754–24761, 2020.
- [304] Peyman Hassanpour, Yunes Panahi, Abbas Ebrahimi-Kalan, Abolfazl Akbarzadeh, Soodabeh Davaran, Aygun N Nasibova, Rovshan Khalilov, and Taras Kavetsky. Biomedical applications of aluminium oxide nanoparticles. *Micro & Nano Letters*, 13(9):1227–1231, 2018.
- [305] S Said, S Mikhail, and MJMSfET Riad. Recent processes for the production of alumina nano-particles. *Materials Science for Energy Technologies*, 3:344–363, 2020.
- [306] Veeradate Piriya Wong, Voranuch Thongpool, Piyapong Asanithi, and Pichet Limsuwan. Preparation and characterization of alumina nanoparticles in deionized water using laser ablation technique. *Journal of Nanomaterials*, 2012: 1–6, 2012.
- [307] Naomi Amoni Ogolo and Mike O Onyekonwu. Potential application of aluminum oxide nanoparticles in the oil and gas industry. *Journal of Oil, Gas and Petrochemical Technology*, 9 (1):8–20, 2022.
- [308] Madhan Nur Agista, Kun Guo, and Zhixin Yu. A state-of-

REFERENCES

- the-art review of nanoparticles application in petroleum with a focus on enhanced oil recovery. *Applied Sciences*, 8(6):871, 2018.
- [309] MA Virji and AB Stefaniak. A review of engineered nanomaterial manufacturing processes and associated exposures. 2014.
- [310] Ho Chang and Yu-Chun Chang. Fabrication of Al_2O_3 nanofluid by a plasma arc nanoparticles synthesis system. *Journal of Materials Processing Technology*, 207(1-3):193–199, 2008.
- [311] Sumio Iijima. Helical microtubules of graphitic carbon. *nature*, 354(6348):56–58, 1991.
- [312] Gilbert D Nessim. Properties, synthesis, and growth mechanisms of carbon nanotubes with special focus on thermal chemical vapor deposition. *Nanoscale*, 2(8):1306–1323, 2010.
- [313] Wei Wu, Quanguo He, and Changzhong Jiang. Magnetic iron oxide nanoparticles: synthesis and surface functionalization strategies. *Nanoscale research letters*, 3:397–415, 2008.
- [314] Sophie Laurent, Delphine Forge, Marc Port, Alain Roch, Caroline Robic, Luce Vander Elst, and Robert N Muller. Magnetic iron oxide nanoparticles: synthesis, stabilization, vectorization, physicochemical characterizations, and biological applications. *Chemical reviews*, 108(6):2064–2110, 2008.
- [315] Chaoping Fu, Haipeng Zhou, Yanan Wang, Dong Liu, Junmeng Li, Haijun Deng, Xiaolong Qi, Tao Chen, Li-Ming Zhang, and Guoxin Li. One-pot synthesis of dextran-coated iron oxide nanoclusters for real-time regional lymph node mapping. *International Journal of Nanomedicine*, pages 3365–3374, 2017.
- [316] Eun Hee Kim, Yangkyu Ahn, and Hyo Sook Lee. Biomedical applications of superparamagnetic iron oxide nanoparticles encapsulated within chitosan. *Journal of Alloys and Compounds*, 434:633–636, 2007.
- [317] Pankaj Gogoi, Ashim J Thakur, Rashmi R Devi, Bodhaditya

REFERENCES

- Das, and Tarun K Maji. Adsorption of as (v) from contaminated water over chitosan coated magnetite nanoparticle: equilibrium and kinetics study. *Environmental nanotechnology, monitoring & management*, 8:297–305, 2017.
- [318] Jingmiao Qu, Guang Liu, Yiming Wang, and Ruoyu Hong. Preparation of fe₃o₄-chitosan nanoparticles used for hyperthermia. *Advanced Powder Technology*, 21(4):461–467, 2010.
- [319] Elham Cheraghipour, Sirius Javadpour, and Ali Reza Mehdizadeh. Citrate capped superparamagnetic iron oxide nanoparticles used for hyperthermia therapy. 2012.
- [320] Tanja Jurkin, Marijan Gotić, Goran Štefanić, and Irina Pucić. Gamma-irradiation synthesis of iron oxide nanoparticles in the presence of peo, pvp or ctab. *Radiation Physics and Chemistry*, 124:75–83, 2016.
- [321] Michela Puddu, Daniela Paunescu, Wendelin J Stark, and Robert N Grass. Magnetically recoverable, thermostable, hydrophobic dna/silica encapsulates and their application as invisible oil tags. *ACS nano*, 8(3):2677–2685, 2014.
- [322] Sulalit Bandyopadhyay, Gurvinder Singh, Ioanna Sandvig, Axel Sandvig, Roland Mathieu, P Anil Kumar, and Wilhelm Robert Glomm. Synthesis and in vitro cellular interactions of superparamagnetic iron nanoparticles with a crystalline gold shell. *Applied surface science*, 316:171–178, 2014.
- [323] JS Weston, RE Jentoft, BP Grady, DE Resasco, and JH Harwell. Silica nanoparticle wettability: Characterization and effects on the emulsion properties. *Industrial & Engineering Chemistry Research*, 54(16):4274–4284, 2015.
- [324] David Margolese, JA Melero, SC Christiansen, BF Chmelka, and GD Stucky. Direct syntheses of ordered sba-15 mesoporous silica containing sulfonic acid groups. *Chemistry of Materials*, 12(8):2448–2459, 2000.

REFERENCES

- [325] Young-Kwon Oh, Lan-Young Hong, Yamini Asthana, and Dong-Pyo Kim. Synthesis of super-hydrophilic mesoporous silica via a sulfonation route. *Journal of Industrial and Engineering Chemistry*, 12(6):911–917, 2006.
- [326] A Torsvik, V Myrseth, N Opedal, B Lund, A Saasen, JD Ytrehus, and Det norske Oljeselskap. Rheological comparison of bentonite based and kcl/polymer based drilling fluids. *Annu. Trans. Nord. Rheol. Soc*, 22:219–224, 2014.
- [327] API Spec et al. Specification for cements and materials for well cementing. 2010.
- [328] Mahmoud Khalifeh, Arild Saasen, Torbjørn Vrålstad, Helge Bøvik Larsen, and Helge Hodne. Experimental study on the synthesis and characterization of aplite rock-based geopolymers. *Journal of Sustainable Cement-Based Materials*, 5(4):233–246, 2016.
- [329] RP Api. 10b-2: Api recommended practice 10b-2, recommended practice for testing well cements. *API RP 10B-2*, 2013.
- [330] M Varela, Andrew R Lupini, K van Benthem, Albina Y Borisevich, Matthew F Chisholm, Naoya Shibata, E Abe, and Stephen J Pennycook. Materials characterization in the aberration-corrected scanning transmission electron microscope. *Annu. Rev. Mater. Res.*, 35:539–569, 2005.
- [331] Arild Saasen and Jan David Ytrehus. Viscosity models for drilling fluids—herschel-bulkley parameters and their use. *Energies*, 13(20):5271, 2020.
- [332] Marilyn Vilorio Ochoa. *Analysis of drilling fluid rheology and tool joint effect to reduce errors in hydraulics calculations*. Texas A&M University, 2006.
- [333] API Rp et al. Recommended practice for field testing water-based drilling fluids. *API Recommendation 13B-1, ISO, 20012009(10414):21*, 2009.
- [334] American Petroleum Institute Recommended Practices. 13b-2

REFERENCES

- recommended practice for field testing oil-based drilling fluids. API Dallas, 2014.
- [335] Jason Maxey. Rheological analysis of static and dynamic sag in drilling fluids. *Annual Transactions-Nordic Rheology Society*, 15:181, 2007.
- [336] TS EN. 196-1. methods of testing cement—part 1: Determination of strength. *European Committee for standardization*, 26, 2005.
- [337] C.ASTM. Standard test method for compressive strength of hydraulic cement mortars (using 2-in. or [50-mm] cube specimens). *Annual Book of ASTM Standards Annual Book of ASTM Standards*, 4, 2013.
- [338] Standard Norge. Ns-en 12390-6: 2009 testing hardened concrete—part 6: Tensile splitting strength of test specimens. 2009.
- [339] ASTM D3967-16. Standard test method for splitting tensile strength of intact rock core specimens. *ASTM International, West Conshohocken, PA, 2016*, 2016.
- [340] Zisis Vryzas, Lori Nalbandian, Vassilis T Zaspalis, and Vassilios C Kelessidis. How different nanoparticles affect the rheological properties of aqueous wyoming sodium bentonite suspensions. *Journal of Petroleum Science and Engineering*, 173:941–954, 2019.
- [341] Jan David Ytrehus, Ali Taghipour, Arash Golchin, Arild Saasen, and Braham Prakash. The effect of different drilling fluids on mechanical friction. *Journal of Energy Resources Technology*, 139(3):034502, 2017.
- [342] Mingzheng Yang and Yuanhang Chen. An experimental evaluation of the effects of filtercake in wellbore strengthening: Filtercake rupture resistance and fracture sealing time. *Journal of Energy Resources Technology*, 142(4):042903, 2020.
- [343] Md Amanullah and CP Tan. A non-destructive method of

REFERENCES

- cake thickness measurement. In *SPE Asia Pacific oil and gas conference and exhibition*, pages SPE-64517. SPE, 2000.
- [344] Bill Rehm, Jerome Schubert, Arash Haghshenas, Jim Hughes, and Amir Saman Paknejad. *Managed pressure drilling*. Elsevier, 2013.
- [345] Helge Hodne, Arild Saasen, and Skule Strand. Rheological properties of high temperature oil well cement slurries. *Annual Transactions-Nordic Rheology Society*, 8:31–38, 2001.
- [346] Arild Saasen and Jan David Ytrehus. Rheological properties of drilling fluids: use of dimensionless shear rates in herschel-bulkley and power-law models. *Applied Rheology*, 28(5):201854515, 2018.
- [347] Z Su, JMJM Bijen, and JA Larbi. Influence of polymer modification on the hydration of portland cement. *Cement and concrete research*, 21(2-3):242–250, 1991.
- [348] Xiangming Kong, Joachim Pakusch, Daniel Jansen, Sebastian Emmerling, Juergen Neubauer, and Friedlinde Goetz-Neuhoeffer. Effect of polymer latexes with cleaned serum on the phase development of hydrating cement pastes. *Cement and Concrete Research*, 84:30–40, 2016.
- [349] Xiangming Kong, Sebastian Emmerling, Joachim Pakusch, Markus Rueckel, and Jörg Nieberle. Retardation effect of styrene-acrylate copolymer latexes on cement hydration. *Cement and Concrete Research*, 75:23–41, 2015.
- [350] Stefan Baueregger, Margarita Perello, and Johann Plank. Influence of carboxylated styrene-butadiene latex copolymer on portland cement hydration. *Cement and Concrete Composites*, 63:42–50, 2015.
- [351] Erez Allouche, Yuri Lvov, Carlos Montes, and Anupam Joshi. Geopolymer with nanoparticle retardant and method, October 2 2018. US Patent 10,087,107.
- [352] Mahmoud Khalifeh, Arild Saasen, Helge Hodne, and

REFERENCES

- Hem Bahadur Motra. Laboratory evaluation of rock-based geopolymers for zonal isolation and permanent p&a applications. *Journal of Petroleum Science and Engineering*, 175:352–362, 2019.
- [353] Zhe Li, Rui Chen, and Lianyang Zhang. Utilization of chitosan biopolymer to enhance fly ash-based geopolymer. *Journal of Materials Science*, 48:7986–7993, 2013.
- [354] MJ Thiercelin, Bernard Dargaud, JF Baret, and WJ Rodriguez. Cement design based on cement mechanical response. *SPE drilling & completion*, 13(04):266–273, 1998.
- [355] H Williams, D Khatri, R Keese, S Le Roy-Delage, J Roye, D Leach, Peter Rottler, O Porcherie, and John Rodriguez. Flexible, expanding cement system (fecs) successfully provides zonal isolation across marcellus shale gas trends. In *SPE Canada Unconventional Resources Conference?*, pages SPE–149440. SPE, 2011.
- [356] Jesus De Andrade and Sigbjørn Sangesland. Cement sheath failure mechanisms: numerical estimates to design for long-term well integrity. *Journal of Petroleum Science and Engineering*, 147:682–698, 2016.
- [357] S Le Roy-Delage, C Baumgarte, M Thiercelin, and B Vidick. New cement systems for durable zonal isolation. In *SPE/IADC Drilling Conference and Exhibition*, pages SPE–59132. SPE, 2000.
- [358] Parth Panchmatia, Nancy S Zhou, Maria Juenger, and Eric van Oort. Monitoring the strength development of alkali-activated materials using an ultrasonic cement analyzer. *Journal of Petroleum Science and Engineering*, 180:538–544, 2019.
- [359] SL Yong, DW Feng, GC Lukey, and JSJ Van Deventer. Chemical characterisation of the steel–geopolymeric gel interface. *Colloids and Surfaces A: Physicochemical and Engineering Aspects*, 302(1-3):411–423, 2007.

REFERENCES

- [360] Yi Huang and Minfang Han. The influence of α -al₂o₃ addition on microstructure, mechanical and formaldehyde adsorption properties of fly ash-based geopolymer products. *Journal of hazardous materials*, 193:90–94, 2011.
- [361] Kang-Wei Lo, Kae-Long Lin, Ta-Wui Cheng, Yu-Min Chang, and Ju-Ying Lan. Effect of nano-sio₂ on the alkali-activated characteristics of spent catalyst metakaolin-based geopolymers. *Construction and building materials*, 143:455–463, 2017.

Appendix

Paper-I:

Alvi, M. A. A., Belayneh, M., Bandyopadhyay, S., & Minde, M. W. (2020). **Effect of iron oxide NPs on the properties of water-based drilling fluids**. *Energies*, 13(24), 6718. <https://doi.org/10.3390/en13246718>



Article

Effect of Iron Oxide Nanoparticles on the Properties of Water-Based Drilling Fluids

Muhammad Awais Ashfaq Alvi ^{1,*}, Mesfin Belayneh ¹, Sulalit Bandyopadhyay ² and Mona Wetrhus Minde ³

¹ Department of Energy and Petroleum Engineering, University of Stavanger, N-4036 Stavanger, Norway; mesfin.a.belayneh@uis.no

² Department of Chemical Engineering, Norwegian University of Science and Technology (NTNU), N-7491 Trondheim, Norway; sulalit.bandyopadhyay@ntnu.no

³ Department of Mechanical, Structural Engineering and Materials Science, University of Stavanger, N-4036 Stavanger, Norway; mona.w.minde@uis.no

* Correspondence: muhammad.a.alvi@uis.no or aawaisalvi@gmail.com

Received: 24 November 2020; Accepted: 16 December 2020; Published: 19 December 2020



Abstract: In recent years, several studies have indicated the impact of nanoparticles (NPs) on various properties (such as viscosity and fluid loss) of conventional drilling fluids. Our previous study with commercial iron oxide NPs indicated the potential of using NPs to improve the properties of a laboratory bentonite-based drilling fluid without barite. In the present work, iron oxide NPs have been synthesized using the co-precipitation method. The effect of these hydrophilic NPs has been evaluated in bentonite and KCl-based drilling fluids. Rheological properties at different temperatures, viscoelastic properties, lubricity, and filtrate loss were measured to study the effect of NPs on the base fluid. Also, elemental analysis of the filtrate and microscale analysis of the filter cake was performed. Results for bentonite-based fluid showed that 0.019 wt% (0.1 g) of NPs reduced the coefficient of friction by 47%, and 0.0095 wt% (0.05 g) of NPs reduced the fluid loss by 20%. Moreover, for KCl-based fluids, 0.019 wt% (0.1 g) of additive reduced the coefficient of friction by 45%, while higher concentration of 0.038 wt% (0.2 g) of NPs shows 14% reduction in the filtrate loss. Microscale analysis shows that presence of NPs in the cake structure produces a more compact and less porous structure. This study indicates that very small concentration of NPs can provide better performance for the drilling fluids. Additionally, results from this work indicate the ability of NPs to fine-tune the properties of drilling fluids.

Keywords: drilling fluids; nanoparticles; iron oxide; KCl; bentonite drilling fluids

1. Introduction

Drilling is the process of connecting the surface to the reservoir. In a rotary drilling operation, drilling fluids play an important role in maintaining well pressure, bringing cuttings to surface, and lubricating and cooling drill bits as well as the wellbore [1,2]. Proper selection of the drilling fluid is one of the key elements for the success of drilling operation. The selection of drilling fluid is usually based on its performance, cost and environmental impact [2].

Due to the interactions between the drilling fluid and the rock, a poorly designed drilling fluid may cause formation damage. The consequences are a negative impact on the log reading and damage to the pore space of the reservoir rock, that reduces its productivity. Increase in fluid loss into the formation will increase the near bore pressure, which as a result will weaken the strength of the wellbore. Moreover, drilling with non-inhibitive water-based drilling fluids will result in shale swelling. If the drilling fluid is poor at holding particles in suspension, cuttings will be accumulated in the

wellbore and result in solid-induced drill string stuck. Also, the thick mud cake may cause differential sticking problems [3,4].

Therefore, in general, drilling fluid design is one of the most important aspects to consider during the well construction and completion phases. The drilling fluid parameters under consideration, among others, are the rheological properties to control the hydraulics (well pressure and hole cleaning), lubricity to control the high torque and drag issues, mud cake properties to control fluid loss and to increase well strength [5,6]. The properties of drilling fluids are determined by the types and the concentration of the chemical additives used in their formulations. The right parameters must be characterized experimentally, and several formulation iterations may be required until the desired properties are achieved.

Typically, water- and oil-based drilling fluids, also known as water-based mud (WBM) and oil-based mud (OBM), are used in oil and gas wells [7]. In terms of lubricity and formation damage control, OBM is better than WBM [8]. The application of OBM is limited in environmentally sensitive areas, and hence, only drilling with water-based fluids is allowed. Moreover, WBM is used to drill the top-hole section where there is no blowout preventer (BOP) in place and drilling fluids can be discharged to the seabed. However, WBM still requires further improvement to provide better lubricity, shale inhibition, and formation damage control.

In recent years, several researchers have reported the impact of nanoparticles (NPs) on the properties of water-based drilling fluids. Studies indicate that the addition of NPs can alter the rheological parameters of drilling fluids under low pressure/low temperature (LPLT) and high pressure/high temperature (HPHT) conditions [9–15], reduce filtrate loss and filter cake thickness [9,16–20], reduce friction [13,15,16,21,22], improve thermal conductivity and heat transfer properties [17,20,23,24] and shale inhibition and wellbore strengthening [25–28]. Iron-based NPs have been added to water-based drilling fluids in several studies. For instance, Jung et al. [29] showed that the addition of iron oxide NPs to a bentonite-based fluid increases the viscosity of the fluid. This study indicated that the NPs interacted with the bentonite and promoted the gelation of the clay particles. In addition, a low concentration of NPs reduces the LPLT fluid loss values of the fluid, however increasing the concentration of NPs results in lesser reduction in fluid loss. Barry et al. [30] also investigated the effect of iron oxide on bentonite drilling fluids and observed higher values of shear stress with the addition of NPs compared to the base fluid. Addition of iron oxide particles at a concentration of 0.5 wt% and with sizes of 3 nm and 30 nm to the bentonite suspension reduced the fluid loss by 27% and 23.4%, respectively. Drilling fluids containing commercial iron oxide were also investigated by Mahmoud et al. [31]. Different concentrations of NPs were tested in this study with, a suspension of Ca-bentonite having 7 wt% concentration as a base fluid. The findings from this work illustrated that yield point and plastic viscosity were changed by the addition of iron oxide NPs to the drilling fluid. In order to enhance the filtration and rheological properties of Na-bentonite-based drilling fluids, Vryzas et al. [32,33] explored some novel iron oxide NPs. These studies illustrated that the apparent viscosity and yield stress become progressively susceptible to the temperature. An increase in apparent viscosity and yield stress was observed at a higher temperature. Moreover, 0.5 wt% of iron oxide NPs reduced the filtrate loss by 40% compared to the base fluid at high pressure and temperature. Recently, Mahmoud et al. [34,35] added iron oxide to a calcium bentonite-based drilling fluid. Addition of 0.5 wt% NPs to the base fluid decreased the fluid loss and produced a filter cake with better packing characteristics under static and dynamic conditions. In addition, the NPs increased the yield strength and gel-forming ability of the drilling fluid.

Our previous study showed the effect of commercial iron oxide NPs on a bentonite/polymer system in the presence of KCl salt [36]. Results from this study showed that NPs can reduce the friction of the drilling fluid. However, barite was not present in the fluid system. Therefore, in this study, the effects of NPs have been studied on a drilling fluid with barite. Further, most of the studies mentioned above focused on bentonite-based fluids, and not many studies available that studied the effect of NPs on KCl-based drilling fluids. Thus, KCl-based fluids without any bentonite were also

prepared as they are effective for shale-based formations. The potassium in KCl inhibits shale swelling by cation exchange with the calcium present in the shale and by reducing the hydration tendency of the shale [37]. Hence, this study focused on both KCl- and bentonite-based drilling fluid with barite.

2. Materials and Methods

Iron (II) chloride tetrahydrate ($\text{FeCl}_2 \cdot 4\text{H}_2\text{O}$) (Arcos Organics, Thermofisher Scientific, Oslo, Norway), Iron (III) chloride hexahydrate ($\text{FeCl}_3 \cdot 6\text{H}_2\text{O}$) and ammonia solution (NH_4OH , 25%) were purchased from Sigma Aldrich (Oslo, Norway) and KCl salt was purchased from VWR Chemicals (Oslo, Norway). Bentonite, barite, xanthan gum and soda ash were provided by a drilling fluid service company. De-ionized water was used for all sample preparations.

2.1. Synthesis of Iron Oxide NPs

NPs were synthesized by conventional co-precipitation of Fe ions in an alkaline environment [38]. First, 84.6 mL of de-ionized water was weighed in a beaker, and to this de-ionized water, 15.4 mL of 25% ammonia solution was added to make 100 mL of 1 M NH_4OH solution. Separately, 2.0 g of $\text{FeCl}_2 \cdot 4\text{H}_2\text{O}$ and 5.4 g of $\text{FeCl}_3 \cdot 6\text{H}_2\text{O}$ was dissolved in 25 mL distilled water in a volumetric flask. Afterward, 10 mL of this rusty coloured solution was transferred to a burette. The solution was then added dropwise into 100 mL of 1 M NH_4OH solution under vigorous stirring. A magnetic stirrer was used. The addition of the iron solution to the ammonia solution resulted in a black coloured solution. After the reaction was completed, the black coloured solution was transferred to centrifuge tubes. A strong magnet was placed under the centrifuge tubes to separate the particles magnetically, and the particles were washed several times with water. The process was repeated to harvest all the particles. Some NPs might stick to the magnetic stirrer. Therefore, it is essential to wash it several times to recover as many particles as possible. Almost clear fluid was obtained as NPs were drawn to a strong magnet after the first cleaning steps of particles with water. However, after several washes with de-ionized water, the particle's separation becomes difficult as less transparent fluid was obtained when a magnet was placed under the solution. It is crucial to stop washing after it gets difficult to avoid the loss of particles.

2.2. Coating of Xanthan Gum on Iron Oxide NPs (Fe-XG)

To coat xanthan gum polymer on iron oxide NPs, a 0.1 g of xanthan gum was added into 50 mL water to make a polymer solution. Afterward, 0.2 g of iron oxide NPs were added to this polymer solution, and the resulting mixture was left for shaking for 24 h. After 24 h, the resulting solution was used to formulate drilling fluid. The term Fe-XG is used for iron oxide NPs coated with xanthan gum throughout the text.

2.3. Formulation of Drilling Fluid

Two types of water-based fluids were formulated, a bentonite-based fluid and a KCl-based fluid. The fluid compositions were selected to produce fluids having comparable viscosity and density [39]. Tables 1 and 2 show the recipes used for both fluids. First base fluids were formulated, and to these fluids, different concentrations of NPs were added to see the effect of NPs on base fluids. In order to prepare bentonite fluid, all chemicals, excluding barite, were mixed with a Hamilton Beach mixer for 5 min followed by additional 5 min mixing to dislodge any material attached to the mixing container's side. Afterward, barite was added and mixed for 5 min and additional 5 min to dislodge adhering materials to attain the uniform mixing of components. To the base fluid, different concentrations of NPs (0.05–0.2 g) were added and again mixed for 5 min to disperse NPs in drilling fluid. To prepare Fe-XG NPs-based drilling fluid, Fe-XG was first mixed with water, and afterward, all components except barite were added and followed the same mixing procedure with 5 + 5 min. After adding barite, the same procedure of 5 + 5 min was followed. The main difference between the two fluids

is the addition of NPs. For iron oxide NPs without xanthan gum, the NPs were added in the end, while Fe-XG were added at the start, followed by other components.

Table 1. Composition of bentonite-based fluid.

Material	Base Fluid	Base Fluid + NPs
Water	350 mL	350 mL
Soda ash	4.8 g	4.8 g
Xanthan gum	0.71 g	0.71 g
Bentonite	10.04 g	10.04 g
Barite	183 g	183 g
Iron oxide NPs in water	-	0.05, 0.1, 0.2 g

Table 2. Composition of KCl-based fluid.

Material	Base Fluid	Base Fluid + NPs
Water	350 mL	350 mL
Soda ash	0.75 g	0.75 g
Xanthan gum	1.5 g	1.5 g
KCl	24.80 g	24.80 g
Barite	175 g	175 g
Iron oxide NPs in water	-	0.05, 0.1, 0.2 g

A similar procedure was followed to mix KCl-based fluids without and with NPs.

2.4. Drilling Fluid and NPs Characterization

Various characterization techniques were used to characterize NPs and drilling fluids with and without NPs. Details of the techniques are provided below.

2.4.1. Scanning Transmission Electron Microscopy (STEM)

A S-5500 STEM instrument (Hitachi, Krefeld, Germany) with a 30 kV accelerating voltage was used to obtain the STEM images of iron oxide NPs. Several drops of NPs solution were dropped on a Formvar carbon-coated copper grid to prepare TEM grids. It is crucial to wipe with Kimberly-Clark wipes after dropping the NPs solution to prevent further aggregation of NPs.

2.4.2. Microscale and Elemental Analysis

A Supra 35VP model scanning electron microscope (SEM, Zeiss, Oberkochen, Germany) was used to gain insights into the structural make-up and the presence of NPs in the mud cake from the fluid loss test. Additionally, images of the iron oxide NPs and Fe-XG were attained. Moreover, to quantify the percentage of different elements present in the structure and mapping, the elemental analysis was done with energy dispersive X-ray spectroscopy (EDS).

2.4.3. Dynamic Light Scattering (DLS) and Zeta Potential Measurements

A Zetasizer Nano-ZS instrument (Malvern, Worcestershire, UK) was used to measure the sizes and zeta potential of NPs. All the measurements were performed in aqueous solutions.

2.4.4. Viscosity

Viscosity parameters were measured using a model 900 viscometer (FANN, Houston, TX 77032, USA). Measurements were performed at 22 °C, 50 °C and 80 °C, and atmospheric pressure.

2.4.5. Mechanical Friction Measurement

The coefficient of friction was measured by using a CSM Tribometer (Anton Paar GmbH, Graz, Austria). The tests were conducted on a steel ball-plate surface filled with drilling fluid. The 13cr steel ball with a diameter of 6 mm was used. For all the tests normal load of 5 N was used that covered a 10 m distance with the rate of 3 cm/s. Measurements were performed at atmospheric pressure and room temperature. Repeat measurements were conducted to report the average value.

2.4.6. Fluid Loss Measurement

An American Petroleum Institute (API) filter press (FANN, Houston, TX 77032, USA) was used to measure the fluid loss at room temperature and 100 psi pressure. Filter paper with a diameter of 2.5 inches was used for the test. API standard, API Recommended Practice 13B-1 [40], was followed to perform the test.

2.4.7. Inductively Coupled Optical Atomic Emission Spectrometry (ICP-OES)

To measure the concentration of different ions, present in the filtrate obtained from the fluid loss test. ICP-OES analysis was performed before the analysis fluids were passed through a 0.2 μm syringe filter and diluted with 5% nitric acid.

2.4.8. Viscoelastic Measurement

Viscoelastic properties of the fluids were measured using a MCR 302 rheometer (Anton Paar GmbH, Graz, Austria). Amplitude sweep with a constant angular frequency of 10 rad/s and varying strain from 0.0005% to 1000% was performed.

3. Results and Discussion

3.1. Size Distribution of Iron Oxide and Fe-XG NPs

Figure 1a,b show the STEM and SEM images, respectively, of the NPs formed. It can be seen that particles have spherical morphology. Figure 2 show the size distribution of iron oxide NPs measured using STEM images. It can be seen in the figure that due to the absence of a stabilizing agent, particles formed have broad size distribution [41]. The average size of NPs formed by this method is 11 ± 2 nm.

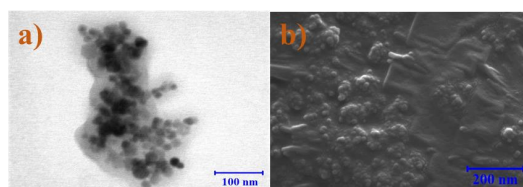


Figure 1. Iron oxide NPs formed by co-precipitation method: (a) STEM image; (b) SEM image.

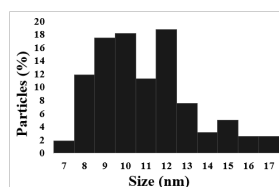


Figure 2. Size distribution of iron oxide NPs measured from STEM images.

Figure 3 shows the SEM images of Fe-XG, and it can be seen that the polymer is coated on the iron oxide NPs. Coating NPs with the polymer increases the particle size compared to the uncoated particles, as shown in Table 3.

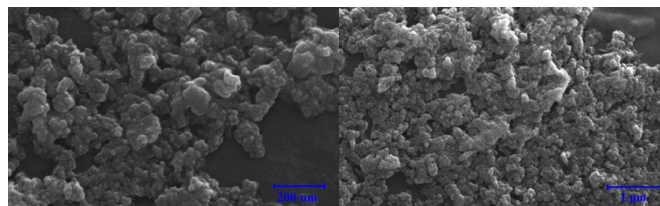


Figure 3. SEM images of Iron oxide NPs coated with xanthan gum (Fe-XG).

Table 3. Surface charges and sizes of NPs.

Material	Size (nm)	Zeta Potential (mV)
Iron oxide NPs at 25 °C	273.5 ± 5.95	−31.3 ± 0.27
Fe-XG NPs at 25 °C	487.60 ± 8.55	−39.23 ± 0.59
Iron oxide NPs at 50 °C	381.17 ± 19.58	−20.17 ± 0.23
Fe-XG NPs at 50 °C	673.57 ± 65.45	−34.37 ± 0.42

3.2. Hydrodynamic Size and Surface Charge of NPs

Table 3 shows the hydrodynamic size and surface charge of the iron oxide NPs and Fe-XG NPs. As shown in table, there is increase in size of NPs after coating of xanthan gum on their surface. Also, results show an increase in the size and decrease in zeta potential at higher temperatures. This indicates that NPs form aggregates at higher temperatures. Higher zeta potential values for Fe-XG indicate that polymer coating provides stability to the NPs and hinders the agglomeration and settling of NPs.

3.3. Rheological Parameters of the Drilling Fluids

3.3.1. Bentonite-Based Fluids

Shear stress values at different shear rates of bentonite-based drilling fluids are presented in Figure 4a–d. For base fluids and fluids with NPs, the shear stress values increase at high temperatures (i.e., 80 °C), especially at low shear rates. This is due to the inter-particle interaction of bentonite, which caused the flocculation of bentonite particles [42,43]. The clay particles agglomerate due to the face-to-face (FF) and edge-to-face (EF) associations [43,44]. A lower concentration (0.05 g) of NPs further increases the shear stress, as indicated in Figure 4a. A possible reason might be attachment of these NPs to edges of the clay platelets and with positively charged barium ions present in the drilling fluid. However, an increase in the NPs concentration (0.1 g) might cause repulsion between the negatively charged NPs and other negatively charged additives in the fluid system, which lowers the fluid's viscosity compared to the 0.05 g NPs as shown in Figure 4b.

Additionally, increasing the NPs concentration to 0.2 g might have caused agglomeration of NPs, which significantly increases the shear stress values, as indicated in Figure 4c. Although, coating of 0.2 g NPs with xanthan gum (Fe-XG) has decreased the shear stress values at a low shear rate, which indicates that polymer coating might have minimized the agglomeration of NPs and negatively charged polymer cause electrostatic repulsion between the negatively charged ions in the fluid system. Increase in zeta potential also indicates the stability of NPs with the polymer coating, see Table 3. In addition, there might be adsorption of polymer chains on the surface of bentonite prevented the

aggregation of bentonite at higher temperature [45]. Vryzas et al. [46] showed a similar behavior for the iron oxide NPs in the water-bentonite suspension. This study shows that bentonite forms a gel structure and aggregates at high temperature, due to the FF association of the platelets. Addition of NPs to these suspensions further increases the viscosity and yield stress due to aggregation of magnetic NPs owing to the high surface energies of the particles. However, the coating of NPs with citric acid minimizes the aggregation of NPs; our study shows a similar behavior with the coating of polymer on the NPs. Moreover, a decrease in the zeta potential of NPs at 50 °C, as indicated in the Table 3, also shows that high temperature reduces the stability of NPs, which causes the aggregation of the particles, especially at high concentration.

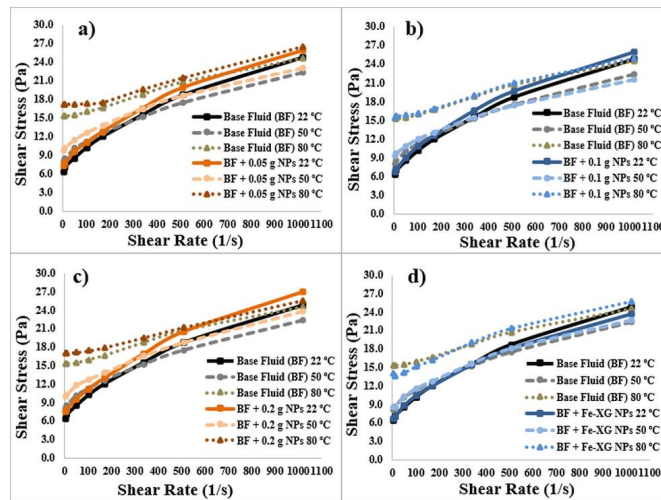


Figure 4. Iron oxide NPs effect on shear stress values of bentonite-based fluids at different shear rates and temperatures: (a) 0.05 g; (b) 0.1; (c) 0.2 g; (d) Fe-XG.

There is a decrease in apparent viscosity values with an increase in the shear rate for all the fluids, indicating the drilling fluid's shear-thinning behavior. Gel strength values (10 s and 10 min) are shown in Figure 5a,b for bentonite drilling fluids. A lower concentration of NPs (0.05 g) caused more increase in the base fluid's gel strength values than the 0.1 g NPs, especially for 10 min gel strength. This shows that NPs might get attached to the bentonite edges at low concentrations without causing the repulsion between the bentonite particles. However, increasing the NPs concentration, causing the deflocculation of the bentonite, precisely at 80 °C. At 80 °C, most of gel strength was attained after 10 s for all the fluids since gel strength did not change much when compared with gel strength measured at 10 min.

Gel strength with a higher concentration of NPs (0.2 g) and Fe-XG is also shown in Figure 5a,b. Increasing the NPs concentration raises the gel strength after 10 s and 10 min due to the agglomeration of NPs. However, coating the NPs surface with the xanthan gum again decreases the gel strength compared to 0.2 g NPs. This shows that the polymer surface on the NPs controls the agglomeration of NPs, and adsorption of polymer on bentonite prevents the gel formation, especially at 80 °C. Gel strength results for the bentonite-based fluid show high gel strength values that could efficiently hold the cutting and provide effective hole cleaning.

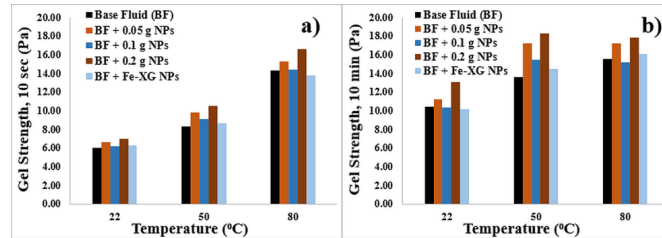


Figure 5. Gel strength of bentonite-based fluids: (a) 10 s gel strength; (b) 10 min gel strength.

3.3.2. KCL-Based Fluids

Figure 6a–d show the shear stress values at varying shear rates for the KCl-based fluids. High concentration of salt present in the fluids decreases the shear stress values at high temperature, as indicated in the figures. The high concentration of KCl salt makes the fluid system dispersive due to the suppression of the electric double layer.

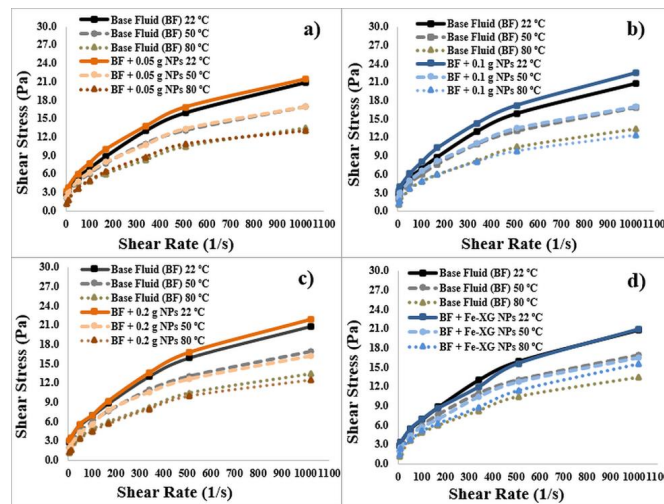


Figure 6. Iron oxide NPs effect on shear stress values of KCl-based fluids at different shear rates and temperatures: (a) 0.05 g; (b) 0.1; (c) 0.2 g; (d) Fe-XG.

Moreover, the addition of 0.05 g of NPs to the fluid system slightly increases the shear stress values at 22 °C and 50 °C, for instance increasing the shear stress values from 2.83 pa to 3.16 pa at 22 °C and 1.97 pa to 2.19 pa at 50 °C for a shear rate of 5.11 1/s. Similarly, for 0.1 g, there is a slight increase in shear stress values at 22 °C and 50 °C, as shown in Figure 6b. In case of 0.2 g, there is an increase in shear stress values at 22 °C. However, at 50 °C, addition of 0.2 g NPs lowers the shear stress value. For Fe-XG, there is not much change in the shear stress values as compared to the base fluid at 22 °C and 50 °C.

At 80 °C, uncoated NPs (0.05, 0.1, 0.2) do not have a significant effect on the shear stress values, in fact there is decrease in shear stress values especially at low shear rate. These results show that at high

temperature, NPs become unstable; this is also supported by the zeta potential measurements shown in Table 3. Polymer coating on the particles increases the shear stress at a higher shear rate for 80 °C compared to the uncoated and base fluid system that shows the improved stability of NPs with the polymer coating. Apparent viscosity in the case of KCl fluids also shows a decrease in values with an increase in the shear rate for all fluids.

Addition of NPs to the KCl drilling fluid slightly increases gel strength at 22 °C and 50 °C for both 10 s and 10 min, as shown in Figure 7a,b. However, at a higher temperature, NPs do not change the gel strength of base fluid. A decrease in zeta potential values of NPs indicates that at high-temperature NPs are agglomerated, which minimizes the interaction between NPs and KCl salt. Moreover, a high concentration of KCl present in the system forms weaker gel structures [47]. Additionally, Increasing the concentration and polymer coating decreases the gel strength compared to a base fluid at 22 °C, as shown in Figure 7. Fe-XG shows a minor increase in the gel strength at 80 °C, which might be due to the system's stability at higher temperatures due to polymer presence compared to the bare NPs.

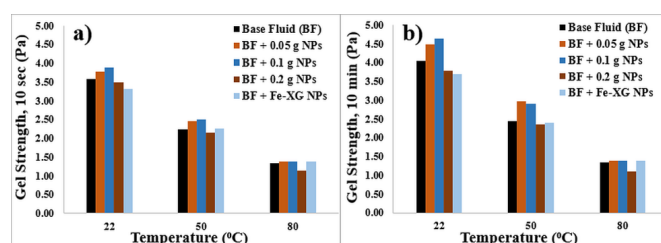


Figure 7. Gel strength values for KCl-based fluids: (a) Effect of temperature and NPs on 10 sec gel strength; (b) Effect of temperature and NPs on 10 min gel strength.

3.4. Viscoelasticity

Drilling fluids possess elastic and viscous properties [48,49]. Viscoelastic properties of the drilling fluids can provide further information about the drilling fluid's internal gel structure under dynamic loading. Storage and loss modules describe the energy stored and lost by the material when the shear is applied, respectively. Viscoelastic behavior of drilling fluids is presented in the next section for both types of fluid.

3.4.1. Bentonite-Based Fluids

Yield stress represents the stress where the deviation from the LVE region occurs and can be estimated from the shear stress and strain/time plot. Deviation of shear stress from linearity is taken as yield stress [50,51]. Flow points represent the point where storage and loss modules are equal. Table 4 shows the yield stress and flow point values for bentonite fluids. Figure 8a,b shows the storage and loss modulus for bentonite-based fluid and fluids with NPs.

Table 4. Yield stress and flow point for bentonite-based fluids.

Samples	Yield Stress (Pa)	Flow Point (Pa)
Base fluid (BF)	4.6	8.5
BF + 0.05 g NPs	5.6	9.3
BF + 0.1 g NPs	4.9	9.5
BF + 0.2 g NPs	5.2	8.9
BF + Fe-XG NPs	5.1	9.4

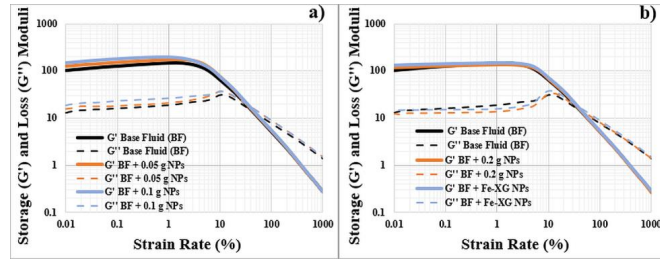


Figure 8. Storage and loss modulus for bentonite-based fluids: (a) Base fluid with low concentration of NPs; (b) Base fluid with high concentration of NPs and Fe-XG.

It can be seen that NPs slightly increases the yield stress values, especially for low concentration. However, increasing the concentration does not significantly alter the yield stress values. Moreover, in case of lower concentration NPs and Fe-XG, there is a slight delay in the flow point. This indicates that NPs provide structural strength to the fluid. However, raising the NPs concentration to 0.2 g slightly decreases the flow point compared to the low concentration.

3.4.2. KCL-Based Fluids

For KCl-based fluids, there is not much difference between the base fluids and fluids having NPs, as shown in Table 5 and Figure 9a,b. NPs addition decreases the flow point values compared to the base fluid in case of uncoated NPs. This shows that NPs addition slightly weakens the gel characteristics of KCl-based fluid. However, for Fe-XG, there is a slight increase in flow point, which shows the polymer’s ability to improve the gel characteristics.

Table 5. Yield stress and flow point for KCl-based fluids.

Samples	Yield Stress (Pa)	Flow Point (Pa)
Base fluid (BF-1)	2.0	4.9
BF-1 + 0.05 g NPs	2.0	4.6
BF-1 + 0.1 g NPs	1.9	4.4
Base fluid (BF-2)	1.6	4.3
BF-2 + 0.2 g NPs	1.4	3.7
BF-2 + Fe-XG NPs	2.0	4.6

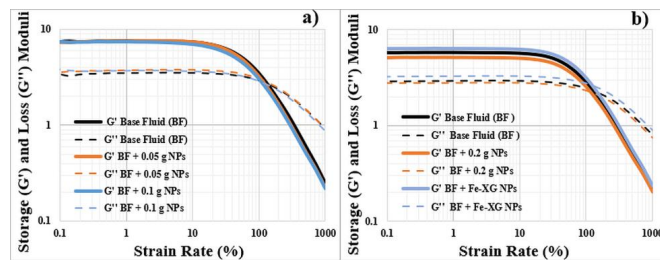


Figure 9. Storage and loss modulus for KCL-based fluid: (a) Base fluid with low concentration of NPs (b) Base fluid with high concentration of NPs and Fe-XG.

3.5. Mechanical Friction

Reducing the drilling fluid’s mechanical friction is crucial to keep the torque and drag to a minimum during the drilling operation. Since minimizing the friction will allow drilling longer distances also, it makes the casing running operation smooth.

3.5.1. Bentonite-Based Fluids

Water-based drilling fluids with bentonite usually show higher values for mechanical friction. Therefore, it is beneficial to increase the lubricity of these fluids. As shown in Figure 10a, NPs have reduced the coefficient of friction of base fluids. NPs with 0.1 g concentration shows the most reduction in friction values. However, a higher concentration of NPs increases friction. The possible reason might be the agglomeration of NPs at higher concentrations.

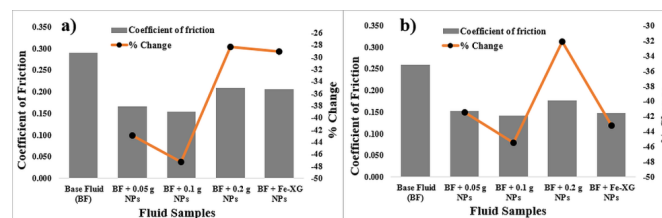


Figure 10. Friction values of: (a) Bentonite-based fluids with NPs; (b) KCl-based fluids with NPs.

3.5.2. KCl-Based Fluids

Since KCl-based fluids do not have bentonite present in them, they show low mechanical friction values compared to bentonite-based fluids, as indicated in Figure 10b. NPs also decrease the coefficient of friction in case of these fluid systems. In this case, also, 0.1 g NPs showed the most reduction in friction values. However, all the other concentrations of NPs still provide a significant reduction in friction. These results for both water-based fluids show that NPs can provide lubricating properties to the drilling fluids. NPs form a lubricating film around the micro-sized material’s harsh surfaces and behave like a fluid in the system.

3.6. Effect of NPs on the Fluid Loss

Since the quality of drilling fluid is dependent on its performance with respect to controlling the filtrate loss to the formation, it is crucial to minimize the fluid loss. The additives and solid particles that form the filter cake are vital in controlling the fluid loss.

3.6.1. Bentonite-Based Fluids

Figure 11a shows the fluid loss results for the bentonite-based fluids with and without NPs. As shown in the figure, NPs have reduced the fluid loss for the base fluids. NPs with 0.05 g, 0.1 g and 0.2 g concentration reduced the fluid loss by 20%, 13% and 19% respectively. NPs coated with xanthan gum reduces fluid loss by 16%. The results indicate that NPs with different concentrations show a similar reduction in fluid loss, with low concentration showing the most reduction. This might be due to the even distribution of NPs on filter cake and the fluid’s stability under pressure. However, 0.2 g NPs show almost the same amount of reduction due to filling the micropores in the filter cake by the NPs.

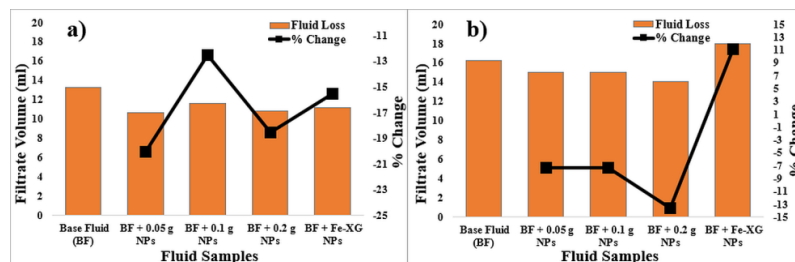


Figure 11. Filtrate volume after fluid loss test for: (a) Bentonite-based fluids with NPs; (b) KCl-based fluids with NPs.

3.6.2. KCL-Based Fluids

For the KCl fluids, a higher concentration (0.2 g) of NPs showed the highest reduction of 14% in fluid loss. Fluids with 0.05 g and 0.1 g concentration NPs reduce fluid loss by 7%, as shown in Figure 11b. However, NPs coated with xanthan gum increases fluid loss. This might be due to the large size of the particles are not able to fill the pores compared to the uncoated particles. It can be seen that KCl based fluid showed higher values for fluid loss due to the absence of bentonite in the system. Moreover, lower apparent viscosity of the KCl-based fluids than the bentonite fluids also contributed to higher values of fluid loss.

3.7. Microscale Analysis of the Filter Cake

3.7.1. Bentonite-Based Fluids

SEM images for the cake formed by bentonite-based fluid are shown in the Figure 12. It can be seen in Figure 12a,b that the cake formed by the base fluid is not compact and there are voids in the cake structure. Addition of NPs results in a less porous and compact structure formation for the base fluid (see Figure 12c,d for iron oxide NPs and Figure 12e,f for Fe-XG NPs). Other studies also report similar results with bentonite-based drilling fluids [30,35,52].

The possible reason for the reduction in fluid loss is the filling of voids in the cake structure by the NPs, as indicated in Figures 13 and 14. However, as indicated in figures for both bare NPs and Fe-XG that there is an agglomeration of NPs, which might hinder the further reduction in the fluid loss due to less particle packing. EDS spectrum of the area pointed by the arrow shows higher concentration of Fe, indicating the presence of iron oxide NPs in the cake.

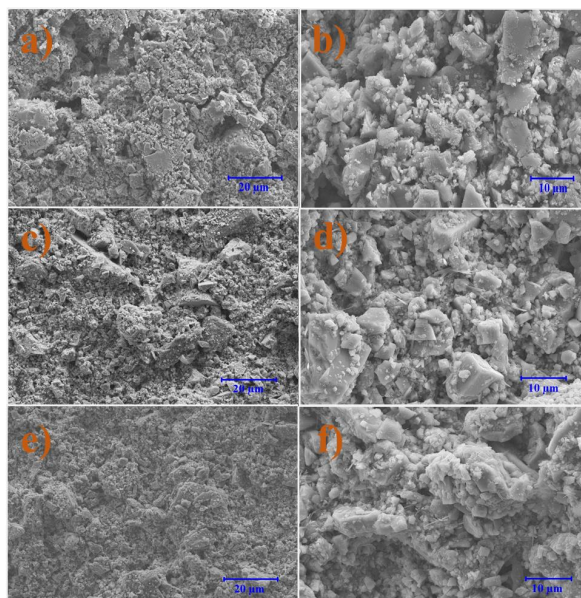


Figure 12. SEM images of filter cake of Bentonite-based fluids: (a,b) Filter cake for base fluids; (c,d) Filter cake for base fluids with Iron oxide NPs; (e,f) Filter cake for base fluids with Fe-XG NPs.

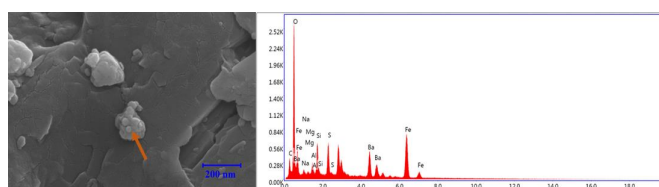


Figure 13. Presence of NPs in the mud cake for bentonite fluids with iron oxide NPs (EDS spectrum shows the analysis done on the area indicated by the arrow).

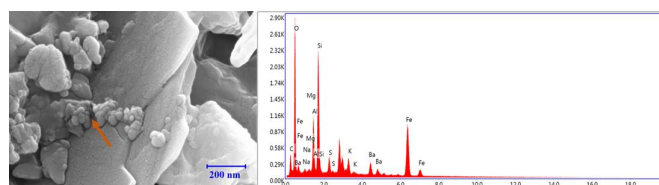


Figure 14. Presence of NPs in the mud cake for bentonite fluids with Fe-XG NPs (EDS spectrum shows the analysis done on the area pointed by the arrow).

3.7.2. KCl-Based Fluids

Figure 15a–f show the SEM images for the KCl-based fluid and base fluids with NPs. NPs can produce a less porous structure by filling the voids in the structure of mud cake. However, as indicated in figures, voids are still present in the cake structure, where they are responsible for higher fluid loss values.

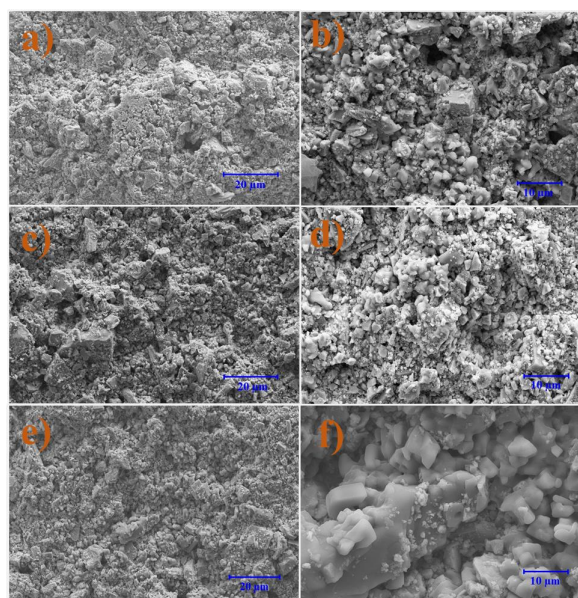


Figure 15. SEM images of filter cake KCl-based fluids: (a,b) Filter cake for base fluids; (c,d) Filter cake for base fluids with Iron oxide NPs; (e,f) Filter cake for base fluids with Fe-XG NPs.

In case of the sample with iron oxide NPs, closer observation of the mud cake structure indicates that for bare NPs, there is a filling of the voids between the micro-sized particles by the NPs as shown in Figure 16. Also, NPs interacted with the salt surface leading to a compact structure compared to microparticles.

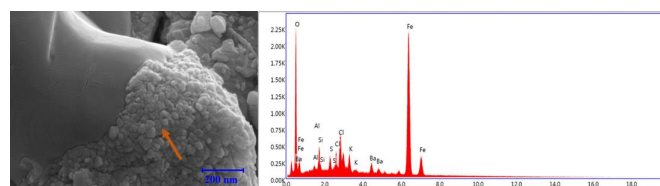


Figure 16. Presence of NPs in the mud cake for KCl fluids with Iron oxide NPs (EDS spectrum shows the analysis done on the area pointed by the arrow).

However, for Fe-XG, the higher values for the fluid loss might be due to NPs got adsorbed on the salt surface and not being able to fill the voids in the cake's structure. Also, large size of the particles did not create compact cake structure, as shown in Figure 17. Moreover, dissociation of salt induces flocculation by reducing the polymer interaction with the other additives and creating voids in the structure.

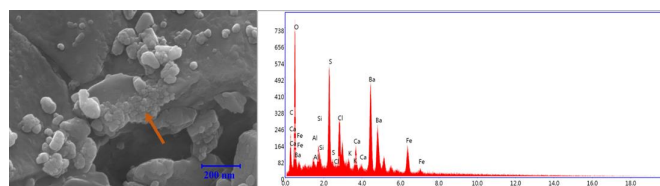


Figure 17. Presence of NPs in the mud cake for KCl fluids with Fe-XG NPs (EDS spectrum shows the analysis done on the area pointed by the arrow).

3.8. EDS Analysis

3.8.1. Bentonite-Based Fluids

The main elements present in the filter cake for the bentonite-based system are sodium, oxygen, barium, sulphur and silicon. Small amounts of magnesium, calcium, aluminum, and strontium are present in the cake formed after the fluid loss test. Figures 18a–c and 19a–c show the presence of iron in the cake structures formed by bentonite-based fluids and KCl-based fluids, respectively. Figure 18b indicates that the iron oxide NPs are distributed in the cake structure, and the iron (Fe) amount also increases compared to the base fluid. However, in case of Fe-XG NPs, as seen in Figure 18c, there is no uniform distribution of NPs. This indicates that the Fe-XG particles remain dispersed in the fluid without contributing to cake formation. Fe content is also lowered in this case compared to the samples with uncoated NPs due to xanthan gum's coating on the surface of the particles.

3.8.2. KCl-Based Fluids

In case of KCl fluids, there is a higher concentration of potassium and chlorine present in the cake structure. Moreover, a lower amount of sodium is present due to the absence of bentonite.

Similarly, in the case of KCl fluids, the iron oxide NPs contributed to cake formation as Fe content increase in case of samples with NPs, see Figure 19b. However, NPs filled few voids in the structure, creating a less compact structure leading to lower fluid loss reduction.

Additionally, mapping results indicate that for Fe-XG, NPs were not uniformly distributed in the cake structure. Also, NPs do not fill the voids in the cake structure, which leads to an increase in the fluid loss values, as shown in Figure 19c.

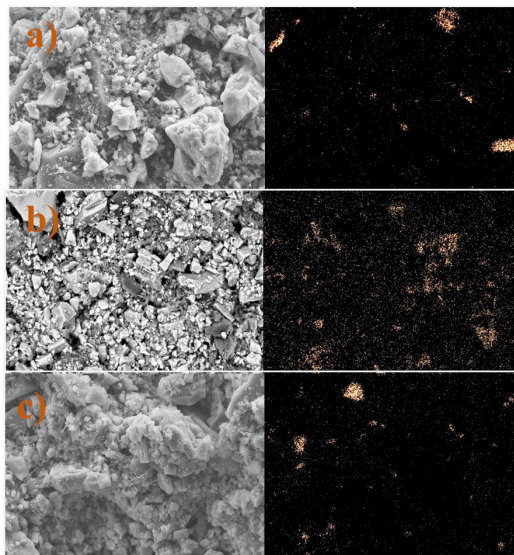


Figure 18. Elemental analysis of filter cake for bentonite-based fluids: (a) Base fluid; (b) Base fluid with NPs; (c) Base fluid with Fe-XG NPs.

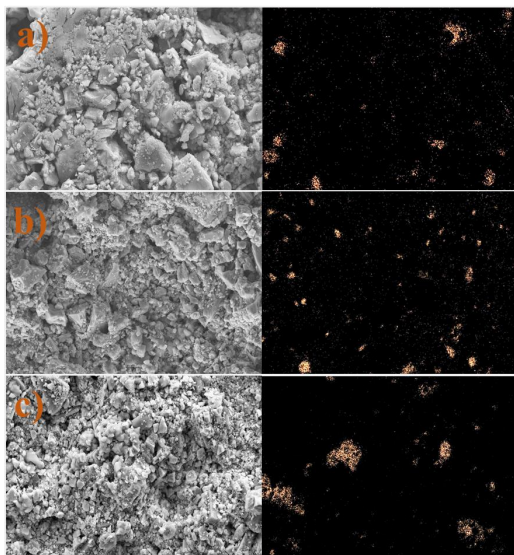


Figure 19. Elemental analysis of filter cake for KCl-based fluids: (a) Base fluid; (b) Base fluid with NPs; (c) Base fluid with Fe-XG NPs.

3.9. Elemental Analysis of Filtrate

Element analysis results are shown in Tables 6 and 7. In case of low concentrations of NPs, there was no iron detected in the filtrate. However, increasing the concentration shows that iron was present in the filtrate. This shows that most of NPs are deposited on a cake or stayed in the drilling fluid at a lower concentration. Even at higher concentrations, there is small amount of iron particles present in the filtrate. Most of the particles stayed on the cake and in the drilling fluid. A high concentration of sodium was detected in the bentonite-based fluids. In comparison, KCl-based fluids showed a higher concentration of potassium cations present in the filtrate. Most of the barite stayed in the cake as low barium and sulfate concentrations were detected, as shown in the tables.

Table 6. Elements from the filtrate loss for bentonite-based fluids.

Elements	Base Fluid	Base Fluid + 0.05 g NPs	Base Fluid + 0.2 g NPs	Base Fluid + Fe-XG
Barium, Ba (mg/L)	0.31	0.27	0.27	0.30
Calcium Ca (mg/L)	0.7	1.0	0.5	0.6
Copper Cu (mg/L)	0.7	0.91	0.6	0.6
Iron Fe (mg/L)	n.d.	n.d.	0.09	<0.06
Potassium K (mg/L)	237	108	123	35
Magnesium Mg (mg/L)	2.2	2.1	2.3	2.4
Sodium Na (mg/L)	5906	5579	5460	5370
Silicon Si (mg/L)	5.6	5.6	4.5	5.3
Strontium Sr (mg/L)	0.9	1.3	0.5	0.3
Aluminium Al (mg/L)	1.4	<0.5	2.0	2.3

Table 7. Elements from the filtrate loss for KCl-based fluids.

Elements	Base Fluid	Base Fluid + 0.05 g NPs	Base Fluid + 0.2 g NPs	Base Fluid + Fe-XG
Barium, Ba (mg/L)	1.8	1.2	1.4	1.6
Calcium Ca (mg/L)	<3	<3	2.1	3.7
Copper Cu (mg/L)	1.9	1.5	1.5	1.4
Iron Fe (mg/L)	n.d.	n.d.	<0.3	<0.3
Potassium K (mg/L)	36,144	35,564	33,400	32,700
Magnesium Mg (mg/L)	4	4	4	3.2
Sodium Na (mg/L)	894	826	820	850
Silicon Si (mg/L)	<3	<3	2.4	2.6
Strontium Sr (mg/L)	9.3	8.6	8.3	8.3
Aluminium Al (mg/L)	<5	<5	<5	<5

3.10. Magnetic Recovery

Magnetic recovery of the NPs from the drilling fluids was done by using a strong magnet. It can be seen that NPs can be recovered from the fluid system. These recovered particles were analyzed using SEM, as shown in Figures 20 and 21 for bentonite and KCl-based fluids, respectively. As seen from the figures, NPs interacted with the other components of the drilling fluids. For both bentonite and KCl fluids high concentration of barium indicated that NPs interacted with the barium. A small amount of sodium and magnesium was also present in bentonite-based fluids indicating the interaction of particles with bentonite. Moreover, the EDS spectrum shows small amounts of potassium and chlorine for the KCl-based fluids.

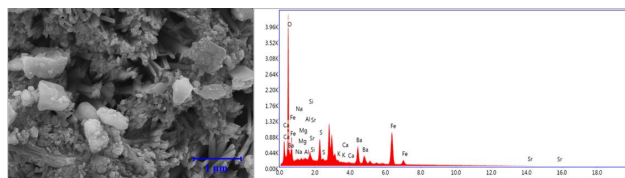


Figure 20. SEM image and EDS spectrum of recovered particles for bentonite-based fluids.

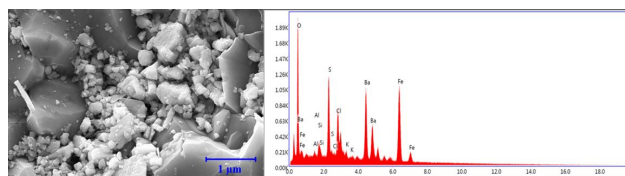


Figure 21. SEM image and EDS spectrum of recovered particles for KCl-based fluid.

4. Conclusions

In this experimental study, iron oxide NPs and Fe-XG NPs effect on two types of water-based drilling fluids (bentonite-based fluids and KCl-based fluids) was studied. The main findings of the study are summarized below:

- Results indicate that NPs can modify the rheological parameters of bentonite-based fluids. NPs increases the viscosity and gel strength of the bentonite-based fluids owing to the agglomeration of magnetic NPs.
- A polymer coating on the NPs slightly reduces the gel strength values at high temperature for bentonite-based fluids.
- Small concentration of NPs was sufficient to reduce the coefficient of friction and fluid loss values of the bentonite-based fluids. NPs with 0.019 wt% (0.1 g) and 0.0095 wt% (0.05 g) reduces the coefficient of friction and fluid loss by 47% and 20%, respectively.
- Fe-XG NPs also reduces the coefficient of friction by 29%, while fluid loss values were reduced by 16% for bentonite-based fluids.
- Filter cake analysis shows that NPs filled the spaces in the structure of the cake and uniform distribution of particles kept the fluid loss values to a minimum compared to the base fluid.
- In addition, elemental analysis shows the even distribution of the NPs throughout the structure of the filter cake.
- In the case of KCl-based fluids, the addition of NPs has a slight impact on rheological parameters owing to the lesser stability of the fluid system due to presence of high salt concentration.

- In case of coefficient of friction and fluid loss, NPs do provide improvements. Addition of 0.038 (0.2 g) wt%, and 0.019 wt% (0.1 g) of NPs reduces fluid loss and friction by 14% and 45%, respectively. However, Fe-XG NPs increase the fluid loss value by 11%.
- Microscale analysis of the cake shows that NPs do interact with the salt and reduce the cake's permeability by forming compact structures.
- Fe-XG NPs increases the fluid loss values due to an increase in size and adsorption of polymer on the salt surface, creating voids in the cake structure.
- This work also shows that magnetic recovery of NPs also provides further information regarding the interaction of NPs with other additives in the drilling fluid system.
- This study shows that low concentration of NPs is sufficient to improve the properties of drilling fluids. Also, NPs can reduce the fluid loss values and friction values of KCl-based fluids without affecting the rheological parameters.

Author Contributions: Conceptualization, methodology, investigation, formal analysis, writing—original draft, writing—review & editing, M.A.A.A.; conceptualization, supervision, project administration, funding acquisition, writing—review & editing, M.B.; conceptualization, supervision, project administration, funding acquisition, S.B.; formal analysis, investigation, validation, resources, M.W.M. All authors have read and agreed to the published version of the manuscript.

Funding: This research was funded by Norwegian Ministry of Education and Research, project number 8050-IN11398 and Norwegian micro- and Nano-Fabrication facility, NorFab project number 245963.

Acknowledgments: Authors would like to thank Kjell Kåre Fjelde for contributing in reviewing the paper and Muhammad Bilal for helping with DLS and zeta potential measurements.

Conflicts of Interest: The authors declare no conflict of interest.

References

1. Bourgoyne, A.T.; Millhelm, K.K.; Chenevert, M.E.; Young, F.S., Jr. *Applied Drilling Engineering*; Textbook Series Vol. 2; Society of Petroleum Engineering: Richardson, TX, USA, 1986.
2. Caenn, R.; Darley, H.C.H.; Gray, G.R. Introduction to Drilling Fluids. In *Composition and Properties of Drilling and Completion Fluids*; Gulf Professional Publishing: Houston, TX, USA, 2017.
3. He, S.; Liang, L.; Zeng, Y.; Ding, Y.; Lin, Y.; Liu, X. The influence of water-based drilling fluid on mechanical property of shale and the wellbore stability. *Petroleum* **2016**, *2*, 61–66. [[CrossRef](#)]
4. Ewy, R.T.; Morton, E.K. Wellbore-Stability Performance of Water-Based Mud Additives. *SPE Drill. Complet.* **2009**, *24*, 390–397. [[CrossRef](#)]
5. Jones, T.G.J.; Hughes, T.L. Drilling Fluid Suspensions. *Adv. Chem. Ser.* **1996**, *251*. [[CrossRef](#)]
6. Al-Yasiri, M.; Awad, A.; Pervaiz, S.; Wen, D. Influence of silica nanoparticles on the functionality of water-based drilling fluids. *J. Pet. Sci. Eng.* **2019**, *179*, 504–512. [[CrossRef](#)]
7. Agarwal, S.; Phuoc, T.X.; Soong, Y.; Martello, D.; Gupta, R.K. Nanoparticle-stabilised invert emulsion drilling fluids for deep-hole drilling of oil and gas. *Can. J. Chem. Eng.* **2013**, *91*, 1641–1649. [[CrossRef](#)]
8. Fink, J. *Petroleum Engineer's Guide to Oil Field Chemicals and Fluids*; Gulf Professional Publishing: Houston, TX, USA, 2012. [[CrossRef](#)]
9. Abdo, J.; Haneef, M.D. Nano-Enhanced Drilling Fluids: Pioneering Approach to Overcome Uncompromising Drilling Problems. *J. Energy Resour. Technol.* **2012**, *134*, 014501. [[CrossRef](#)]
10. Abdo, J.; AL-Sharji, H.; Hassan, E. Effects of nano-sepiolite on rheological properties and filtration loss of water-based drilling fluids. *Surf. Interface Anal.* **2016**, *48*, 522–526. [[CrossRef](#)]
11. Ghanbari, S.; Kazemzadeh, E.; Soleymani, M.; Naderifar, A. A facile method for synthesis and dispersion of silica nanoparticles in water-based drilling fluid. *Colloid Polym. Sci.* **2016**, *294*, 381–388. [[CrossRef](#)]
12. Jain, R.; Mahto, V.; Sharma, V.P. Evaluation of polyacrylamide-grafted-polyethylene glycol/silica nanocomposite as potential additive in water based drilling mud for reactive shale formation. *J. Nat. Gas Sci. Eng.* **2015**, *26*, 526–537. [[CrossRef](#)]
13. Katende, A.; Boyou, N.V.; Ismail, I.; Chung, D.Z.; Sagala, F.; Hussein, N.; Ismail, M.S. Improving the performance of oil based mud and water based mud in a high temperature hole using nanosilica nanoparticles. *Colloids Surf. A Physicochem. Eng. Asp.* **2019**, *577*, 645–673. [[CrossRef](#)]

14. Sadeghalvaad, M.; Sabbaghi, S. The effect of the TiO₂/polyacrylamide nanocomposite on water-based drilling fluid properties. *Powder Technol.* **2015**, *272*, 113–119. [[CrossRef](#)]
15. Alvi, M.A.A.; Belayneh, M.; Saasen, A.; Fjelde, K.K.; Aadnøy, B.S. Effect of MWCNT and MWCNT functionalized -OH and -COOH nanoparticles in laboratory water based drilling fluid. In Proceedings of the ASME 37th International Conference on Ocean, Offshore & Arctic Engineering (OMAE), Madrid, Spain, 17–22 June 2018. [[CrossRef](#)]
16. Aftab, A.; Ismail, A.R.; Khokhar, S.; Ibpupoto, Z.H. Novel zinc oxide nanoparticles deposited acrylamide composite used for enhancing the performance of water-based drilling fluids at elevated temperature conditions. *J. Pet. Sci. Eng.* **2016**, *146*, 1142–1157. [[CrossRef](#)]
17. Halali, M.A.; Ghotbi, C.; Tahmasbi, K.; Ghazanfari, M.H. The Role of Carbon Nanotubes in Improving Thermal Stability of Polymeric Fluids: Experimental and Modeling. *Ind. Eng. Chem. Res.* **2016**, *55*, 7514–7534. [[CrossRef](#)]
18. Song, K.; Wu, Q.; Li, M.C.; Wojtanowicz, A.K.; Dong, L.; Zhang, X.; Ren, S.; Lei, T. Performance of low solid bentonite drilling fluids modified by cellulose nanoparticles. *J. Nat. Gas Sci. Eng.* **2016**, *34*, 1403–1411. [[CrossRef](#)]
19. Song, K.; Wu, Q.; Li, M.; Ren, S.; Dong, L.; Zhang, X.; Lei, T.; Kojima, Y. Water-based bentonite drilling fluids modified by novel biopolymer for minimizing fluid loss and formation damage. *Colloids Surf. A Physicochem. Eng. Asp.* **2016**, *507*, 58–66. [[CrossRef](#)]
20. William, J.K.M.; Ponmani, S.; Samuel, R.; Nagarajan, R.; Sangwai, J.S. Effect of CuO and ZnO nanofluids in xanthan gum on thermal, electrical and high pressure rheology of water-based drilling fluids. *J. Pet. Sci. Eng.* **2014**, *117*, 15–27. [[CrossRef](#)]
21. Mao, H.; Qiu, Z.; Shen, Z.; Huang, W. Hydrophobic associated polymer based silica nanoparticles composite with core-shell structure as a filtrate reducer for drilling fluid at ultra-high temperature. *J. Pet. Sci. Eng.* **2015**, *129*, 1–14. [[CrossRef](#)]
22. Taha, N.M.; Lee, S. Nano Graphene Application Improving Drilling Fluids Performance. In Proceedings of the International Petroleum Technology Conference, Doha, Qatar, 6–9 December 2015. [[CrossRef](#)]
23. Fazelabdolabadi, B.; Khodadadi, A.A.; Sedaghatzadeh, M. Thermal and rheological properties improvement of drilling fluids using functionalized carbon nanotubes. *Appl. Nanosci.* **2015**, *5*, 651–659. [[CrossRef](#)]
24. Sadegh Hassani, S.; Amrollahi, A.; Rashidi, A.; Soleymani, M.; Rayatdoost, S. The effect of nanoparticles on the heat transfer properties of drilling fluids. *J. Pet. Sci. Eng.* **2016**, *146*, 183–190. [[CrossRef](#)]
25. Kang, Y.; She, J.; Zhang, H.; You, L.; Song, M. Strengthening shale wellbore with silica nanoparticles drilling fluid. *Petroleum* **2016**, *2*, 189–195. [[CrossRef](#)]
26. Nwaoji, C.O.; Hareland, G.; Husein, M.; Nygaard, R.; Zakaria, M.F. Wellbore strengthening- nano-particle drilling fluid experimental design using hydraulic fracture apparatus. In Proceedings of the SPE/IADC Drilling Conference, Amsterdam, The Netherlands, 5–7 March 2013. [[CrossRef](#)]
27. Sharma, M.M.; Zhang, R.; Chenevert, M.E.; Ji, L.; Guo, Q.; Friedheim, J. A new family of nanoparticle based drilling fluids. In Proceedings of the SPE Annual Technical Conference and Exhibition, San Antonio, TX, USA, 8–10 October 2012. [[CrossRef](#)]
28. Aramendiz, J.; Imqam, A. Water-based drilling fluid formulation using silica and graphene nanoparticles for unconventional shale applications. *J. Pet. Sci. Eng.* **2019**, *179*, 742–749. [[CrossRef](#)]
29. Jung, Y.; Barry, M.; Lee, J.-K.; Tran, P.; Soong, Y.; Martello, D.; Chyu, M. Effect of nanoparticle-additives on the rheological properties of clay-based fluids at high temperature and high pressure. In Proceedings of the AADE National Technical Conference and Exhibition, Houston, TX, USA, 12–14 April 2011; pp. 1–4.
30. Barry, M.M.; Jung, Y.; Lee, J.K.; Phuoc, T.X.; Chyu, M.K. Fluid filtration and rheological properties of nanoparticle additive and intercalated clay hybrid bentonite drilling fluids. *J. Pet. Sci. Eng.* **2015**, *127*, 338–346. [[CrossRef](#)]
31. Mahmoud, O.; Nasr-El-Din, H.A.; Vryzas, Z.; Kelessidis, V.C. Characterization of filter cake generated by nanoparticle-based drilling fluid for HP/HT applications. In Proceedings of the SPE International Conference on Oilfield Chemistry, Montgomery, TX, USA, 3–5 April 2017. [[CrossRef](#)]
32. Vryzas, Z.; Mahmoud, O.; Nasr-El-Din, H.; Zaspalis, V.; Kelessidis, V.C. Incorporation of Fe₃O₄ nanoparticles as drilling fluid additives for improved drilling operations. In Proceedings of the ASME 35th International Conference on Ocean, Offshore & Arctic Engineering (OMAE), Busan, Korea, 19–24 June 2016. [[CrossRef](#)]
33. Vryzas, Z.; Zaspalis, V.; Nalbantian, L.; Mahmoud, O.; Nasr-El-Din, H.A.; Kelessidis, V.C. A comprehensive approach for the development of new iron oxide nanoparticles giving smart drilling fluids with superior properties for HP/HT applications. In Proceedings of the International Petroleum Technology Conference, Bangkok, Thailand, 14–16 November 2016. [[CrossRef](#)]

34. Mahmoud, O.; Nasr-El-Din, H.A.; Vryzas, Z.; Kelessidis, V.C. Effect of ferric oxide nanoparticles on the properties of filter cake formed by calcium bentonite-based drilling muds. *SPE Drill. Complet.* **2018**, *33*. [[CrossRef](#)]
35. Mahmoud, O.; Nasr-El-din, H.A.; Vryzas, Z.; Kelessidis, V.C. Using ferric oxide and silica nanoparticles to develop modified calcium bentonite drilling fluids. *SPE Drill. Complet.* **2018**, *33*. [[CrossRef](#)]
36. Alvi, M.A.A.; Belayneh, M.; Saasen, A.; Aadnøy, B.S. The effect of micro-sized boron nitride BN and iron trioxide Fe₂O₃ nanoparticles on the properties of laboratory bentonite drilling fluid. In Proceedings of the SPE Norway One Day Seminar, Bergen, Norway, 18 April 2018. [[CrossRef](#)]
37. Shi, X.; Wang, L.; Guo, J.; Su, Q.; Zhuo, X. Effects of inhibitor KCl on shale expansibility and mechanical properties. *Petroleum* **2019**, *5*, 407–412. [[CrossRef](#)]
38. Puddu, M.; Paunescu, D.; Stark, W.J.; Grass, R.N. Magnetically recoverable, thermostable, hydrophobic DNA/silica encapsulates and their application as invisible oil tags. *ACS Nano* **2014**, *8*, 2677–2685. [[CrossRef](#)]
39. Torsvik, A.; Myrseth, V.; Opedal, N.; Lund, B.; Saasen, A.; Ytrehus, J.D. Rheological comparison of bentonite based and KCl/polymer based drilling fluids. *Annu. Trans. Nord. Rheol. Soc.* **2014**, *22*, 219–224.
40. API. *Recommended Practice for Field Testing Water-Based Drilling Fluids*; 13B-1 APIRP; API: Washington, DC, USA, 2009.
41. Sharma, A.; Foppen, J.W.; Banerjee, A.; Slimani, S.; Bachhar, N.; Peddis, D.; Bandyopadhyay, S. Magnetic Nanoparticles to Unique DNA Tracers—Effect of Functionalization on Physico-Chemical Properties. *Nanoscale Res. Lett.* **2020**. [[CrossRef](#)]
42. Darley, H.C.H.; Gray, G.R. *Composition and Properties of Drilling and Completion Fluids*; Gulf Professional Publishing: Houston, TX, USA, 1988.
43. Vryzas, Z.; Kelessidis, V.C.; Nalbandian, L.; Zaspalis, V.; Gerogiorgis, D.I.; Wubulikasimu, Y. Effect of temperature on the rheological properties of neat aqueous Wyoming sodium bentonite dispersions. *Appl. Clay Sci.* **2017**, *136*, 26–36. [[CrossRef](#)]
44. Mouzon, J.; Bhuiyan, I.U.; Hedlund, J. The structure of montmorillonite gels revealed by sequential cryo-XHR-SEM imaging. *J. Colloid Interface Sci.* **2016**, *465*, 58–66. [[CrossRef](#)]
45. Ahmad, H.M.; Kamal, M.S.; Al-Harathi, M.A. Rheological and filtration properties of clay-polymer systems: Impact of polymer structure. *Appl. Clay Sci.* **2018**, *160*, 226–237. [[CrossRef](#)]
46. Vryzas, Z.; Nalbandian, L.; Zaspalis, V.T.; Kelessidis, V.C. How different nanoparticles affect the rheological properties of aqueous Wyoming sodium bentonite suspensions. *J. Pet. Sci. Eng.* **2019**, *173*, 941–954. [[CrossRef](#)]
47. Chang, W.Z.; Leong, Y.K. Ageing and collapse of bentonite gels—Effects of Li, Na, K and Cs ions. *Rheologica Acta* **2014**, *53*, 109–122. [[CrossRef](#)]
48. Bui, B.; Saasen, A.; Maxey, J.; Ozbayoglu, M. Viscoelastic Properties of Oil-Based Drilling Fluids. *Annu. Trans. Nord. Rheol. Soc.* **2012**, *20*, 33–47.
49. Saasen, A.; Liu, D.; Marken, C.D. Prediction of barite sag potential of drilling fluids from rheological measurements. In Proceedings of the SPE/IADC Drilling Conference, Amsterdam, The Netherlands, 28 February–2 March 1995. [[CrossRef](#)]
50. Barnes, H.A.; Nguyen, Q.D. Rotating vane rheometry—A review. *J. Nonnewtonian Fluid Mech.* **2001**, *98*, 1–14. [[CrossRef](#)]
51. Fernandes, R.R.; Andrade, D.E.V.; Franco, A.T.; Negrão, C.O.R. Correlation between the gel-liquid transition stress and the storage modulus of an oil-based drilling fluid. *J. Nonnewton Fluid Mech.* **2016**, *231*, 6–10. [[CrossRef](#)]
52. Vryzas, Z.; Mahmoud, O.; Nasr-El-din, H.A.; Kelessidis, V.C. Development and testing of novel drilling fluids using Fe₂O₃ and SiO₂ nanoparticles for enhanced drilling operations. In Proceedings of the International Petroleum Technology Conference (IPTC), Doha, Qatar, 6–9 December 2015. [[CrossRef](#)]

Publisher's Note: MDPI stays neutral with regard to jurisdictional claims in published maps and institutional affiliations.



© 2020 by the authors. Licensee MDPI, Basel, Switzerland. This article is an open access article distributed under the terms and conditions of the Creative Commons Attribution (CC BY) license (<http://creativecommons.org/licenses/by/4.0/>).

Paper-II:

Alvi, M. A. A., Belayneh, M., Fjelde, K. K., Saasen, A., & Bandyopadhyay, S. (2021). **Effect of hydrophobic iron oxide NPs on the properties of oil-based drilling fluids**. *Journal of Energy Resources Technology*, 143(4). <https://doi.org/10.1115/1.4048231>

This paper is not included in the repository due to copyright restrictions.

Paper-III:

Alvi, M. A. A., Khalifeh, M., & Agonafir, M. B. (2020). **Effect of NPs on properties of geopolymers designed for well cementing applications.** Journal of Petroleum Science and Engineering, 191, 107128. <https://doi.org/10.1016/j.petrol.2020.107128>



Contents lists available at ScienceDirect

Journal of Petroleum Science and Engineering

journal homepage: <http://www.elsevier.com/locate/petrol>



Effect of nanoparticles on properties of geopolymers designed for well cementing applications

Muhammad Awais Ashfaq Alvi^{*}, Mahmoud Khalifeh, Mesfin Belayneh Agonafir

Dept. of Energy and Petroleum Engineering, University of Stavanger, Norway

ARTICLE INFO

Keywords:
Well cementing
Geopolymer
Rock-based
Nanoparticles

ABSTRACT

Recently the focus of the oil and gas industry is to find the alternative material for well barrier applications. Geopolymers are among the suggested materials, which could be used in the future to solve the well integrity issues rooted by the properties of Portland cement. Previous study with rock-based geopolymer indicates the potential of geopolymer to be used as a barrier material. However, there are still some shortcomings of geopolymer material, which need to be improved to make it a possible option for well cementing applications. This study aims to improve the properties of the geopolymer. Al_2O_3 and multi walled carbon nanotubes functionalized with hydroxyl group (MWCNT-OH) nanomaterials were used to study their effect on rheological, filtration loss, and mechanical properties of the geopolymer. Moreover, the effect of nanomaterials on the setting time and microstructure of the geopolymer has been studied. Results obtained from this work indicate that, nanomaterials-based geopolymers have better mechanical properties and setting time compared to the neat geopolymer. Addition of nanomaterials produced a more ductile structure with higher compressive and tensile strengths. Microstructure and element analysis confirmed the formation of a more compact and dense structure with the presence of MWCNT-OH and Al_2O_3 throughout the structure of the geopolymer.

1. Introduction

In hydrocarbon wells, cement is one of the important well barrier elements used during well construction, completion, and Plug and Abandonment (P&A) phases. When well productivity is not economical, or the well experience uncontrolled leakage, the fate of the well is to be permanently plugged and abandoned. The primary function of well cementing is to seal annular spacing between casing-casing or casing-formation, hinder formation-casing communication, providing structural integrity, and preventing formation fluid from leaking to the surface (Nelson and Guillot, 2006). Fig. 1 presents possible leak scenarios that occurred due to improper zonal isolation. Possible leak paths from the well could be: through cement due to permeability of cement, through cracks caused by downhole stresses (e.g. thermal shocks, tectonic stresses, post-cement operations) and brittleness of cement, in the microannuli at the interface of casing-cement or cement-formation caused due to shrinkage of cement and/or insufficient wetting to ensure bonding between casing and cement. Properly designed slurry, as well as good cementing practices, are the key factors for successful cementing operation. For any civil engineering works, it is important to

follow recommended practices and standards. NORSOK D-10 (2013) defines well integrity as “the application of a technical, operational, and organizational solution to minimize the risk of an undesired leak during the lifetime of the well.”

Well integrity issues are reported in several parts of the world. For instance, Vignes and Aadnøy (2010) have audited the integrity status of the Norwegian Continental Shelf (NCS) wells based on the information obtained from seven operators. As shown in Fig. 2, their investigation indicated that out of the 75 wells (i.e., 48 production and 27 injection wells), casing and cement integrity issues recorded 11% of well integrity issues each. A recent survey performed by the Petroleum Safety Authority (PSA) Norway on 1995 wells from 13 operators shows that 30% of the wells have well integrity issues (Norway, 2019).

Moreover, Watson and Bachu (2009) have statistically assessed the leakage potential of several abandoned wells in Alberta, Canada. This study indicates that improper zonal isolation is one of the causes of leak to the environment.

Depending on the well design and completion, qualified cement can be counted either as a well barrier element in the primary or secondary barrier envelope (see Fig. 1). Although cement has been the prime

^{*} Corresponding author. University of Stavanger, 4036 Stavanger, Norway.
E-mail address: muhammad.a.alvi@uis.no (M.A.A. Alvi).

<https://doi.org/10.1016/j.petrol.2020.107128>

Received 1 November 2019; Received in revised form 24 February 2020; Accepted 25 February 2020

Available online 4 March 2020

0920-4105/© 2020 The Author(s).

Published by Elsevier B.V. This is an open access article under the CC BY-NC-ND license

(<http://creativecommons.org/licenses/by-nc-nd/4.0/>).

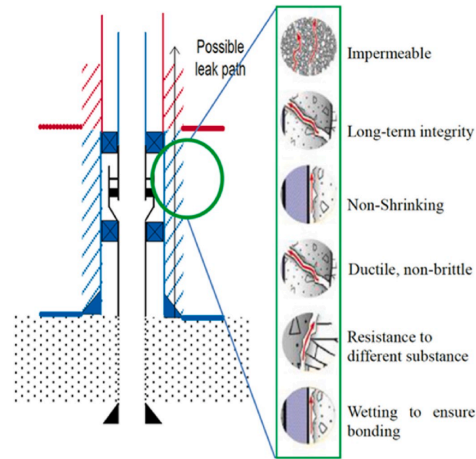


Fig. 1. Well barrier envelopes (blue as primary and red as secondary) and NORSOK D-10 cement requirement (Belayneh and Aadnøy, 2015; Norsok, 2013). (For interpretation of the references to colour in this figure legend, the reader is referred to the Web version of this article.)

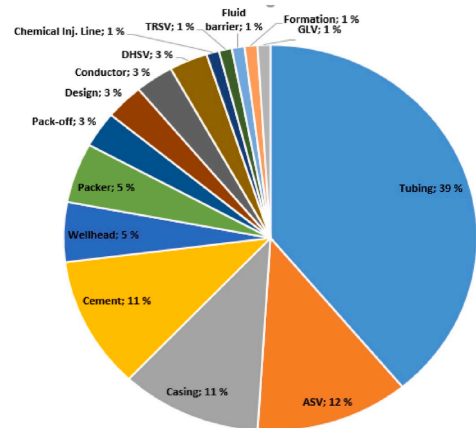


Fig. 2. Categories of well barrier element failures in the Norwegian sector of the North Sea (Vignes and Aadnøy, 2010).

material used for zonal isolation and P&A, the enacted mechanical and long-term durability requirements by different authorities make the use of alternative barrier materials important. NORSOK D-10 (2013) reminds that any barrier material used for zonal isolation or P&A shall be impermeable, able to withstand mechanical loads/impact, and non-shrinking. In addition, the candidate material shall resist downhole chemicals and ensure bonding with steel and formation. Obtained results by different researchers and dialogue with operators suggest that the use of alternative material to Portland cement might be necessary to reduce the risk of well barrier failure (Teodoriu et al., 2013; Jafariesfad

et al., 2017a; Kiran et al., 2017; Salehi et al., 2017; Vrålstad et al., 2018).

The primary failure mechanisms associated with the Portland cement are addressed as, but not limited to, changes of temperature and pressure regimes that cause cement cracks, brittleness (low ductility) of cement, volume changes causing possible microannuli (Vrålstad et al., 2018). Furthermore, poor cementing practices can result in channels through cement (Shenold and Teodoriu, 2016) and tectonic stresses (Lavrov and Torsæter, n.d; Jafariesfad et al., 2017a; Vrålstad et al., 2018) are circumstances that intensify the risk of material failure. However, due to the above shortcomings with the Portland cement, researchers are trying to look for supplementary materials. Several alternative materials such as bismuth-based materials (Carragher and Fulks, 2018), resins, creeping formation, and geopolymer have been proposed or used as an alternative to Portland cement (Khalifeh et al., 2013, 2014; Vrålstad et al., 2018).

Geopolymers have been used in the construction industry and suggested as a supplementary material to cement for well construction (Khalifeh et al., 2014, 2018; Liu et al., 2017; Salehi et al., 2019). Geopolymers are inorganic polymers made of a long chain of aluminosilicate materials formed by the process of geopolymerization. Geopolymerization is the term introduced by Joseph Davidovits in 1978 (Davidovits, 1982, 1991). In this process, reactive alumina and silica-based materials, known as precursors, act as source material. The source material is mixed with a hardener, which is an alkali silicate solution to activate the geopolymerization process. Three different mechanisms (dissolution, orientation and polycondensation) are involved during the geopolymerization process (Duxson et al., 2007; Davidovits, 2005). A variety of precursor materials based on natural minerals such as feldspar, metakaolin, kaolinite, and solid wastes like fly ash, blast furnace slag, rice husk, and several others can be used to produce geopolymers. The geopolymer structure has a 3-D network gel consisting of SiO_4 and AlO_4 tetrahedrons that are bonded alternately by sharing the oxygen ions as Si-O-Al-O (Davidovits, 2005; Komnitsas, 2011). The stability and strength of the geopolymer depend on the properties of the source material. Some of these properties may include, but not limited to, fineness, particle size distribution, chemical composition and reactive content of the geopolymeric precursors (Singh et al., 2015). Moreover, the concentration of soluble silicate, water content, and pH level of the hardener are also important factors (Duxson et al., 2007).

Different researchers studied the advantages and current limitations of geopolymers compared to conventional cement. Some of the advantages include durability at corrosive environments (Nasvi et al., 2014; Khalifeh et al., 2017), lower permeability (Gao et al., 2013; Salehi et al., 2016; Nasvi et al., 2014), higher structural flexibility (Khalifeh et al., 2015), lower chemical shrinkage (Salehi et al., 2016, 2017; Paiva et al., 2018; Khalifeh et al., 2018) and lower CO_2 emission during production (Gao et al., 2013). However, there are current limitations that limit the application of geopolymer for well construction. These include lower tensile strength compared to Portland cement and issues related to controlling the pumpability of geopolymer slurry at elevated temperature for a reasonable time (Khalifeh et al., 2018). Another main barrier is that technology has not been field tested and, therefore, not yet qualified for use.

1.1. Nanomaterials in cement and geopolymer

In recent years, research results have shown that nanomaterials (1–100 nm) can significantly improve the properties of conventional drilling fluid, oil well cement, and enhanced oil recovery processes. Nanomaterials have shown great potential to solve engineering problems related to the oil and gas industry. Due to a very small size and high surface area to volume ratio, nanomaterials have the ability to create smart materials with improved rheological and mechanical properties. For instance, the application of nanoparticles in cement has shown improved properties such as increase in compressive strength (Li et al.,

2004; Meng et al., 2012; Safi et al., 2018), flexural strength (Li et al., 2004; Safi et al., 2018), tensile strength (Jalal et al., 2012) and reduced permeability (Ozyildirim and Zegetosky, 2010). Researchers working in the areas of well cementing have also introduced nanomaterials to their mix designs to achieve better properties of the cement material (Ershadi et al., 2013; Pang et al., 2014; de Paula et al., 2014; Khan et al., 2016; Murtaza et al., 2016; Jafariefad et al., 2017b; Li et al., 2017).

Moreover, the application of nanoparticles in geopolimer has shown impacts on different properties. Many studies are available which show the impact of nanoparticles on workability (Hassan et al., 2015; Phoo-ngernkham et al., 2014; Rodríguez et al., 2013; Gao et al., 2014), microstructure (Assaedi et al., 2016; Phoo-ngernkham et al., 2014), chemical shrinkage (Yang et al., 2015) and density and porosity (Deb et al., 2016; Assaedi et al., 2015, 2016). Additionally, the effect of nanoparticles on the mechanical properties of geopolymers has been studied by some authors (Assaedi et al., 2016; Phoo-ngernkham et al., 2014; Naskar and Chakraborty, 2016). However, very few studies are available to address the effect of nanoparticles on the properties of geopolymers for oil well cementing (Ridha and Yerikania, 2015; Khalifeh et al., 2019a,b).

In geopolimer technology, the presence of aluminium oxide plays an important role. By decreasing the ratio of Si/Al, the final geopolimer material can be more flexible with a higher degree of resistivity to corrosive chemicals (Provis and Van Deventer, 2009). In addition, the use of aluminium for producing lightweight and sound-isolating geopolymers have been studied by some researchers (Hajimohammadi et al., 2017; Leiva et al., 2019). We also know that the hydroxyl group plays a role in the geopolymerization reaction. Therefore, the use of nanoparticles functionalized with OH⁻ involves the nanoparticles in geopolimer reactions to further enhance the properties of geopolymers.

In this study, MWCNT functionalized with a hydroxyl group (MWCNT-OH), and Al₂O₃ nanoparticles (AL-0450) have been used to study their effect on the properties of rock-based geopolimer. The impact of Al₂O₃ nanoparticles and MWCNT on different geopolimer systems have been previously studied. For instance, Guo et al. (2014) have added γ -Al₂O₃ to fly-ash based geopolimer. This study shows that Al₂O₃ nanoparticles have modified the pore structure of the geopolimer and produced a material structure with a narrow pore distribution based on the FT-IR spectrum and SEM analysis. Also, nanoparticles improved the compressive strength of the fly ash-based geopolimer, 2.0 wt% of Al₂O₃ nanomaterials increase the strength from 50 MPa to 56.8 MPa for neat geopolimer after 28 days. Another study shows that the addition of Al₂O₃ nanoparticles to high calcium fly-ash based geopolimer decrease the setting time of the slurry (Chindaprasit et al., 2012). Phoo-ngernkham et al. (2014) showed that the microstructure of the Al₂O₃ based high calcium fly ash geopolimer was improved, with the formation of denser structure. Additionally, nanoparticles improved elastic modulus, compressive, and flexural strength of the geopolimer paste.

MWCNTs have also been used in geopolymers to improve mechanical properties (i.e. compressive and tensile strengths as well as Young modulus) because of the superior mechanical properties of carbon nanotubes. Saafi et al. (2013) introduced MWCNT to a low calcium fly ash-based geopolimer. The addition of MWCNT having a concentration of up to 1 wt% by weight of the geopolimer improved flexural strength and Young modulus of the geopolimer. However, Saafi et al. (2013) reported that a lower concentration of the MWCNT in the geopolimer matrix gave better results due to sufficient dispersion of the nanotubes in the slurry. The effect of carbon nanotubes on the compressive strength and modulus of elasticity of fly ash-based geopolimer has been reported by Rovnanik et al. (2016). According to Rovnanik et al. (2016), the best result for compressive strength and modulus of elasticity of the geopolimer obtained when low concentration (0.15 wt%) of MWCNT was used in the mix. Published results by Abbasi et al. (2016) show that carbon nanotubes improve the strength of metakaolin-based geopolymers. According to them, an addition of 0.5% nanotubes had increased compressive strength by 32% and flexural strength by 28% of

the geopolimer. Moreover, SEM analysis confirmed the bonding of MWCNT with the geopolimer, as nanotubes bridged the microcracks in the structure of the geopolimer.

One important criterion to be considered in the selection of nanoparticles is to obtain sufficient dispersion. Agglomeration of nanomaterials may lead to a negative impact on the properties of geopolimer or other cement-based materials. Furthermore, lower concentration of nanomaterials has a better performance compared to the use of large amounts, which ultimately may lead to non-reacted nanoparticles in the cement-based materials (Guo et al., 2014; Riahi and Nazari, 2012; Sumesh et al., 2017; Khater and Abd El Gawad, 2016).

In this paper, the intent is to study the effects of the AL-0450 and MWCNT-OH nanoparticles on rheological properties, static fluid loss, pumping time, and mechanical properties of a neat rock-based geopolimer (GP). The mechanical, elastic, and physical properties are used to quantify and analyze the quality of cementitious material. In an oil and gas well, cement can experience compressive and tensile loads. Hence, in this paper, the elastic properties of geopolymers are characterized through the uniaxial and Brazilian (indirect tensile) tests. Additionally, the microstructure of the geopolymers containing the nanoparticles was examined.

2. Experimental procedures

2.1. Materials

Granite is an intrusive igneous rock, and its main constituents are quartz and alkali feldspars. Granite was used as geopolimer precursor, in this work, to produce rock-based geopolimer. Veldé Pukk AS provided powdered granite, and it was used without any further processing. The particle size of powder granite was below 63 μ m. To achieve the required chemical composition of geopolymers precursors, the chemical composition of granite was normalized by introducing silica flour and ground granulated blast furnace slag. The chemical composition of the geopolimeric precursor is presented in Table 1. The development of the rock-based geopolimer and its reaction is extensively presented in work done by Khalifeh et al. (2016).

Ground Granulated Blast Furnace Slag (GGBFS) is an industrial by-product of the steel industry. The GGBFS has calcium and magnesium content, but the precursor mix is designed so that the final calcium content is less than 10 wt%. The GGBFS used in this study was supplied by MEROX, Sweden, with the product name Merit 5000.

Silica flour is natural quartz sand, and it was supplied by Halliburton. It was introduced to the mix design to adjust the Si/K₂O ratio.

In this research work, a potassium silicate solution was used as a hardener, which had a modulus number (SiO₂/K₂O) of 2.30. Deionized water was used to adjust the water content of the binder. The chosen nanoparticles were introduced to the binder prior to the addition of precursor.

To this liquid phase, suitable amounts of AL-0450 and MWCNT-OH were added. Nanomaterials in the liquid phase (aqueous) were used in this study. As nanomaterials are dispersions in the water phase, liquid to solid ratio of the geopolimer slurry was adjusted according to the liquid content of the nanomaterials.

2.1.1. Nanomaterials

MWCNT-OH used in this study were purchased from US Research Nanomaterials, Inc. Functionalization of MWCNT is done to improve their properties such as better dispersion, interfacial bonding strength, better flexibility as well as better surface activity. Hydroxyl functionalized nanotubes were used in this study to achieve possible reaction with the geopolimer. In addition, a non-ionic surfactant containing aromatic groups without having Alkylphenol Ethoxylates (APEO) is used to disperse MWCNT in water. Ultra-sonication and centrifugation were used to disperse the tubes and to form a stable dispersion of MWCNT in water. Properties of MWCNT-OH are presented in Table 2.

Table 1
Chemical composition of the geopolymeric precursor.

Chemical composition	SiO ₂	Al ₂ O ₃	Fe ₂ O ₃	CaO	MgO	Na ₂ O	K ₂ O	TiO ₂	MnO	SrO	BaO	S ₂	LOI	Total
Wt. %	65.77	10.04	0.58	11.98	6.37	1.89	1.78	0.91	0.01	0.01	0.01	0.48	0.17	99.99

AL-0450 was purchased from the Alfa Aesar. AL-0450 is a colloidal dispersion in 50% H₂O with dispersant, see Table 3 for properties of AL-0450. Fig. 3 shows SEM images of the nanomaterials used in this study.

2.2. Test methods and preparation of test specimens

2.2.1. Characterization and test methods

Temperature and Pressure Conditions – For this study, the temperature was chosen to be 50 °C and 70 °C. The ramp-up rate of 1 °C/min was selected for both cases. Additionally, curing pressure used for pressurized consistency, uniaxial compressive strength, as well as ultrasonic cement analyser was 14 MPa. This was done to mimic the possible downhole temperature and pressure conditions in a well.

Shear Stress Measurement – Fann viscometer was employed to measure the rheological behaviour of the geopolymeric slurries. Atmospheric consistometer was used to do the conditioning of the geopolymer slurry at 50 °C. After reaching 50 °C, the slurry was conditioned for 20 min to achieve uniform temperature.

Consistency – In order to map pumpability and effect of pressure on the pumpability of the slurries, atmospheric consistometer and pressurized consistometer recommended by API RP 10B-2 standard (API, 2013) were employed.

Static Fluid Loss – To measure the fluid loss of the slurries; first the slurries were conditioned in the atmospheric consistometer at 50 °C (BHCT). Then, high temperature and high pressure (HTHP) fluid loss cell was used to measure the drained fluid. The achieved differential pressure was 5.2 MPa. As the slurry was already conditioned at 50 °C, the ambient temperature was used during the measurement, and all the slurries were passed through the 850 µm sieve. The pressure was applied by using carbon dioxide cartridges.

Uniaxial Compressive Strength – To measure the unconfined compressive strength of the samples, a Toni Technik-H mechanical tester was used. A loading rate of 27.6 MPa/min was selected according to the API RP 10B-2 standard (API, 2013). All the samples were cured in an autoclave at 14 MPa and 70 °C. Samples were cured in plastic cylinders having dimensions of 100 mm length and 52 mm diameter. After curing for the required time, samples were removed from the plastic molds and were cut from both ends to achieve flat surfaces before measuring the compressive strength. The specimen is loaded between parallel plates, and the loading is on the surface of the cylindrical geopolymer plug. The testing procedure is according to NS-EN 196-1 standard (Norway, 2005; ASTM, 2013), and the compressive strength is given by:

$$\sigma_c = \frac{F}{\pi R^2} \quad (1)$$

Table 2
Properties of MWCNT-OH

Properties	Values
Purity	>95 wt% (carbon nanotubes) >97 wt% (carbon content)
Content of -OH	1.76 wt%
Outside diameter	20–30 nm
Inside diameter	5–10 nm
Length	10–30 µm
Specific surface area (SSA)	>110 m ² /g
Color	Black
Electrical conductivity	>100 S/cm
Tap density	0.28 g/cm ³
True density	~2.1 g/cm ³

Table 3
Properties of AL-0450.

Properties	Values
Purity	50% in water, colloidal dispersion
Formula	Al ₂ O ₃
Form	45 nm APS for dry powder
Formula Weight	101.96
Surface Area	32–40 m ² /g
Refractive Index	1.768
Color	White

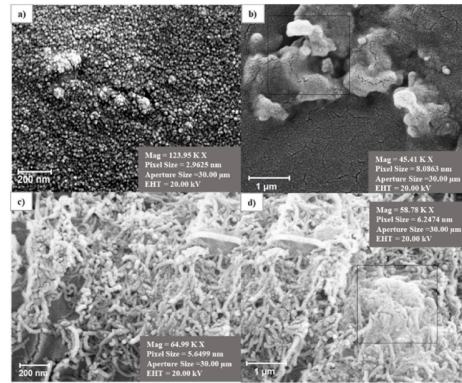


Fig. 3. SEM images of AL-0450 NPs showing the distribution of nanoparticles (a and b), SEM images of MWCNT-OH showing the nanotubes (c and d).

Where F is maximum recorded compressive load (kN) and R is radius of the specimen (mm).

Indirect Tensile Strength Measurement – Brazilian tests were conducted by employing Zwick/Z020 mechanical testing machine. TestXpertII software was used to record the applied force on the sample. The loading rate of 50 N/s, which is equivalent to 0.05 MPa/s was selected according to the ASTM D3967-16 (Standard, n.d.). Unlike steel materials, rock and cement like structures exhibit weak tensile strength. Hence, the indirect test method is used to determine the tensile strength of such materials. The Brazilian tensile tests were conducted according to the procedure described in NS-EN 12390-6:2009 standard (Norway, 2009). The specimen is placed between parallel curved plates, and the applied load is continuously increased until failure. The tensile strength is given as (Norway, 2005; ASTM, 2013):

$$\sigma_t = \frac{2F}{\pi DL} \quad (2)$$

Where F is the maximum load (Newton), D is the diameter (mm), and L is the length of the specimen (mm). The unit of the tensile strength is N/mm².

Sonic Strength Development – Sonic Strength of the geopolymers mixed with the nanoparticles were measured by Chandler Ultrasonic Cement Analyser (UCA). The downhole temperature of 70 °C was used

to map the sonic strength development. UCAs are designed to compute the sonic strength of Portland cement by applying a pre-defined algorithm and using the travel time of ultrasound through the cement slurry. Therefore, to estimate the values for new materials, it is necessary to develop a new algorithm. For this study, a customized algorithm feature was used from UCA to accommodate geopolymer-based slurries. A polynomial equation generated from the plot between transit time and measured compressive strength from UCS was put into the UCA software using a custom algorithm option in the instrument to calculate the sonic compressive strength.

X-ray diffraction (XRD) – Bruker D8 ADVANCE Eco diffractometer (having Cu-K α radiation source, $\lambda = 1.5406 \text{ \AA}$, 40 kV, and 25 mA) was used to study the X-Ray diffraction of the geopolymer and geopolymer with nanomaterials. The X-Ray patterns were recorded in the 2 θ range of 5–70 $^\circ$.

Microstructure and Elemental Analysis – To get an insight into internal structural make-up of the geopolymer, Zeiss Supra 35VP model scanning electron microscope was used. Additionally, to quantify the percentage of different elements present in the structure, the elemental analysis was conducted with element dispersion spectra (EDS).

2.2.2. Slurry preparation

Slurry mix designs are presented in Tables 4 and 5. First, the pulverized granite rock was normalized with other industrial wastes to prepare a unique chemical composition, which gives repeatable results. Separately the hardener was prepared by mixing potassium silicate solutions with deionized water. Then, suitable amounts of either AL-0450 or MWCNT-OH were added to the hardener and mixed with a high shear rate mixer. The normalized geopolymeric precursors were mixed with the nanoparticle blended hardener by using the commercial Waring blender according to the API RP 10B-2 (API, 2013). The slurries were conditioned with the atmospheric consistometer to make sure that the system is homogenous. The sample preparations were conducted according to the API RP 10B-2 (API, 2013). The liquid to solid ratio (L/S) of the samples was 0.55. The specimens for compressive strength and tensile strength measurements were poured in the plastic molds.

3. Results and discussions

3.1. Rheological properties

3.1.1. Shear Stress Measurement

The rheological properties of the neat geopolymer show non-Newtonian (Bingham Plastic) behaviour as indicated by the previous study. The addition of nanomaterials shows similar trends but with the higher shear stress values for the same shear rate. Hence, nanomaterials increase the viscosity of the material, see Fig. 4. As indicated by Hodne et al. (2001) addition of micro-sized silica particles increased the viscosity of the cement slurry. A similar trend is observed in this study; the addition of nanoparticles to the slurry increases the solid content.

A sharp change in the rheological profile of the mix design containing MWCNT-OH was noticed at high shear rate when the temperature increased from 40 to 50 $^\circ\text{C}$. The reason for the behaviour remained unknown. However, shear rates of more than 250 1/s are not commonly experienced in the field, except the Bottom Hole Assembly (Saasen and Ytrehus, 2018). Fig. 5 shows the apparent viscosity of the slurries at different temperatures. It can be seen that nanoparticles have increased the apparent viscosity. Moreover, for all the slurries increase in temperature decreases the apparent viscosities.

The Casson model is a two parameter model, which was used to

Table 4
Composition of the AL-0450 modified geopolymer.

Component	Precursor	Hardener	Water	Nanomaterials (AL-0450)
Weight (g)	735	324.45	81.9	0.36

Table 5
Composition of the MWCNT-OH modified geopolymer.

Component	Precursor	Hardener	Water	Nanomaterials (MWCNT-OH)
Weight (g)	735	324.45	81.9	0.18

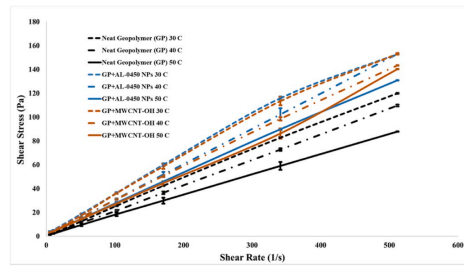


Fig. 4. Effect of temperature and the nanoparticles on the rheological behaviour of geopolymer.

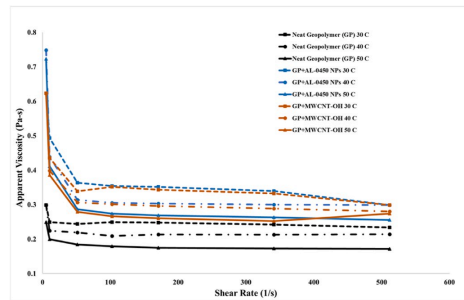


Fig. 5. Apparent viscosity of neat geopolymer and neat geopolymer modified with AL-0450 and MWCNT-OH.

calculate the Casson yield stress and Casson plastic viscosity. The Casson model provided a good fit for the measured shear stress and shear strain values. At both high and low shear rates, the Casson model provides more accurate results (Ochoa, 2006). The model is given (Nelson and Guillot, 2006) as,

$$\tau^{0.5} = \tau_c^{0.5} + \mu_c^{0.5} \gamma^{0.5} \quad \text{For } \tau < \tau_c \quad (3)$$

$$\gamma = 0 \quad \text{For } \tau \geq \tau_c \quad (4)$$

Where,

- τ is the shear stress (Pa)
- τ_c is the Casson yield stress (Pa)
- μ_c is the Casson plastic viscosity (Pa)
- γ is the shear rate (sec^{-1})

Table 6 shows the values for yield stress and plastic viscosity for neat geopolymer and geopolymer mixes having nanomaterials. Yield stress and plastic viscosity of cement-based materials are critical with respect to displacement and the pumpability of the slurry. Higher values of yield stress and plastic viscosity of the geopolymer mix with nanomaterial

Table 6
Casson Yield stresses and Casson plastic viscosities.

Temperature (°C)	Casson Yield Stress-Neat Geopolymer (Pa)	Casson Plastic Viscosity-Neat Geopolymer (Pa)	Casson Yield Stress-GP + AL-0450 (Pa)	Plastic Viscosity-GP + AL-0450 (Pa)	Casson Yield Stress- GP + MWCNT-OH (Pa)	Plastic Viscosity-GP + MWCNT-OH (Pa)
30	0.015	0.23	0.36	0.29	0.25	0.29
40	0.009	0.21	0.22	0.27	0.21	0.26
50	0.014	0.17	0.34	0.23	0.15	0.24

thickens the system and control the segregation of materials by providing better cohesion. This increase in viscosity does not have effect on the pumpability of the slurry, as indicated by the setting time results, but it can have an impact on pump pressures and friction in the well, causing larger downhole pressures when circulating.

3.2. Fluid-loss test

Fluid-loss values for cement slurries are generally high when additives are not used, which can contribute to problems such as gas migration as well as maintaining the hydrostatic pressure and incomplete hydration of cement. Geopolymerization does not involve hydration reaction and requires less amount of water, but hardener loss may result in loss of hydrostatic pressure or incomplete reaction. Our measurements confirmed that lower values of fluid loss are associated with the geopolymer. As shown in Fig. 6, very low values of fluid loss were recorded after 30 min. The mix containing AL-0450 nanoparticles showed a significant increase in fluid loss values. The possible reason might be a delay in the hardening of slurry with AL-0450, as indicated in Fig. 7. However, in the case of MWCNT-OH, there is a significant decrease in fluid loss values. Perhaps, attachment of MWCNT particles to the oligomers is a possible scenario.

3.3. Pumpability

For oilfield applications, geopolymeric slurry should set at the desired time. Therefore, it is crucial to have control over the setting time of the slurry. Retarders (such as lignosulfonates, and derivatives of carbohydrate) are commonly used to delay the setting time of Portland cement used in oil fields. However, these are not effective in case of the geopolymers. Borax based retarders are suggested for the geopolymer; however, a significant decrease in mechanical strength has been reported (Allouche et al., 2017). Therefore, nanomaterials might be used to prolong the pumpability of the geopolymer slurries by acting as a retarder. Fig. 7 shows that the addition of nanomaterials almost doubles the available pumping time of the geopolymers. Different mechanisms could be involved here, which causes the delay in the setting of

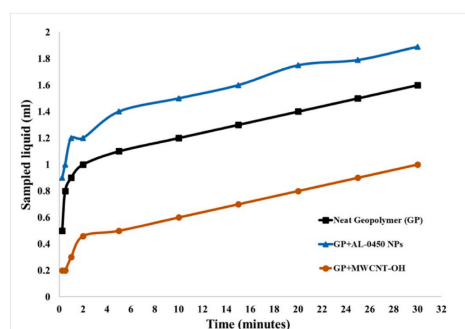


Fig. 6. Effect of AL-0450 nanoparticles and MWCNT-OH on static fluid loss of the geopolymeric slurries.

nanomaterials-based geopolymer slurries. A possible scenario could be that the nanomaterials might act as a shield between the aluminosilicate precursor and hardener and reduce the rate of dissolution of alumina-silicates (Allouche et al., 2017).

Delaying the gelation step can significantly prolong the setting of the geopolymer slurry. As with the addition of nanoparticles, there are more charged particles in the system, the electrostatic repulsion between the similar charges in the system may be promoted. Also, surfactants that are used to disperse the nanoparticles might act as retarders and delay the setting time of the geopolymer slurries. The addition of the nanomaterials prolonged the pumping time to 3 hrs, see Fig. 7.

Our study shows that pressure does not have a significant effect on pumping time, see Fig. 7, which is aligned with previous results obtained by Khalifeh et al. (2019a) on the neat geopolymers.

3.4. Mechanical properties

3.4.1. Uniaxial compressive strength (UCS)

The unconfined compressive strength tests were performed after the specimens being aged at 12hr, 24hr, 3, 7, and 28 days. For each curing time, three specimens were crushed, and the average strength values are reported as a representative for the unconfined compressive strength. Even though the geopolymer specimens were cured in autoclaves, the mechanical destructive tests were conducted at ambient conditions. Fig. 9 shows a continuous increase in the strength development of geopolymers with the incorporation of MWCNT-OH and AL-0450 NPs. This shows that nanoparticles are integrated into the material structure. As indicated in Fig. 9, there is not a very significant difference between the compressive strength between 7 days and 28 days. This indicates that samples attained most of the strength in the first 7 days. However, there is a continuous increase in strength with time. Introducing nanomaterials to the geopolymeric slurry might provide additional nucleation sites for the aluminosilicate reaction, forming a more homogeneous and denser geopolymer paste. Narrow pore distribution and elimination of weaker zones within the geopolymer matrices could lead to an increase in compressive strength. Hydroxyl groups on the surface of the MWCNT may either react with the geopolymer structure and releasing a hydroxyl group or make a hydrogen bond, as illustrated in Fig. 8. This incorporates the MWCNT throughout the structure of the geopolymer, as indicated by the microstructure analysis. It can ultimately produce nanotubes reinforced geopolymer having higher mechanical properties such as compressive strength. Li et al. (2013) have shown that the incorporation of Carboxymethyl chitosan improves the mechanical properties of the fly ash-based geopolymer due to the created hydrogen bond between the hydroxyl groups in N-Carboxymethyl chitosan and the geopolymer.

In case of AL-0450 NPs, the smaller size of these particles may also act as a filler and fill the pores in the structure of the geopolymer, consequently yielding a more compact structure.

3.4.2. Stress and strain curves

Fig. 10 shows the measured stress-strain. As shown, the nanoparticle treated system exhibited a longer deformation as well as a higher load carrying capacity depending on the curing time. All the geopolymer samples showed creeping behaviour, which means more ductility. However, it is important to mention here that this behaviour is dependent on the curing time, as indicated in Fig. 10, after 28 days

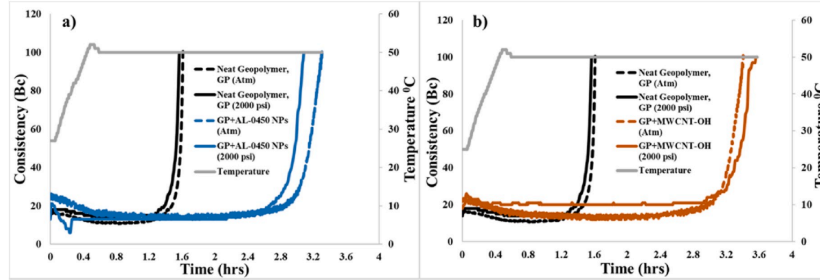


Fig. 7. a) Effect of AL-0450 nanoparticles on setting time of the geopolymer slurry b) Effect of MWCNT-OH on setting time of the geopolymer slurry.

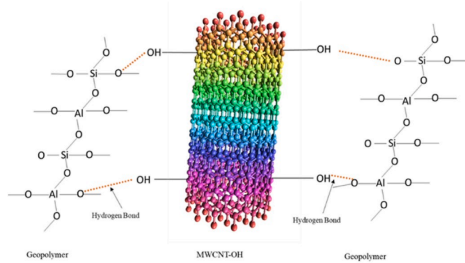


Fig. 8. Hydrogen bond formation between MWCNT-OH and geopolymer.

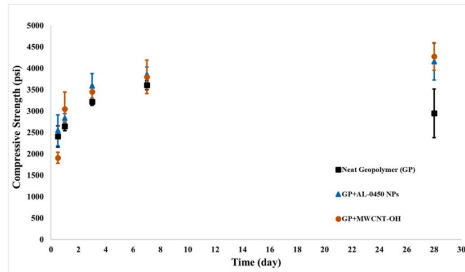


Fig. 9. Trend for unconfined compressive strength build up from 12 h to 28 days for neat geopolymer, and modified geopolymers with nanomaterials AL-0450 and MWCNT-OH.

nanomaterials-based system because less ductile with the time.

3.4.3. Modulus of elasticity

Tensile strength requirements for the oil well cement are dependent on Young's modulus (E) of cement and formation rock (Thiercelin et al., 1998; Williams et al., 2011). Downhole stresses caused by temperature or pressure changes, throughout the well life-cycle, can result in the failure of cement sheath integrity (De Andrade and Sangesland, 2016). Thiercelin et al. (1998) stated that higher compressive and tensile strengths are not always the solution, and the flexibility of cement is required in several cases to minimize the damage. Due to limitations to use tri-axial cell, the piston displacement measurements, from uniaxial

compressive strength measurement, were used to study the elasticity. Although the estimated values are lower than real elasticity, the relative elasticities still remain comparable. As shown in Fig. 11, the introduction of nanomaterials to geopolymers did not significantly increase Young's modulus of the geopolymers. After 28 days, there is a minor increase in Young's modulus values, which is because of an increase in the unconfined compressive strength of the nanomaterials based geopolymers. In fact, higher compressive strength and tensile strength with low Young's modulus are beneficial for oil well cementing applications. The flexibility of the MWCNT-OH based geopolymer is expected to be due to a flexible nanotube structure. Also, functionalization with the -OH groups incorporate more flexibility in the structure of the geopolymer. In case of AL-0450, there is a sharp increase in the Young modulus values in the first 3 days. This is due to the higher unconfined compressive strength achieved by this sample in the first 3 days. As shown in Fig. 9, AL-0450 based system attained most of his strength in 3 days, and afterward, there is a slow increase in the strength.

3.4.4. Compressive strength to young modulus ratios

Increase in the ratio of unconfined compressive strength to Young's modulus values for the nanomaterials based geopolymer indicates that nanomaterials-based system has higher compressive strength with lower values for Young's modulus. A decrease in the value after 28 days is due to an increase in both compressive strength and Young's modulus. However, for nanomaterials-based system, the ratio is slightly better than the neat geopolymer, see Fig. 12.

3.4.5. Tensile strength (TS)

As geopolymers are known to possess lower values of tensile strength, it is vital to improve their tensile strength for well cementing applications. Nanomaterials used in this work have improved the tensile strength of the neat geopolymer until 7 days. AL-0450 and MWCNT-OH have significantly improved the tensile strength for 7 days; the latter has even more effect on the tensile strength (see Fig. 13). The MWCNT-OH additive improved the tensile strength of the geopolymer by 123% while the AL-0450 additive leads to a 68% improvement for 7 days. Higher tensile strength of the modified geopolymers with nanomaterials make them more stable against tensile failures. However, for longer curing time, the increase in the tensile strength is not very significant compared to the neat geopolymer. After 28 days, mixtures with nano-additives showed a decrease in tensile strength values compared to 7 days. However, in the case of MWCNT-OH, tensile strength values are still better compared to neat geopolymer after 28 days, see Fig. 13. It is important to mention here, that new batch of materials was used for 28 days tensile strength, therefore this could be the reason of lower values compared to 7 days test.

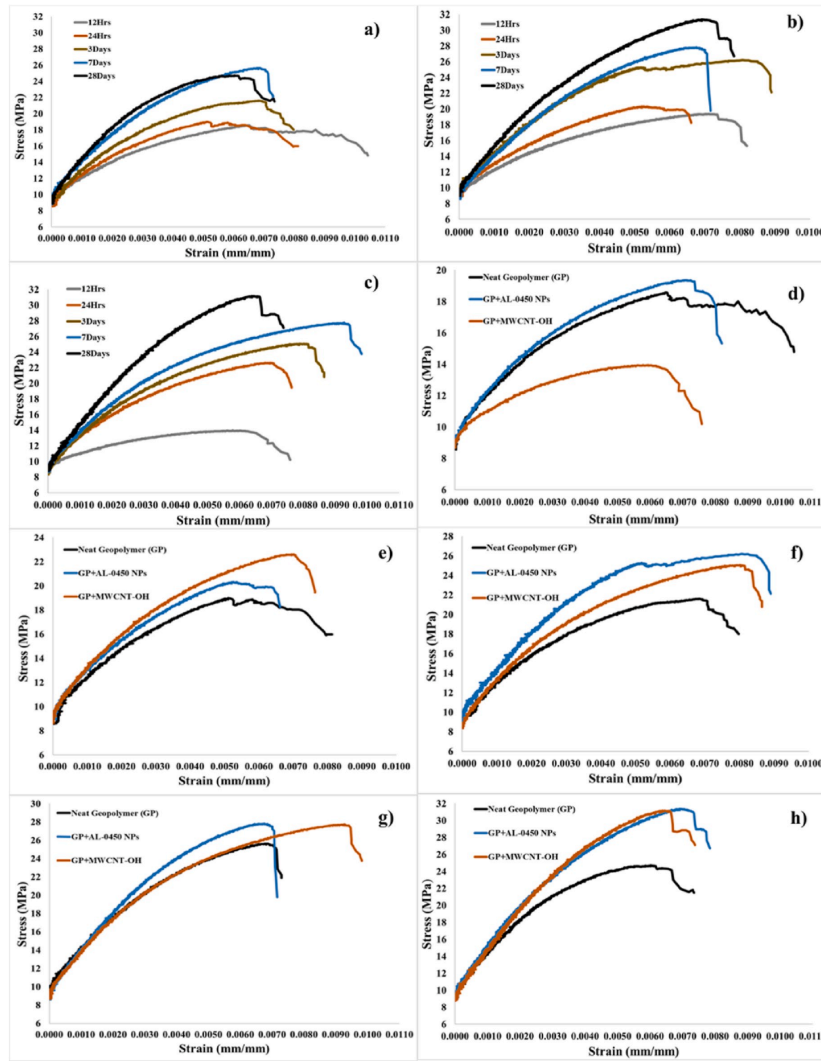


Fig. 10. Strain vs Stress curves of samples cured at different days; 70 °C and 14.7 MPa a) Neat geopolymer b) Neat geopolymer and nano AL-0450 modified c) Neat geopolymer and nano MWCNT-OH modified d) Comparison of Neat geopolymer with AL-0450 and MWCNT-OH modified geopolymer after 12 hrs e) Comparison of Neat geopolymer with AL-0450 and MWCNT-OH modified geopolymer after 24 hrs f) Comparison of Neat geopolymer with AL-0450 and MWCNT-OH modified geopolymer after 3 days g) Comparison of Neat geopolymer with AL-0450 and MWCNT-OH modified geopolymer after 7 days h) Comparison of Neat geopolymer with AL-0450 and MWCNT-OH modified geopolymer after 28 days.

3.4.6. Tensile strength to Young's modulus ratios

There is a significant increase in the ratio of tensile strength to Young's modulus for the rock-based geopolymer modified with the nanomaterials for 7 days (see Fig. 14). This substantial increase, especially in case of MWCNT-OH, could be attributed to the high tensile

strength of the nanomaterials formulated geopolymer slurry. At the same time, Young's modulus is relatively low. In order to minimize the mechanical damage to the cement sheath, it is beneficial to have a high strength to Young's modulus ratio (Roy-Delage et al., 2000). However, after 28 days, the increase is not very significant compared to the neat

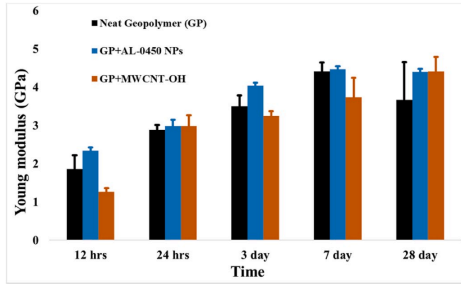


Fig. 11. Estimated Young's modulus values for neat geopolymer, nano AL-0450 and MWCNT-OH modified geopolymers.

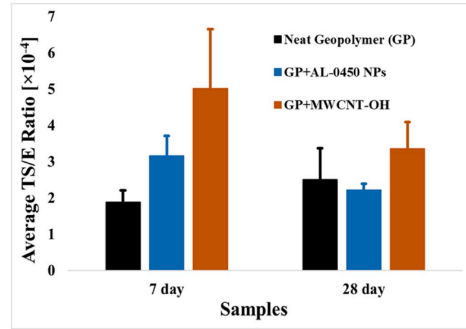


Fig. 14. Ratio of average tensile strength to Young's modulus of the samples.

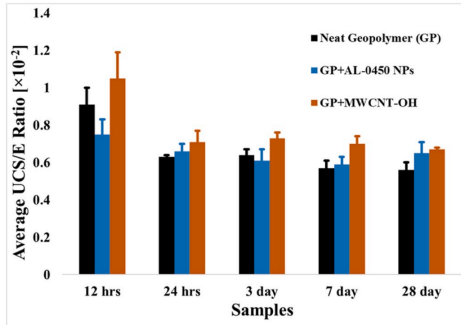


Fig. 12. Ratio of unconfined compressive strength to Young's modulus at different curing time.

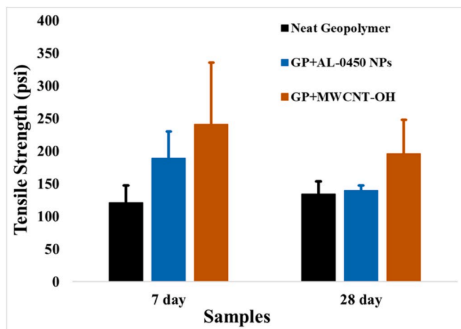


Fig. 13. Indirect tensile strength of the samples cured at 70 °C and 14.7 MPa.

geopolymer. In case of AL-0450, there is a slight decrease in ratio compared to the neat geopolymer, while for MWCNT-OH, the ratio still showed improvement.

3.5. Sonic strength

Table 7 shows the empirical correlation developed in this study to be used for estimating the sonic strength development of the geopolymers and geopolymers modified with nanomaterials. The sonic strength measurements show that the maximum strength development occurs on the first day. A comparison of the UCA and consistency results show that the geopolymers set a little faster in static conditions compared to the dynamic situation (compare Figs. 7 and 15). It could be due to a delay in gelation caused by a continuous mixing of the slurry. High values of transit time at the start are due to the ramp-up of the temperature to 70 °C, which reduces the viscosity of the slurry as also shown in Figs. 4 and 5 that high temperature decreases the viscosity of the slurries (Panchmatia et al., 2019). Moreover, additives used could also affect the ultrasonic wave transmission, which can influence the transit time (Liu, 2017).

3.6. X-ray diffraction

X-ray analysis of the neat geopolymer and geopolymer with nanomaterials is shown in Fig. 16. XRD pattern of neat geopolymer showed that quartz (SiO₂), albite Na(AlSi₃O₈), microcline (K(AlSi₃O₈)), illite (K_{0.65}Al_{2.0}[Al_{0.65}Si_{3.35}O₁₀](OH)₂) and clinoptilolite-Na ((Na,K,Ca)₂₋₃Al₃(Al,Si)₂Si₁₃O₃₆·12H₂O) are the main phases present in the geopolymer structure. Minor peaks for oligoclase ((Ca,Na)(Al,Si)₄O₈) are also present.

Similar phases are also present in the nanomaterials based geopolymer structures. Fig. 17a-d shows that additional peaks are present for geopolymer with AL-0450. For instance, peak at 8.75° is due to the formation of phyllosilicates minerals from mica group like phlogopite (KMg₃(AlSi₂)O₁₀(OH)₂). Small peaks at 9.9, 11.1°, and 13-14° are due to the formation of zeolite-based mineral (e.g. clinoptilolite-Na and albite). Moreover, smaller additional peaks at 19-20° for geopolymer having AL-0450 additive are due to the formation of illite. Peaks present at 21-25° are due to the formation of albite, microcline, oligoclase, and illite. The broad peak at 26° is due to quartz, there is a minor shift in the peak for geopolymer with AL-0450 due to the formation of microcline and albite, and an additional peak at 26.7° is for microcline.

Table 7

Empirical Correlations obtained from the plot between uniaxial compressive strength and Transit time.

Samples	Empirical Correlation
GP + AL-0450	$y = 27.658x^2 - 1775.7x + 27797$
GP + MWCNT-OH	$y = 66.938x^2 - 3583.8x + 47808$

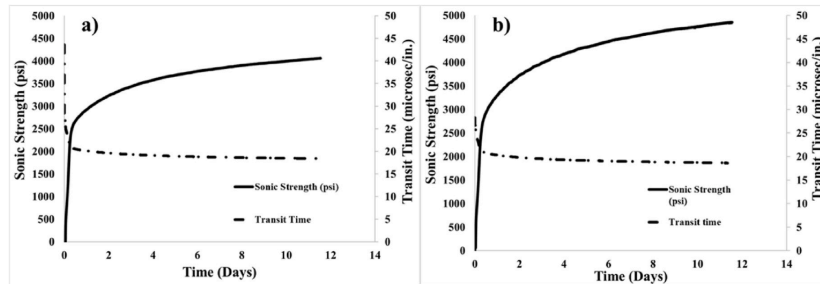


Fig. 15. a) Sonic Strength development of geopolymers modified with nano AL-0450 b) Geopolymers modified with nano MWCNT-OH.

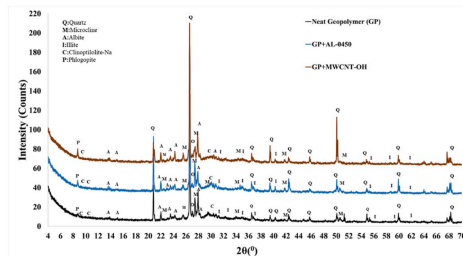


Fig. 16. XRD pattern for the neat geopolymer and geopolymer with AL-0450 NPs and MWCNT-OH.

Similar to neat geopolymer, peaks at 27–33° are due to albite, illite, and microcline phases with few additional peaks for the same phases for geopolymer with AL-0450. New peaks at 34.64° are formed due to the formation of almandine ($\text{Fe}_3\text{Al}_2(\text{SiO}_4)_3$). Also, there are minor peaks for alumino-magnesiotsaramite ($\text{Na}(\text{CaNa})(\text{Mg}_3\text{Al}_2)(\text{Si}_6\text{Al}_2)\text{O}_{22}(\text{OH})_2$) at 34–35°. A peak at 41.8° is for diaspore ($\text{AlO}(\text{OH})$) for a geopolymer with AL-0450.

There are also additional peaks for berlinite (AlPO_4) at 20.9–26.6° and 34–68°, specifically at 64.1–67.9°. The sharp peak at 60.08° is due to the formation of mullite ($3\text{Al}_2\text{O}_3 \cdot 2\text{SiO}_2$). Moreover, additional albite, illite, and microcline are also present throughout 30–70° for geopolymer with AL-0450 additive.

The additional sharp peak at 8.75° is also present for MWCNT-OH due to the formation of phyllosilicates minerals. In case of MWCNT-OH geopolymer, the broad peak around 13.6° is associated with graphite, while other peaks are due to additional aluminosilicate minerals like albite. In addition, the carbon peak is formed at 20.96° for MWCNT-OH. There is a peak shift for MWCNT-OH at 26° is due to the graphite peak at 25.60° is overlapping with a quartz peak. There is also a broad peak at around 27.44° because of graphite for MWCNT-OH. Additional peaks for MWCNT-OH at 28.2° is due to microcline. A peak at 39.5° is due to the formation of albite and illite. Minor peaks at 42.3, 42.5, and 44.6° are due to graphite. In addition, minor peaks at 54–55° are also due to graphite. X-ray analysis indicates that additional phases are formed in case of geopolymer slurries with nano-additives. It shows that nanoparticles took part in the reaction. The stability of nano-materials dispersion might be the reason for the effective reaction between nano-additive and other raw materials used to formulate geopolymer slurries. Moreover, in case of MWCNT-OH, the hydroxyl groups might be a possible reason for taking part in the reaction, see

Fig. 8.

3.7. Microstructure analysis

Microstructure analysis shows that nanomaterials have reacted with the geopolymer components and contributed in the geopolymerization. As shown in Fig. 19 a-d, the AL-0450 nanoparticles based geopolymer has form dense microstructure as compared to the neat geopolymer, see Fig. 18 a-d. Nanomaterials are able to form a structure that is more compact and improved interlocking morphology, as shown in Fig. 19 d). AL-0450 nanoparticles produced highly ordered geopolymer structure, as revealed in Fig. 19, due to the low ratio of Si/Al. Yong et al. (2007) have observed similar behaviour where a decrease in Si/Al ratio contributed to higher chemical interactions and a more ordered structure. Studies have indicated that nanomaterials fill the gaps in the structure of a geopolymer, which constructed a more homogenous and compact structure (Huang and Han, 2011; Lo et al., 2017). In addition, this structure produced materials with higher strength, as confirmed by the compressive strength results.

Similarly, for MWCNT-OH based geopolymer, the nanotubes have reacted with the geopolymer and produced a structure that is more compact without any pores and empty spaces in the structure. As mentioned previously in the introduction that MWCNT bonded the surfaces of the geopolymer and uniformly distributed in the geopolymer structure as indicated in Fig. 20 b. Moreover, nanotubes bridged the microcracks in the structure of the geopolymer. Since the samples used for the SEM analysis are from the compressive strength test, therefore there are cracks in the structures as indicated by the SEM images.

3.7.1. EDX analysis

Fig. 21 shows the elemental analysis for the neat geopolymer, and it can be seen that a lower amount of aluminium is present in the neat geopolymer. Additionally, carbon is not present in the geopolymer without MWCNT-OH.

EDX analysis for the geopolymer with nanomaterials showed that both AL-0450 and MWCNT-OH contributed to the geopolymerization reactions. As shown in Figs. 22 and 23, both AL-0450 and MWCNT-OH are uniformly distributed throughout the structure of the geopolymer. Stable dispersions of nanoparticles in dispersants may be contributed to this phenomenon. The uniform distribution of nanomaterials is critical to improve the properties of the geopolymer. Mapping of the geopolymer structure with AL-0450 and MWCNT-OH also indicates that addition nanoparticles increase the percentage of aluminium and carbon respectively in the geopolymer structure.

Testing results performed in this work indicates the potential of nano-additives in altering properties of geopolymer mixtures. Rheology results showed that nanomaterials could increase the viscosity of the slurries, however for both neat geopolymer slurries and slurries with

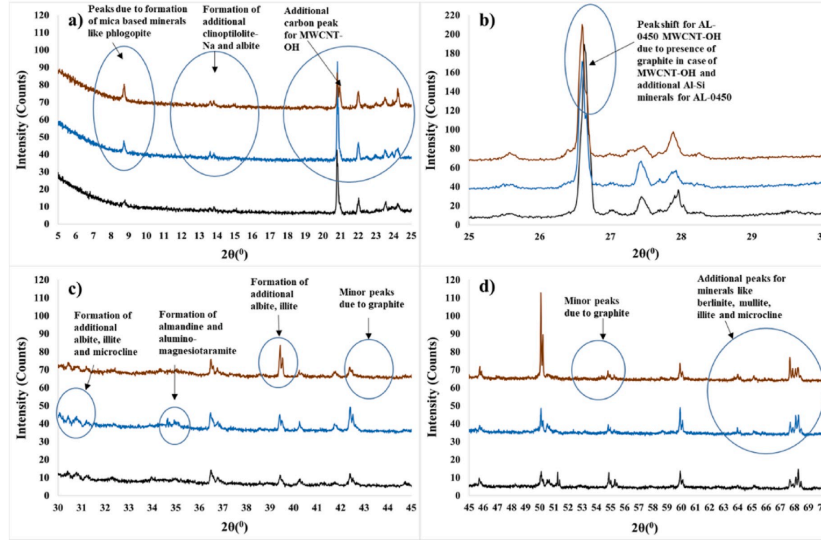


Fig. 17. (a-d) XRD pattern for the neat geopolymer and geopolymer with AL-0450 NPs and MWCNT-OH indicating additional peaks and peak shifts for geopolymer with nanomaterials.

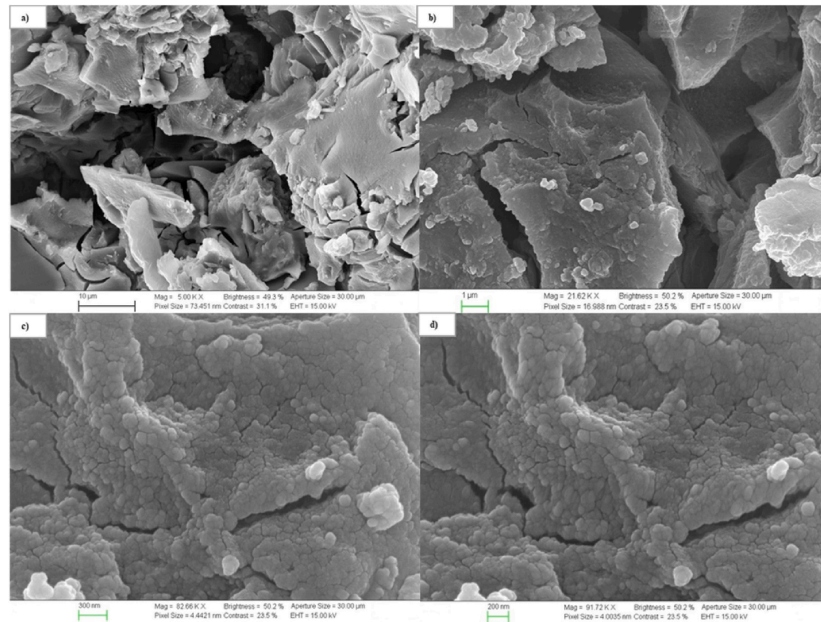


Fig. 18. SEM images of the neat geopolymer.

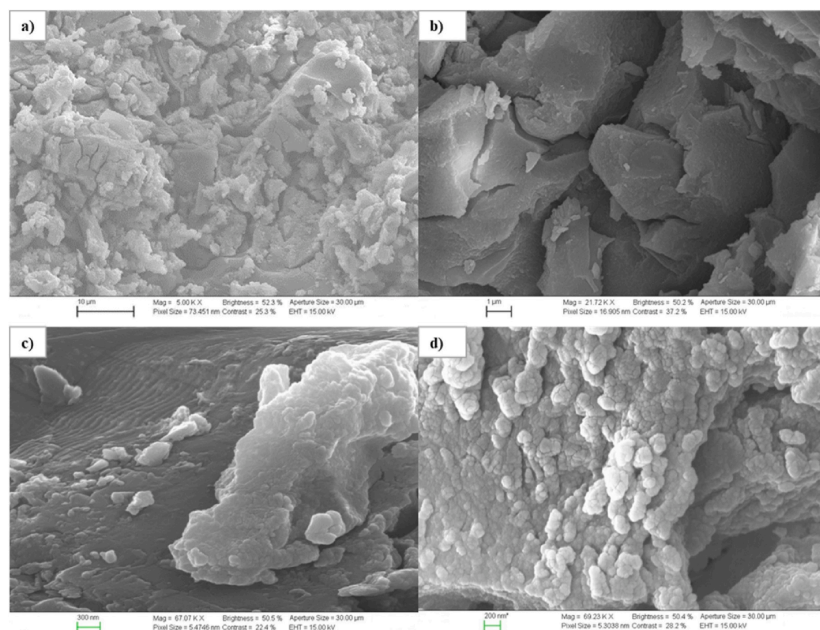


Fig. 19. SEM images of geopolymer with AL-0450 NPs a) overview of the structure b) Internal structure showing AL-0450 NPs and geopolymer c) AL-0450 NPs presence in the structure of geopolymer d) Compact structure of geopolymer with AL-0450 NPs.

nano-additives, viscosity decreased with temperature. Moreover, nano-additives also increase the plastic viscosity, apparent viscosity, and yield point of the geopolymer. However, as indicated in Fig. 7 an increase in viscosity does not have effect on pumpability. Also, the fluid loss result in Fig. 6 showed that geopolymer having AL-0450 nanoparticles have more fluid loss, which might be due to delay in the setting of the slurry. While in the case of MWCNT-OH, delay in setting did not affect the fluid loss and, in fact, improved the fluid loss compared to neat geopolymer. It could be explained from Fig. 8, which suggests the attachment of MWCNT-OH with the oligomers. The attachment of tube structures with the geopolymer structure controls the loss of fluid.

Fig. 7 showed the ability of nano additives to delay the setting of geopolymers, additionally setting time of slurries is not affected by pressure, and as slurries with nano-additives took almost the same time to set under atmospheric and high pressure. Unconfined compressive strength results showed that nano-additives could improve the compressive strength of neat geopolymer. The geopolymer achieves most of the strength in the first 3 days, see Figs. 9 and 15. After 3 days, there is a steady increase in the compressive strength values, and there is not a very significant difference between 7 and 28 days. Therefore, no test was performed for 14 days. However, it would be interesting to check in the future how the materials behave after 14 days. Stress-strain curves in Fig. 10 indicates that until 7 days nanomaterials-based slurries showed longer deformation and higher load carrying capacities. While, as curing time increases, mixtures with nanomaterials become less ductile, which indicates that materials could become more brittle with the time. Fig. 11 also confirms this phenomenon where Young's modulus of the geopolymer mixture with nanomaterials is higher than neat geopolymer, which suggests that mixtures with nanomaterials become less ductile after 28 days. This could be disadvantage for long-term

wellbore integrity. However, Fig. 12 indicates that the ratio of UCS and Young's modulus for the mixtures with nanomaterials after 28 days is slightly better than the neat geopolymer. Moreover, Fig. 10 h also showed that mixtures with nanomaterials still showed higher load carrying capacity and reasonable deformation compared to the neat geopolymer. Future study with curing samples for 6 months can provide the answer if nanomaterials-based mixture becomes more brittle or not.

Tensile strength results indicate that nanomaterials have improved the tensile strength of neat geopolymer for 7 days. However, after 28 days, mixtures with nanomaterials showed lower tensile strength values compared to 7 days. It indicates that for longer period nanomaterials based geopolymers lost their tensile strength. However, further studies are needed to find the reason for these phenomena and to confirm that nanomaterials might not improve the strength of neat geopolymer for longer periods.

Sections 3.5 to 3.7 are the test performed to compliment the tests in the previous section. Sonic strength result showed that reduction in viscosity causes the transit time to increases, which supports the reduction in viscosity with temperature, as indicated in Fig. 15. Also, this test supports that mixtures attained most of their strength during the early stages of curing. X-ray analysis, SEM, and EDX analysis confirms the involvement of nanomaterials during geopolymerization.

New minerals formation, as indicated by X-ray analysis, confirms the presence of nanomaterials in the mixture. SEM analysis shows the compact structure formation for the geopolymer mixtures with nanomaterials. Which, also indicates that nanomaterials are well mixed with precursor and other raw materials used to formulate geopolymer. EDX results conformed the uniform distribution of the elements present in the nanomaterials, which again confirms the proper reaction between nano additives dispersions and other additives used to formulate geopolymer

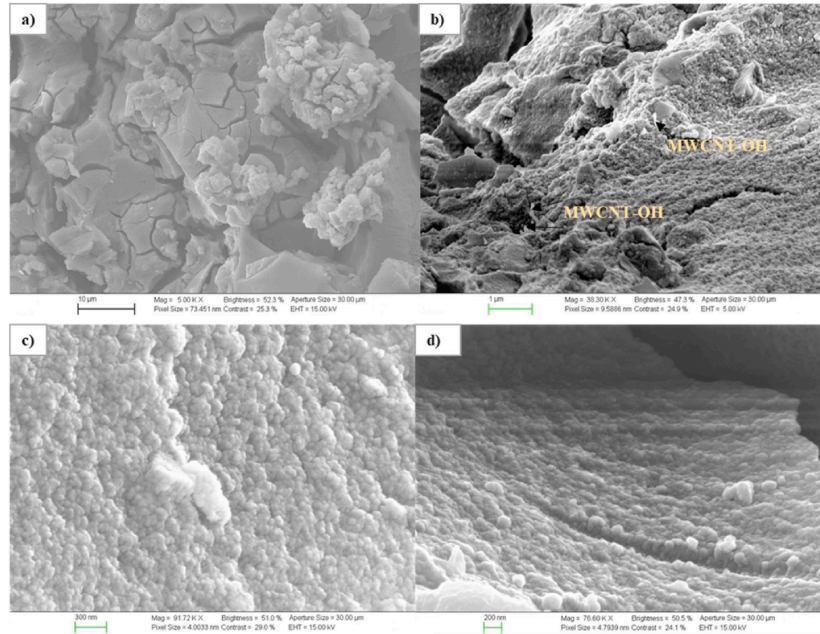


Fig. 20. SEM images of Geopolymer with MWCNT-OH a) overview of the structure b) Internal structure showing MWCNT-OH and geopolymer c) MWCNT-OH presence in the structure of geopolymer d) Compact structure of geopolymer with MWCNT-OH.

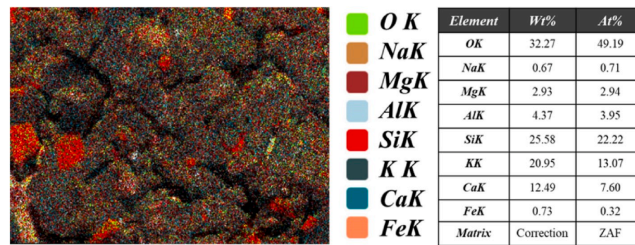


Fig. 21. Element analysis of geopolymer.

as well as stability of nano-additive dispersions.

4. Conclusion

This work indicates that nanomaterials have the ability to contribute in geopolymer structure, showing improved mechanical properties and modified structure.

- Findings from this work have shown that nanomaterials have significantly enhanced the pumping time of the neat geopolymer slurry. Results showed that nano-additives increase the thickening time to 3 hrs at 50 °C and 14.7 MPa.
- Nanomaterials have increased the viscosity of the geopolymer slurry.

- MWCNT-OH decreased the fluid loss of the geopolymer. However, AL-0450 increases fluid loss compared to neat geopolymer.
- AL-0450 and MWCNT-OH both increased the compressive strength of the neat geopolymer from to 2945 psi to 4154 psi and 4274 psi respectively after 28 days.
- Stress strain curves showed better load carrying capacity and deformation for AL-0450 and MWCNT-OH based mixtures. However, after 28 days, mixtures become less ductile.
- Nanomaterials based mixtures did not show a significant increase in Young's modulus values compared to the neat geopolymer. AL-0450 showed more increase in Young's modulus after 3 days, due to high compressive strength.

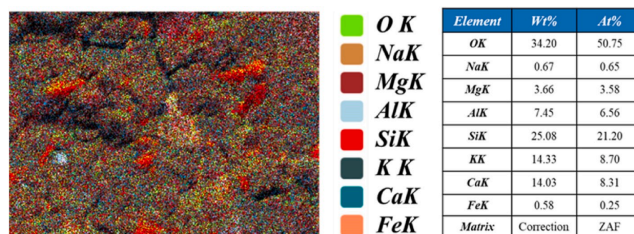


Fig. 22. Element analysis of geopolymer with AL-0450 NPs.

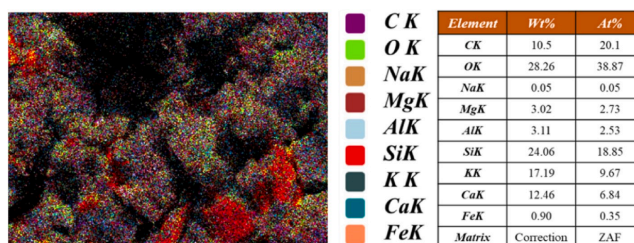


Fig. 23. Element analysis of geopolymer with MWCNT-OH particles.

- AL-0450 and MWCNT-OH based mixtures slightly increase the ratio of UCS and E after 28 days.
- In case of tensile strength, both AL-0450 and MWCNT-OH based mixtures showed improvement after 7 days. However, after 28 days, the increase is not very significant in case of AL-0450, while MWCNT-OH based mixture still showed improvement compared to neat geopolymer.
- Incorporation of nanomaterials produced a more flexible geopolymer structure until 7 days, with a significant increase in the tensile strength to Young's modulus ratio compared to neat geopolymer. However, after 28 days, tensile strength to Young's modulus for AL-0450 slightly decreases compared to neat geopolymer, while for MWCNT-OH ratio is improved compared to neat geopolymer, but decreases compared to 7 days.
- UCA results confirm the maximum strength development occurs at the early stages of curing.
- The XRD analysis showed the formation of new minerals that was an indication of the chemical reaction of nanoparticles with geopolymers.
- Dense and compact microstructure formation with the nanomaterials is being confirmed from the SEM analysis. Moreover, elemental analysis indicates the uniform distribution of nanomaterials in the geopolymer structure.
- This study indicates that nanomaterials can produce geopolymer material with improved mechanical strength and flexibility for a curing period of 7 days, however, for longer curing periods, nanomaterials might lose these properties as observed in this work. Therefore, future work should investigate the ability of nanomaterials to provide long term integrity.

Declaration of competing interest

The authors declare that they have no known competing financial interests or personal relationships that could have appeared to influence

the work reported in this paper.

CRedit authorship contribution statement

Muhammad Awais Ashfaq Alvi: Conceptualization, Methodology, Investigation, Data curation, Writing - original draft, Writing - review & editing. **Mahmoud Khalifeh:** Conceptualization, Methodology, Writing - review & editing, Investigation, Resources, Supervision. **Mesfin Belayneh Agonafir:** Conceptualization, Supervision, Project administration, Funding acquisition.

Acknowledgment

Authors would like to thank Master student Saeed Abdolahpour for helping in part of laboratory work. Moreover, authors would like to thank Kjell Kåre Fjelde for contributing during writing the paper. Also, author would like to thank Mohammadreza Kamali for helping with tensile strength tests and Mona Minde for helping during SEM analysis. The first author would like to thank the Faculty of Science and Technology, University of Stavanger, for funding this project.

Appendix A. Supplementary data

Supplementary data to this article can be found online at <https://doi.org/10.1016/j.petrol.2020.107128>.

References

Abbasi, S.M., Ahmadi, H., Khalaj, G., Ghasemi, B., 2016. Microstructure and mechanical properties of a metakaolinite-based geopolymer nanocomposite reinforced with carbon nanotubes. *Ceram. Int.* <https://doi.org/10.1016/j.ceramint.2016.06.080>.
 Allouche, E., Lvov, Y., Montes, C., Joshi, A., 2017. Geopolymer with Nanoparticle Retardant and Method.
 API, R.P., 2013. 10B-2: recommended practice for testing well cements. *API Recomm. Pract. B* 10.

Appendix - Paper III

M.A.A. Abvi et al.

Journal of Petroleum Science and Engineering 191 (2020) 107128

- Assaedi, H., Shaikh, F.U.A., Low, I.M., 2016. Effect of nano-clay on mechanical and thermal properties of geopolymers. *J. Asian Ceram. Soc.* <https://doi.org/10.1016/j.jascer.2015.10.004>.
- Assaedi, H., Shaikh, F.U.A., Low, I.M., 2015. Utilization of nanoclay to reinforce flex fabric-geopolymer composites. *Int. J. Chem. Mol. Nucl. Mater. Metall. Eng.* *ASTM*, C., 2013. Standard test method for compressive strength of hydraulic cement mortars (using 2-in. or [50-mm] cube specimens). *Annu. B. ASTM Stand. B. ASTM Stand.* 4, 1-9.
- Belayneh, M., Aadnoy, B.S., 2015. Effect of nano and micro sized particle additives on the mechanical strength of cement plug. In: *Proceedings of the International Conference on Offshore Mechanics and Arctic Engineering - OMAE*. <https://doi.org/10.1115/OMAE201541756>.
- Carragher, P.J., Fuls, J., 2018. Well abandonment solutions utilizing bismuth and thermite. In: *Proceedings of the Annual Offshore Technology Conference*.
- Chindaprasirt, P., De Silva, P., Sagoe-Crentsil, K., Hanjitsuwan, S., 2012. Effect of SiO₂ and Al₂O₃ on the setting and hardening of high calcium fly ash-based geopolymer systems. *J. Mater. Sci.* <https://doi.org/10.1007/s10853-012-6353-y>.
- Davidovits, J., 2005. Geopolymer, Green Chemistry and Sustainable Development Solutions Chimie Verte et Solutions, Geopolymer chemistry and sustainable Development. The Poly(silicate) terminology: a very useful and simple model for the promotion and understanding of green-chemistry.
- Davidovits, J., 1991. Geopolymers - inorganic polymeric new materials. *J. Therm. Anal.* <https://doi.org/10.1007/BF01912193>.
- Davidovits, J., 1982. Mineral Polymer and Methods of Making Them. United States Pat. U.S. Patent No. 4,349,386. <https://patents.google.com/patent/US4349386A/en>.
- De Andrade, J., Sangesland, S., 2016. Cement sheath failure mechanisms: numerical estimates to design for long-term well integrity. *J. Pet. Sci. Eng.* <https://doi.org/10.1016/j.petrol.2016.08.032>.
- de Paula, J.N., Calixto, J.M., Ladeira, L.O., Ludvig, P., Souza, T.C.C., Rocha, J.M., de Melo, A.A.V., 2014. Mechanical and rheological behavior of oil-well cement slurries produced with clinker containing carbon nanotubes. *J. Pet. Sci. Eng.* <https://doi.org/10.1016/j.petrol.2014.07.020>.
- Deb, P.S., Sarker, P.K., Barbhuiya, S., 2016. Sorptivity and acid resistance of ambient-cured geopolymer mortars containing nano-silica. *Cem. Concr. Compos.* <https://doi.org/10.1016/j.cemconcomp.2016.06.017>.
- Duxson, P., Fernández-Jiménez, A., Provis, J.L., Lukey, G.C., Palomo, A., Van Deventer, J.S.J., 2007. Geopolymer technology: the current state of the art. *J. Mater. Sci.* <https://doi.org/10.1007/s10853-006-0637-z>.
- Ershadi, V., Ebadi, T., Rabani, A., Ershadi, L., Soltanian, H., 2013. The effect of nanosilica on cement matrix permeability in oil well to decrease the pollution of receptive environment. *Int. J. Environ. Sci. Dev.* <https://doi.org/10.7763/ijesd.2011.v2.109>.
- Gao, K., Lin, K.-L., Wang, D., Shiu, H.-S., Hwang, C.-L., Cheng, T.-W., 2013. Effects of nano-SiO₂ on setting time and compressive strength of alkali-activated metakaolin-based geopolymer. *Open Civ. Eng. J.* <https://doi.org/10.2174/1874149501307010084>.
- Gao, K., Lin, K.L., Wang, D., Hwang, C.L., Shiu, H.S., Chang, Y.M., Cheng, T.W., 2014. Effects SiO₂/Na₂O molar ratio on mechanical properties and the microstructure of nano-SiO₂ metakaolin-based geopolymers. *Constr. Build. Mater.* <https://doi.org/10.1016/j.conbuildmat.2013.12.063>.
- Guo, X., Hu, W., Shi, H., 2014. Microstructure and self-solidification/stabilization (S/S) of heavy metals of nano-modified CFA-MSWFA composite geopolymers. *Constr. Build. Mater.* <https://doi.org/10.1016/j.conbuildmat.2014.01.062>.
- Hajmohammadi, A., Ngo, T., Mendis, P., 2017. How does aluminum foaming agent impact the geopolymer formation mechanism? *Cem. Concr. Compos.* <https://doi.org/10.1016/j.cemconcomp.2017.03.022>.
- Hassaan, M.M., Khater, H.M., El-Mahllawy, M.S., El Nagar, A.M., 2015. Production of geopolymer composites enhanced by nano-kaolin material. *J. Adv. Ceram.* <https://doi.org/10.1007/s40145-015-0156-y>.
- Hodne, H., Saasen, A., Strand, S., 2001. Rheological properties of high temperature oil well cement slurries. In: *Annual Transactions of the Nordic Rheology Society*.
- Huang, Y., Han, M., 2011. The influence of α -Al₂O₃ addition on microstructure, mechanical and formaldehyde adsorption properties of fly ash-based geopolymer products. *J. Hazard. Mater.* <https://doi.org/10.1016/j.jhazmat.2011.07.025>.
- Jafariefad, N., Geiker, M.R., Gong, Y., Skalle, P., Zhang, Z., He, J., 2017a. Cement sheath modification using nanomaterials for long-term zonal isolation of oil wells: Review. *J. Pet. Sci. Eng.* <https://doi.org/10.1016/j.petrol.2017.06.047>.
- Jafariefad, N., Khalifeh, M., Skalle, P., Geiker, M.R., 2017b. Nanorubber-modified cement system for oil and gas well cementing application. *J. Nat. Gas Sci. Eng.* <https://doi.org/10.1016/j.jngse.2017.10.002>.
- Jalal, M., Mansouri, E., Sharifpour, M., Pouladkhan, A.R., 2012. Mechanical, rheological, durability and microstructural properties of high performance self-compacting concrete containing SiO₂ micro and nanoparticles. *Mater. Des.* <https://doi.org/10.1016/j.matdes.2011.08.037>.
- Khalifeh, M., Hodne, H., Korsnes, R.I., Saasen, A., 2015. Cap Rock Restoration in Plug and Abandonment Operations; Possible Utilization of Rock-Based Geopolymers for Permanent Zonal Isolation and Well Plugging. <https://doi.org/10.2523/iptc-18454-ms>.
- Khalifeh, M., Hodne, H., Saasen, A., Vralstad, T., 2013. Techniques and Materials for North Sea Plug and Abandonment Operations. <https://doi.org/10.4043/23915-ms>.
- Khalifeh, M., Saasen, A., Hodne, H., Godoy, R., Vralstad, T., 2018. Geopolymers as an alternative for oil well cementing applications: a review of advantages and concerns. *J. Energy Resour. Technol.* <https://doi.org/10.1115/1.4040192>.
- Khalifeh, M., Saasen, A., Hodne, H., Motra, H.B., 2019a. Laboratory evaluation of rock-based geopolymers for zonal isolation and permanent P&A applications. *J. Pet. Sci. Eng.* <https://doi.org/10.1016/j.petrol.2018.12.065>.
- Khalifeh, M., Saasen, A., Vralstad, T., Hodne, H., 2014. Potential utilization of class C fly ash-based geopolymer in oil well cementing operations. *Cem. Concr. Compos.* <https://doi.org/10.1016/j.cemconcomp.2014.06.014>.
- Khalifeh, M., Saasen, A., Vralstad, T., Larsen, H.B., Hodne, H., 2016. Experimental study on the synthesis and characterization of apelite rock-based geopolymers. *J. Sustain. Cem. Mater.* <https://doi.org/10.1080/21650373.2015.1044049>.
- Khalifeh, M., Salehi, S., Jamrozik, A., Kimanzi, R., Abdollahpour, S., 2019b. Nano-modified rock-based geopolymers as supplement to Portland cement for oil well cementing. In: *Proceedings of the International Conference on Offshore Mechanics and Arctic Engineering*.
- Khalifeh, M., Todorovic, J., Vralstad, T., Saasen, A., Hodne, H., 2017. Long-term durability of rock-based geopolymers aged at downhole conditions for oil well cementing operations. *J. Sustain. Cem. Mater.* <https://doi.org/10.1080/21650373.2016.1196466>.
- Khan, W.A., Rahman, M.K., Mahmoud, M.A., Sarmah, P., 2016. MWCNT for Enhancing Mechanical Properties of Oil Well Cement for HPHT Applications. <https://doi.org/10.2118/178175-ms>.
- Khater, H.M., Abd El Gawaad, H.A., 2016. Characterization of alkali activated geopolymer mortar doped with MWCNT. *Constr. Build. Mater.* <https://doi.org/10.1016/j.conbuildmat.2015.10.121>.
- Kiran, R., Teodorici, C., Daidmohammadi, Y., Nygaard, R., Wood, D., Mokhtari, M., Salehi, S., 2017. Identification and evolution of well integrity and causes of failure of well integrity barriers (A review). *J. Nat. Gas Sci. Eng.* 45, 511-526. <https://doi.org/10.1016/j.jngse.2017.05.009>. <https://www.sciencedirect.com/science/article/pii/S1875510017302184#>.
- Komnitsas, K.A., 2011. Potential of geopolymer technology towards green buildings and sustainable cities. In: *Procedia Engineering*. <https://doi.org/10.1016/j.proeng.2011.11.2108>.
- Lavrov, A., Torsæter, M., n.d. *Physics and Mechanics of Primary Well Cementing*. Springer.
- Leiva, C., Luna-Galiano, Y., Arenas, C., Alonso-Fariñas, B., Fernández-Pereira, C., 2019. A porous geopolymer based on aluminum-waste with acoustic properties. *Waste Manag.* <https://doi.org/10.1016/j.wasman.2019.06.042>.
- Li, H., Xiao, H., gang, Ou, J., ping, 2004. A study on mechanical and pressure-sensitive properties of cement mortar with nanophase materials. *Cem. Concr. Res.* <https://doi.org/10.1016/j.cemconres.2003.08.025>.
- Li, M., Deng, S., Meng, F., Hao, J., Guo, X., 2017. Effect of nanosilica on the mechanical properties of oil well cement at low temperature. *Mag. Concr. Res.* <https://doi.org/10.1680/jmacr.16.00394>.
- Li, Z., Chen, R., Zhang, L., 2013. Utilization of chitosan biopolymer to enhance fly ash-based geopolymer. *J. Mater. Sci.* <https://doi.org/10.1007/s10853-013-7610-4>.
- Liu, X., 2017. Mud-to-cement conversion of synthetic-based drilling muds using geopolymers (Doctoral Dissertation) Retrieved from. <https://repositories.lib.utexas.edu/handle/2152/63651>.
- Liu, X., Ramos, M.J., Nair, S.D., Lee, H., Espinoza, D.N., van Oort, E., 2017. True Self-Healing Geopolymer Cements for Improved Zonal Isolation and Well Abandonment. <https://doi.org/10.2118/184675-ms>.
- Lo, K.W., Lin, K.L., Cheng, T.W., Chang, Y.M., Lan, J.Y., 2017. Effect of nano-SiO₂ on the alkali-activated characteristics of spent catalyst metakaolin-based geopolymers. *Constr. Build. Mater.* <https://doi.org/10.1016/j.conbuildmat.2017.03.152>.
- Meng, T., Yu, Y., Qian, X., Zhan, S., Qian, K., 2012. Effect of nano-TiO₂ on the mechanical properties of cement mortar. *Constr. Build. Mater.* <https://doi.org/10.1016/j.conbuildmat.2011.10.047>.
- Murtaza, M., Rahman, M.K., Al-Majed, A.A., 2016. Effect of Nanoclay on Mechanical and Rheological Properties of Oil Well Cement Slurry under HPHT Environment. <https://doi.org/10.2523/iptc-18989-ms>.
- Naskar, S., Chakraborty, A.K., 2016. Effect of nano materials in geopolymer concrete. *Perspect. Sci.* <https://doi.org/10.1016/j.pisc.2016.04.049>.
- Nasvi, M.C.M., Ranjith, P.G., Sanjayam, J., Bui, H., 2014. Effect of temperature on permeability of geopolymer: a primary well sealant for carbon capture and storage wells. *Fuel*. <https://doi.org/10.1016/j.fuel.2013.09.007>.
- Nelson, D.G.E.B., Guillot, D., 2006. *Well Cementing*, second ed. Schlumberger, Sugar Land, Texas.
- Norsok, D., 2013. 010. Well integrity in drilling and well operations. *Stand. Norway. Rev* 4.
- Norway, P., 2019. PSA - RNNP Presentation 2019 [WWW Document]. *Well Integr. Semin.* 2019. <https://www.norskolejeoggass.no/contentassets/61374c11e854015bc457be3f9b51c0/psa-rnnp-presentasjon-2019-wif-seminar-13.6.2019-til-wif-with-out-film.pdf>.
- Norway, S., 2009. NS-EN 12390-6:2009 Testing Hardened Concrete - Part 6:Tensile Splitting Strength of Test Specimens.
- Norway, S., 2005. NS-EN 196-1: Methods of Testing Cement Part 1 (Determination of strength).
- Ochoa, M.V., 2006. *Analysis of Drilling Fluid Rheology and Tool Joint Effect to Reduce Errors in Hydraulics Calculations*. Texas A&M University.
- Ozyildirim, C., Zegetosky, C., 2010. Exploratory investigation of nanomaterials to improve strength and permeability of concrete. *Transp. Res. Rec. J. Transp. Res. Board.* <https://doi.org/10.3141/2142-01>.
- Paiva, M.D.M., Silva, E.C.C.M., Melo, D.M.A., Martinelli, A.E., Schneider, J.F., 2018. A geopolymer cementing system for oil wells subject to steam injection. *J. Pet. Sci. Eng.* <https://doi.org/10.1016/j.petrol.2018.06.022>.
- Panchmatia, P., Zhou, N.S., Juenger, M., van Oort, E., 2019. Monitoring the strength development of alkali-activated materials using an ultrasonic cement analyzer. *J. Pet. Sci. Eng.* <https://doi.org/10.1016/j.petrol.2019.05.070>.

Appendix - Paper III

M.A.A. Abvi et al.

Journal of Petroleum Science and Engineering 191 (2020) 107128

- Pang, X., Boul, P.J., Cuello Jimenez, W., 2014. Nanosilicas as accelerators in oilwell cementing at low temperatures. *SPE Drill. Complet.* <https://doi.org/10.2118/168037-pa-Complet>.
- Phoo-ngernkham, T., Chindaprasit, P., Sata, V., Hanjitsuwan, S., Hatanaka, S., 2014. The effect of adding nano-SiO₂ and nano-Al₂O₃ on properties of high calcium fly ash geopolymer cured at ambient temperature. *Mater. Des.* <https://doi.org/10.1016/j.matdes.2013.09.049>.
- Provis, J.L., Van Deventer, J.S.J., 2009. Geopolymers: Structures, Processing, Properties and Industrial Applications. <https://doi.org/10.1533/9781845696382>.
- Riahi, S., Nazari, A., 2012. The effects of nanoparticles on early age compressive strength of ash-based geopolymers. *Ceram. Int.* <https://doi.org/10.1016/j.ceramint.2012.02.021>.
- Ridha, S., Yerikania, U., 2015. The Strength Compatibility of Nano-SiO₂ Geopolymer cement for oil well under HPHT conditions. *J. Civ. Eng. Res.* 5, 6–10.
- Rodríguez, E.D., Bernal, S.A., Provis, J.L., Paya, J., Monzo, J.M., Borrachero, M.V., 2013. Effect of nanosilica-based activators on the performance of an alkali-activated fly ash binder. *Cem. Concr. Compos.* <https://doi.org/10.1016/j.cemconcomp.2012.08.025>.
- Rovnanik, P., Simonová, H., Topolár, L., Schmid, P., Kersner, Z., 2016. Effect of carbon nanotubes on the mechanical fracture properties of fly ash geopolymer. In: *Procedia Engineering*. <https://doi.org/10.1016/j.proeng.2016.07.350>.
- Roy-Delage, L., Baumgarde, C., Thiercelin, M., Vidick, B., 2000. New cement systems for durable zonal isolation. In: *IADC/SPE Drilling Conference. Society of Petroleum Engineers*.
- Saafi, M., Andrew, K., Tang, P.L., McGhon, D., Taylor, S., Rahman, M., Yang, S., Zhou, X., 2013. Multifunctional properties of carbon nanotube/fly ash geopolymeric nanocomposites. *Constr. Build. Mater.* <https://doi.org/10.1016/j.conbuildmat.2013.08.007>.
- Saasen, A., Ytrehus, J.D., 2018. Rheological properties of drilling fluids: use of dimensionless shear rates in Herschel-Bulkley and power-law models. *Appl. Rheol.* <https://doi.org/10.3933/applrheol-28-54515>.
- Safi, B., Aknouche, H., Mechakra, H., Aboutaleb, D., Bouali, K., 2018. Incorporation mode effect of Nano-silica on the rheological and mechanical properties of cementitious pastes and cement mortars. In: *IOP Conference Series: Earth and Environmental Science*. <https://doi.org/10.1088/1755-1315/143/1/012015>.
- Salehi, S., Ali, N., Khattak, M.J., Rizvi, H., 2016. Geopolymer Composites as Efficient and Economical Plugging Materials in Peanuts Price Oil Market. <https://doi.org/10.2118/181426-ms>.
- Salehi, S., Khattak, J., Saleh, F.K., Igbojekwe, S., 2019. Investigation of mix design and properties of geopolymers for application as wellbore cement. *J. Pet. Sci. Eng.* <https://doi.org/10.1016/j.petrol.2019.03.031>.
- Salehi, S., Khattak, M.J., Ali, N., Ezeakacha, C., Saleh, F.K., 2017. Study and use of geopolymer mixtures for oil and gas well cementing applications. *J. Energy Resour. Technol.* <https://doi.org/10.1115/1.4037713>.
- Shenold, C., Teodoriu, C., 2016. Development of a structured workflow for enhanced well cement integrity: lessons learned and the way ahead. *J. Nat. Gas Sci. Eng.* <https://doi.org/10.1016/j.jngse.2016.10.042>.
- Singh, B., Ishwarya, G., Gupta, M., Bhattacharya, S.K., 2015. Geopolymer concrete: a review of some recent developments. *Constr. Build. Mater.* <https://doi.org/10.1016/j.conbuildmat.2015.03.036>.
- Standard, A., n.d. D3967-16 (2016) Standard Test Method for Splitting Tensile Strength of Intact Rock Core Specimens. ASTM Int. West Conshohocken, USA.
- Sumesh, M., Alengaram, U.J., Jumaat, M.Z., Mo, K.H., Alnahhal, M.F., 2017. Incorporation of nano-materials in cement composite and geopolymer based paste and mortar – a review. *Constr. Build. Mater.* <https://doi.org/10.1016/j.conbuildmat.2017.04.206>.
- Teodoriu, C., Kosinowski, C., Amani, M., Schubert, J., Shadravan, A., 2013. Wellbore Integrity AND cement failure at hpht conditions. *Int. J. Eng. Appl. Sci.*
- Thiercelin, M.J., Dargaud, B., Baret, J.F., Rodriguez, W.J., 1998. Cement design based on cement mechanical response. *SPE Drill. Complet.* 13, 266–273.
- Vignes, B., Aadnøy, B.S., 2010. Well-integrity issues offshore Norway. In: *SPE Production and Operations*. <https://doi.org/10.2118/112535-PA>.
- Vrålstad, T., Saasen, A., Fjær, E., Øia, T., Ytrehus, J.D., Khalifeh, M., 2018. Plug & abandonment of offshore wells: ensuring long-term well integrity and cost-efficiency. *J. Pet. Sci. Eng.*
- Watson, T.L., Bachu, S., 2009. Evaluation of the potential for gas and CO₂ leakage along wellbores. *SPE Drill. Complet.* <https://doi.org/10.2118/106817-pa>.
- Williams, R.H., Khatri, D.K., Keese, R.F., Le Roy-Delage, S., Roye, J.M., Leach, D.L.R., Porcherie, O., Rottler, P., Rodriguez, J., 2011. Flexible, Expanding Cement System (FECS) Successfully Provides Zonal Isolation across Marcellus Shale Gas Trends. <https://doi.org/10.2118/149440-ms>.
- Yang, L.Y., Jia, Z.J., Zhang, Y.M., Dai, J.G., 2015. Effects of nano-TiO₂ on strength, shrinkage and microstructure of alkali activated slag pastes. *Cem. Concr. Compos.* <https://doi.org/10.1016/j.cemconcomp.2014.11.009>.
- Yong, S.L., Feng, D.W., Lukey, G.C., van Deventer, J.S.J., 2007. Chemical characterisation of the steel-geopolymeric gel interface. *Colloids Surfaces A Physicochem. Eng. Asp.* <https://doi.org/10.1016/j.colsurfa.2007.03.004>.

Paper-IV:

Alvi, M. A. A., Belayneh, M., Saasen, A., & Bandyopadhyay, S. (2021, June). **Impact of Various NPs on the Viscous Properties of Water Based Drilling fluids**. In International Conference on Offshore Mechanics and Arctic Engineering (Vol. 85208, p. V010T11A066). American Society of Mechanical Engineers.
DOI: 10.1115/OMAE2021-62612

This paper is not included in the repository due to copyright restrictions.